ROLE OF COMPLEMENT COMPONENT 1, Q SUBCOMPONENT BINDING PROTEIN (C1QBP) IN BREAST CARCINOGENESIS

OLIVIA JANE SCULLY

NATIONAL UNIVERSITY OF SINGAPORE

2015

ROLE OF COMPLEMENT COMPONENT 1, Q SUBCOMPONENT BINDING PROTEIN (C1QBP) IN BREAST CARCINOGENESIS

OLIVIA JANE SCULLY
(BSc, UPM)

A THESIS SUBMITTED
FOR THE DEGREE OF DOCTOR OF PHILOSPHY
DEPARTMENT OF ANATOMY
NATIONAL UNIVERSITY OF SINGAPORE

2015

DECLARATION

I hereby declare that this thesis is my original work and it has been written by me in its entirety. I have duly acknowledged all the sources of information which have been used in the thesis.

This thesis has also not been submitted for any degree in any university previously.

_____

Olivia Jane Scully

3 August 2015

ACKNOWLEDGEMENTS

First and foremost, my sincere thanks and gratitude to my supervisor, **Professor Bay Boon Huat**, Head of Department of Anatomy, Yong Loo Lin (YLL) School of Medicine, National University of Singapore (NUS), for providing me with an opportunity to pursue my doctorate degree. Prof. Bay has tirelessly given his support, guidance and motivation throughout my studies, and his valuable suggestions, dedication, ideas and critical comments, are pivotal for the success of this project. Apart from his professionalism and great leadership, Prof. Bay leads an exemplary life, treating everyone with kindness and compassion. He is truly a source of inspiration in my life.

I would also like to take this opportunity to thank my co-supervisor, **Associate Professor Yip Wai Cheong, George**, Department of Anatomy, YLL School of Medicine, NUS for his advice, support and guidance in data analyses and experiments that are of great help in this project. In addition, I would also like to thank **Dr. Harve Subramhanya Karthik**, Department of Anatomy, YLL School of Medicine, NUS, my thesis advisory committee member for his comments regarding this project. I am also very grateful to all the collaborators involved in this project: Firstly, **Professor Tan Puay Hoon**, Senior Consultant and Head of Department of Pathology, Singapore General Hospital (SGH), for kindly providing the breast cancer tissue microarrays (TMAs), and also, for her important pathological evaluations; **Dr. Aye Aye Thike**, Department of Pathology, SGH, for her patience, guidance and verification for the scoring of TMAs; My utmost gratitude to **Dr. Ken Matsumoto**, Laboratory of Cellular Biochemistry, Institute of Physical and

Chemical Research (RIKEN) for generously providing the C1QBP and YB-1 antibodies and plasmids, and for his immense support and assistance in this project; **Dr. Agus Salim**, Department of Mathematics and Statistics, La Trobe University, Australia, for his invaluable assistance in the statistical analysis of the breast cancer TMA data; and **Dr. Jayantha Gunaratne**, Institute of Molecular and Cell Biology, for his help and discussion in the proteomics study.

My heartfelt appreciation to Mrs. Ng Geok Lan, Mrs. Yong Eng Siang, Mr. Poon Jun Wei, Miss Chan Yee Gek and Mr. Low Chun Peng for their technical assistance, and Mdm Ang Lye Gek, Carolyne, Mdm Teo Li Ching, Violet and Mdm Diljit Kaur for their administrative assistance.

I am deeply grateful to Dr. Yu Yingnan, Dr. Guo TianTian and Dr. Ding Jian for teaching and sharing their research experiences, skills and advice during the course of my PhD. I would also like to thank Dr. Jasmine Li Jia'En, Dr. Alice Zin Mar Lwin, Dr. Ng Cheng Teng, Dr. Chua Pei Jou, Dr. Sukanya Shyamasundar, Miss Cynthia Ong, Miss Lim Jia Pei, Miss Sheila Chee Min Yao, Ms Sunitha Nair and Miss Tan Shay Ping, for their candid discussions and friendship.

Without the financial help in the form of the NUS research scholarship, I would not have been able to further my studies and for that I am extremely grateful to NUS. I am also thankful for the Singapore Ministry of Education MOE2013-T2-1-129 Grant and Biomedical Research Council BMRC/10/1/21/24/638 Grant that has provided the funding for this project.

Last but not least, this would not have been possible without the support, love and understanding of my parents, Mr. and Mrs Patrick William Scully and my husband, Mr. Dominic Leng Han, thus, my greatest gratitude, thanks and love to them.

TABLE OF CONTENT

SUMMARY

Breast cancer is the most common cancer afflicting women globally, and its progression is the result of complex genetic and molecular processes. Once breast cancer acquires metastatic features, no effective cure is available, and treatments are meant for palliative purposes. Hence, a search of molecular biomarkers for the diagnosis and treatment of breast cancer holds great importance. One such molecule is the complement component 1, q subcomponent binding protein (C1QBP), which has been reported to play important roles in cancer development, including proliferation and metastasis. Although much work has been done on C1QBP and its role in cancer, the mechanistic role of C1QBP in breast cancer has not been fully elucidated. Therefore, the current study aims to determine the effect of C1QBP on breast cancer progression, and elucidate the underlying molecular pathways, to provide a better understanding of the roles of C1QBP in breast cancer.

Immunohistochemical analysis of C1QBP in tissue microarrays (TMAs) of breast cancer, revealed significant associations with age, tumor size and lymph node spread. Furthermore, in progesterone receptor-positive patients, C1QBP was found to be an independent predictor of tumor size, after performing multivariate analysis. Immunostaining of C1QBP in breast cancer TMAs appeared granular in nature and predominantly localized to the cytoplasm. In MDA-MB-231 and T47D breast cancer cell lines, immunofluorescence staining of C1QBP indicated that it was mainly localized to the mitochondria. The depletion of C1QBP in a progesterone receptor-positive breast cancer cell line, T47D, diminished cell proliferation,

substantiating the data from the TMAs. In addition, depletion of C1QBP in MDA-MB-231 breast cancer cells, a metastatic cell line, decreased cell proliferation and cell migration, but not cell invasion, while overexpression of C1QBP in MDA-MB-231 cells increased cell proliferation, migration and invasion. Further evaluation into the cell cycle profile after overexpression of C1QBP, showed an elevated G1 to S progression, accompanied by changes in Cyclin D1 and CDK6 expression. Chemoresistance studies showed that C1QBP affects chemosensitivity to Doxorubicin hydrochloride treatment. Furthermore, constitutively higher levels of C1QBP were observed in Doxorubicin hydrochloride-resistant MCF7 cells compared to its parental counterpart.

Using gene microarray analysis and an antibody array, C1QBP was found to be involved in the regulation of p-STAT3 (Y705) and the ERK1/2 signalling pathways. Overexpression of C1QBP increased p-ERK1/2 and p-MEK1/2, both of which are main regulators of the ERK1/2 pathways. In addition, C1QBP also affected the downstream targets of p-STAT3 (Y705), such as Bcl2, Mcl1 and p53. These are cell survival signals, and could contribute to the increase of cell survival seen in C1QBP-overexpressing cells. Additionally, the p-STAT3 and ERK1/2 pathways are also known to be upstream regulators of Cyclin D1, and hence, could indirectly affect cell proliferation. Cell migration and cell invasion have also been reported to be potentially regulated by these two pathways. The antibody array also revealed a possible role of C1QBP in the Akt-pathway but this needs to be further validated.

SILAC-immunoprecipitation quantitative proteomics was carried out to determine C1QBP's interactome, and YB-1 was identified as one of its interacting partners. Further studies revealed that this interaction is partially involved in cell proliferation, migration and invasion, and other factors may also influence these functions. Taken together, the findings provided a further understanding of the role of C1QBP in breast cancer, and may be useful for future development of a molecular target in breast cancer.

LIST OF TABLES

LIST OF FIGURES

LIST OF ABBREVIATIONS

18-FDG	Fluorodeoxyglucose
ABC	ATP-binding cassette
AJCC	American Joint Committee on Cancer
ASF/SF2	Serine/Arginine-rich Splicing Factor 1
BCL2	B-cell Lymphoma 2
BRCA	Breast Cancer Type
BSA	Bovine Serum Albumin
C1QBP	Complement component 1, q subcomponent binding protein
CDK	Cyclin-dependent Kinase
DAVID	Database for Annotation, Visualization and Integrated Discovery
DCIS	Ductal Carcinoma *In Situ*
DMEM	Dulbecco's Modified Eagle Medium
ER	Estrogen Receptor
ERK	Mitogen Activated Protein Kinase 1
FNA	Fine Needle Aspiration
GAPDH	Glyceraldehyde-3-phosphate Dehydrogenase
GSK-3β	Glycogen Synthase Kinase 3 beta
HER2	Human Epidermal Growth Factor Receptor 2
MAP3K8	Mitogen-activated Protein Kinase Kinase Kinase 8
MCL1	Myeloid Cell Leukemia 1
MEK1	Mitogen-activated Protein Kinase Kinase 1
MMP2	Matrix Metallopeptidase 2
MRI	Magnetic Resonance Imaging
MSK1	Ribosomal Protein S6 Kinase, 90 kDa
MT1-MMP	Matrix Metallopeptidase 14
mTOR	Mechanistic Target of Rapamycin
p53	Tumor Protein p53
PCNA	Proliferating Cell Nuclear Antigen
PCR	Polymerase Chain Reaction
PI3K/AKT	Phosphatidylinositol-3-Kinase/ Protein Kinase B
PKC	Protein Kinase C
PR	Progesterone Receptor
PSA	Prostate-specific Antigen
PVDF	Polyvinylidene Fluoride
RAF	Raf-1 Proto-oncogene
RASGRP1	RAS Guanyl Releasing Protein 1
RIPA	Radioimmunoprecipitation assay buffer
RPMI	Roswell Park Memorial Institute
SDS-PAGE	Sodium Dodecyl Sulphate- Polyacrylamide Gel Electrophoresis
SILAC	Stable Isotope Labelling by Amino Acids in Cell Culture
STAT	Signal Transducer and Activator of Transcription
TBST	Tris Buffer Saline with Tween 20
TFIIB	Transcription Factor II B
TMA	Tissue Microarray
WAI	Weighted Average Index
WHO	World Health Organization
YB-1	Y-box binding protein 1

LIST OF PUBLICATIONS

Journals

Scully, O.J., Bay, B.H., Yip, G., and Yu, Y. (2012). Breast cancer metastasis. Cancer Genomics Proteomics 9, 311-320.

Scully, O.J., Yu, Y., Salim, A., Thike, A.A., Yip, G.W., Baeg, G.H., Tan, P.H., Matsumoto, K., and Bay, B.H. (2015). Complement component 1, q subcomponent binding protein is a marker for proliferation in breast cancer. Exp Biol Med (Maywood) 240: 846-853.

Meeting proceedings

Scully, O.J., Thike, A.A., Yip, G.W., Tan, P.H., Matsumoto, K., Bay, B.H. (2014). Y-box binding protein-associated acidic protein promotes breast cancer progression and is a potential molecular target. In: American Association for Cancer Research (AACR) Annual Meeting 2014, 5-9 April 2014.

Scully O.J. (2013). Gene profile of Y-box protein associated acidic protein (YBAP1) in breast cancer. In: Microscope Society (Singapore) Annual General and Scientific Meeting 2013, 10 April 2013. Awarded with 'Best Oral Presentation'.

Scully, O.J., Yu, Y., Matsumoto, K., Bay, B.H. (2013). Silencing of Y-box binding protein-associated acidic protein (YBAP1) affects cell migration in breast cancer. In: YLLSOM 3rd Annual Graduate Scientific Congress National University of Singapore, 30 January 2013.

Scully, O.J., Yu, Y., Matsumoto, K., Bay, B.H. (2012). Gene profile of Y-box binding protein-associated acidic protein (YBAP1) in breast cancer. In: 2nd International Anatomical Sciences and Cell Biology Conference (IASCBC 2012). Chiang Mai, Thailand: Proceedings of the Anatomy Association of Thailand, 6-8 December 2012.

Scully, O.J., Guo, T., Yu, Y., Matsumoto, K., Yip, G.W., Bay, B.H. (2012). Localization of Y-box binding protein 1 (YB-1) in cancer cells. In: 2nd International Anatomical Sciences and Cell Biology Conference (IASCBC 2012). Chiang Mai, Thailand: Proceedings of the Anatomy Association of Thailand, 6-8 December 2012. Awarded with 'Best Poster award'.

CHAPTER 1
INTRODUCTION

1 INTRODUCTION

1.1 Breast cancer

1.1.1 Epidemiology of breast cancer

The breast or mammary gland contains milk-secreting lobules, which drain into ducts that coalesce into the larger lactiferous ducts, which empty into the nipple (Marieb et al., 2014). The breast is only functional in lactating females when milk is produced to nourish the infant. Breast cancer has been reported to be the 2nd most common cancer and ranked 5th as the cause of cancer deaths worldwide. In the global female population, an estimated 1.7 million breast cancer cases and 521,900 breast cancer deaths have been recorded, making it the most frequently diagnosed type of cancer and leading cause of cancer death among females (Ferlay, 2013). Incidence rates of breast cancer vary across the world, where slightly more cases are seen in less developed countries compared to developed countries. The differences in rates reflect the accessibility of early intervention and risk factors (Torre et al., 2015). Breast cancer death rates have seen a plateau or decline in Northern America and developed European countries, mainly due to advanced treatments and early detection via mammography (Bosetti et al., 2012). On the contrary, breast cancer incidence is increasing in the South America, Africa and Asia region, most likely caused by westernized lifestyles and lack of facilities for diagnosis and treatment (Youlden et al., 2012).

The Singapore Cancer Registry Interim Annual Report released in May 2015, indicated that breast cancer is the most common cancer among female residents of Singapore from the year 2010 to 2014 (Figure 1.1).

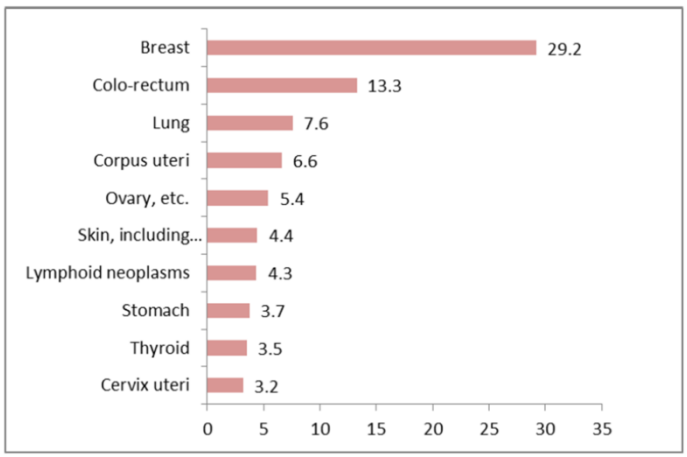

Figure 1.1. Percentages of 10 most frequent cancers in Singapore females, 2010-2014. *(Used with permission from National Registry of Diseases Office, Health Promotion Board)*

Likewise, the mortality rate for breast cancer is the highest among other cancer deaths in Singapore's female population. It was also noted that the age-standardized incidence rate of newly diagnosed breast cancer has been increasing drastically over the years from 23.8 per 100000 in 1975-1979 to 64.7 per 100000 in 2010-2014.

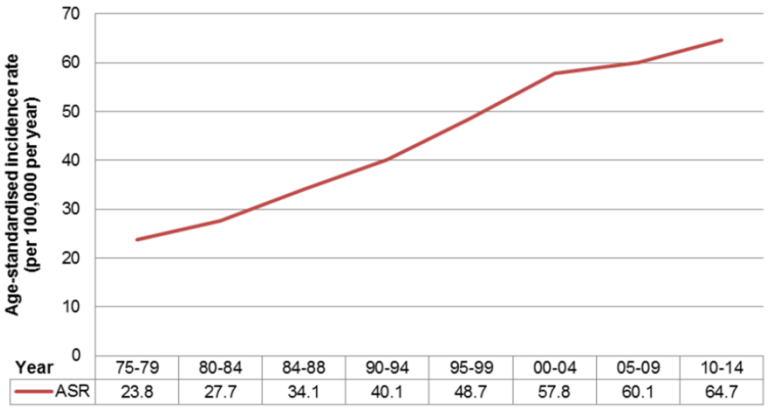

Figure 1.2. Age-standardized incidence rates for Singapore female breast cancer, 1975-2014. *(Used with permission from National Registry of Diseases Office, Health Promotion Board)*

The incidence rate is highest in Chinese females, followed by Malay and Indian females. There is also a steep increase of incidence rate in the 30-39 age group onwards with the highest incidence rate recorded in the 60-69 age group. On a more positive note, survival rates of breast cancer patients were slightly increased for all ethnicities and age group (except for the 65-74 age group) in the years 2010-2014 compared to 2005-2009 (NRDO, 2015).

1.1.2 Risk factors of breast cancer

Breast cancer predisposition is not the same among women. Several risk factors have been identified to increase the chances of breast cancer development. These include biological factors, hormonal factors and lifestyle choices.

1.1.2.1 Biological factors – family history, age and breast conditions

Risk factors such as family history, age and breast conditions are biological risk factors for breast cancer. Epidemiological studies have shown that individuals with predisposing gene mutations, have a 50-85% chance of having breast cancer (Evans, 2013). In addition, it was estimated that women with a first degree relative having a history of breast cancer, have a higher risk of developing cancer, compared to women without such history (Dumalaon-Canaria et al., 2014). The likelihood is increased if the first degree relatives were affected by breast cancer, when they are below 40 years of age (Claus et al., 1994). Inheritable gene mutations, such as *BRCA1* and *BRCA2* mutations, have been associated with a cumulative lifetime risks of 85% for breast cancer (Evans et al., 2008).

Age has also been identified as a significant risk factor of breast cancer. Approximately 75% of breast cancer cases happen in postmenopausal women. The risk of breast cancer for women in their 70s is 1 to 30, which is about 8 fold higher than women in their 30s (NBOCC, 2009).

Physically, an individual's breast density is a risk factor of breast cancer. It has been estimated that women with breast density of more than 75%, are 4 times more likely to develop breast cancer, than women with less dense breast (Dumalaon-Canaria et al., 2014).

1.1.2.2 Hormonal factors

The hormonal environment of breast tissue has been associated with increased risk factor of breast cancer. Cumulative exposure to estrogen influenced by early menarche, late menopause, late first pregnancy, not having children and not breastfeeding has been associated with a higher risk of breast cancer (Evans, 2013; Dumalaon-Canaria et al., 2014). A meta-analysis of over 100 epidemiological studies, showed that the risk of breast cancer is increased by 5% per year for every younger year of menarche. Additionally, the use of oral contraceptive pill has been associated with a 20% increase of breast cancer risk, which persists for 10 years after use (Evans, 2013). The strongest association between these reproductive factors and breast cancer risks, exist for hormone receptor-positive breast cancer (Anderson et al., 2014).

1.1.2.3 Lifestyle factors – physical activity, diet, body size and alcohol consumption

Physical activity, diet, body size and alcohol consumption have been associated with the development of breast cancer. There is convincing evidence that breast cancer risk is inversely related to physical activity. Constant physical activity from adolescence to adulthood has been shown to reduce the risk of breast cancer by approximately 30% (Maruti et al., 2008; Colditz et al., 2014). Nine percent of breast cancer death has been attributed to obesity. In addition, weight gain and abdominal fat accumulation have been associated with higher risk of breast cancer in postmenopausal women (Dumalaon-Canaria et al., 2014). Dietary factors, such as high cholesterol and triglycerides intake, have also been shown to increase the risk of breast cancer while diets high in fibres, fruits and vegetable, have been shown to be protective against breast cancer (Rossi et al., 2014). Also, intake of alcohol is considered a risk factor for breast cancer. Alcohol has been classified by the International Agency for Research on Cancer (IARC) as 'carcinogenic to human' with alcohol being attributed to 5% of breast cancer-related death (Colditz et al., 2014; Dumalaon-Canaria et al., 2014).

1.1.3 Symptoms of breast cancer

The most common presentation of breast cancer is a painless lump in the breast. Other symptoms are changes in the size and shape of the breast, nipple discharge and changes, breast pain and breast skin changes. These symptoms are usually evaluated in terms of their duration, persistence and variation with the menstrual cycle (Morrow, 2014). However, it should also be

noted that not all breast lumps are malignant (Bleicher, 2014). In addition, some early stage breast cancers are asymptomatic. Therapeutic intervention at an earlier stage of malignancy will greatly increase survival chances (Benson, 2013). Thus, regular breast examination and screening, are important for early detection of breast cancer. In agreement, trials have shown that in women over 50 years old, breast screening reduced the mortality rate of breast cancer by 25 to 30% (Benson, 2013).

1.1.4 Diagnosis of breast cancer

Diagnosis of breast cancer is done based on triple assessment, which is a combination of clinical assessment, radiological assessment and pathological assessment. Clinical assessment includes clinical breast examination, while radiological and pathological assessments, are based on imaging techniques and biopsy, respectively. Each assessment will be categorised as either normal, benign, indeterminate, suspicious or malignant. The 'worse' conclusion from the clinical and radiological assessment, must be used to interpret the pathological assessment (Mathew and Cheung, 2013).

1.1.4.1 Breast examination

Breast examination can be divided into breast self-examination, or clinical breast examination. As the name suggests, breast self-examination can be perform by women themselves, to detect any presence of lumps or changes in the appearance of the breasts. It is recommended to be done monthly, a week after menstruation. Although the effectiveness of breast self-examination in reducing breast cancer mortality seemed weak, it has been shown to assist

in the early detection of breast cancer (Kamproh and Fungpong, 2008; Lee and Elmore, 2014).

Clinical breast examination is done by a certified health professional. Several studies have assessed the effectiveness of clinical breast examination, combined with mammography, in reducing breast cancer mortality. The final conclusion of its effectiveness is still in debate, where some argued that higher false negative or false positive rates are observed with clinical breast examination (Chiarelli et al., 2009; Lee and Elmore, 2014). Nonetheless, it was also reported that the quality of clinical breast examination, can be greatly improve and beneficial, when it is done by highly trained personnel (Chiarelli et al., 2009; Lee and Elmore, 2014).

1.1.4.2 Radiological assessment – mammography, ultrasonography, magnetic resonance imaging and radionuclide breast imaging

Mammography is the mainstay of breast cancer screening. Randomized clinical trials conducted have shown that breast screening using mammography, reduced mortality rate by 30% (Lewin, 2011). Women at the age of 40 and above, are recommended to attend yearly mammography screenings. Screening should start about 7 to 10 years earlier for women with higher risk of breast cancer, such as for women with family history or prior chest radiation therapy (Jochelson, 2014). A weakness of traditional film mammography, is its reduced sensitivity with dense breast tissue. Digital mammography has largely replaced film mammography and improved sensitivities in this situation (Lewin, 2011; Jochelson, 2014). In addition, several advancements have been made such as digital breast tomosynthesis

and contrast-enhanced mammography, which could improve accuracy and sensitivity of digital mammography (Jochelson, 2014).

Ultrasonography is another widely used method to aid diagnosis of breast cancer. Apart from differentiating cystic and solid mass in the breast, ultrasonography can be used to distinguish benign and malignant characteristics of the tumor (Lewin, 2011; Jochelson, 2014). It is also used to confirm negative mammograms of palpable mass in the breast. Additionally, this method is also applied for guiding core needle biopsies (Lewin, 2011). A pitfall of the ultrasonography method compared to mammography, is its inefficiency of detecting ductal carcinoma *in situ* and microcalcifications (Jochelson, 2014). The reproducibility of this technique is also highly dependent on the operator of the ultrasound transducer, thus, reproducibility is sub-optimal (Sedgwick, 2014). Nevertheless, the development of Automated Whole Breast Ultrasound, reduces dependency on the operators and increases reproducibility of the results (Jochelson, 2014).

Magnetic resonance imaging (MRI) is a breast cancer detection technique, that uses gadolinium contrast medium with no radiation exposure (Weinstein and Roth, 2014). Unlike mammography and ultrasonography, the use of MRI enabled the determination of tumor size, and presence of multifocal and multicentric tumors. Furthermore, the detection of contralateral disease of the breast and lymph node spread are possible with MRI (Lewin, 2011). Although the sensitivity of MRI in detecting invasive breast cancer reaches almost a 100%, its specificity is low resulting in more false-positive results (Pointon and Down, 2013; Weinstein and Roth, 2014). The MRI is especially useful for screening of high-risk younger women – below 50 years

old – where repeated radiation exposure is of concern, or screening by mammography alone is not satisfactory. With a combination of both MRI and mammography, the sensitivity and specificity of cancer detection are increased (Pointon and Down, 2013). Other ways being develop to improve the specificity of MRI are the addition of Diffusion-Weighted Imaging and MR spectroscopy to conventional MRI (Jochelson, 2014).

Radionucleotide breast imaging detects abnormalities based on the physiology of the breast, and it is not affected by breast densities (Jochelson, 2014). In this technique, low-level radioactive compounds will be introduced into the body or specific sites for subsequent detection. The commonly used traces are sestamibi and 18F-fluorodeoxyglucose (18F-FDG) (Jochelson, 2014). Sestamibi imaging is usually indicated for evaluating the extent of breast cancer in known patients, and in patients where MRI cannot be performed. Specificity and sensitivity of breast cancer detection using sestamibi, are greatly improved using detector systems, such as the breast-specific gamma imaging system. Though, it is to be noted that sestamibi imaging is dependent on patients' hormone status (Jochelson, 2014). On the other hand, 18F-FDG is not dependent on both breast density and hormone status. It is widely utilized for whole body Positron Emission Tomography (PET) to determine the stage and progression of lymphoma and solid tumors. However, the sensitivity for primary breast tumor detection is very low (Jochelson, 2014). Positron Emission Mammography (PEM) using 18F-FDG was developed for improved breast imaging, and its specificity seemed to be better than that of MRI (Berg et al., 2011). In addition, PEM could also direct biopsy of the lesion (Jochelson, 2014). However, usage of radionucleotide

imaging methods need to be limited, due to their radiation dose (Jochelson, 2014).

1.1.4.3 Pathological assessment – fine needle aspiration cytology and needle core and surgical biopsy

A simple and fast technique: fine-needle aspiration (FNA) is a low-cost, relatively comfortable procedure, that can be helpful in diagnosis of malignancy (Prier, 2011). Despite that, the use of FNA has been markedly limited due to frequent poor sampling, inability to distinguish ductal carcinoma *in situ* and invasive carcinoma, difficulty in characterizing receptor status, and most importantly, FNA has a high false positive rate with low accuracy (Prier, 2011; Sung and Comstock, 2014). Consequently, FNA is routinely used for sampling of axillary nodes or lesions which are not suitable for biopsy (Sung and Comstock, 2014).

Core needle biopsy is usually done using an automated or vacuum-assisted 14-gauge needle, to obtain breast tissue samples for analysis. The method is superior to that of FNA as sufficient samples are obtained, for more accurate histological diagnosis and immunohistochemical analysis. Additionally, it is also possible to discriminate between *in situ* and invasive cancer (Prier, 2011). Core needle biopsy is further enhanced by assistance from imaging procedures, such as ultrasound and MRI. Ultrasound-guided core biopsy is less invasive, accurate and permits better access to lesions which are difficult to reach (Sung and Comstock, 2014).

1.1.5 Breast cancer classification

Breast cancer development arises from a complex series of molecular events, that oversee the progression of breast cells from normal cells to *in situ* carcinoma, and eventually invasive and metastatic disease (Simpson et al., 2005; Bombonati and Sgroi, 2011). Since development of breast cancer entails the disease with altered pathological and clinical features at different stages, classification of breast cancer is important for diagnosis and treatment of the disease. Breast cancer can be classified using a few methods. Staging of breast cancer according to the American Joint Committee on Cancer (AJCC) remains the mainstay in evaluating prognosis and treatment of a breast cancer patient (Yalcin, 2013). The World Health Organization (WHO) classification of breast cancer, is mostly a histopathological classification of breast cancer, which is based on morphological characteristics of the cells (Viale, 2012). Another way to categorize breast cancer is the grouping of the disease based on its molecular features.

1.1.5.1 American Joint Committee on Cancer (AJCC) staging system

The AJCC staging system uses TNM classification where T defines the size and extent of the primary breast tumor, N defines the spread to neighbouring lymph nodes, and M defines the presence of distant metastases (Harris, 2014). Based on this features, the staging of breast cancer is as follows:

Stage 0 : Carcinoma *in situ*

Stage I : Primary tumor of 2 cm or less with no lymph node metastasis

Stage IIA : Primary tumor not detected with lymph node spread in axillary lymph nodes; or primary tumor of 2 cm or less with lymph

node spread in axillary lymph nodes; or primary tumor larger than 2 cm but smaller than 5 cm without lymph node spread

Stage IIB : Primary tumor of more than 2 cm but less than 5 cm with axillary lymph node spread; or primary tumor size is larger than 5 cm without lymph node spread

Stage IIIA : Primary tumor not detected but presence of fixed or matted axillary lymph node metastasis or metastasis to internal mammary nodes; or tumor size of less than 5 cm with fixed or matted axillary lymph node metastasis or metastasis to internal mammary nodes; or tumor size of more than 5 cm with axillary lymph node spread; or tumor size of more than 5 cm with fixed or matted axillary lymph node spread or internal mammary nodes spread

Stage IIIB : Primary tumor of any size that extent to chest wall or skin without lymph node spread or with axillary lymph node spread or internal mammary nodes spread

Stage IIIC : Primary tumor of any size with metastasis in ipsilateral infraclavicular or both axillary lymph nodes and internal mammary nodes or supraclavicular lymph nodes

Stage IV : Primary tumor of any size with any lymph node spread status and the presence of distant metastasis

Although still important, more emphasis is given to the rapidly growing molecular classifications of breast cancer, which will be discussed later. Nonetheless, these newer methods are used complementarily with staging of breast cancer for therapeutic decisions (Harris, 2014).

1.1.5.2 World Health Organization (WHO) classification

The WHO classification, which has been primarily based on morphological aspects of breast cancer, has been updated to include some molecular expression of the tumors (Sinn and Kreipe, 2013; Austreid et al., 2014). Among others, it includes classification of precursor lesions, benign epithelial proliferations, fibroepithelial, epithelial tumors and invasive breast carcinoma. Several subtypes are included in invasive breast carcinoma, including invasive breast carcinoma of no special type, invasive lobular carcinoma, tubular carcinoma and so on. A majority of breast cancer falls

under the invasive breast carcinoma of no special type category. This constitutes the group of breast cancers, which do not belong to other breast cancer categories, and it is previously known as invasive ductal carcinoma (Sinn and Kreipe, 2013).

1.1.5.3 Breast cancer molecular subtype

Traditionally, breast cancer has also been classified according to the presence of hormone receptors, and human epidermal growth factor receptor 2 (HER2) status, in order to assess the use of adjuvant systemic therapy (Goldhirsch et al., 2009; Viale, 2012). In the advent of gene expression profiling, more detailed breast cancer subtypes have since been unveiled. The luminal breast cancer subtypes, consisting of luminal A and luminal B subtypes, have been identified as subtypes with positive hormone receptors while HER2-enriched, basal-like and claudin-low groups are under the hormone receptors-negative group (Schnitt, 2010).

The luminal A subtype is generally enriched with estrogen receptors (ER), progesterone receptors (PR) and genes associated with ER activation. In addition, this subtype contains low levels of proliferation gene clusters, mainly Ki67 (Schnitt, 2010; Carey et al., 2014; Sonnenblick et al., 2014). On the other hand, the luminal B breast cancer subtype, has relatively less ER-gene clusters although still positive for ER and/or PR and high Ki67 expression. In addition, variable HER2 expression is present (Schnitt, 2010; Sonnenblick et al., 2014). The HER2-enriched group contains elevated HER2 gene cluster expression, accompanied by low levels of luminal and basal-like gene cluster. Apart from that, this subtype also exhibits high proliferation clusters, with TP53 mutations

commonly detected (Carey et al., 2014). The basal-like breast cancer subtype has low levels of luminal characteristics and HER2 expression, with high expression of proliferation genes. In addition, what makes this subtype unique, is the greater presence of the basal gene clusters which consists of basal epithelial cytokeratins, such as CK5, 6, epidermal growth factor receptor, c-Kit, vimentin, P-Cadherin and αB-crystallin (Schnitt, 2010; Carey et al., 2014). Claudin-low subtype is similar to basal-like breast cancer subtype, in that, it has low luminal genes and HER2 expression. However, the claudin-low subtypes differ from the basal-like breast cancer, in terms of their low level of proliferation genes and cell-cell adhesion proteins. Additionally, claudin-low subtypes also contain elevated immune system response genes, such as interleukin-6 and CD4 (Carey et al., 2014).

Although much has been done to elucidate the molecular subtypes of breast cancer, the use of molecular subtypes alone, is not enough for decisions on staging, treatment and follow-up of breast cancer (Sonnenblick et al., 2014). However, several ongoing clinical trials based on gene expression signatures, such as the Amsterdam 70-gene prognostic profile (Agendia Mammaprint®), and Treatment for Positive Node, Endocrine Responsive Breast cancer (RxPONDER) trial, are being conducted to determine the prognostic and therapeutic value of these classifications (Carey et al., 2014; Sonnenblick et al., 2014).

1.1.6 Treatment of breast cancer

There are several options for treatment of breast cancer, and these are dependent on the staging and spread of the cancer, hormone receptor status,

patient's menopausal status, age and also patient's choices (Maughan et al., 2010). Basically, breast cancer treatment options ranged from surgery, systemic therapy to targeted therapy.

1.1.6.1 Surgery

Generally, breast conserving surgery is done for patients with early-stage disease, and smaller tumor size (<5cm) in relation to breast size. Tumor-to-breast size is important to ensure clear resection of tumor, while preserving the breast appearance (Harris and Morrow, 2014). Breast conserving surgery is usually followed by radiation therapy, and this has been shown to reduce local recurrence, and at the same time, improve long-term survival of patients (Clarke et al., 2005). Another form of surgical therapy for breast cancer is the removal of whole breast or mastectomy. The procedure applies to breast cancer patients who are unable to undergo breast conserving surgery. This could be due to the inability to reduce the tumor burden, and inability for patients to receive safe radiation therapy. Simple mastectomy involves the removal of the whole breast, without the removal of axillary lymph nodes, while modified radical mastectomy involves the removal of breast, plus axillary lymph nodes (Morrow and Golshan, 2014).

1.1.6.2 Radiation therapy

Radiation therapy utilizes ionizing radiation to kill cancerous cells. Whole breast irradiation includes radiation of the chest wall and the supraclavicular lymph nodes. This is usually done after surgery to remove residual local disease, and reduce the chances of local recurrence (Khan and Haffty, 2014). In addition, radiation therapy may also be administered before

surgery to reduce the size of tumor, so that, breast conserving surgery can be performed (Harris and Morrow, 2014).

1.1.6.3 Chemotherapy

Chemotherapy is administered to breast cancer patients, as a neoadjuvant or adjuvant treatment. Preoperative chemotherapy or neoadjuvant chemotherapy, is used to downstage tumors, enabling the removal of previously unresectable tumors (Bardia and Baselga, 2014). Adjuvant chemotherapy after surgical resection, is done to remove remaining malignant cells, and is based on histological parameters and the molecular subtypes (Dang and Hudis, 2014). Both preoperative and adjuvant chemotherapy, have shown good clinical outcomes in the treatment of breast cancer (Bardia and Baselga, 2014; Dang and Hudis, 2014). Some examples of chemotherapeutic drugs, are Doxorubicin hydrochloride, Epirubicin hydrochloride and 5-Fluorouracil (Eisner and Luoh, 2011).

1.1.6.4 Targeted therapy

A deeper understanding of the molecular signatures of breast cancer, has led to the development of targeted therapy, where treatments are directed to specific molecules of cancer cells. One of the earliest forms of targeted therapy is the endocrine therapy, which is recommended for breast cancer patients whose tumors have high levels of ERs. An example of such drug is tamoxifen (Lumachi et al., 2011; Rimawi and Osborne, 2014). Aside from targeting ERs, trastuzumab which is a monoclonal antibody targeting the HER2 receptor, is fundamental in the development of targeted therapies (Munagala et al., 2011). In addition, due to the advancements of tumor

genetics, many new targeted therapies are being developed, which includes phosphatidylinositol-3 kinase/protein kinase B (PI3K/AKT) inhibitors, cyclin-dependent kinase inhibitors, mitogen-activated protein/extracellular signal-regulated kinase (MEK) inhibitors and matrix metalloproteinases inhibitors (Munagala et al., 2011).

1.1.6.5 Challenges associated with current breast cancer treatment

Although advancements in breast cancer treatment have improved the prognosis of breast cancer patients, 15% of patients still develop distant metastasis, for which there is no cure (Austreid et al., 2014). Chemoresistance and drug resistance remain the main issues in the treatment of breast cancer (Austreid et al., 2014). In addition, patients undergoing breast cancer treatment, often face acute and chronic adverse side effects, such as cardiac toxicity and neurotoxicity (Odle, 2014). Chemotherapeutic drugs in combination with targeted therapies, such as anti-HER2, have been shown to counteract drug resistance (Austreid et al., 2014). However, the efficacy of combination therapy of new drugs, such as mTOR inhibitors, CDK inhibitors and so on, have given mixed results or are not yet established (Austreid et al., 2014; Ziauddin et al., 2014). Yet, the development of targeted therapies are still widely pursued, because of their potential use to battle drug resistance, and at the same time, reduce toxicity of treatment due to their specificity to malignant cells (Austreid et al., 2014; Odle, 2014; Ziauddin et al., 2014). Hence, it is important to continually unearth potential biomarkers, to develop therapeutic and prognostic targets for breast cancer.

1.2 Complement component 1, q subcomponent binding protein (C1QBP)

Complement component 1, q subcomponent binding protein (C1QBP) is a protein known by many names, such as receptor for the globular head of C1q (gC1qR), hyaluronan-binding protein 1 (HABP1), Y-box protein-associated acidic protein (YBAP1) and mitochondrial matrix protein p32 (p32). Initially purified from Raji cells, it was found to bind to globular heads of C1q molecules (Ghebrehiwet et al., 1994). The *C1QBP* gene originates from chromosome 17p13.3, spanning 6055 bp of DNA (Ghebrehiwet and Peerschke, 1998; Tye et al., 2001). The gene contains 6 exons and 5 introns, encoding a pre-pro protein of 282 amino acid residues, which is eventually cleaved to form the mature protein of 209 amino acid residues, beginning on the 74^{th} (Leu) amino acid residue (Ghebrehiwet et al., 1994; Ghebrehiwet and Peerschke, 1998). The cleaved section contains the mitochondrial localization signal necessary for mitochondrial localization of C1QBP (Muta et al., 1997; Dedio et al., 1998). In addition, C1QBP has also been found to be present in the cell nucleus and cell surface (Dedio et al., 1998; Ghebrehiwet and Peerschke, 1998; Soltys et al., 2000; Brokstad et al., 2001). Due to its high charge, the mature C1QBP protein is very acidic with a pI value of 4.15 (Ghebrehiwet and Peerschke, 1998). The crystal structure of C1QBP revealed that C1QBP exists as a trimeric doughnut-shaped quarternary complex, with assymetrical charge distribution (Jiang et al., 1999). Although predicted to be a 24.3 kDa protein, the C1QBP protein appears as a 33 kDa protein on SDS-PAGE (Ghebrehiwet et al., 1994; Ghebrehiwet and Peerschke, 1998).

1.2.1 Physiological functions of C1QBP

C1QBP is a multifunctional protein, evident from its interaction with diverse proteins of different functions. One of the early discoveries of C1QBP's functions, is its role in infection and inflammation (Peerschke and Ghebrehiwet, 2007). C1QBP contributes to infection by facilitating binding to antigens from microbes, such as *Listeria monocytogenes*, Hepatitic C virus and *Staphylococcus aureus* (Ghebrehiwet and Peerschke, 1998; Peerschke and Ghebrehiwet, 2007). For example, persistent infection of hepatitis C virus due to T cell suppression is mediated by C1QBP, through its interaction with the hepatitis C virus core protein. This blocks the G1 to S phase progression of T cell and thus, inhibits proliferation (Yao et al., 2003). C1QBP also modulates the classical complement pathway, contributing to inflammation. In atherosclerotic lesions, C1QBP facilitated inflammation by binding to C1q and influencing the kinin systems (Peerschke et al., 2004).

Apart from that, C1QBP has also been shown to be involved in transcription. It has been reported to interact with proteins involved in transcription regulation, such as CCAAT-binding factor- B subunit and human immunodeficiency virus type 1 Tat transactivator, as well as, transcription factor II B (TFIIB) (Yu et al., 1995; Chattopadhyay et al., 2004). In addition, C1QBP influences the pre-mRNA splicing process, by deterring the functions of serine/arginine-rich splicing factor 1 (ASF/SF2), an important protein for this process (Petersen-Mahrt et al., 1999). ASF/SF2, functions as both splicing repressor and activator, depending on the site of its binding on pre-mRNA. C1QBP inhibits ASF/SF2 dual functions by preventing the binding of ASF/SF2 to RNA, thus allowing the formation of pre-spliceosome, and by

hindering phosphorylation of ASF/SF2, which is required for spliceosome assembly (Petersen-Mahrt et al., 1999). C1QBP has also been shown to interact with Y-box binding protein 1 (YB-1 or YBX1) and relieves the translational repression of YB-1, which is a multifunctional transcription factor (Matsumoto et al., 2005).

The predominant localization of C1QBP in the mitochondria, indicates a role of C1QBP in mitochondrial-related functions. Mitochondrial C1QBP has been shown to be an essential factor in maintaining mitochondrial oxidative phosphorylation, and its depletion affects ATP synthesis (Muta et al., 1997). C1QBP has also been reported to be involved in apoptosis. In normal fibroblastic cells, the up-regulation of C1QBP increased the production of reactive oxygen species, leading to apoptosis via elevation of Bax (Meenakshi et al., 2003; Chowdhury et al., 2008). Additionally, C1QBP also modulates ARF-induced p53-dependent apoptosis (Itahana and Zhang, 2008). However, C1QBP has also been reported to prevent cell death induced by oxidative stress, by inhibition of the mitochondrial permeability transition pore (McGee and Baines, 2011).

The role of C1QBP also extends to the nervous system. In hippocampal neurons isolated from rats, C1QBP was found to interact with γ-Aminobutyric acid type A ($GABA_A$) receptor (Schaerer et al., 2001). Furthermore, studies done on the *Drosophila melanogaster* model, showed that C1QBP is located within the presynaptic mitochondria, and is important for synaptic transmission (Lutas et al., 2012).

C1QBP has also been implicated in the embryonic development and reproduction system. C1QBP-knockout mice displayed mid-gestation lethality, with severe disruption of mitochondrial DNA-encoded protein synthesis (Yagi et al., 2012). Placental cytotrophoblast proliferation, which is needed for sustenance of the fetus during pregnancy, is regulated by C1QBP, and the ablation of C1QBP, was highly observed in placentas with fetal growth restriction (Matos et al., 2014).

In addition to all these functions, C1QBP has also been reported to be involved in early nucleolar ribosome biogenesis, via its interaction with Nop52 and fibrillarin (Yoshikawa et al., 2011). Other than that, C1QBP has also been shown to interact with Protein Kinase C μ (PKCμ) and lamin B (Simos and Georgatos, 1994; Storz et al., 2000). Altogether, these findings showed that C1QBP is involved in a plethora of cell processes and functions.

1.2.2 Role of C1QBP in tumorigenesis

Given its multifunctional role, it is not surprising that the dysregulation of C1QBP could give rise to tumorigenesis. The overexpression of C1QBP has been reported in various carcinomas, including breast, lung, colon, thyroid, gastric, esophagus, pancreas, ovarian and endometrial cancers (Rubinstein et al., 2004; Chen et al., 2009b; Amamoto et al., 2011; Dembitzer et al., 2012; Yu and Wang, 2013; Zhao et al., 2015). In clinical breast cancer tissue samples, mRNA expression of *C1QBP* was correlated with lymph node spread, and low survival rate for breast cancer patients (Chen et al., 2009b). In addition, the high levels of C1QBP protein in breast cancer tissue, were also recently reported to be associated with distant metastasis of breast cancer

(Zhang et al., 2013). Overexpression of C1QBP in ovarian cancer, has been shown to produce poor outcomes. In a study done on stage III and stage IV serous ovarian cancer, C1QBP was highly expressed in cisplatin-resistant cases, and overexpression of C1QBP was associated with poorly differentiated carcinomas, residual tumor size, lymph node spread and lower overall survival (Yu and Wang, 2013). Moreover, the expression of C1QBP was seen to gradually increase from the primary lesions to metastatic lesions of epithelial ovarian cancer. The expression of C1QBP in this cancer, was also associated with peritoneal invasion and lymph node spread (Yu et al., 2013). Similarly, increased tumor recurrence and metastasis, were associated with high levels of C1QBP expression in endometrial cancer, which led to an unfavourable prognosis for patients with this disease (Zhao et al., 2015). In prostate cancer tissue samples, the expression of C1QBP showed an inverse relationship with survival of patients. In addition, C1QBP was associated with Gleason score, prostate-specific antigen (PSA) and pathological stage, all of which are prognostic factors for prostate cancer (Amamoto et al., 2011).

There are several ways in which C1QBP exerts its tumorigenic functions. True to its physiological function, C1QBP sustains tumor growth and progression, by maintaining oxidative phosphorylation in tumor cells (Fogal et al., 2010). Depletion of C1QBP switched tumor metabolism from oxidative phosphorylation to glycolysis, which reduces tumor growth and progression (Fogal et al., 2010). This function contradicts with the well-known Warburg effect, where cancer cells rely on glycolysis for metabolism in the hypoxic environment (Dang, 2010). In liver carcinoma cells, C1QBP caused the maintenance of hyaluronan synthesis, and increased expression of β-

catenin, ras and Cyclin D1, which promotes cell survival (Kaul et al., 2012). C1QBP mediates cell migration by regulating lamellipodia formation in lung carcinoma cells. It is known to be condensed in the lamellipodia protrusions with lamellipodial components, and aided in the lamellipodial formation, by regulating receptor tyrosine kinases signalling (Kim et al., 2011). The binding of C1QBP to matrix metallopeptidase 14 (MT1-MMP), which has roles in tumor invasion has also been recorded (Rozanov et al., 2002). In line with this, melanoma cells exposed to exogenously introduced C1QBP, led to interaction with $\alpha_v\beta_3$ integrin and phosphorylation of nuclear factor inducing kinase, which caused an increase of MT1-MMP and MMP2 expression, accompanied by cell migration and tumor growth (Prakash et al., 2011). In contrast to its tumorigenic role, C1QBP has also been shown to repress the phosphorylation of YB-1, which is an oncogene in renal carcinoma. It was also reported that high C1QBP expression and low nuclear YB-1 expression, gave a better prognosis for renal carcinoma patients (Wang et al., 2015).

In breast cancer, C1QBP has been shown to positively regulate cell proliferation, migration and resistance to Doxorubicin hydrochloride (McGee et al., 2011). Although the mechanism has not been fully elucidated, the interaction of C1QBP with protein kinase C ζ (PKCζ), has been shown to enhance cell polarity and migration in breast cancer (Zhang et al., 2013).

1.3 Scope of study

The development of breast cancer is a complex interplay of molecular events, which primes the breast cancer cells for survival, metastasis and resistance to current therapeutic interventions (Simpson et al., 2005;

Bombonati and Sgroi, 2011). Thus, continual investigations of potentially useful biomarkers for monitoring and therapeutic purposes are always in progress. The role of C1QBP in breast cancer progression, has been demonstrated in various studies. C1QBP has been associated with proliferation, migration and chemoresistance in breast cancer (McGee et al., 2011). In addition, a recent study showed that distant metastasis is associated with C1QBP expression, and cell migration could be mediated through PKCζ (Zhang et al., 2013). Therefore, it is of interest to have a comprehensive look into the role of C1QBP in breast cancer.

The hypothesis of the current study is that, C1QBP promotes breast cancer progression by regulating fundamental processes, such as cell proliferation, migration and invasion. In order to prove this hypothesis, the following objectives were delineated:

1. Analyse the expression of C1QBP in clinical breast cancer tissue samples, in association with clinicopathological parameters.
2. Evaluate the expression of C1QBP in breast cancer cell lines, and determine the association of C1QBP with cell proliferation, migration, invasion and chemosensitivity, by manipulation of C1QBP expression in breast cancer cell lines.
3. Determine the potential signalling pathways that C1QBP is involved in, by genome wide analysis, antibody array and stable isotope labelling by amino acids in cell culture (SILAC)-immunoprecipitation quantitative proteomics for proteome and interactome profiling.

CHAPTER 2
MATERIALS AND METHODS

2 MATERIALS AND METHODS

2.1 Gene expression profiling of C1QBP in breast cancer tissues

Gene expression profile of C1QBP was determined by performing real-time PCR on Human Breast Cancer Panel I TissueScan™ qPCR Array (Origene, Rockville, MD, USA). The array contained 48 cDNA samples from normal and breast cancer tissues diagnosed at various clinical stages – 7 samples from normal breast tissues, 13 samples from Stage IIa breast cancer, 7 samples from Stage IIb breast cancer, 8 samples from Stage IIIa breast cancer and 3 samples from Stage IIIc breast cancer. Patients' age ranged from 31 to 82 years old. The samples were normalized using a housekeeping gene, β-actin.

The ABI Prism 7500 thermocycler (Applied Biosystems®, Carlsbad, CA, USA) was used for the real-time RT-PCR procedures. Prior to that, a pre-mix solution, comprising of 750 µl of SYBR Green Master Mix, 50 µl of C1QBP forward primer, 50 µl of reverse primer and 650 µl of ddH_2O was made. The sealing film from the array was removed, and 30 µl of the pre-mix was loaded into each well. A new adhesive cover sheet was used to seal the wells tightly. Any air bubbles formed were removed by gently tapping the plate. The plate was left on ice for 15 minutes to dissolve the dried cDNA. The thermal cycling program started with an activation step at 95°C for 15 minutes, after which, a cycle, comprising of denaturation at 94°C for 15 sec, annealing at 60°C for 30 sec and extension at 72°C for 30 sec, was repeated for 40 PCR cycles.

2.2 Immunostaining of C1QBP in invasive ductal breast carcinoma tissues

2.2.1 Tissue microarray specimens and clinicopathological parameters

Tissue microarrays (TMAs) were constructed by the Department of Pathology, Singapore General Hospital. The microarrays comprised of 1 mm core from paraffin-embedded breast cancer specimens. These samples were collected from patients between the year 2004 and 2007. Ethics approval was granted by the Institutional Review Board of Singapore General Hospital.

Briefly, areas of breast tumours were preselected, marked and punched out from 'donor' blocks, using a 1 mm punch. The tissue cores of 1 mm in diameter were sequentially arranged into 'recipient' blocks, by the tissue microarrayer. Five 'recipient' blocks with a total of 132 cases were used for this study. The recipient blocks were also prepared with control tissues of 1 mm in diameter, which include normal lung, liver, colon, tonsil, thyroid and testis tissues. Sections of 4 μm from the TMA blocks were sliced and mounted on silane-coated glass slides (3-aminopropyltriethoxysilane; Sigma-Aldrich, St. Louis, MO, USA) and left to dry at 37°C, overnight.

Clinicopathological data of the patients were recorded by the Department of Pathology, Singapore General Hospital. These include patients' age, race, tumor size, histological grade, pathological staining, lymph node spread, mitotic index, extent as well as, grade of ductal carcinoma *in situ*, and presence of ER, PR and HER2. Data for matching normal controls is not available.

2.2.2 Immunohistochemical staining of C1QBP and PCNA of invasive ductal breast carcinoma tissue microarrays

The Leica BOND-MAX^{TM} System with a standard protocol F, was used to stain the TMA sections. Rabbit polyclonal anti-C1QBP antibody was used as the primary antibody, at a dilution of 1:1000. The antibody was produced against the recombinant C1QBP-His_6 protein, and subsequently purified through a protein G Sepharose column (Matsumoto et al., 2005). Tissue sections were deparaffinised, and pre-treated with epitope retrieval solution 2 (EDTA buffer, pH 8.8) for 20 minutes at 90°C. The slides were washed thrice, and the sections were blocked for peroxidase, with Bond Polymer Refine Detection Kit DC9800 (Leica Biosystems Inc., Buffalo Grove, IL, USA) for 10 min. After washing, the tissue sections were incubated with primary antibody for 30 min. Excess primary antibody was removed by washing the tissue sections thrice. Subsequently, the tissue sections were incubated with polymer for 10 min and DAB-chromogen for 10 min. Each step was followed by washing steps. Upon completion of standard protocol F, hematoxylin was used to counterstain the sections, followed by three washing steps. After staining, the TMA sections were dehydrated with three changes of absolute ethanol and three changes of histoclear. The TMA sections were mounted with a coverslip. The omission of primary antibody on breast cancer tissue was used as the negative control. Mouse monoclonal anti-proliferating cell nuclear antigen (PCNA) antibody (Sigma-Aldrich; 1:10000 dilution) was also used to stain the TMAs, with the same immunostaining procedures as mentioned above.

2.2.3 Scoring system of invasive ductal breast carcinoma tissue microarrays

The TMAs were viewed under the light microscope, at magnifications of 100X and 400X. The percentage and corresponding staining intensity of C1QBP in malignant epithelial cells with immunopositive staining, was scored by assigning '0' for non-detectable staining, '1+' for weak staining, '2+' for moderate staining and '3+' for strong staining. The scores were validated independently by a researcher and a pathologist from the Department of Pathology, Singapore General Hospital. The weighted average index (WAI) score was then computed as followed:

$$\text{WAI}=\frac{\sum(\text{intensity of each staining x percentage of cells stained with each intensity})}{\text{Total percentage of immunopositive staining}}$$

For analysis of PCNA, only the total percentage of PCNA staining was recorded.

2.2.4 Statistical analyses of TMA samples

Statistical analyses were carried out by the STATA version 10 software, to determine the association of the immunohistochemical expression of C1QBP with patients' clinicopathological parameters. The analysis was first performed by univariate analysis, using chi-square test. A *P*-value of less than 0.05 is considered as statistically significant. The correlation of the expression of C1QBP and PCNA was done using Pearson's correlation.

Multivariate analysis was subsequently done using binary logistic regression, to define the association between the main predictor and outcome, after correcting for confounders. The outcome of interest included tumor size,

grade of tumour, associated ductal carcinoma *in situ* (DCIS) grade, associated DCIS extent, tubule formation, pleomorphism, mitotic index and lymph node spread. These are categorized into binary variables as depicted in Table 3.3. Age, ER status, PR status and HER2 status were considered as the potential confounders.

In the initial model, the potential confounders were incorporated for every main outcome of interest. This was followed by backward stepwise regression, where the potential confounder having the highest p-value (>0.05) was dropped from the model. The stepwise regression was repeated until all potential confounders retained, achieved statistical significance, or no confounder was left in the model. Following that, non-significant predictor variables will then be removed from the model until all predictors retained achieve statistical significance, or no predictor of interest was left in the model.

2.3 Cell culture

2.3.1 Culture conditions for breast cancer cell line

MDA-MB-231 (HTB-26), T47D (HTB-133), ZR-75-1 (CRL-1500) and MCF7 (HTB-22) breast cancer cell lines, were included in this study. The breast cancer cell lines were obtained from the American Tissue Culture Collection (ATCC, Manassas, VA, USA). The main breast cell line used was MDA-MB-231 breast cancer cell line. It is a highly metastatic epithelial breast cancer cell line, which was derived from the pleural effusion of a 51 years old Caucasian woman with breast adenocarcinoma (Cailleau et al., 1974). Another cell line, the T47D breast cancer cell line, which was also used in this study,

originated from the pleural effusion of a 54 years old female diagnosed with infiltrating ductal carcinoma of the breast (Keydar et al., 1979). The MCF7 and ZR-75-1 breast cancer cell lines, were isolated from adenocarcinoma and ductal carcinoma, respectively (Soule et al., 1973; Engel et al., 1978). Among these cell lines, MDA-MB-231 breast cancer cell line does not express ER and PR (Kao et al., 2009). On the other hand, T47D and MCF7 breast cancer cells are positive for both ER and PR, while ZR-75-1 is only positive for ER (Kao et al., 2009).

The culture medium used for MDA-MB-231, T47D and ZR-75-1 breast cancer cell lines was Roswell Park Memorial Institute (RPMI) 1640 medium (GE Healthcare Life Sciences, Buckinghamshire, UK), supplemented with 10% FBS (GE Healthcare Life Sciences). The Dulbecco's modified Eagle's medium (DMEM) comprising 10% FBS, was used to culture the MCF7 cells. All the cell lines were incubated at 37°C with atmospheric content of 5% CO_2. Cells were grown to approximately 80% confluence before splitting. Cells were detached from the surface of the flask using 1X Trypsin-EDTA, which was prepared by diluting 10X 0.5% Trypsin-EDTA (Invitrogen^{TM}, Life Technologies, Carlsbad, CA, USA) with 1X PBS. The activity of Trypsin-EDTA was halted by the addition of three times the volume of fresh complete culture medium to the flask. Cells were resuspended and dispensed into a new flask, at a ratio of 1:4. For the purpose of seeding, the suspension of cells was spun for 5 minutes at 1000 rpm. After discarding the supernatant, the cells were resuspended in fresh complete medium. Cell density for seeding was determined by counting cells using a haemocytometer or cell counter.

2.3.2 Cryopreservation of breast cancer cell lines

Cell lines with 90% confluency were used for cryopreservation. Cells were trypsinized, resuspended and centrifuged according to the method in Section 2.3. Cells were then resuspended in their respective medium with 20% FBS and 10% DMSO, and 1 ml was aliquoted into each cryotube. The cryotubes were then stored at -80°C overnight in a Cryo 1 ºC Freezing Container (Nalge Nunc International, Rochester, NY, USA). The cryotubes were then transferred to a liquid nitrogen tank for long term storage.

2.4 Quantitative real-time polymerase chain reaction

2.4.1 Extraction of total RNA from breast cancer cell lines

Total RNA was extracted from breast cancer cell lines grown to approximately 80% confluence, in 6-well microtitre plates using the RNeasy Minikit (Qiagen, Hilden, Germany). Firstly, monolayer cells were washed with 1X PBS, to completely discard the culture medium. Cell lysis was done using 350 µl of RLT buffer, supplemented with 1% β-mercaptoethanol. The lysate was scraped and collected in a 1.5 ml microcentrifuge tube, and homogenized by passing the lysate through a blunt 21-gauge needle, fitted with a RNase-free syringe. The same amount of 70% ethanol was pipetted into the homogenized lysate and gently mixed. The ensuing solution was transferred into an RNeasy spin column, and centrifuged at full speed for a minute. After which, the flow-through was disposed of, and 700 µl of Buffer RW1 was added to the spin column. Centrifugation was done as before, and flow-through removed. Traces of ethanol were removed by washing and spinning with 500 µl of Buffer RPE twice – 1 min for the first time and 2 min

for the second time – at full speed. Flow-through was discarded both times. Complete removal of possible Buffer RPE carryover and residual flow-through was done, by full speed centrifugation in a new 2 ml collection tube for 1 min. Finally, total RNA was eluted in a new 1.5 ml collection tube, with 30 µl of RNase-free water, by centrifugation at maximum speed for 1 min. For RNA extraction from cells seeded in 24-well microtitre plates, RNeasy micro kit was used. The procedures in this kit were similar to RNeasy Minikit.

For the RNeasy micro kit, 80% ethanol was used to wash the membrane of the spin column after the first wash with Buffer RPE. In addition, the spin column membrane was dried by centrifugation at full speed for 5 min, with the lid opened. The elution of RNA was done with 14 µl of RNase-free water, instead of 30 µl of RNase-free water. The quality and concentration of the RNA were determined by A_{260}nm/A_{280}nm, determined by nanodrop ND-100 spectrophotometer (Thermo Fisher Scientific, Waltham, MA, USA). High purity RNA should yield an A_{260}/A_{280} value of 1.8 to 2.1.

2.4.2 Complementary DNA (cDNA) synthesis

The extracted RNA was converted to cDNA, by using the SuperScript III First-Strand Synthesis System (Invitrogen™). A total of 1 µg or 2 µg of RNA was added to 1 µl of 50 ng/µl of random hexamers, and 1 µl of 10mM dNTP mix. RNase-free water was added to the mixture to a volume of 10 µl. The solution was then incubated for 5 minutes at 65°C and then, at 4°C for a minute. A cDNA Synthesis Mix was prepared by adding 2 µl of 10X RT buffer, 4µl of 25mM $MgCl_2$, 2µl of 0.1M DTT, 1µl of RNaseOUT™ (40U/µl) and 1µl of SuperScript™ III RT (200U/µl). Both solutions were incubated at

25°C for 10 min, followed by 50°C for 50 min. The reaction was terminated by incubating the mixture at 85°C for 5 min. Subsequently, the cDNA product was stored at -20°C.

2.4.3 Quantitative real-time polymerase chain reaction (Real-time PCR)

Primers were designed by Primer3 software (http://bioinfo.ut.ee/primer3-0.4.0/), and primer specificities were determined by Basic Local Alignment Search Tool (BLAST®; http://blast.ncbi.nlm.nih.gov/Blast.cgi). The primer sequences (1st Based, Singapore) used are depicted in Table 2.1.

Table 2.1. Primer sequences used in real-time PCR

Primers	Forward sequence (3'-5')	Reverse sequence (5'-3')
AP4B1	CAAGGGACCTTTGCTAGCTG	CTGCTGCACATTCTCATCGT
ASMTL	GAGTGTCAAGCACGACTCCA	CAGGCCCTTGGATAGCATAA
BCL2	GGTGGGGTCATGTGTGTGG	CGGTTCAGGTACTCAGTCATCC
C1QBP	AGAAGCGAAATTAGTGCGGAA	CCACGAAATTGGGAGTTGATGTC
CDC14B	GCGCCAGATTAGTAGGCAAC	TTGTTTGGCTGAGAACACGG
FGD1	GGAGTTGACTGTGCAGCAAA	AGAGAAGATGCCGTGGACAA
FOXD3	AAGCCCAAGAACAGCCTAGT	GTTGAGTGAGAGGTTGTGGC
GAPDH	GAAGGTGAAGGTCGGAGTCAACG	TGCCATGGGTGGAATCATATTGG
HCAR3	CAGGGCAGCATCATATTCCT	GCTGAAGCTGATGCACACAT
HPR	GCGTGTGGGTTACGTGTCT	GTTATGCAATCGTATTGGTCAGC
IL15RA	ACGACTGAGAAGAGGTGCAA	TGTATTCCAGGCAGCTCACA
IL23A	ACTCAGCAGATTCCAAGCCT	CCATGGAGATCTGAGTGCCA
MAP3K8	CCCTGGAGAGAAACCCCAAT	CGTTGCCTCTTGAGCATCTC
MCM4	ACCTGGTCGCACTGTACTAC	TAGCTGTCGAGGGTATGCAG
MMP23B	AGGCTTCTACCCGATCAACC	ACGCCTTTCTTCCAGCTGTA
TPTE	CGACGACACAAGACCTCAGA	ATACGTGCCTCTGGGTTCAC
YB-1	AAGTGATGGAGGGTGCTGAC	TTCTTCATTGCCGTCCTCTC

2.4.4 LightCycler 2.0 System

The LightCycler 2.0 System (Roche Applied Science, Inc., Penzberg, Germany) was used for real-time PCR. The PCR reaction mixtures contained 3 µl of RNase-free water, 0.5 µl each of 10 µM forward and reverse primers, 5

µl of 2X QuantiTect SYBR Green PCR master mix (Qiagen) and 1 µl of cDNA, that made up a total volume of 10 µl. The PCR conditions were set up as followed:

Step 1: Initial denaturation of cDNA and polymerase activation at 95°C for 15 min.

Step 2: Amplification process which includes a cycle of denaturation at 94°C for 15 s, annealing at 60°C for 25 s and extension at 72°C for 15 s. This cycle was repeated for 45 cycles.

Step 3: Melting curve analysis conditions were fixed as followed: denaturation at 95°C for 0 s with a temperature transition rate of 20°C/s, which is followed by incubation of 15 s at 65°C and 95°C with transition rate of 0.1°C/s.

Step 4: The final step was to cool the Lightcycler rotor and carousel chamber at 40°C for 30 s.

The product of the PCR reaction from the LightCycler 2.0 system was subsequently used to run the agarose gel electrophoresis, to determine its primers' specificity.

2.4.5 Analysis of PCR product using agarose gel electrophoresis

The verification of the specificity of primers was done using 2% agarose gel electrophoresis. The agarose gel was prepared by heating a mixture of 1 g of agarose in 50 ml of 1X TAE buffer. The mixture was left to cool for about 5 min, and 0.5 µg/ml of Ethidium bromide (EtBr) was swirled into the mixture. The mixture was then poured into a gel cast and left to solidify. The amplified PCR product from each sample obtained from the LightCycler 2.0 system was mixed with 6X DNA loading dye (Promega

Coorporation, Madison, WI, USA) at a ratio of 5:1. The resulting samples were loaded into the wells of the casted agarose gel. A 100 bp DNA ladder standard (Promega Corporation) was also loaded to measure the size of the PCR products. The electrophoresis program was performed at 100 V for 1 h. The ChemiDoc™ MP imaging system was used to visualize and capture the gel image.

2.4.6 HT7900 FAST Realtime PCR system

Real-time PCR was also performed using the HT7900 FAST Realtime PCR system (Applied Biosystems®). Each PCR reaction consisted of 3 µl of RNase-free water, 0.5 µl each of forward and reverse primers with concentration of 10 µM, and 5 µl of Fast SYBR® Green Master Mix (Applied Biosystems®), together with 1 µl of diluted cDNA template (5X dilution). The mixture for each sample was loaded into each well of a MicroAmp® Fast Optical 96-well Reaction Plate (Applied Biosystems®). The FAST Realtime PCR thermal cycling run was programmed with an initial activation at 95°C for 20 s, prior to 40 cycles of the amplification process which consists of melting at 95°C for 1 s, and annealing of primer as well as, extension at 60°C for 20 s.

2.4.7 Analysis of data obtained from real-time PCR

Cycle threshold (Ct) is the number of cycles needed for the fluorescent intensity of the SYBR Green to exceed a fixed threshold. The relative gene expression of target genes obtained from real-time PCR was assessed based on the ΔΔCt value and $2^{-\Delta\Delta Ct}$ value. The expression level of a target gene was normalized to a housekeeping gene (*GAPDH*) by subtracting the Ct value of

the housekeeping gene, from the Ct value of the target gene, subsequently producing the ΔCt value. To obtain ΔΔCt, ΔCt of a control group was deducted from ΔCt of a treatment group. In short, $\Delta\Delta Ct = [(Ct_{target} - Ct_{housekeeping})$ of treatment group] – $[(Ct_{target} - Ct_{housekeeping})$ of control group]. Finally, the formula $2^{-\Delta\Delta Ct}$ was used to calculate the relative fold change of the target gene from the treatment group, compared to the control group.

2.5 Relative quantification of protein expression through western blot

2.5.1 Extraction of total protein from cell lines

Total protein extraction was carried out on cells grown in 6-well or 24-well cell culture plate. The cells were fasted for 24 h prior to nourishment with complete medium for 24 h or 48 h, before extraction of protein. Firstly, cells were washed with chilled 1X PBS twice. A mixture of Thermo Fisher Scientific RIPA Lysis and Extraction Buffer (Pierce Biotechnology, Rockford, IL, USA), Halt™ Protease and Phosphatase Inhibitor Cocktail (Pierce Biotechnology), and 0.5M EDTA at a ratio 100:1:1 was prepared as the lysis buffer, which was incubated with the cells on ice for 15 min. The cell lysate was then scraped and collected into a 1.5 ml microcentrifuge tube. Then, the lysate was centrifuged for 10 min, at 14000 g at 4°C. Cell pellet containing cell debris was discarded, while the resulting supernatant was transferred to a new tube and kept at -80°C.

2.5.2 Quantification and denaturation of protein samples

Protein samples were relatively quantified based on the Bradford method. The colorimetric change of the dye from the Bio-Rad Protein Assay

Dye Reagent Concentrate (Bio-Rad Laboratories, Hercules, CA, USA) correlates with various concentrations of protein, and evaluation to a standard curve delivers a relative measurement of the protein concentration. The concentrated dye reagent was diluted with deionized water, using 1 part of dye reagent and 4 parts of deionized water. A series of bovine serum albumin (BSA) concentration, ranging from 0.05 mg/ml to 0.5 mg/ml, was used as protein standards. Protein samples were subjected to 10X dilution with deionized water. Ten microliters of each protein standards and protein samples was pipetted into separate wells in triplicates. Then, 200 µl of the diluted dye reagent was dispensed into each well. After thorough mixing, absorbance was measured at 595 nm, with the GENios plate reader (Tecan Group Ltd, Mannedorf, Switzerland). A standard curve was derived from the protein standards' absorbance values. From the standard curve, the concentrations of each protein sample were deduced.

The protein concentrations obtained were used to calculate the volume of protein, and deionized water needed to prepare 1.25 µg/µl, 2.5 µg/µl or 3.125 µg/µl of protein samples. Depending on each samples' volume, 5X protein loading dye was added to each protein samples to produce protein samples with a final concentration of 1 µg/µl, 2 µg/µl or 2.5 µg/µl, respectively. The resulting solution was mixed and denatured at 95°C for 5 min. The denatured protein samples were immediately used for subsequent experiments or stored at -20°C for future use.

2.5.3 Sodium dodecyl sulphate-polyacrylamide gel electrophoresis (SDS-PAGE)

Differential percentage of resolving gel, and a stacking gel (5%) was used for SDS-PAGE, depending on the size of target proteins, using the formula depicted in Table 2.2.

Table 2.2. Reagents for resolving gel and stacking gel

Reagent	**Resolving gel (ml)**			**5% Stacking gel (ml)**
	8%	**10%**	**15%**	
Milipore water	4.6	4.0	2.3	3.4
30% acrylamide	2.7	3.3	5.0	0.83
1.5 M Tris (pH8.8)	2.5	2.5	2.5	-
1.0 M Tris (pH6.8)	-	-	-	0.63
10% SDS	0.1	0.1	0.1	0.05
10% ammonium persulfate (1mg/ml)	0.1	0.1	0.1	0.05
TEMED	0.006	0.004	0.004	0.005
Total	**10**	**10**	**10**	**5**

Clean glass plates and spacer plates were assembled, according to the manufacturer's instructions (Bio-Rad Laboratories). Ammonium persulfate (APS) and N,N,N',N'-tetramethylethylenediamine (TEMED) were mixed in at the last step in the resolving gel solution. As soon as TEMED was added, the mixture was swirled and immediately poured into the gap between the spacer plate and glass plate, with sufficient space left for the stacking gel. Acrylamide solution was overlaid with isopropanol, to acquire an even gel surface. The polymerization of the resolving gel was allowed to be completed for at least 30 minutes. The overlaid isopropanol was removed, and the top of the gel was washed several times with deionized water. Likewise, APS and TEMED were added last to the stacking gel and immediately poured onto the resolving gel.

Without delay, a clean comb was inserted, ensuring that air bubbles were not introduced. Similarly, stacking gel was allowed to polymerize for approximately 30 min.

The polymerized SDS-PAGE gel was then mounted to the electrophoresis apparatus. 1X Tris/Glycine/SDS buffer (Bio-Rad Laboratories), which was prepared by diluting 10X Tris/Glycine/SDS buffer (Bio-Rad Laboratories; 25 mM Tris, 192 mM glycine, 0.1% SDS, pH8.3) with deionized water, were added to the electrophoresis tank. The comb was then cautiously removed from the gel. Equal amount of denatured protein samples, which were prepared as detailed in the previous section, were loaded into each well. To assess the molecular weight of the protein samples, Precision Plus Protein^{TM} Dual Color Standard Marker (Bio-Rad Laboratories) was also loaded. The SDS-PAGE was carried out at 70V for 1 hour and followed by 100V, until the dye front reaches the end of the resolving gel.

2.5.4 Transfer of protein to polyvinyl difluoride membrane

The protein separated by SDS-PAGE was transferred to a polyvinyl difluoride (PVDF) membrane (Bio-Rad Laboratories). Prior to the transfer, the PVDF membrane was soaked in 100% methanol for approximately 20 s. The membrane was then rinsed with deionized water. The membrane, together with filter pads, were immersed in 1X transfer buffer, which contained 25 mM Tris, 192 mM glycine and 20% (v/v) methanol. A piece of filter pad was placed on the TransBlot SD Semi-Dry Transfer Cell (Bio-Rad Laboratories), and the equilibrated PVDF membrane was laid on that filter pad. The SDS-PAGE gel was then placed on top of the membrane, and lastly, another filter

pad was used to cover the gel, creating a ‘gel sandwich’. Trapped air bubbles were removed by rolling the ‘gel sandwich’ with a glass rod. The lid was closed, and protein was transferred at 15 V for 1 h.

2.5.5 Blocking and probing of the membrane

The membrane containing the transferred protein was blocked for unspecific sites, before probing with antibodies. The blocking reagent used was 5% non-fat milk (Bio-Rad Laboratories), prepared in 1X TBST (Tris-buffered saline with 0.1% (v/v) Tween 20). On the other hand, 5% BSA in 1X TBST was used instead of milk, when phosphorylated proteins were targeted. The membrane was blocked with either milk or BSA, for 1 h at room temperature. After which, it was washed with 1X TBST thrice, where each wash lasted for 5 min. The membrane was then incubated with primary antibody overnight at 4°C, with slow shaking. Following that, the membrane was washed three times as before, to remove excess antibodies. The appropriate secondary antibody was added to the membrane and incubated for 1.5 h, with slow shaking at room temperature. This was followed by washing of the membrane with 1X TBST twice, for 10 minutes each. The final wash was done with 1X TBS for 10 min. The housekeeping protein, β-actin was measured to ensure equal loading. The primary antibodies used are shown in Table 2.3.

Table 2.3. Primary antibodies' sources and dilution used for western blot

Antibody	Source	Host species	Dilution
Bcl-2	Cell Signaling, Danvers, MA, USA	Rabbit	1:1000
C1QBP	RIKEN, Wako, Japan	Rabbit	1:1000
Cdc25a	Cell Signaling, Danvers, MA, USA	Rabbit	1:1000
Cdk4	Cell Signaling, Danvers, MA, USA	Mouse	1:1000
Cdk6	Cell Signaling, Danvers, MA, USA	Mouse	1:1000
Cyclin D1	Cell Signaling, Danvers, MA, USA	Rabbit	1:2000
Mcl-1	Cell Signaling, Danvers, MA, USA	Rabbit	1:1000
p53	Cell Signaling, Danvers, MA, USA	Mouse	1:1000
Phospho-c-Raf (Ser 338)	Cell Signaling, Danvers, MA, USA	Rabbit	1:500
Phospho-ERK1/2 (Thr202/Tyr204)	Cell Signaling, Danvers, MA, USA	Rabbit	1:2000
Total ERK1/2	Cell Signaling, Danvers, MA, USA	Rabbit	1:1000
Phospho-MEK1/2 (Ser 217/221)	Cell Signaling, Danvers, MA, USA	Rabbit	1:1000
Total MEK1/2	Cell Signaling, Danvers, MA, USA	Rabbit	1:1000
Phospho-Msk1 (Thr 581)	Cell Signaling, Danvers, MA, USA	Rabbit	1:1000
Phospho-Stat3 (Y705)	Cell Signaling, Danvers, MA, USA	Rabbit	1:1000
Total Stat3	Cell Signaling, Danvers, MA, USA	Rabbit	1:1000
YB-1	RIKEN, Wako, Japan	Rabbit	1:1000
β-actin	Sigma-Aldrich, St Louis, MO, USA	Mouse	1:6000

2.5.6 Detection and densitometric analysis of protein bands

Enhanced chemiluminescence (ECL) via Supersignal West Pico Chemiluminescent substrate (Pierce Biotechnology) was used to detect the protein bands. The ECL substrates provided were mixed well at a 1:1 ratio, and pipetted onto the membrane. The membrane was incubated with the

solution for 5 min at room temperature. The membrane was then exposed to clear blue x-ray films, which were developed in an automatic film processor.

The densitometer (Model GS-710; Bio-Rad Laboratories) was utilized to scan and obtain the images of the protein bands formed on the x-ray film, and subsequently, using Quantity-One Image Analysis software version 4.62 (Bio-Rad Laboratories) or ImageJ, the intensity of the protein bands were quantified. The relative protein expression of the protein samples were obtained by calculating the ratio of the optical density (O.D.) of the target proteins, to the O.D. of the respective β-actin.

2.6 Immunofluorescence

Breast cancer cell lines were grown on coverslips, in 6 well plates or Lab-Tek® 4-Chambered Coverglass (Nalge Nunc International), until 70% to 80% confluent. Paraformaldehyde (4%) was used for cells fixation for 15 min. This was followed by washing with 1X wash buffer (0.05% Tween-20 in 1X PBS). Subsequently, 0.1% Triton X-100 in 1X PBS was used to permeabilize the cells for 5 min. Unspecific sites were blocked with 1% BSA, at room temperature for 30 min. Primary antibody was then added to the cells and incubated at 4°C overnight (Table 2.4). After three series of washing with 1X wash buffer, cells were incubated with secondary antibody conjugated with Cy-3 or FITC (Sigma-Aldrich) for 1 h at room temperature, followed by thorough washing. The coverslip or coverglass was removed and mounted with Vectashield® fluorescence mounting medium with 4,6-diamidino-2-phenylindole (DAPI, Vector Laboratories), to counterstain the nucleus and mount the slides at the same time. The slides were visualized using the

Olympus Fluoview FV1000 Laser Scanning Confocal Microscopy. Negative controls were included where primary antibody was omitted.

Table 2.4: Primary antibodies' sources used for immunofluorescence staining and dilution used

Antibody	Source	Host species	Dilution
C1QBP	RIKEN, Wako, Japan	Rabbit	1:200
YB-1	RIKEN, Wako, Japan	Rabbit	1:200
Actin cytoskeleton and focal adhesion staining kit	Millipore, Billerica, MA, USA	Mouse	1:100
c-myc	Santa Cruz, Dallas, TX, USA	Mouse	1:100

2.6.1 Mitochondrial staining

Mitochondrial staining was done using MitoTracker® Red CMXRos (Invitrogen™). Culture medium from cells, which were grown on coverslips or Lab-Tek® 4-Chambered Coverglass, was replaced and incubated with pre-warmed culture medium (37°C) containing 250 nM MitoTracker® probe, for 30 min at 37°C. Pre-warmed 1X PBS was used for washing to remove residual medium, before fixation with 4% paraformaldehyde for 15 min. The subsequent steps were as detailed in Section 2.6.

2.7 Down-regulation of C1QBP and STAT3 in breast cancer cell lines

2.7.1 Silencing of C1QBP in MDA-MB-231 and T47D breast cancer cell line via siRNA targeting C1QBP

Twenty four hours prior to transfection, 2.5 X 10^5 cells of MDA-MB-231 cells or T47D cells were seeded in each well of a 6-well microtitre plate.

The ON-TARGETplus SMARTpool siRNA targeting C1QBP, which consisted of 4 siRNA sequences (Table 2.5) and the non-targeting siRNA pool, were commercially available from GE Dharmacon (Lafayette, CO, USA). The transfection reagent used, DharmaFECT2, was also purchased from GE Dharmacon. From here on, siRNA targeting C1QBP and non-targeting siRNA, will be referred to as siC1QBP and NT respectively.

Table 2.5. Sequences of siRNA used in the study

siRNA	**Source ID**	**Target sequence**
C1QBP	J-011225-13	GCGAAAUUAGUGCGGAAAG
	J-011225-14	CGCAAGGGCAGAAGGUUGA
	J-011225-15	UUUCGUGGUUGAAGUUAUA
	J-011225-16	GAAGUUAGCUUUCAGUCCA

The stock siRNA stock solution was 20 µM. The appropriate amount of transfection reagent and diluted siRNA were then combined and mixed to give a final concentration of 20 nM of siRNA for administration to the cells in each well, which were then incubated at 37°C in 5% CO_2.

The transfection procedure applied to cells cultured in 24-well plate was similar to the above with the final concentration of siRNA at 20 nM. For 24-well plates, 0.625 X 10^5 cells were seeded in each well, with a total volume of 1 ml/well.

The transfection medium was replaced with 2 ml or 1 ml of complete culture medium (RPMI1640 containing 10% FBS), for each well of a 6-well or 24-well plate, respectively, 24 h post-transfection. Silencing efficiency at the gene and protein levels were examined at 48 h and 72 h, after transfection respectively. Additionally, cells were fasted for 24 h with serum-free medium

and replenished with complete culture medium for 24 h, before harvesting or using the cells for further experiments.

2.7.2 Silencing of STAT3 in MDA-MB-231 breast cancer cell line

The methods used to silence STAT3 in MDA-MB-231 breast cancer cell line were identical to the conditions mentioned above. The only exception was the volume of siRNA diluted. The siRNA targeting STAT3 (Santa Cruz Biotechnology, Dallas, TX, USA) was supplied as a stock of 10 µM. Thus, the transfection procedure for STAT3 required twice the amount of siRNA needed previously to obtain a final siRNA concentration of 20 nM. The amount of culture medium was adjusted accordingly.

2.7.3 Double knockdown of YB-1 and C1QBP in MDA-MB-231 cells

Conditions such as, cell seeding density, culture medium, siRNA, transfection reagent and incubation time remained the same as the transfection process for individual siRNA. The volume of siRNA was modified for optimal silencing of the two genes. Four different treatment groups were constructed and supplied with different concentration of siRNAs as followed:

Group 1: 10 nM of siYB-1 + 10 nM of NT
Group 2: 10 nM of siC1QBP + 10 nM of NT
Group 3: 10 nM of siYB-1 + 10 nM of siC1QBP
Group 4: 20 nM of NT

2.7.4 Knockdown of C1QBP in MDA-MB-231 cells overexpressing YB-1

MDA-MB-231 cells stably overexpressing YB-1 were established previously (Yu, 2010). The conditions, concentration and cell density of the transfection is the same as Section 2.7.1.

2.8 Establishment of MDA-MB-231 cells overexpressing C1QBP

Full length human C1QBP cDNA with a C-terminal c-myc tag was inserted into pCI-neo (Promega Corporation), to produce a C1QBP expression vector, pCI-neo-C1QBP, a gift from Dr. Ken Matsumoto from RIKEN, Japan. pCI-neo-C1QBP and pCI-neo empty plasmids were transfected into MDA-MB-231 cells using 4 µl of Lipofectamine2000 at a concentration of 1µg, respectively. Neomycin-resistant colonies were selected in the presence of Geniticin® (Gibco®, Life Technologies, Grand Island, NY, USA) at a concentration of 400µg/ml. The overexpression of C1QBP was determined using real-time PCR and western blot, at the gene and protein levels, respectively. The resulting cells were labelled 231.Vec for MDA-MB-231 cells transfected with pCI-neo empty plasmids, and 231.C1QBP for MDA-MB-231 cells transfected with pCI-neo-C1QBP.

2.9 Assessment of cell proliferation and cell growth

Breast cancer cell lines were initially fasted for 24 h with serum-free medium, and re-nourished with complete medium supplemented with 10% FBS, before subjecting to cell proliferation assays. Briefly, at 48 h post-transfection, transiently transfected cells were starved for 24 h with serum-free medium. After starvation, the cells were supplied with fresh complete medium

for 24 h before collection or experimentation. On the other hand, C1QBP-overexpressing cells were starved for 24 h with serum-free medium, and replenished with fresh complete medium with 10% FBS for 48 h, before harvesting. In total, cells were maintained in culture for 96 h.

2.9.1 CellTiter 96® AQ_{ueous} Non-Radioactive Cell Proliferation (MTS) assay

The MTS assay (Promega Corporation) was employed for assessment of cell proliferation. The assay is a tetrazolium-based assay, which consists of MTS, a tetrazolium compound and phenazine methosulfate (PMS), an electron coupling reagent. The reduction of MTS into a soluble formazan dye in the presence of metabolic activity by living cells reflects the number of viable cells. The working solution was prepared by mixing MTS/PMS solution with complete culture medium at a ratio of 1:5. As proliferation assay was performed in 24-well culture plates, 1 ml of this solution was added to each well of the culture plates and incubated for 1 to 4 hours at 37°C, 5% CO_2. The absorbance was read at 490 nm using a plate reader (GENios, Tecan Group Ltd).

2.9.2 Growth curve analysis using alamarBlue® assay

The alamarBlue® assay (Invitrogen^{TM}) was used to attain cell growth curves. The system, a minimally toxic oxidation-reduction indicator, was able to detect fluorometric and colorimetric changes during cellular metabolism in living cells. As such, the same set of cells can be used repeatedly for this assay, to obtain its growth curve. The working reagent consisted of a mixture of alamarBlue® reagent and complete culture medium at a 1:10 ratio. The

working reagent was thoroughly mixed, and 1 ml of the reagent was added to each well of a 24-well culture plate. The culture was incubated at 37°C in 5% CO_2 for 1 to 4 hours, and the fluorescent intensity was measured at excitation and emission wavelengths of 530 nm and 590 nm, respectively. To reuse the set of cells, the alamarBlue® mixture was replaced with culture medium and cells were incubated at 37°C with 5% CO_2. The procedures above were repeated every 24 h for up to 168 h.

2.9.3 Cell cycle analysis

Propidium iodide (PI), an intercalating agent which binds to DNA enabled the profiling of the DNA content in cell cycle analysis (Pozarowski and Darzynkiewicz, 2004). Cell cycle analysis entailed the collection of all cells within the culture medium. Therefore, culture media from each set of cells was collected, and 1X PBS used to wash the cells was not dispensed but collected as well. Adhered cells were collected using the trypsin-EDTA method. The cells were centrifuged at 1700 rpm at 4°C for 5 min and washed thrice with 1X PBS. The supernatant was discarded each time. After the last wash, cells were resuspended in 500 µl of 1X PBS. For fixation, the cell suspension was added, drop by drop into 4.5 ml of ice cold 70% ethanol, while vortexing the solution. The cells were fixed at 4°C, overnight, and collected by centrifuging at 1700 rpm for 5 min. Traces of ethanol was removed by washing the cells twice with 1X PBS. Meanwhile, 200 µl of 1mg/ml PI, 2 mg of RNase A (Sigma-Aldrich) and 0.1% Triton-X 100 in PBS, were prepared to a final volume of 10 ml. The PI dye solution was used to resuspend the cells. After 30 min of incubation in the dark, the stained cells were run through the CyAn^{TM} ADP Analyzer (Beckman Coulter, Inc., Indianapolis, IN, USA) for

cell cycle analysis. The data obtained was analysed by the Summit version 4.3 software (Beckman Coulter).

2.10 Cell migration assay

2.10.1 Wound healing assay

Wound healing or wound scratch assay was carried out for cells transfected with siC1QBP. A straight gap was created with a yellow pipette tip, in the middle of each well of a 6-well culture plate, 48 h after transfection. The well was washed twice with 1X PBS to remove floating cells, and complete culture medium was added after the last wash. The images of the 'wound' were taken at 0 h and 6 h. The gap of the 'wound' was measured and the difference in measurement between 0 h and 6 h was calculated.

2.10.2 Transwell migration assay

The transwell migration assay was carried out by using transwell inserts, with a polycarbonate membrane diameter of 6.5 mm and 8.0 µm pores (Corning Inc., Corning, NY, USA). Hydration of the inserts were carried out by submerging them into 600 µl of serum-free RPMI1640 medium in a 24 well plate, and loading 200 µl of the same medium into the upper chamber of the inserts, followed by incubation at 37°C with 5% CO_2 overnight. Prior to seeding, MDA-MB-231 cells were resuspended in serum-free RPMI1640 medium. After removal of the hydration medium, the lower chamber of the inserts were filled with 600 µl of RPMI1640 medium containing 15% FBS, while the upper chamber of the inserts were seeded with 3 X 10^4 cells in 200 µl of serum-free medium. The transwell system was then incubated at 37°C in

5% CO_2 for 20 h. Following that, the inserts were washed twice with 1X PBS, and fixed with 100% methanol for 15 min. Residual methanol was removed by air-drying the inserts. Crystal violet (0.5% (w/v) in 20% methanol) was used for staining of migrated cells, on the membrane of the inserts. Residual crystal violet solution was removed by rinsing the inserts in 2 changes of clean water. Non-migratory cells were swabbed off with a moist cotton bud. The transwell inserts were left to dry, and viewed under a Nikon SMZ 1500 stereo microscope at 10X magnification. Number of cells in the middle and 4 peripheral fields of the membrane was counted.

2.11 Cell invasion assay

BD BioCoat™ Matrigel™ Invasion Chamber with 8 μm pore size PET membrane (BD Biosciences, Franklin Lakes, NJ, USA) was used for cell invasion assay. Firstly, the inserts were thawed to room temperature and rehydrated, by adding 600 μl and 400 μl of serum-free RPMI1640 medium into the lower and upper chambers of the inserts, respectively. The inserts were incubated at 37°C in 5% CO_2 overnight. After careful removal of the medium, 3 X 10^4 MDA-MB-231 cells in 200 μl of serum-free medium, were dispensed in the upper chamber of the inserts and 600 μl of RPMI1640 containing 15% FBS, was dispensed to the lower chamber of the inserts. Incubation of the inserts was done at 37°C in 5% CO_2 for 20 h. Subsequent washing, fixing, staining and viewing steps were done in the same way as for the cell migration assay.

2.12 Determination of chemoresistance of chemotherapeutic drugs

2.12.1 Chemotherapeutic drugs

Doxorubicin hydrochloride, Epirubicin hydrochloride and 5-Fluorouracil were obtained from Sigma-Aldrich. Stock solution of each of these drugs were prepared at a concentration of 10 mM, by dissolving 10 mg of Doxorubicin hydrochloride in 1.724 ml of DMSO; 5 mg of Epirubicin hydrochloride in 0.862 ml of DMSO and 2.6 mg of 5-Fluorouracil in 2 ml of DMSO. These drugs were kept at 4°C for further experiments. Working drug solutions for treatment of cells were prepared from the stock, by diluting with complete culture medium.

2.12.2 Assessment of half maximal inhibitory concentration (IC_{50}) of chemotherapeutic drugs after silencing or overexpression of C1QBP in MDA-MB-231 breast cancer cell line

MDA-MB-231 cells were seeded at 0.625 X 10^5 cells/well in 24-well plates. The cells were then transfected with siC1QBP or NT siRNA, following the procedures in Section 2.7.1. Drugs with a range of concentrations were added at 48 h post transfection. The concentrations used were as followed: Doxorubicin hydrochloride and Epirubicin hydrochloride: 0 µM, 0.1 µM, 0.3 µM, 0.5 µM, 1 µM and 2 µM; 5-Fluorouracil: 0 µM, 0.5 µM, 1.0 µM, 2.5 µM, 4 µM and 5 µM. The cells were incubated with the drugs for 48 h at 37°C with 5% CO_2. The cell viability was evaluated using MTS assay following the protocol in Section 2.9.1. The percentage of survival for each set of cells was plotted against the log concentration of drug, and the IC_{50} was compared. Two-way ANOVA was done for statistical analysis. The same methods

applied to C1QBP-overexpressing cells. However, the cells were fasted for 24 h and replenished with complete medium for 48 h, before addition of the drugs.

2.12.3 Determination of expression of C1QBP in doxorubicin hydrochloride-resistant MCF7 cells and parental MCF7 cells

Doxorubicin hydrochloride-resistant MCF7 cell line (MCF7R) was a gift from Professor Eric Lam from Imperial College London. The MCF7R cells were cultured in DMEM medium containing 10% FBS and 0.01 mg/ml of Doxorubicin hydrochloride. These cells together with parental MCF7 cells, were subjected to treatment with 0.6 µM of Doxorubicin hydrochloride for 0 h, 12 h, 24 h and 48 h, and the protein lysate from both, cells in the medium and adhered cells were collected. Western blot was conducted to determine the expression of C1QBP in these two cell lines. The concentration of Doxorubicin hydrochloride used that is 0.6 µM, is the IC25 obtained from 'kill-curve' plotted from treatment of parental MCF7 cells with Doxorubicin hydrochloride for 48 h. The lower concentration used is to prevent massive cell death.

2.13 Gene expression profiling by GeneChip ST 2.0 microarray

Total RNA was collected from MDA-MB-231 cells transfected with siC1QBP and NT siRNA on the 2nd day after transfection. Silencing efficiency of siC1QBP was verified through real time PCR, before delivery to Origen Labs (Singapore) for further processing. The Shimadzu spectrophotometer (BioSPEC-Mini, Shimadzu Corporation, Kyoto, Japan) and Agilent Bioanalyzer, were used to measure the concentration and RNA integrity

number (RIN) of the RNA samples, respectively. The processing of the samples was in accordance to the Affymetrix and NuGEN recommended protocols, while the Ribo-SPIA RNA Amplification/Encore Biotin Fragmentation and Labeling was done using Origen Laboratory's Standard Operating Procedure. In short, 100 ng of total RNA was reverse transcribed to create a cDNA/mRNA hybrid molecule, which was used as a template to produce double stranded cDNA, with a DNA/RNA heteroduple on one end. Single stranded anti-sense DNA was produced by amplifying the unique double stranded cDNA through SPIA (Single Primer Isothermal Amplification). Biotin-labelled sense target cDNA was produced by post-SPIA modification. Hybridization of these cDNA to the Affymetrix Human Gene 2.0 ST array was done with constant rotation at 60 rpm at 45°C for 18 h. The FS450_0007 fluidics protocol was employed for the washing and staining steps. The array was then scanned using an Affymetrix 3000 7G scanner. Hybridization efficiency was elucidated through the scanned images and quality control (QC) was carried out in Expression Console (EC) 1.1 software.

2.13.1 Data analysis for microarray

The genome-wide gene expressions between MDA-MB-231 cells treated with siC1QBP and NT siRNA was compared. Analysis of CEL files were carried out by GeneSpring 11.5 software (Silicon Genetics, Redwood City, CA, USA) and Partek Genomics Suite (Partek Inc., St. Louis, MI, USA). Potential gene candidates were screened by a cut-off point of ±1.5 fold change with $P<0.05$. The Partek Genomics Suite and Database for Annotation, Visualization and Integrated Discovery (DAVID) 6.7 were further used to determine the potential pathways and genetic annotations involved.

2.14 Protein expression of signalling molecules in C1QBP-overexpressing cells

The PathScan® Intracellular Signaling Array Kit (Chemiluminescent Readout) (Cell Signaling) is an antibody array, which utilized the enzyme-linked immunosorbent assay (ELISA) principle. The kit enabled the detection of 18 well-characterized signalling molecules in its active form (phosphorylated or cleaved). The antibodies provided in the array are depicted in Table 2.6.

Table 2.6. Antibodies included in the PathScan® Intracellular Signaling Array Kit

Target	Phosphorylation Site	Modification
ERK1/2	Thr202/Tyr204	Phosphorylation
Stat1	Tyr701	Phosphorylation
Stat3	Tyr705	Phosphorylation
Akt	Thr308	Phosphorylation
Akt	Ser473	Phosphorylation
AMPKα	Thr172	Phosphorylation
S6 Ribosomal Protein	Ser235/236	Phosphorylation
mTOR	Ser2448	Phosphorylation
HSP27	Ser78	Phosphorylation
Bad	Ser112	Phosphorylation
P70 S6 Kinase	Thr389	Phosphorylation
PRAS40	Thr246	Phosphorylation
p53	Ser15	Phosphorylation
p38	Thr180/Tyr182	Phosphorylation
SAPK/JNK	Thr183/Tyr185	Phosphorylation
PARP	Asp214	Cleavage
Caspase-3	Asp175	Cleavage
GSK-3β	Ser9	Phosphorylation

MDA-MB-231 cells stably overexpressing C1QBP and MDA-MB-231 cells containing empty vector were seeded at 2.5 X 10^5 cells, in 2 ml of complete medium supplemented with 10% FBS and 0.4 mg/ml of geneticin, in each well of a 6-well culture plate, and allowed to adhere for 24 h in a 37°C

incubator supplied with 5% CO_2. Cells were then fasted for 24 h with serum-free medium and subsequently, replenished with complete medium for 48 h before collection.

Protein collection was done using 1X Cell Lysis Buffer #7018, which was included in the kit. The lysis buffer was thawed and mixed with Halt™ Protease and Phosphatase Inhibitor Cocktail (Pierce Biotechnology) and 0.5M EDTA at a ratio 100:1:1. Medium from the cell culture was removed, and cells were washed with ice-cold 1X PBS once. PBS was discarded and 100 µl of ice-cold lysis buffer was added to each well. The cells were lysed for 2 min on ice. The resulting lysate was scraped, collected and centrifuged at maximum speed at 4°C for 3 min, to remove cell debris. Supernatant was collected and stored at -80°C as single-use aliquots. The protein concentration of the lysate was quantified just before performing the assay, and diluted with Array Diluent Buffer to a final concentration of 1.0 mg/ml.

Glass slides and blocking buffer were equilibrated to room temperature before use. 1X Array Wash Buffer was prepared by diluting 1 ml of 20X Array Wash Buffer in 19 ml of deionized water. The multi-well gasket was fixed to the glass slide, and assembled as designated in the manufacturer's protocol. Each well was then filled with 100 µl of Array Blocking Buffer, covered with sealing tape and incubated for 15 min at room temperature on an orbital shaker. The blocking buffer was then discarded. 75 µl of the protein lysate was then added to each well, covered with sealing tape and incubated overnight at 4°C on an orbital shaker. The lysate was removed and wells were washed with 1X Array Wash Buffer for 5 min on a shaker at room temperature. The washing step was repeated 3 times and each time, the

contents were discarded. Next, 75 µl of 1X Detection Antibody Cocktail was added to each well, covered with a sealing tape and incubated at room temperature for an hour on an orbital shaker. The wells were then washed for 4 times, as described previously. After the last wash, 75 µl of HRP-linked Streptavidin was added to each well, covered with sealing tape and incubated for 30 min at room temperature on a shaker. Again, wells were washed as before. The multi-well gasket was then removed and separated from the glass slide. The glass slide was washed with 10 ml of 1X Array Wash Buffer. LumiGLO®/Peroxide reagent was used to produce the chemiluminescent signal. Immediately before use, 9 ml of deionized water, 0.5 ml of 20X LumiGLO® and 0.5 ml of 20X Peroxide, were combined to produce 1X LumiGLO®/Peroxide chemiluminescent reagent. The wash buffer was removed and slide was covered with 1X LumiGLO®/Peroxide chemiluminescent reagent. The slide image was captured directly by the ChemiDoc^{TM} MP system (Bio-Rad Laboratories). The intensity of each dots were measured by ImageLab Version 5.0 (Bio-Rad Laboratories).

2.15 Stable isotope labelling by amino acids in cell culture (SILAC)-immunoprecipitation quantitative proteomics analysis

2.15.1 SILAC

MDA-MB-231 cells containing empty vector and MDA-MB-231 cells overexpressing the myc-tagged C1QBP plasmid, were differentially labelled to incorporate isotopic forms of lysine and arginine present in DMEM media. Media containing normal (or 'light' (L)) isotypes of L-lysine ($^{12}C6^{14}N2$) (143 µg/ml; Sigma-Aldrich) and L-arginine-($^{12}C6^{14}N4$) (83 µg/ml, Sigma-Aldrich),

was used to culture 231.Vec cells, while 231.C1QBP cells were cultured in media containing 'heavy' (H) isotopes of L-lysine-($^{13}C6^{15}N2$) and L-arginine-($^{13}C6^{15}N4$) (Cambridge Isotope Laboratory, Tewksbury, MA, USA). Cells were grown in their respective SILAC media for at least 5 to 6 doublings, to ensure complete incorporation of labelled amino acids. Subsequently, these cells were harvested for immunoaffinity purification of protein complexes.

2.15.2 Immunoaffinity Purification of Protein Complexes

Cell pellets were lysed in ice-cold modified RIPA buffer (50mM Tris pH7.5, 150mM NaCl, 1% NP40) containing Complete, Mini, EDTA-free Protease Inhibitor Cocktail Tablet and PhosSTOP Phosphatase Inhibitor Cocktail Tablet (Roche Diagnostic, Basel, Switzerland), and centrifuged at 20000 g for 20 min at 4°C. For the immunoaffinity experiments, 10mg of extracts from each differentially labelled cell line were affinity purified separately by overnight incubation at 4ºC, with equal amount of normal mouse IgG (Santa Cruz Biotechnology) or anti-c-myc antibody (Santa Cruz Biotechnology) for 231.Vec and 231.C1QBP cells, respectively. The following day, each of the antibody-bound samples were added to protein A/G Plus agarose beads (Santa Cruz Biotechnology) and incubated at 4°C for 2 to 3 h. The beads were combined carefully after one wash step in RIPA buffer, and were washed for an additional three times with RIPA buffer thereafter. To elute the bound proteins from the anti-myc agarose beads, a 1.5X bead-volume of 2X lithium dodecyl sulfate sample buffer with reducing agent was added, and the matrix was boiled for 5 min. Separation of proteins were conducted on NuPAGE 4-12% Bis-Tris gels (Invitrogen^{TM}), that were then stained with Colloidal Blue (Invitrogen^{TM}), followed by overnight destaining, before being

processed for mass spectrometry. Mass Spectrometry and Data Analysis Eluted protein complexes were separated and digested as detailed previously (Shevchenko et al., 2006). Samples were analysed on an Orbitrap or Orbitrap XL (Thermo Fisher Scientific), coupled to a Proxeon Easy-nLC. The MS spectra and protein identity, as well as quantification, was obtained as described previously (Gunaratne et al., 2011). Briefly, the Mascot version 2.2 software (Matrix Science, London, UK) was used to identify and quantify proteins, against a database prepared from the human International Protein Index (IPI) (version 3.68), with addition of common contaminants such as, human keratins, porcine trypsin and proteases. MaxQuant version 1.0.13.13 with default settings was used for SILAC peptide and protein quantification, with a maximum false discovery rates (FDR) of 0.01 (Cox and Mann, 2008).

2.15.3 Validation of YB-1 as an interacting partner of C1QBP by co-immunoprecipitation

Modified RIPA buffer (50mM Tris pH7.5, 150mM NaCl, 1% NP40) supplemented with Halt^{TM} Protease and Phosphatase Inhibitor Cocktail (Pierce Biotechnology), was used to obtain protein lysate from MDA-MB-231 cells overexpressing C1QBP. Cell pellet obtained from cells, was lysed with 3X the cell pellet volume of modified RIPA buffer and incubated for 20 min on ice. The lysate was then centrifuged at 15000 g for 20 min at 4°C and supernatant was kept. At least 1 mg of protein was used for co-immunoprecipitation. The protein lysate was incubated with either 2 µg of YB-1 antibody, 1 µg of c-myc antibody (Santa Cruz Biotechnology) or 1 µg of appropriate IgG (Santa Cruz Biotechnology) and topped-up to 1 ml with modified RIPA buffer at 4°C, overnight. The rabbit polyclonal YB-1 antibody was a gift from Dr. Ken

Matsumoto from RIKEN, Japan. Forty microliters of protein A/G sepharose beads (Sigma-Aldrich) were washed with 500 µl of modified RIPA buffer twice, by spinning at 2000 rpm for 2 min at 4°C. After each wash, supernatant was discarded. Pre-incubated lysate with antibodies was then mixed with the protein A/G beads and incubated for 3 h at 4°C. The complex formed was then washed with 1 ml modified RIPA buffer to remove unspecific binding, by centrifugation at 2000 rpm for 2 min at 4°C. After each wash, supernatant was removed with gel loading tips and this was repeated for 4 times. Peptide elution using K13 peptide (Genescript, Piscataway, NJ, USA) for YB-1 and myc peptide (Sigma-Aldrich) for anti-myc, was then carried out. Approximately 30 µl of peptide (2.5 mg/ml) was incubated with the beads. The tube was placed in a tube shaker for 20 min at 4°C. Then, the mixture was centrifuged at 2000 rpm for 2 min at 4°C. The supernatant was transferred to another tube and loading dye was added to the supernatant, as well as the leftover beads. The samples were boiled at 95°C for 5 min and run on SDS-PAGE.

2.15.4 Immunostaining of C1QBP and YB-1 in MDA-MB-231 cells overexpressing C1QBP

To represent C1QBP, mouse monoclonal anti-myc was used, as C1QBP-overexpressing cells were tagged with myc. The immunofluorescence procedure was detailed in Section 2.6. The dilution factor of mouse monoclonal anti-myc used was 1:100, while for rabbit polyclonal YB-1 antibody, the dilution factor used was 1:200. Secondary antibodies were diluted at 1:200, for both anti-mouse and anti-rabbit. Anti-mouse and anti-

rabbit secondary antibodies were used for cells incubated with anti-myc and anti-YB-1, respectively.

2.16 Statistical analyses used for *in vitro* experiments

Statistical analyses were carried out by GraphPad Prism 5 (GraphPad Prism, San Diego, CA, USA). Two-tailed student t-test was done for comparison of means between two groups. When more than two groups were involved, one-way ANOVA was used instead. Data are presented as mean ± SEM and a $P<0.05$ was considered as statistically significant. Two-way ANOVA was used when two variables were introduced. For two-way ANOVA, *P*-value of less than 0.05 for interaction between variables was considered statistically significant. Experiments were carried out with at least triplicates and repeated for at least two independent times.

CHAPTER 3
RESULTS

3 RESULTS

3.1 Gene expression profile of C1QBP in breast cancer tissue samples

The mRNA expression profile of C1QBP was carried out in Human Breast Cancer Panel I TissueScanTM Tissue qPCR Array, which consisted of 48 cDNA samples from normal and cancerous breast tissue specimens (Adenocarcinoma of the breast, ductal: 39 samples; Adenocarcinoma of the breast, lobular: 2, Normal breast tissue: 7). The clinicopathological data are provided in Table 3.1. The term 'Not applicable' refers to clinicopathological data which is not relevant for the normal tissue samples, while the term 'Unavailable' refers to data that is not provided.

Table 3.1. Clinicopathological parameters of samples from Human Breast Cancer Panel I TissueScan™ Tissue qPCR Array (n=48)

Clinicopathological data	Number of cases	Clinicopathological data	Number of cases
Breast cancer stage		***Estrogen receptor***	
Normal	7	Positive	15
Stage I	10	Negative	17
Stage IIa	13	Borderline	1
Stage IIb	7	Not applicable	7
Stage IIIa	8	Unavailable	8
Stage IIIc	3		
Tumor size		***Progesterone receptor***	
Stage 1	11	Positive	15
Stage 2	24	Negative	14
Stage 3	6	Borderline	1
Not applicable	7	Not applicable	7
		Unavailable	11
Lymph node spread		***HER2 receptor***	
Positive	18	Positive	10
Negative	18	Negative	23
Not applicable	7	Borderline	1
Unavailable	5	Equivocal	1
		Not applicable	7
		Unavailable	6

The gene expression of *C1QBP* was evaluated in breast cancer stages which had been divided into two groups, – AJCC stage normal to stage IIa and AJCC stage IIb to IIIc – the latter being the more advanced stages of breast cancer. In the advanced stages of breast cancer, the expression of *C1QBP* was significantly increased (P=0.0109, Figure 3.1A). Apart from that, *C1QBP* expression was also remarkably higher in tissues of breast cancer patients with lymph node spread (P=0.0169, Figure 3.1B) and in T3 tumor size compared to T1 and T2 tumor sizes (P=0.0502, Figure 3.1C).

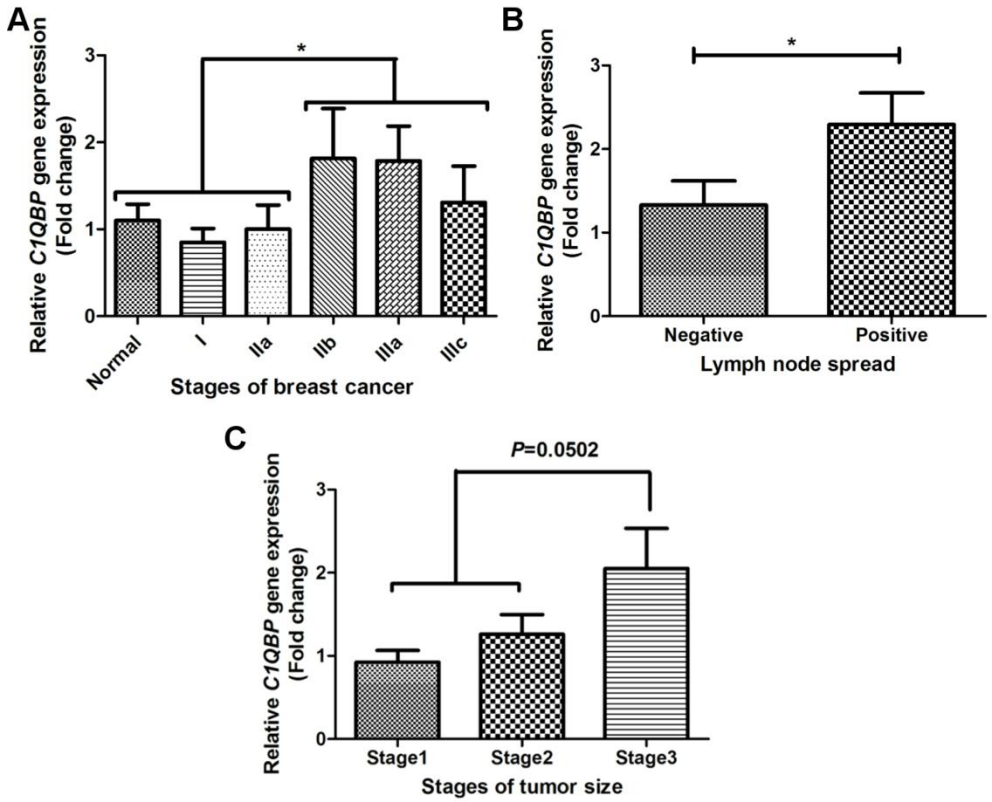

Figure 3.1. Relative gene expression of *C1QBP* in breast cancer tissue samples. The expression of *C1QBP* gene was increased in (A) higher stages of breast cancer, (B) positive lymph node spread and (C) tumor size of stage 3 compared to tumor sizes of stage 1 and 2. The panel contained 48 pre-normalized breast cancer tissue mRNA samples. The relative expression of *C1QBP* was obtained by comparing each sample's Ct value to mean Ct value of normal breast tissues. The values are represented as mean ± SEM. $P<0.05$ was considered statistically significant.

The amplification curve which plots ΔRn to PCR cycle number, reflected the quantitative expression of *C1QBP* in the array (Figure 3.2A). ΔRn represents the log of normalized reporter signal without the baseline signal. The single peak of the melting curve indicated that the primer used to target *C1QBP* was specific (Figure 3.2B).

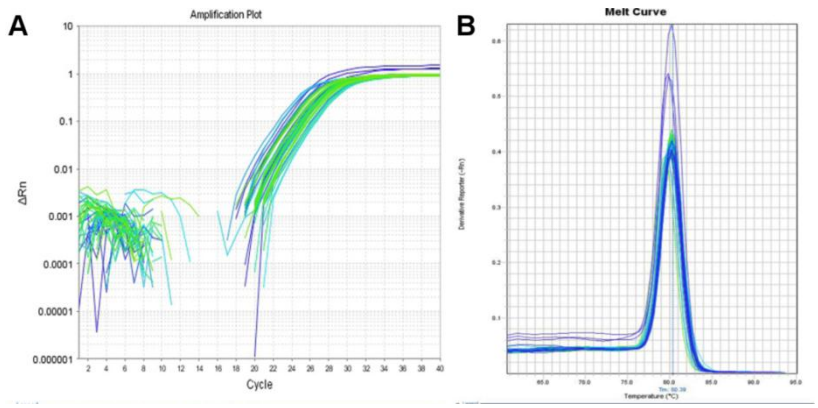

Figure 3.2. (A) Amplification plot and (B) melting curve indicated the Ct value and specificity of the C1QBP primer, respectively.

3.2 Immunohistochemical analysis of C1QBP in breast cancer tissue microarray samples

3.2.1 Clinicopathological parameters of breast cancer patients diagnosed with invasive ductal carcinomas

Following the assessment of the gene expression of *C1QBP* in clinical samples, protein expression of C1QBP was evaluated in breast cancer TMAs. Only tissue sections from patients diagnosed with invasive ductal carcinoma were included in the study. A total of 132 out of 199 breast cancer tissue sections were used for the study. The excluded sections accounted for different subtypes of breast cancer, and also, loss of sections during processing of TMAs and immunohistochemical staining. The statistical distribution of clinicopathological parameters containing continuous variables are shown in Table 3.2 and clinicopathological parameters of the tissues from the breast cancer patients are shown in Table 3.3.

Table 3.2. Statistical distribution of parameters with continuous variable (age and tumor size)

Parameters	Statistical distribution		
	Minimum	Maximum	Mean
Age (years)	23	88	56
Tumor size (mm)	10	140	41

All tissue sections of the study were obtained from female patients. Patients' age ranged from 23 to 88 years old, with a mean age of 56 years old (Table 3.2). A majority of the patients were Chinese (77.3%), followed by Malay (9.8%) and Indian (1.5%). Other ethnic races accounted for 10.6% of the total study population. Histological grade of the tissue sections were available for 126 patients and 6.1% of the tissues were classified under Grade 1, while 89.4% were Grade 2 and 3. The extent of DCIS was known for 118 cases of which, 72.0% were categorized as negative or minimal, and 17.4% as extensive. Information for DCIS grade was available for 85 cases. Among the cases, 3% were graded low while 61.4% were graded as intermediate or high. Information on tumor size was available for 130 cases. Tumor size was stratified according to its mean of 41 mm (Table 3.2). Out of the available cases, 63.6% of the tumors were 41 mm or less, and 34.8% of the tumors were larger than 41 mm. ER status, PR status and HER2 receptor status were recorded for 129 patients. 37.1% of the tissues were ER-positive while 60.6% were negative. Patients with PR-negative and PR-positive tumors made up 47.0% and 50.8% of the available cases, respectively. Out of the 129 specimens, 64.4% of them were HER2-negative, while 33.3% were HER2-positive.

Table 3.3. Clinicopathological parameters of the study population (n=132)

Clinicopathological parameters	N	%
Age (years)		
≤56	66	50.0
>56	66	50.0
Race		
Chinese	102	77.3
Malay	13	9.8
Indian	2	1.5
Others	14	10.6
Unavailable	1	0.8
Histological Grade		
1	8	6.1
2 and 3	118	89.4
Unavailable	6	4.5
Nuclear Pleomorphism Score		
1	4	3.0
2 and 3	121	91.7
Unavailable	7	5.3
Tubule Formation Score		
1 and 2	33	25.0
3	92	69.7
Unavailable	7	5.3
Mitotic index		
1	20	15.2
2 and 3	105	79.5
Unavailable	7	5.3
Associated DCIS extent		
None/Minimal	95	72.0
Extensive	23	17.4
Unavailable	14	10.6
Associated DCIS grade		
Low	4	3.0
Intermediate or High	81	61.4
Unavailable	47	35.6
Tumor size		
≤41mm	84	63.6
>41mm	46	34.8
Unavailable	2	1.5
Estrogen receptor status		
Negative	49	37.1
Positive	80	60.6
Unavailable	3	2.3
Progesterone receptor status		
Negative	62	47.0
Positive	67	50.8
Unavailable	3	2.3
HER2 status		
Negative	85	64.4
Positive	44	33.3
Unavailable	3	2.3

3.2.2 Association between immunohistochemical expression of C1QBP and clinicopathological parameters

3.2.2.1 Expression of C1QBP in breast cancer tissues

The expression of C1QBP in breast cancer tissues was determined by immunohistochemical staining, and its expression was associated with clinicopathological parameters via Chi-square analysis. The various intensities of C1QBP staining are shown in Figure 3.3A-C. The expression of C1QBP was scored based on the staining intensity with 1+ for weak staining, 2+ for moderate staining and 3+ for strong staining, respectively. A negative control was included with omission of primary antibody (Figure 3.3D). The immunostaining of C1QBP in breast cancer epithelial cells was predominantly cytoplasmic and mainly observed to be granular in nature. Although there seemed to be accentuation of the staining at the cell membrane, no distinct membrane staining was observed.

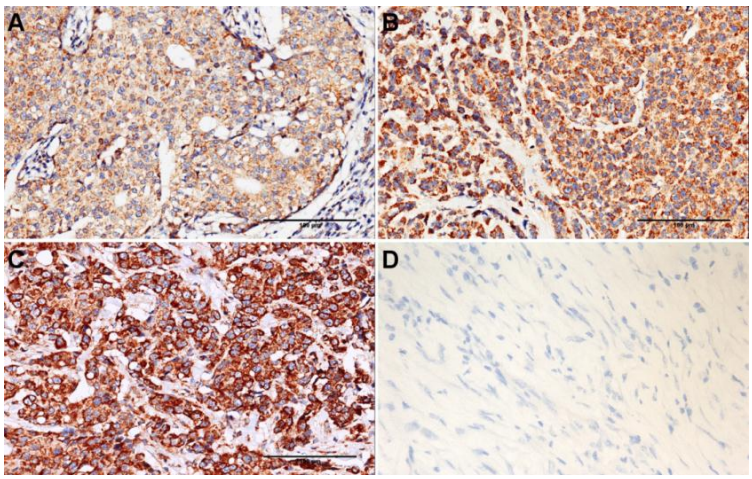

Figure 3.3. Representative images of immunohistochemical staining of C1QBP in breast cancer tissue microarrays. The intensity of the staining was assigned as (A) 1+ for weak staining, (B) 2+ for moderate staining and (C) 3+ for strong staining. Scale bar: 100 µm. (D) Absence of staining in the negative control tissues where primary antibody was omitted. Image was taken at 400X magnification.

3.2.2.2 Statistical analysis of association between immunohistochemical expression of C1QBP and clinicopathological parameters

Out of 132 cases, only one case did not show immunopositive staining. The immunostaining of C1QBP was quantified by the weighted average index (WAI) score. The minimum WAI score was recorded as 0 while the maximum WAI score reached 2.5. Mean WAI score was 1.5 (Table 3.4).

Table 3.4. Statistical distribution of WAI score for C1QBP immunohistochemical expression

Parameters	**Statistical distribution**		
	Minimum	**Maximum**	**Mean**
Weighted average index (WAI)	0.0	2.5	1.5

With a cut-off point at 1.5, the WAI scores were grouped into two sets. Number of cases with WAI of less than or equal 1.5 accounted for 58.3% (n=77) of the cases, while number of cases with WAI of more than 1.5 accounted for 41.7% (n=55) of the total cases (Table 3.5).

Table 3.5. Statistical distribution of C1QBP immunostaining in breast cancer tissue microarray (n=132)

Immunoscores of C1QBP	**Number of patients (%)**
C1QBP staining	
Negative	1 (0.8%)
Positive	131 (99.2%)
WAI	
WAI≤1.50	77 (58.3%)
WAI>1.50	55 (41.7%)

Chi-square analysis was used to determine the association of C1QBP expression and clinicopathological parameters. The associations between the expression of C1QBP and histological grade, nuclear pleomorphism, tubule formation, mitotic index, DCIS extent and grade, ER status, PR status and HER2 status were not statistically significant. Breast cancer tissue expression of C1QBP was significantly up-regulated in patients who are more than 56 years old (P=0.001), patients having tumor of more than 41 mm in size (P=0.002) and positive lymph node spread (P=0.027). The data is summarized in Table 3.6.

Table 3.6. Univariate analysis for C1QBP immunostaining with clinicopathological parameters by Chi-square analysis

Clinicopathological parameters[#]	**WAI≤1.50 N(%)**	**WAI>1.50 N(%)**	***P*-value**
Age (years)			
≤56	48 (70%)	18 (30%)	0.001**
>56	29 (40%)	37 (60%)	
Histological Grade			
1	6 (75%)	2 (25%)	0.312
2 and 3	67 (57%)	51 (43%)	
Nuclear Pleomorphism			
1	4 (100%)	0 (0%)	0.086
2 and 3	69 (57%)	52 (43%)	
Tubule Formation			
1 and 2	15 (45%)	18 (55%)	0.079
3	58 (63%)	34 (37%)	
Mitotic Index			
1	14 (70%)	6 (30%)	0.251
2 and 3	59 (56%)	46 (44%)	
Associated DCIS Extent			
None/Minimal	57 (60%)	38 (40%)	0.494
Extensive	12 (52%)	11 (48%)	
Lymph Node Spread			
Negative	44 (68%)	21(32%)	0.027*
Positive	31 (48%)	33 (52%)	
Associated DCIS Grade			
Low	2 (50%)	2 (50%)	0.676
Intermediate/High	49 (60%)	32 (40%)	
Tumor Size			
≤41mm	57 (76%)	18 (24%)	0.002**
>41mm	27 (49%)	28 (51%)	
Estrogen Receptor Status			
Negative	25 (51%)	24 (49%)	0.200
Positive	50 (63%)	30 (38%)	
Progesterone Receptor Status			
Negative	34 (55%)	28 (45%)	0.465
Positive	41 (61%)	26 (39%)	
HER2 Status			
Negative	54 (64%)	31 (36%)	0.085
Positive	21 (48%)	23 (52%)	

[#]Unavailable cases for each parameter are shown in Table 3.3

Statistical significance: *P<0.05, **P<0.01

Multivariate analysis using backwards logistic binary regression was then carried out to determine the independence of C1QBP as a predictor of tumor size and lymph node spread. After adjustment of confounding factors, which include age, ER status, PR status and HER2 status, C1QBP was determined to be independently associated to tumor size in PR-positive breast cancer patients (P<0.001, Table 3.7). A WAI value of more than 1.5 increased the odds ratio of possessing a tumor size that is larger than 41 mm, by 10.8 times. Also from the analysis, C1QBP was not an independent predictor for lymph node spread.

Table 3.7. Multivariate analysis by backwards logistic binary regression

Parameters	**Odds Ratio**	**Standard error**	***P*-value**	**95% Cl**
Tumor size				
PR Positive Patients				
C1QBP	10.7919	0.6571	<0.001***	(2.9771,39.1203)
PR Negative Patients				
C1QBP	1.3572	0.5166	0.591	(0.4931,3.7357)
Mitotic index				
ER	0.1342	0.7665	0.0088**	(0.0299,0.6030)
HER2	3.3525	0.6595	0.0666	(0.9204,12.2108)
Associated DCIS extent				
PR status	2.6690	0.3898	0.0118*	(1.2432,5.7300)

Statistical significance: *P<0.05, **P<0.01, ***P<0.001

3.2.3 Association of C1QBP expression and Proliferating Cell Nuclear Antigen (PCNA)

3.2.3.1 Expression of PCNA in breast cancer tissue samples

As tumor size is a gauge for tumor proliferation, the association of C1QBP expression and PCNA, which is a well-known marker of proliferation was determined. A total number of 66 cases were used for comparison of PCNA. All tissue sections were positive for PCNA staining with percentage of

staining in tissue sections ranging from 5% to 100%. PCNA staining was mostly seen in the nucleus (Figure 3.4).

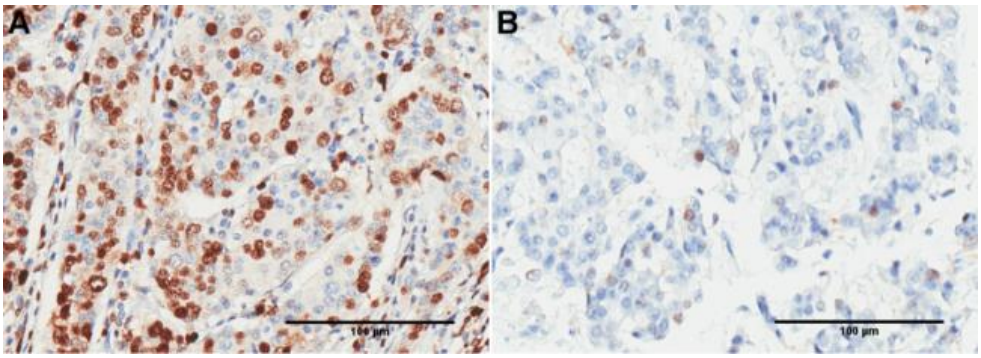

Figure 3.4. Representative micrographs of PCNA immunostaining in breast cancer tissue microarrays. Tissue sections with (A) high and (B) low expressions of PCNA. Scale bar: 100 µm.

3.2.3.2 Correlation between immunohistochemical expression of C1QBP and PCNA

The expression of C1QBP has a significant correlation to the expression of PCNA as determined by Pearson's correlation (*P*=0.0229, Pearson's R=0.2863).

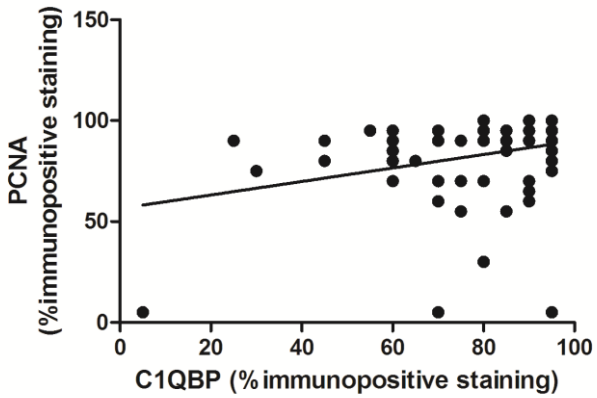

Figure 3.5. Correlation between C1QBP and PCNA immunopositive staining; Pearson's correlation R = 0.2863 (**P*=0.0229).

3.3 Expression of C1QBP in breast cancer cell lines

3.3.1 Characteristics of various breast cancer cell lines

To uncover the functional characteristics of C1QBP in breast cancer, *in vitro* experimentation was performed. The breast cancer cell lines that were used included, ZR-75-1, T47D, MCF7 and MDA-MB-231. The ZR-75-1 cells are positive for ER and negative for PR. T47D and MCF7 cell lines are positive for both ER and PR, while MDA-MB-231 cells are negative for both hormone receptors (Kao et al., 2009). The potential of the cell lines to invade varied widely with ZR-75-1 cells, and MCF7 cells being non-invasive, T47D cells are less invasive while MDA-MB-231 cells are highly invasive (Tai et al., 2003). This is summarized in Table 3.8.

Table 3.8: Breast cancer cell lines with its respective estrogen receptor, progesterone receptor and invasiveness status.

Breast cancer cell line	**ER status**	**PR status**	**Invasiveness (Tai et al., 2003)**
ZR-75-1	+	-	Non-invasive
T47D	+	+	Less invasive
MCF7	+	+	Non-invasive
MDA-MB-231	-	-	Highly invasive

'+': positive; '-': negative

ZR-75-1 cells, T47D cells and MCF7 cells displayed an epithelial-like morphology, while MDA-MB-231 cells possessed spindle-like shaped cells (Figure 3.6).

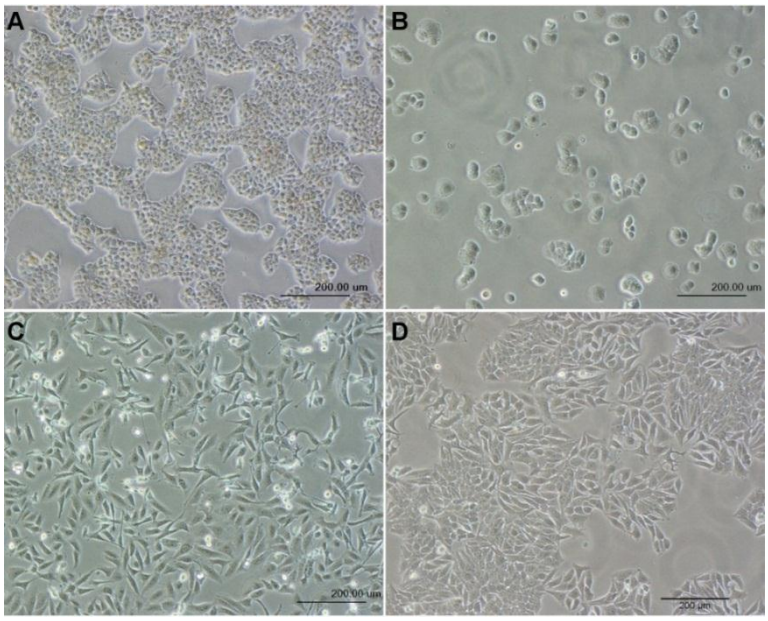

Figure 3.6. Breast cancer cell lines used in this study. (A) ZR-75-1 (B) T47D (C) MDA-MB-231 (D) MCF7 breast cancer cell lines. Scale bar: 200 µm.

3.3.2 Gene profile of *C1QBP* in breast cancer cell lines

The *C1QBP* gene was constitutively expressed in all the breast cancer cell lines examined. ZR-75-1 had the lowest gene expression of *C1QBP*. The expression of *C1QBP* was relatively higher in T47D, MDA-MB-231 and MCF7 breast cancer cell lines (Figure 3.7).

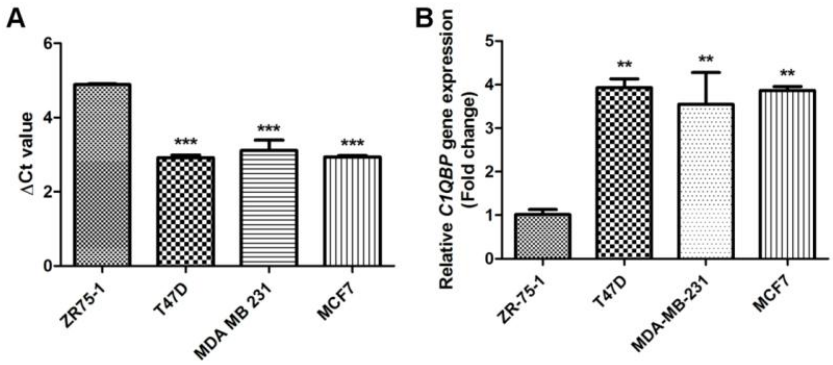

Figure 3.7. Real-time PCR of *C1QBP* in breast cancer cell lines. (A) ΔCt values of *C1QBP* in breast cancer cell lines obtained by normalization to *GAPDH*, a housekeeping gene. (B) Relative expression of *C1QBP* in breast cancer cell lines compared to ZR-75-1. Values are presented as mean ± SEM. $^{**}P<0.01$, $^{***}P<0.001$. Experiments were done in triplicates and repeated three independent times.

Primer specificity of the primers for *C1QBP* and *GAPDH* were determined by gel electrophoreses. A single band was seen from the gel indicating the specificity of the primers (Figure 3.8).

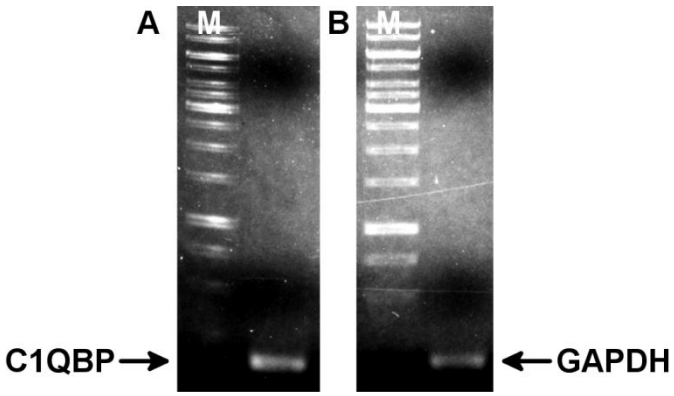

Figure 3.8. Representative gel electrophoresis image for real-time PCR products of (A) *C1QBP* and (B) *GAPDH*, with sizes of 161 bp and 160 bp, respectively. The first lane, Lane M, represents the DNA ladder marker.

3.3.3 Protein expression of C1QBP in breast cancer cell lines

The protein expression of C1QBP was next examined in the breast cancer cell lines. Consistently, ZR-75-1 cells had the lowest expression of C1QBP. However, the expression of C1QBP was highest in MCF7 cells, followed by MDA-MB-231 cells and T47D cells. There was no significance difference between the expression of C1QBP in T47D, MCF7 and MDA-MB-231 cell lines (Figure 3.9).

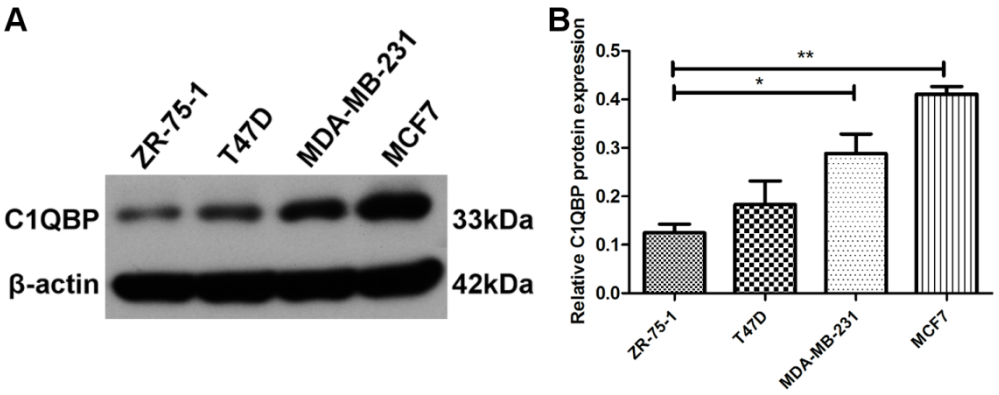

Figure 3.9. Protein expression of C1QBP in breast cancer cell lines. (A) Western blot representation of C1QBP and β-actin protein expression in breast cancer cell lines. (B) O.D. ratio of C1QBP to β-actin in breast cancer cell lines. O.D. ratio are presented as mean ± SEM. Statistical significance was achieved at *P<0.05 and **P<0.01. Experiments were done in triplicates and repeated three independent times

Intracellular localization of C1QBP was observed by immunofluorescence staining in both the MDA-MB-231 and T47D breast cancer cell lines (Figure 3.10). From the images, C1QBP was observed to be present in both the cytoplasm and nucleus. Cytoplasmic expression of C1QBP appeared spotty in nature.

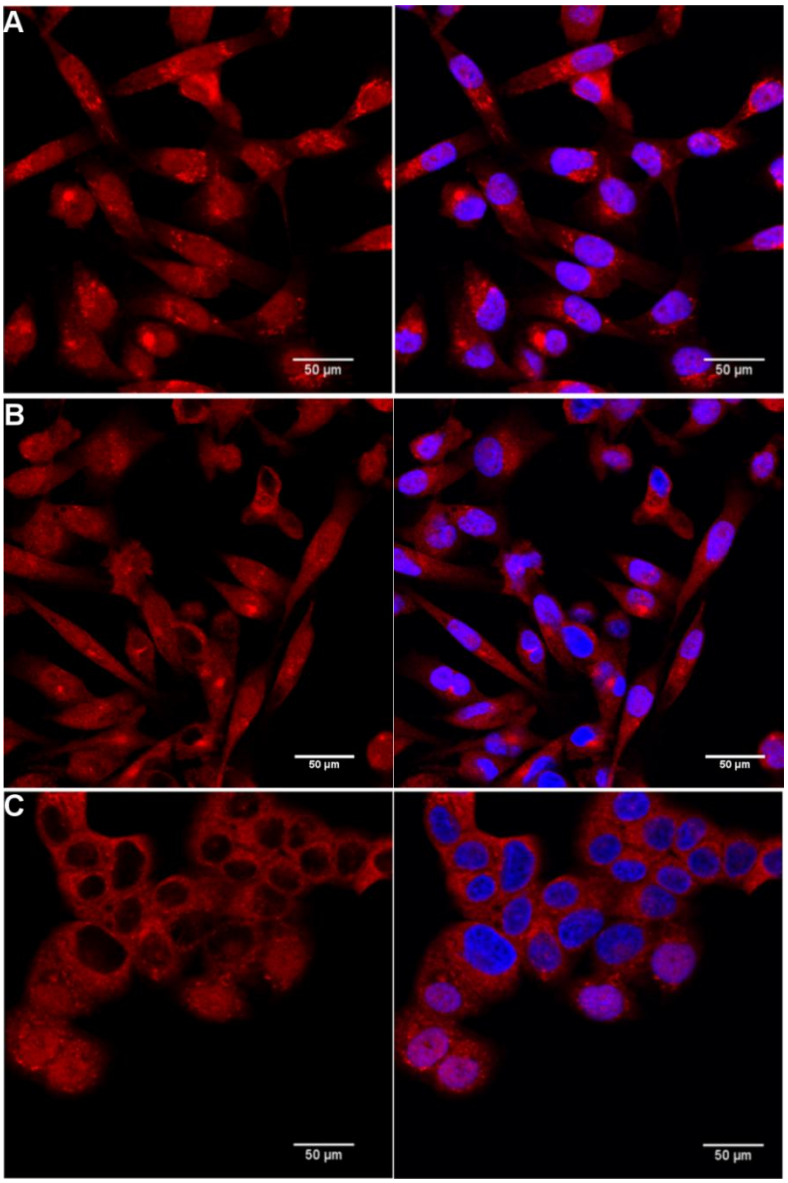

Figure 3.10. Immunofluorescence images of C1QBP in (A) MDA-MB-231 indicating nuclear and cytoplasmic staining and (B) MDA-MB-231 cells indicating only a proportion of cells have nuclear staining. (C) Immunofluorescence images of T47D breast cancer cell lines showing that C1QBP expression was localized in the cytoplasm and nucleus of the cells. Scale bar: 50 µm.

The localization of C1QBP was further validated by double staining of C1QBP and MitoTracker® Red CMXRos in MDA-MB-231 cells and T47D cells, to determine the co-localization of C1QBP and mitochondria. Indeed, the expression of C1QBP in both cell lines was mainly observed to co-localize with the red mitochondrial staining when the images were merged as depicted in Figure 3.11.

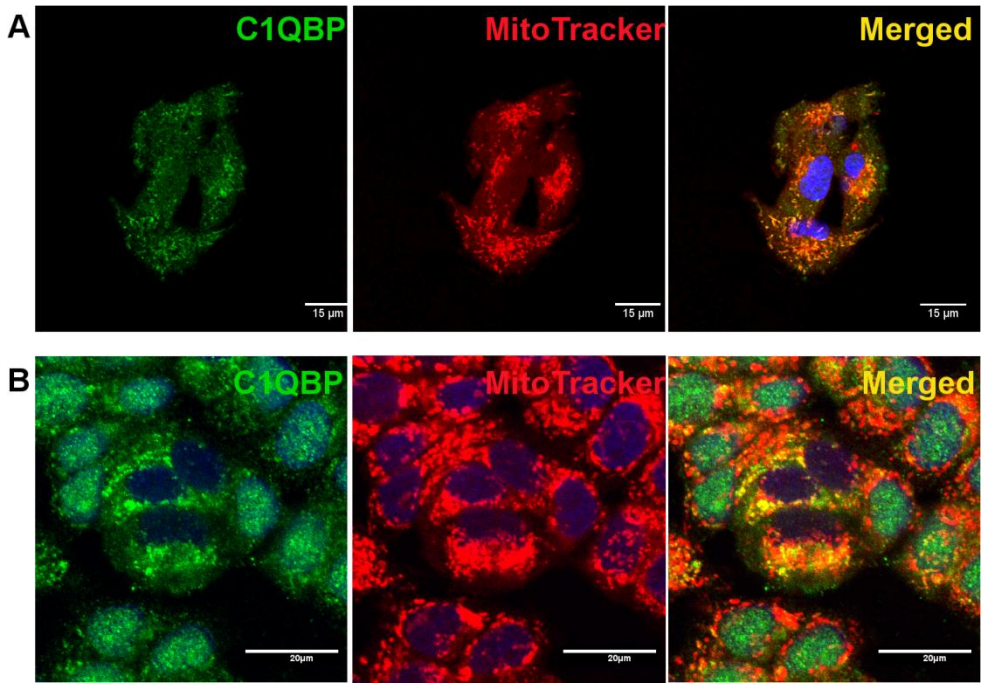

Figure 3.11. Co-localization of C1QBP with mitochondria in (A) MDA-MB-231 and (B) T47D. C1QBP was stained green with FITC-conjugated antibody while mitochondria were stained red with MitoTracker® Red CMXRos. The co-localization of C1QBP and mitochondria was displayed as yellow in the merged images. Scale bar: (A) 15µm (B) 20 µm.

3.4 Transient down-regulation of C1QBP in breast cancer cell lines

3.4.1 Knockdown of C1QBP in MDA-MB-231 breast cancer cell line

MDA-MB-231 breast cancer cells were used as the main cell line in the study, as the gene and protein expression of C1QBP were relatively high. In addition, MDA-MB-231 is a metastatic cell line with high invasive capabilities, which are not present in the other cell lines.

The transfection efficiency of DharmaFECT2 transfection reagent in MDA-MB-231 was assessed using a cy3-conjugated non-targeting siRNA, warranting that the siRNA complex entered the cells. More than 90% of the cells were transfected with the siRNA using the DharmaFECT2 transfection reagent (Figure 3.12).

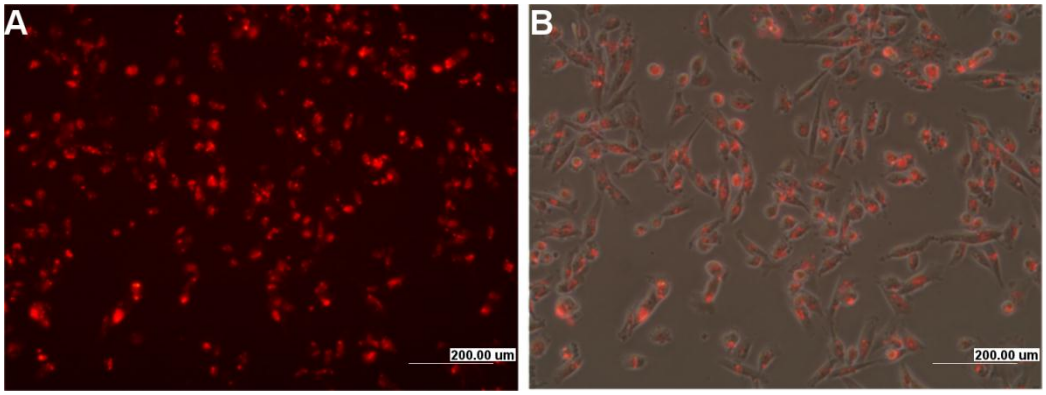

Figure 3.12. DharmaFECT2 transfection efficiency in MDA-MB-231 observed by using cy3-conjugated non-targeting siRNA. (A) Cy3-conjugated non-targeting siRNA transfected into MDA-MB-231 cells using DharmaFECT2 transfection reagent. (B) Cy3 staining superimposed onto corresponding MDA-MB-231 cells bright field image indicating a transfection efficiency of more than 90%. Scale bar: 200 µm.

Knockdown of C1QBP in MDA-MB-231 cells at the gene and protein levels, were established by real-time PCR and western blot respectively. The expression of *C1QBP* at the gene level was depleted by 94% (Figure 3.13), while the protein expression of C1QBP was depleted by 76%, after transfection with siRNA targeting C1QBP (Figure 3.14).

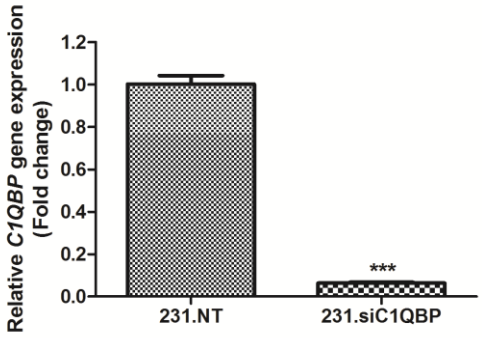

Figure 3.13. Relative *C1QBP* gene expression in MDA-MB-231 cells 48 h after transfection with siC1QBP. The *C1QBP* gene level was reduced by approximately 94% in MDA-MB-231 cells. Values are presented as mean ± SEM, ****P*<0.001. Experiments were done in triplicates and repeated twice.

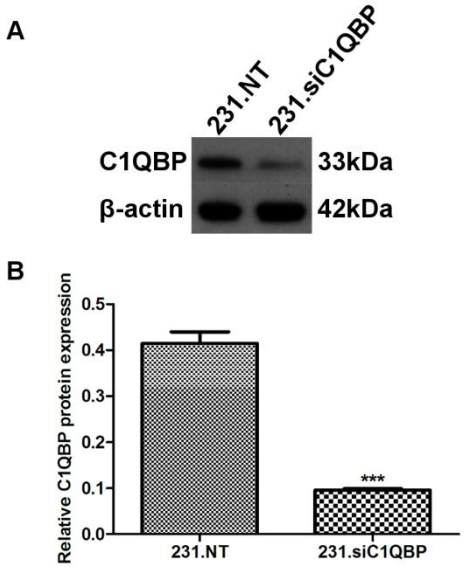

Figure 3.14. Silencing efficiency of siC1QBP at the protein level in MDA-MB-231 breast cancer cell lines 72 h after transfection. (A) Western blot showed an obvious reduction of C1QBP protein in MDA-MB-231 cells transfected with siC1QBP. (B) The protein level was decreased by 76% compared to cells transfected with non-targeting siRNA. Relative protein expression are presented as mean ± SEM. ****P*<0.001. Experiments were done in triplicates and repeated twice.

3.4.2 Knockdown of C1QBP in T47D breast cancer cell lines

T47D breast cancer cell line was also used, to verify the effect of C1QBP on proliferation in PR-positive breast cancer cells. Silencing efficiency of siC1QBP in T47D cells was attained at 85% and 81% at the gene and protein level, respectively (Figure 3.15 and Figure 3.16).

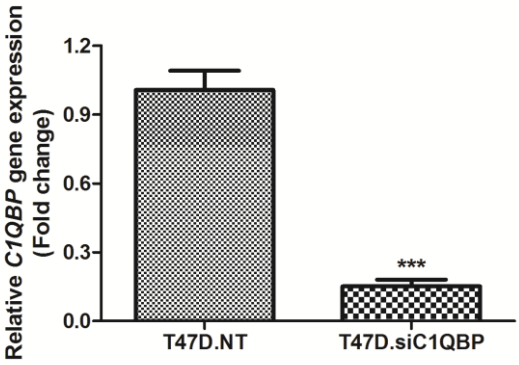

Figure 3.15. Down-regulation of C1QBP gene in T47D breast cancer cell line, 96 h after transfection. Silencing efficiency was achieved at approximately 85%. Fold change are presented as mean ± SEM. ****P*<0.001. Experiments were done in triplicates and repeated twice.

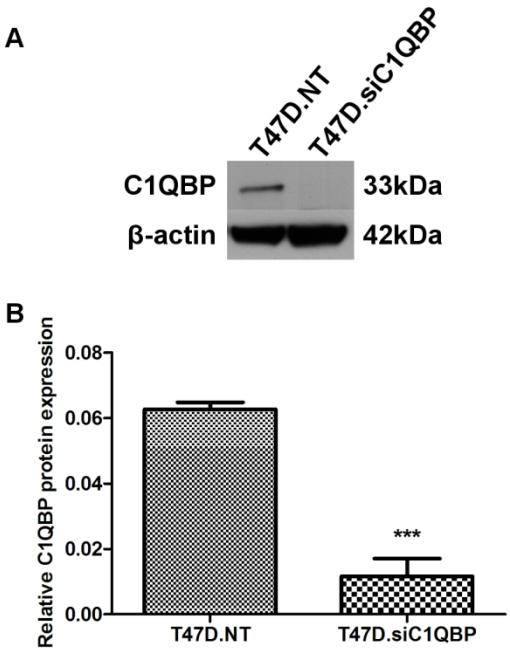

Figure 3.16. Knockdown of C1QBP protein in T47D breast cancer cell line 96 h post-transfection. (A) Western blot of the knockdown efficiency of siC1QBP in T47D cells. (B) Graph showing about 81% reduction of C1QBP protein expression in T47D cells. Relative protein expression are presented as mean ± SEM. ****P*<0.001. Experiments were done in triplicates and repeated twice.

3.5 Association of C1QBP knockdown with cell proliferation

3.5.1 Knockdown of C1QBP affected cell proliferation in MDA-MB-231 cell line

In MDA-MB-231 cells, cell proliferation was measured using MTS assay after knockdown of C1QBP. The cells were fasted for 24 h before measurement of MTS at 72 h and 96 h. At both these time points, cell proliferation was significantly decreased in MDA-MB-231 cells transfected with siC1QBP (*P*=0.0115, *P*=0.0029, Figure 3.17).

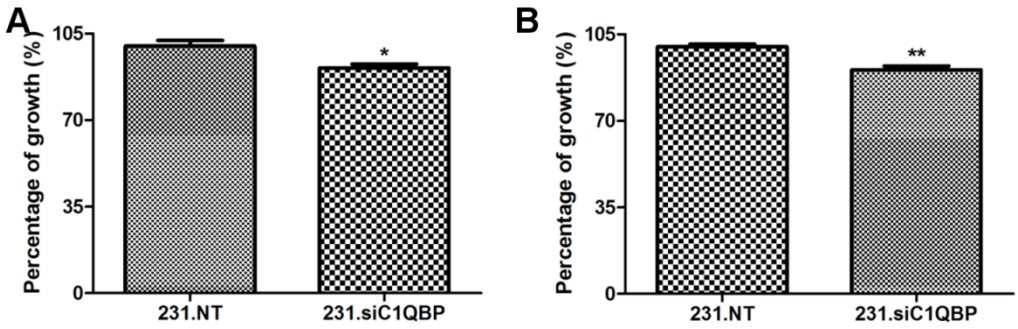

Figure 3.17. Down-regulation of C1QBP decreased cell proliferation in MDA-MB-231 cells at (A) 72 h and (B) 96 h post-transfection, as measured by MTS assay. Cells were fasted on the 3rd day after transfection and replenished with complete medium after 24 h. Absorbance value of MTS assay was read at 490 nm. Each column represents the percentage of growth ± SEM. **P*<0.05, ***P*<0.01. Experiments were done in quadruplicates and repeated at three independent times.

In addition, cell growth curve was also plotted for MDA-MB-231 cells, after knockdown of C1QBP for a period of 96 h (Figure 3.18). The measurements were taken every 24 h using the alamarBlue assay. Using two-way ANOVA, the cell growth was found to be significantly lower in 231.siC1QBP cells which reflected the results from the MTS assay (*P*=0.0005).

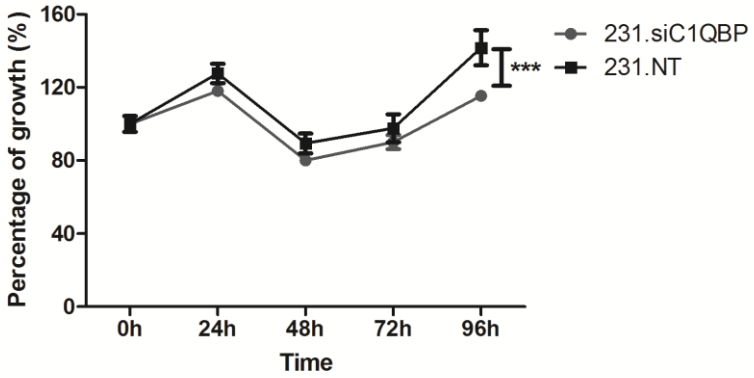

Figure 3.18. Knockdown of C1QBP significantly decreased the cell growth of MDA-MB-231 cells. Cell growth curve was plotted by measurements from alamarBlue assay taken at 0 h, 24 h, 48 h, 72 h and 96 h. Percentage of measurements ± SEM are shown. Statistical significance was determined by two-way ANOVA (***P<0.001). Experiments were done in quadruplicates and repeated twice.

Cell proliferation could be governed by the cell cycle process. The cell cycle process is controlled by regulatory molecules, such as the cyclins and cyclin-dependent kinases (CDKs), which determine the progression of cells to subsequent cell cycle phases. Hence, several main regulatory proteins of the cell cycle process were examined after knockdown of C1QBP (Figure 3.19). There was a significant decrease of Cyclin D1 after knockdown of C1QBP compared to control cells (*P*=0.007). In addition, there was a decrease in CDK4 expression (*P*=0.0882). The expressions of CDC25a and CDK6 were unchanged after knockdown of C1QBP in MDA-MB-231 cells.

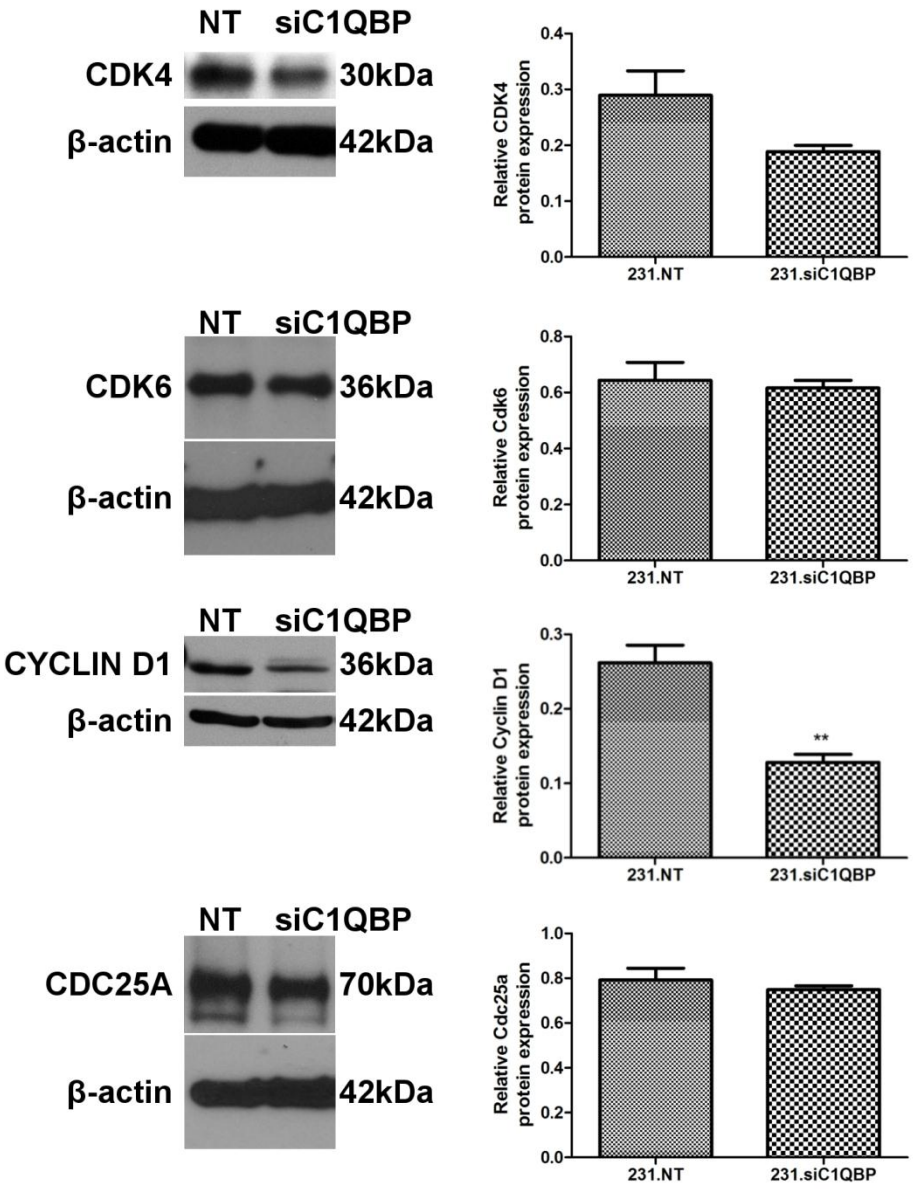

Figure 3.19: Cell cycle-related proteins' expression after knockdown of C1QBP. The expression of CDK4 and Cyclin D1 was downregulated after knockdown of C1QBP in MDA-MB-231 cells. The protein levels of CDC25A and CDK6 were not affected. Although the difference was not statistically significant, the difference in protein expression of CDK4 between the two groups was marginally significant (P=0.0882). Statistical significance was achieved at $^{**}P<0.01$. Values are presented as mean ± SEM. Experiments were done in triplicates and repeated at three independent times.

3.5.2 Knockdown of C1QBP in T47D breast cancer cell line affected proliferation

Based on the TMA results shown earlier, C1QBP seemed to affect tumor growth in PR-positive breast cancer patients. Therefore, knockdown of C1QBP in T47D breast cancer cell lines was carried out to determine the effect of C1QBP on proliferation in a PR-positive cell line. At 72 h after transfection, there was no significant difference in cell growth as measured by MTS assay (*P*=0.8854, Figure 3.20A). However, cell growth measured by the same method was significantly reduced in T47D cells 96 h after transfection with siC1QBP (*P*=0.0015, Figure 3.20B). The alteration of cell growth by C1QBP was further verified by the alamarBlue assay (Figure 3.20C). A decrease in cell growth of T47D cells was observed, when measured by alamarBlue assay over 168 h. The difference was statistically significant (*P*=0.0008).

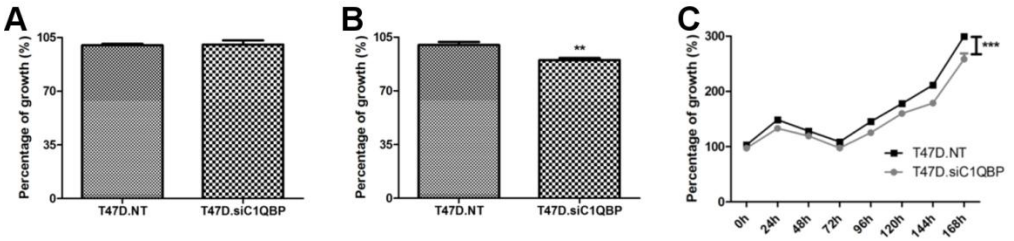

Figure 3.20. Cell growth and proliferation were affected after knockdown of C1QBP in T47D breast cancer cell line. Cell proliferation measured by MTS assay was not affected at (A) 72 h, but significantly decreased at (B) 96 h after transfection of siC1QBP in T47D breast cancer cell line. Bar chart was presented as mean(%) ± SEM. ***P*<0.01. (C) AlamarBlue assay indicated a decrease in cell growth over 168h, after knockdown of C1QBP. The difference was statistically significant with *P*=0.0008, determined by two-way ANOVA. Experiments were done in quadruplicates and repeated at two independent times.

3.6 Effect of knockdown of C1QBP on cell migration and invasion in MDA-MB-231 cells

Cell migration was measured using the wound scratch method, and limited to 6 h to prevent interference from cell proliferation. In addition, transwell migration assay was carried out. Knockdown of C1QBP significantly decreased cell migration in MDA-MB-231 cells as measured by wound scratch assay (Figure 3.21, P=0.0006).

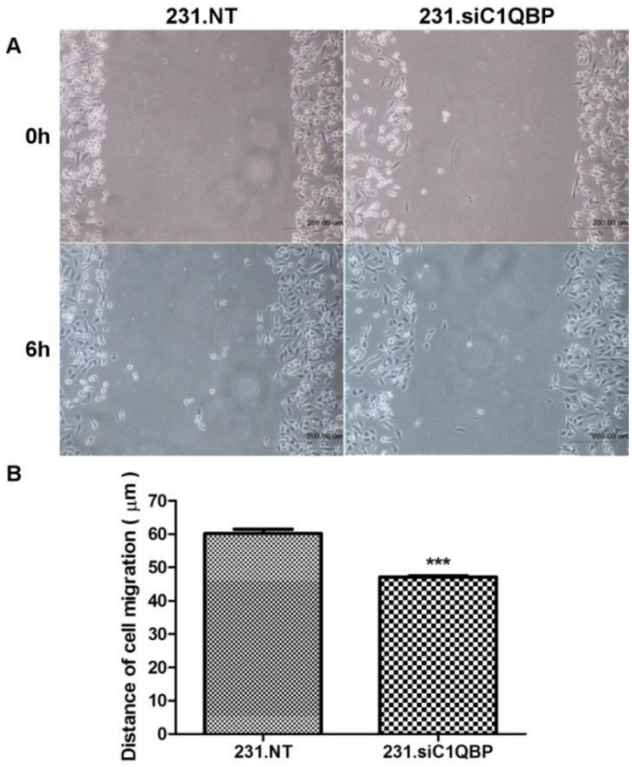

Figure 3.21. Decreased expression of C1QBP inhibited cell migration in MDA-MB-231 cells via wound healing assay. A gap was created using a yellow tip at 72 h after transfection. (A) Images were taken at 0 h and 6 h thereafter. Five fields were taken for each sample and five measurements were made for each field. Scale bar: 200 μm. The width of the gap was measured at 0 h and 6 h, using ImageJ software. (B) The distance of cell migration was determined by the difference of the gap measurements at 0 h and 6 h. Each bar in the bar chart are presented as mean ± SEM. ***P<0.001. Experiments were done in triplicates and repeated at three independent times.

In addition, transwell migration assay was carried out after down-regulatin of C1QBP. Knockdown of C1QBP significantly decreased cell migration in MDA-MB-231 cells as measured by transwell migration assay (Figure 3.22, *P*=0.0435).

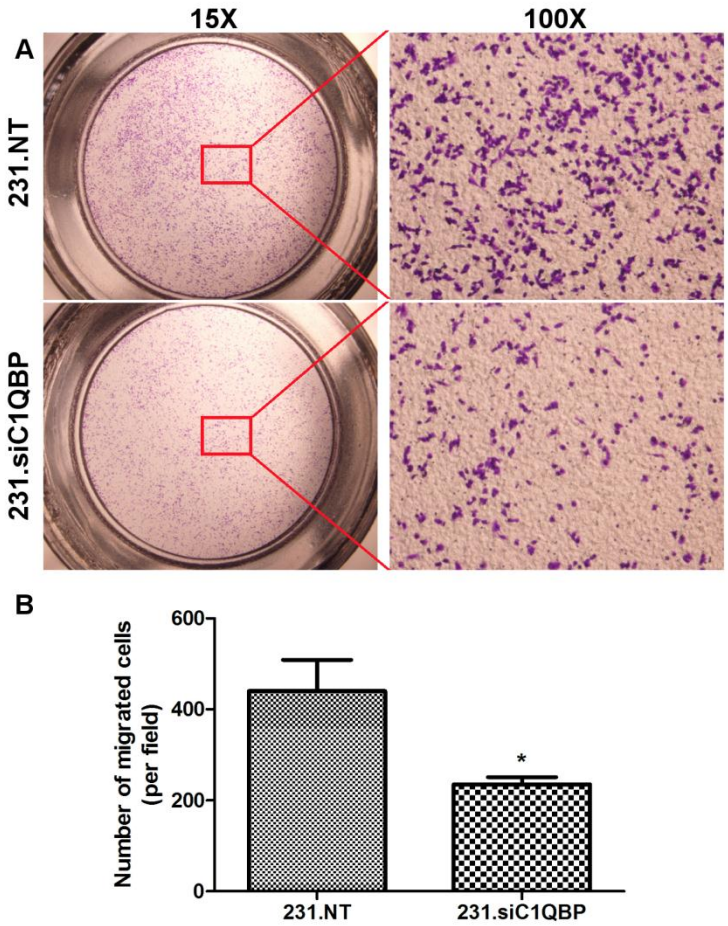

Figure 3.22: Knockdown of C1QBP in MDA-MB-231 cells decreased cell migration as observed in transwell migration assay. (A) Representative images of the transwell inserts and the respective membranes at 15X magnification and 100X magnification, respectively. (B) Cell migration was significantly decreased after knockdown of C1QBP in MDA-MB-231 cells. Experiment was done in triplicates. *, *P*<0.05.

Cell invasion was also assessed after knockdown of C1QBP. Although a general decrease was observed, it was statistically not significant (*P*=0.3623, Figure 3.23).

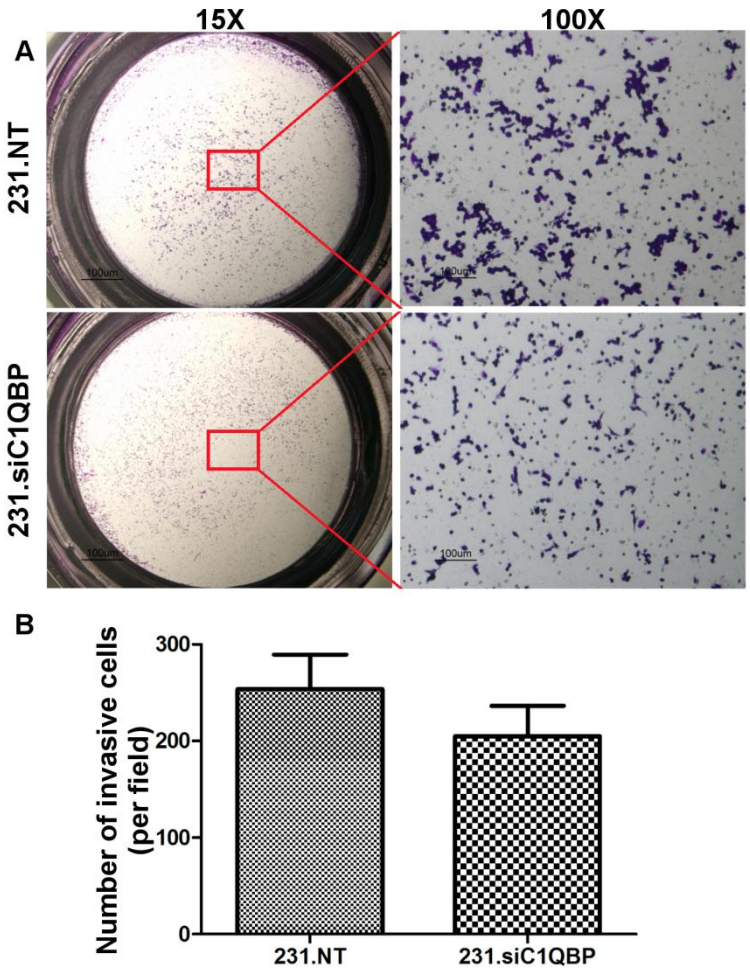

Figure 3.23. Invasion assay using transwell inserts after knockdown of C1QBP in MDA-MB-231 breast cancer cells. (A) Representative images of the transwell inserts and the respective membranes at 15X magnification and 100X magnification, respectively. (B) Although cell invasion was slightly diminished after knockdown of C1QBP, the difference was not statistically significant. Experiments were done in triplicates and repeated at three independent times.

3.7 Effect of C1QBP attenuation on chemosensitivity of MDA-MB-231 cells

Chemosensitivity of MDA-MB-231 cells towards Doxorubicin hydrochloride, Epirubicin hydrochloride and 5-Fluorouracil were examined after transient knockdown of C1QBP. After 48 h of treatment with the drugs, cells with reduced expression of C1QBP displayed lower percentage of cell viability (Figure 3.24). The IC50 values for each treatment generally exhibited a lower IC50 value after knockdown of C1QBP. Statistically, only treatment of cells with Doxorubicin hydrochloride demonstrated a marginal difference when C1QBP was diminished (*P*=0.0579).

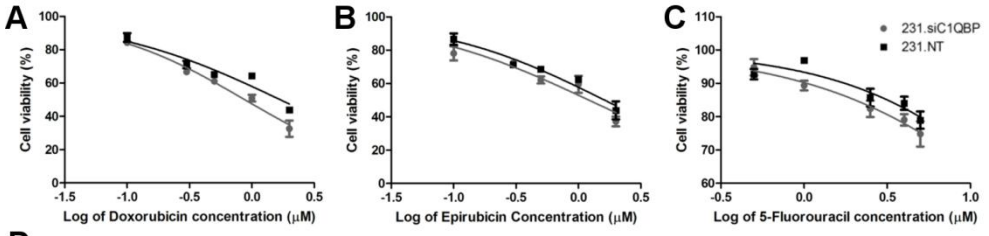

D

Drugs	IC50 of drug (μM)		Statistical analysis *(Two-way ANOVA)*
	231. NT	231. siC1QBP	
(A) Doxorubicin hydrochloride	1.691	0.8774	0.0579[#]
(B) Epirubicin hydrochloride	1.629	1.220	0.6381
(C) 5-Fluorouracil	28.90	24.79	0.5388

[#]Borderline significance

Figure 3.24. Chemosensitivity of MDA-MB-231 breast cancer cell line to various drugs - (A) Doxorubicin hydrochloride (B) Epirubicin hydrochloride and (C) 5-Fluorouracil – was increased after knockdown of C1QBP. Cell viability measurements are presented as mean ± SEM. (D) IC50s of chemotherapeutic drugs were determined for MDA-MB-231 breast cancer cell line transfected with non-targeting and siRNA targeting C1QBP, respectively. Statistical analysis was done using two-way ANOVA. Experiments were done in quadruplicates and repeated at least twice.

3.8 Stable overexpression of C1QBP in MDA-MB-231 breast cancer cell line

The full-length human C1QBP cDNA with a C-terminal c-myc tag, was inserted into pCI-neo (Promega Corporation) to produce a C1QBP expression vector, pCI-neo-C1QBP. Stable overexpression of C1QBP was established in MDA-MB-231 breast cancer cell line by transfection of pCI-neo-C1QBP plasmid into MDA-MB-231 cells. MDA-MB-231 cells were also transfected with empty pCI-neo plasmid, which acted as the control cells. The C1QBP insert was sequenced to ensure its specificity (Figure 3.25).

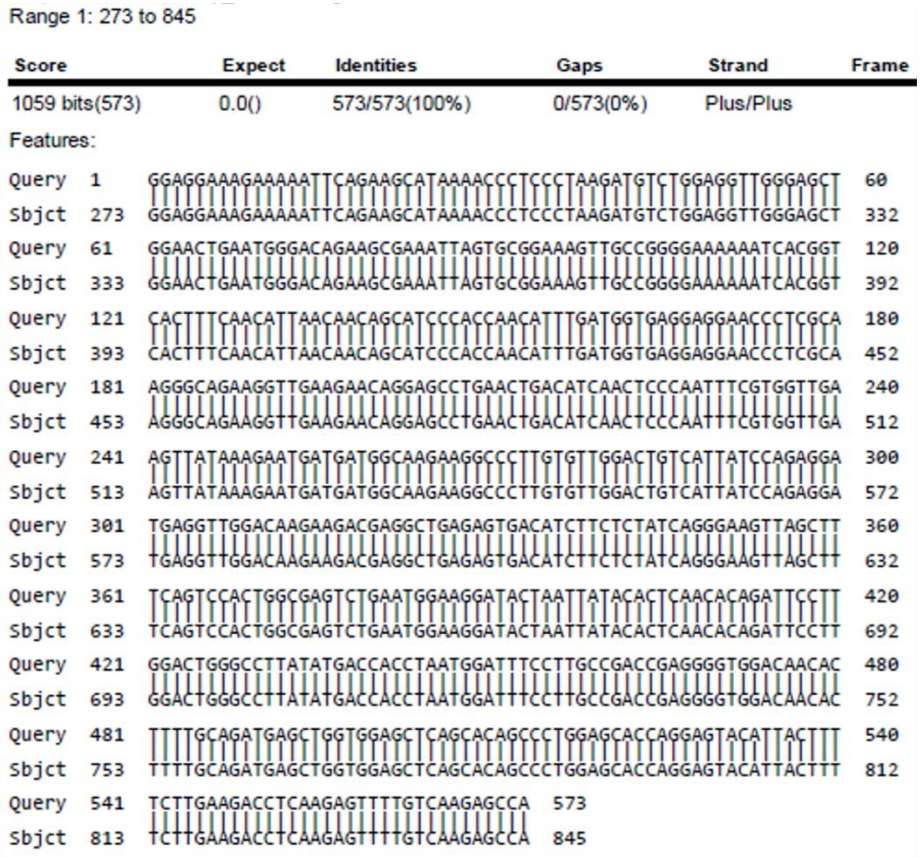

Range 1: 273 to 845

Score	Expect	Identities	Gaps	Strand	Frame
1059 bits(573)	0.0()	573/573(100%)	0/573(0%)	Plus/Plus	

Features:

```
Query  1    GGAGGAAAGAAAAATTCAGAAGCATAAAACCCTCCCTAAGATGTCTGGAGGTTGGGAGCT  60
Sbjct  273  GGAGGAAAGAAAAATTCAGAAGCATAAAACCCTCCCTAAGATGTCTGGAGGTTGGGAGCT  332
Query  61   GGAACTGAATGGGACAGAAGCGAAATTAGTGCGGAAAGTTGCCGGGGAAAAAATCACGGT  120
Sbjct  333  GGAACTGAATGGGACAGAAGCGAAATTAGTGCGGAAAGTTGCCGGGGAAAAAATCACGGT  392
Query  121  CACTTTCAACATTAACAACAGCATCCCACCAACATTTGATGGTGAGGAGGAACCCTCGCA  180
Sbjct  393  CACTTTCAACATTAACAACAGCATCCCACCAACATTTGATGGTGAGGAGGAACCCTCGCA  452
Query  181  AGGGCAGAAGGTTGAAGAACAGGAGCCTGAACTGACATCAACTCCCAATTTCGTGGTTGA  240
Sbjct  453  AGGGCAGAAGGTTGAAGAACAGGAGCCTGAACTGACATCAACTCCCAATTTCGTGGTTGA  512
Query  241  AGTTATAAAGAATGATGATGGCAAGAAGGCCCTTGTGTTGGACTGTCATTATCCAGAGGA  300
Sbjct  513  AGTTATAAAGAATGATGATGGCAAGAAGGCCCTTGTGTTGGACTGTCATTATCCAGAGGA  572
Query  301  TGAGGTTGGACAAGAAGACGAGGCTGAGAGTGACATCTTCTCTATCAGGGAAGTTAGCTT  360
Sbjct  573  TGAGGTTGGACAAGAAGACGAGGCTGAGAGTGACATCTTCTCTATCAGGGAAGTTAGCTT  632
Query  361  TCAGTCCACTGGCGAGTCTGAATGGAAGGATACTAATTATACACTCAACACAGATTCCTT  420
Sbjct  633  TCAGTCCACTGGCGAGTCTGAATGGAAGGATACTAATTATACACTCAACACAGATTCCTT  692
Query  421  GGACTGGGCCTTATATGACCACCTAATGGATTTCCTTGCCGACCGAGGGGTGGACAACAC  480
Sbjct  693  GGACTGGGCCTTATATGACCACCTAATGGATTTCCTTGCCGACCGAGGGGTGGACAACAC  752
Query  481  TTTTGCAGATGAGCTGGTGGAGCTCAGCACAGCCCTGGAGCACCAGGAGTACATTACTTT  540
Sbjct  753  TTTTGCAGATGAGCTGGTGGAGCTCAGCACAGCCCTGGAGCACCAGGAGTACATTACTTT  812
Query  541  TCTTGAAGACCTCAAGAGTTTTGTCAAGAGCCA  573
Sbjct  813  TCTTGAAGACCTCAAGAGTTTTGTCAAGAGCCA  845
```

Figure 3.25. Partial sequence of C1QBP inserted into pCI-neo plasmid.

The resulting colonies after selection with G418 were elected and cultured. The selected colony has a stable overexpression of *C1QBP* gene, 8 folds higher than cells transfected with empty plasmids (Figure 3.26).

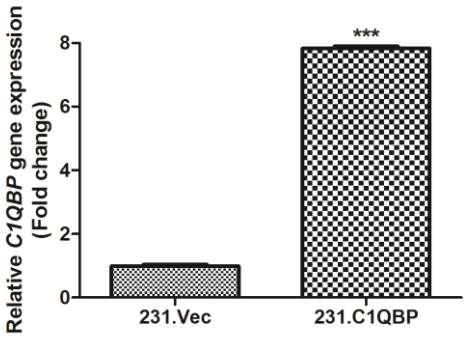

Figure 3.26. Stable overexpression of *C1QBP* gene in MDA-MB-231 breast cancer cell line. The *C1QBP*-overexpressing cells expressed approximately 8 folds higher expression of the *C1QBP* gene, compared to cells stably transfected with empty vector. Experiments were done in triplicates and repeated twice.

Measurements of the protein levels in C1QBP-overexpressing cells indicated that protein expression of C1QBP was approximately 3.3 times higher compared to control cells (Figure 3.27).

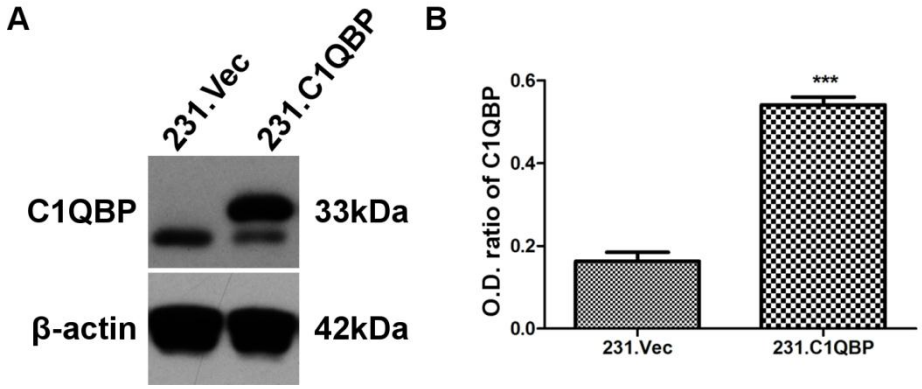

Figure 3.27. Protein overexpression of C1QBP in MDA-MB-231 breast cancer cells stably transfected with pCI-neo-C1QBP. (A) Representation of western blot images showing an increase expression of C1QBP in MDA-MB-231 cell line stably transfected with C1QBP-containing plasmid, compared to cells transfected with plasmid without inserts. β-actin served as the loading control. (B) C1QBP was significantly overexpressed in selected MDA-MB-231 breast cancer cell line transfected with C1QBP-containing plasmid compared to cells transfected with empty vector. O.D. ratios are presented as mean ± SEM. ****P*<0.001. Experiments were done in triplicates and repeated twice.

The overexpression of C1QBP was also validated by immunofluorescence staining (Figure 3.28). Increased FITC staining was observed in C1QBP-overexpressing cells. The increased expression of C1QBP also co-localized with Mitotracker, indicating that the overexpression of C1QBP mostly occurred in cell mitochondria.

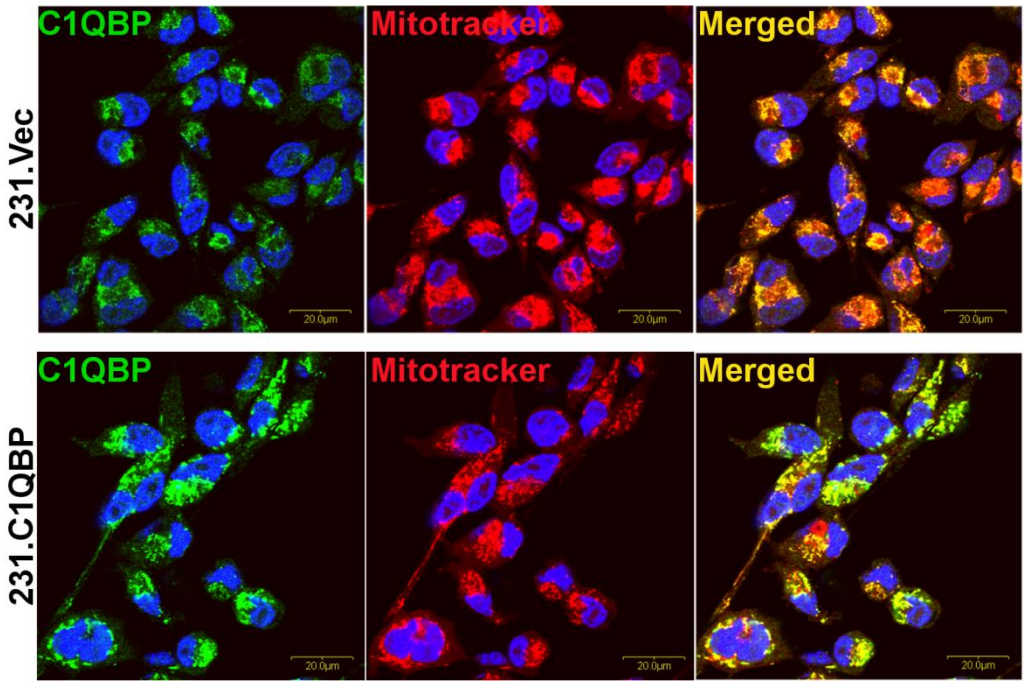

Figure 3.28. Immunofluorescence images of MDA-MB-231 cells overexpressing C1QBP. C1QBP-overexpressing cells showed more intense FITC staining (green), indicating a higher presence of C1QBP protein compared to cells transfected with empty vector. When the images were merged with the Mitotracker dye, overexpression of C1QBP protein was primarily observed in the mitochondria of the cells. Scale bar: 20 µm.

3.9 Association of C1QBP overexpression and cell proliferation

After establishing C1QBP-overexpressing cells, cell proliferation was measured using MTS or alamarBlue assays. The stable overexpression of C1QBP in MDA-MB-231 cells increased cell growth, as measured by MTS at 72 h after seeding (Figure 3.29A). Growth curve of the C1QBP-overexpressing cells, plotted using readings from alamarBlue taken over 96 h, also showed a remarkable escalation compared to control cells (Figure 3.29B).

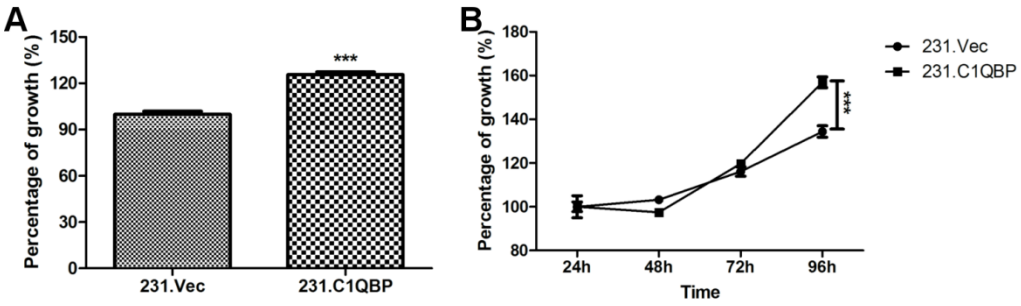

Figure 3.29. Stable overexpression of C1QBP increased cell growth in MDA-MB-231 breast cancer cell line. (A) Measurements done by MTS assay showed that the overexpression of C1QBP significantly increased cell viability in MDA-MB-231 cells. Bar chart are presented as mean(%) ± SEM. ***P<0.001. (B) The growth curve of MDA-MB-231 stably overexpressing C1QBP displayed accelerated growth rate compared to control cells. The graph was generated by alamarBlue fluorescence measurements taken, up till 96 h. Each point in the growth curve was presented as mean(%) ± SEM. Statistical analysis was done by two-way ANOVA. ***P<0.001. Experiments were done in quadruplicates and repeated twice.

Cell cycle analysis was then carried out by flow cytometry at 72 h after seeding (Figure 3.30A). The cell cycle profile revealed that a lower percentage of C1QBP-overexpressing cells was in sub-G1 phase (231.Vec: 2.46% vs 231.C1QBP: 1.33%, P=0.0234) and the G1 phase (231.Vec: 70.02% vs 231.C1QBP: 64.83%, P=0.0155), compared to the control cells (Figure 3.30B). Concomitantly, there was an increase percentage of C1QBP-overexpressing cells in the S phase (231.Vec: 7.31% vs 231.C1QBP: 10.37%,

P=0.0185) and G2/M phase (231.Vec: 20.45% vs 231.C1QBP: 23.99%, *P*=0.0195). Overall, the cell cycle profiling has implied that C1QBP promotes cell cycle progression.

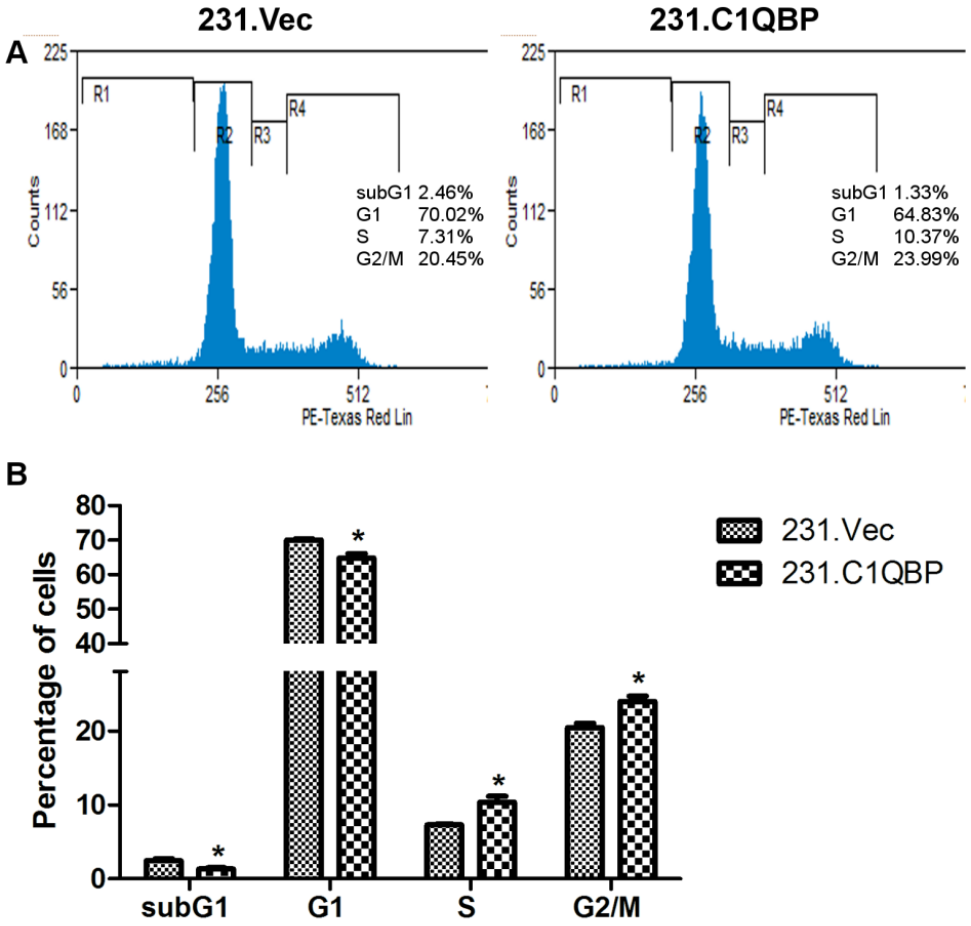

Figure 3.30. Overexpression of C1QBP promoted progression of cell cycle from the G1 phase to the G2/M phase. (A) Representation of the cell cycle profiles obtained by flow cytometry from 231.Vec and 231.C1QBP cells, respectively. (B) Percentage of cells within each phase of the cell cycle detected by flow cytometry by PI staining. Percentages are presented as mean ± SEM. **P*<0.05. Experiments were done in triplicates and repeated twice.

Since cell cycle progression was dysregulated after overexpression of C1QBP in MDA-MB-231 cells, cell cycle regulatory proteins for the G1 to S progression were measured. In C1QBP-overexpressing cells, there was a significant increase of CDK6 (*P*=0.0115) and Cyclin D1 (*P*=0.0035), proteins involved in the G1 to S phase checkpoint (Figure 3.31). Contrary to the

findings after knockdown of C1QBP, the expression of CDK4, another protein involved in the G1 to S phase checkpoint was not affected. CDC25a, was also not affected in C1QBP-overexpressing cells.

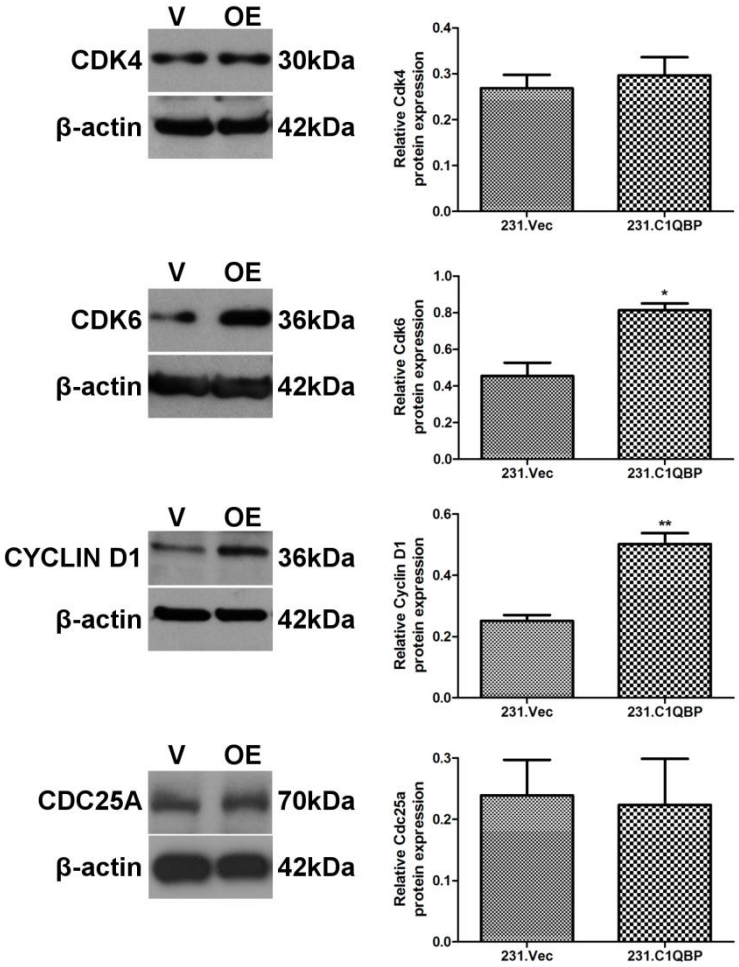

Figure 3.31. Expression of cell cycle proteins in C1QBP-overexpressing cells. Left panel: Representations of western blots for the respective proteins and its molecular weight. The first lane, V, represents protein from 231.Vec cells and the second lane, OE, represents protein from 231.C1QBP cells. Right panel: Relative quantification of protein expression by densitometry analysis. The expression of CDK6 and Cyclin D1 were significantly upregulated in C1QBP-overexpressing cells. The protein level of CDK4 and CDC25A remained unchanged. Relative protein expression are presented as mean ± SEM. **P*<0.05, ***P*<0.01. Experiments were done in triplicates and repeated twice.

3.10 Effect of C1QBP overexpression on cell migration and cell invasion

3.10.1 Effect of C1QBP overexpression on cell migration

The effect of C1QBP overexpression in MDA-MB-231 breast cancer cell line on cell migration was evaluated using the transwell migration system. The stable overexpression of C1QBP increased the cells' migration capability through the polycarbonate membrane (Figure 3.32A). Quantitatively, the number of C1QBP-overexpressing cells migrating through the membrane, was higher compared to the control cells (Figure 3.32B, *P*=0.0262).

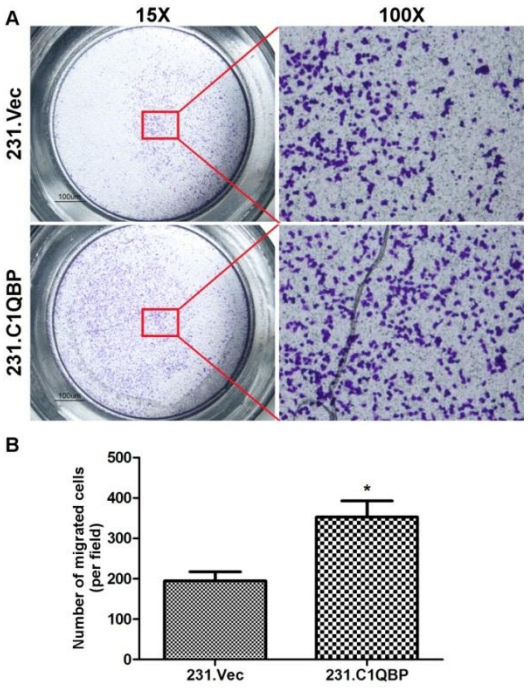

Figure 3.32. MDA-MB-231 breast cancer cells overexpressing C1QBP demonstrated a higher ability to migrate through the membrane of the transwell inserts. (A) Representative images of C1QBP-overexpressing MDA-MB-231 cells and control cells migrating through the transwell membrane after incubation at 37°C in 5% CO_2 for 20 h. Images were taken at 15X and 100X magnification. (B) Bar chart showed that a higher number of cells migrated through the transwell membrane from the C1QBP-overexpressing cells group, compared to the control group. The average number of migratory cells/field for each insert was obtained from 5 fields per insert. Data shown are presented as mean number of migrated cells ± SEM. **P*<0.05. Experiments were done in triplicates and repeated twice.

3.10.2 Changes in cytoskeletal structure of C1QBP-overexpressing cells

As cell migration was affected after overexpression of C1QBP in MDA-MB-231 cells, the cytoskeletal structure and the expression of vinculin, a focal adhesion protein was ascertained in C1QBP-overexpressing cells. This was done by treatment of cells with phalloidin to stain F-actin and immunostaining with vinculin. As shown in Figure 3.33, C1QBP-overexpressing cells displayed prominent actin stress fibres and punctate vinculin staining as compared to control cells, indicating changes in cytoskeletal structure and diminished focal adhesion.

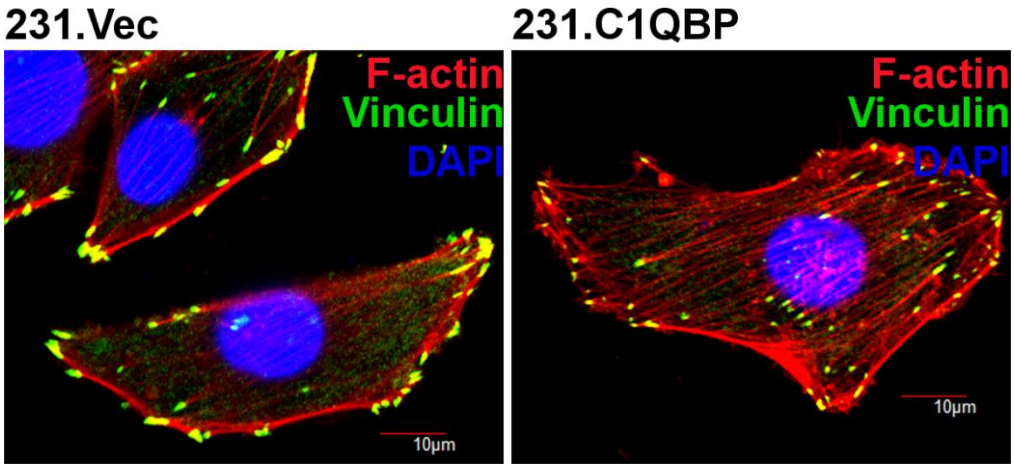

Figure 3.33: Immunostaining of F-actin and vinculin in C1QBP-overexpressing cells. C1QBP-overexpressing cells displayed prominent actin stress fibres and punctate vinculin staining as compared to control cells. Scale bar: 10 μm.

3.10.3 Effect of C1QBP overexpression on cell invasion

Cell invasion was also carried out using the transwell invasion system. The overexpression of C1QBP in MDA-MB-231 cells increased the invasiveness of the cells compared to control cells (Figure 3.34A). The number of C1QBP-overexpressing cells that were able to invade through the membrane was significantly higher compared to the control cells (Figure 3.34B, *P*=0.0151).

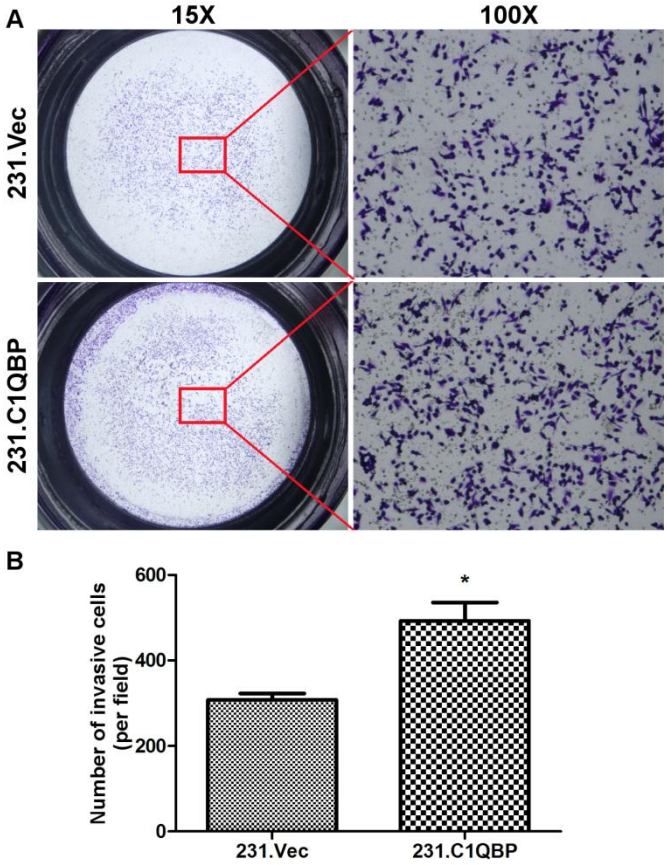

Figure 3.34. Cell invasion was increased in C1QBP-overexpressing cells. (A) Representative images of the transwell inserts and the corresponding field showed an apparent increase of invasion from the C1QBP-overexpressing cells compared to control cells. Images were taken at 15X and 100X magnification. (B) A count of invading cells confirmed that C1QBP-overexpressing cells possessed an augmented ability to invade compared to control cells. Data are presented as mean ± SEM. **P*<0.05. Experiments were done in triplicates and repeated twice.

3.11 Cytotoxic effect of doxorubicin in C1QBP-overexpressing cells

Since treatment with Doxorubicin hydrochloride produced a marginally significant difference in MDA-MB-231 cells after knockdown of C1QBP, the effect of Doxorubicin hydrochloride on C1QBP-overexpressing cells was evaluated. MDA-MB-231 cells overexpressing C1QBP were observed to be more resistant to Doxorubicin hydrochloride treatment compared to the control cells (Figure 3.35). Evaluation of the IC50 of Doxorubicin hydrochloride treatment showed that C1QBP-overexpressing cells possessed a higher IC50 (1.096 μM) compared to the control cells (0.9126 μM). The difference between the two curves was also statistically significant as determined by two-way ANOVA (*P*=0.0117).

A

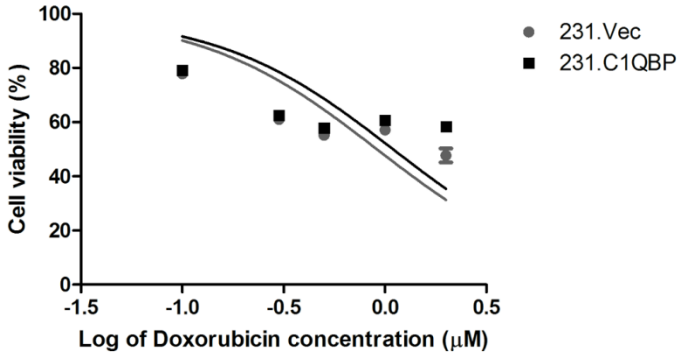

B

Drug	IC50 of drug (μM)		Statistical analysis *(Two-way ANOVA)*
	231. Vec	231. C1QBP	
Doxorubicin hydrochloride	0.9126	1.096	0.0117*

*$P<0.05$

Figure 3.35. (A) Increased chemoresistance to Doxorubicin hydrochloride was observed in MDA-MB-231 cells overexpressing C1QBP. Values are presented as mean ± SEM. (B) IC50 of Doxorubicin hydrochloride on MDA-MB-231 cells with and without overexpression of C1QBP. *$P<0.05$. Experiments were done in quadruplicates and repeated twice.

3.12 Expression of C1QBP in parental MCF7 cells and Doxorubicin hydrochloride-resistant MCF7 cell line

Next, the expression of C1QBP in Doxorubicin hydrochloride-resistant MCF7 cells was compared to parental MCF7 cells. The dose of Doxorubicin hydrochloride used for treatment of the MCF7 cell lines, was obtained from a 'kill-curve' of cells treated with Doxorubicin hydrochloride, at a range of concentration for 48 h. The IC25 concentration of Doxorubicin hydrochloride i.e., 0.6 µM was used to treat the parental MCF7 and MCF7R cell line to reduce cell death rate. The cells were treated for 0 to 48 h, and the protein expression of C1QBP was obtained. The constitutive expression of C1QBP in MCF7 cells was lower than in MCF7R cells. The treatment of these cells with Doxorubicin hydrochloride for 12 h, 24 h and 48 h gradually increased the expression of C1QBP in MCF7 cells. However, the expression of C1QBP in MCF7R cells remained unchanged.

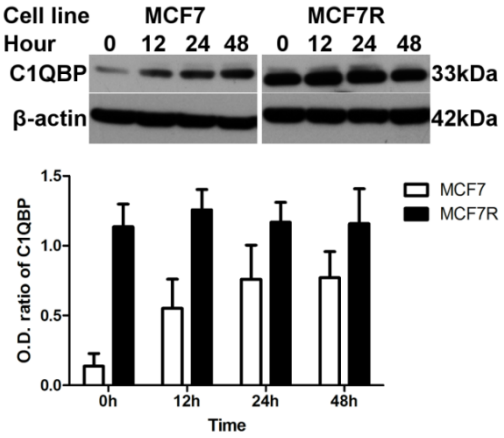

Figure 3.36. Expressions of C1QBP in parental MCF7 and Doxorubicin hydrochloride-resistant MCF7 cell line, after treatment with Doxorubicin hydrochloride in a time-dependent fashion. The expression of C1QBP in parental MCF7 cells was increased in a time-dependent manner after treatment with Doxorubicin hydrochloride, while the C1QBP expression was not altered in Doxorubicin hydrochloride-resistant MCF7 cell line. Experiments were done in triplicates and repeated twice.

3.13 Genome-wide analysis of MDA-MB-231 cells with diminished C1QBP expression

Genome-wide analysis using gene microarray, is a widely used technology enabling the simultaneous study of the expression of many genes. Previously, the study has shown that the knockdown of C1QBP affected the function and characteristics of MDA-MB-231 cells. Gene expression profiling of MDA-MB-231 cells with knockdown of C1QBP, was carried out to gain an understanding of the underlying molecular pathway that could possibly be involved in its functional changes.

3.13.1 Quality control of total RNA extracted from MDA-MB-231 cells with diminished expression of C1QBP

Good quality total RNA is required to obtain reliable data from the microarray. Extracted RNA was first assessed by obtaining the A_{260}/A_{280} ratio using Nanodrop ND-1000. Only RNA samples with A_{260}/A_{280} ratio of more than 1.9 were considered. The silencing efficiency was then confirmed by real-time PCR to be approximately 90% before further processing (Figure 3.37).

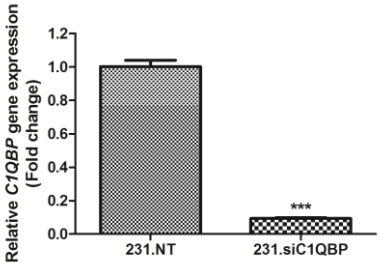

Figure 3.37. Silencing efficiency of siC1QBP in MDA-MB-231 breast cancer cell lines that were used for the gene microarray analysis. The gene expression of *C1QBP* was diminished by 90%. Relative gene expression are presented as mean ± SEM. ****P*<0.001.

The quality of RNA was again verified using spectrophotometric methods. All samples showed A_{260}/A_{280} ratios of between 2.00-2.07, with concentrations ranging from 389.65 ng/µl to 484.86 ng/µl (Table 3.9). The RNA Integrity Number (RIN) reflects RNA integrity. The RIN score ranges from 1 to 10, where the score 10 indicates a completely intact RNA. All samples have RIN of 9.8 to 10, demonstrating that RNA integrity was satisfactory (Table 3.9).

Table 3.9. Quality control of RNA samples determined by spectrophotometric reading

Sample	**OD_{260}/OD_{280}**	**Concentration (ng/µl)**	**RIN**
231.siC1QBP A	2.026	448.24	9.9
231.siC1QBP B	2.004	458.98	10
231.siC1QBP C	2.074	450.68	9.9
231.NT A	2.051	389.65	9.8
231.NT B	2.047	469.73	10
231.NT C	2.077	484.86	9.8

The RIN was obtained from the Agilent Bioanalyzer which produced a gel-like image and electrophoregram from its analyses. The gel-like image showed two distinct bands indicating mostly intact RNA (Figure 3.38A). The electrophoregram of the 6 samples, showed two distinct ribosomal peaks representing the 18S fragment and 28S fragment (Figure 3.38B). The first peak represented the marker, while the 2^{nd} and 3^{rd} peaks represented the 18S fragment and 28S fragment, respectively. The RIN values obtained was without anomalies and showed a highly intact RNA.

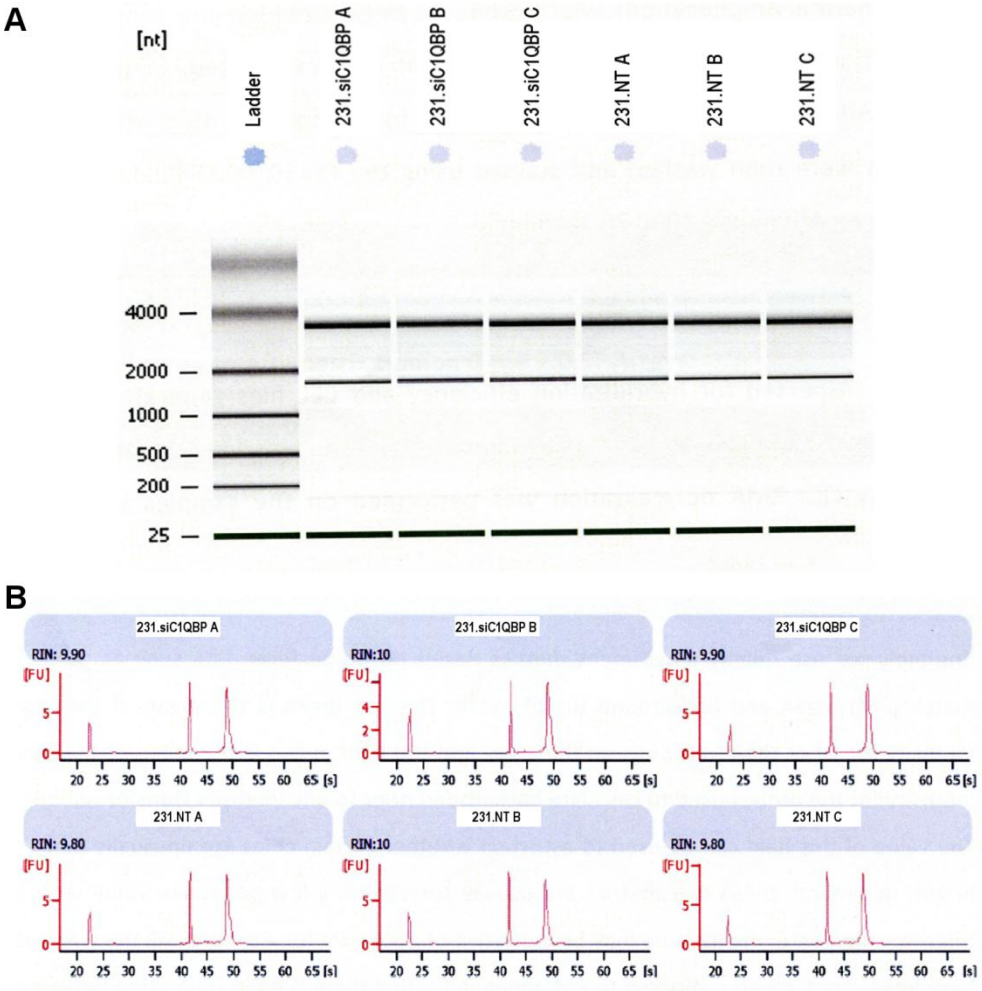

Figure 3.38. The Agilent Bioanalyzer analysis produced (A) a gel-like image and (B) electrophoregram of the 6 samples.

Ribo-SPIA assay was carried out using 100 ng total RNA according to Origen Labs SOP. The processing of the samples yielded good purity with a high concentration, and the results are shown in Table 3.10.

Table 3.10. Spectrophotometric reading of purified sense target cDNA

Sample	**OD_{260}/OD_{280}**	**Concentration (µg/µl)**	**Yield (µg)**
231.siC1QBP A	1.844	539.73	8.10
231.siC1QBP B	1.753	528.89	7.93
231.siC1QBP C	1.840	467.92	7.02
231.NT A	1.837	531.15	7.97
231.NT B	1.822	471.53	7.07
231.NT C	1.775	385.72	5.79

3.13.2 Array quality control (QC) metrics

The arrays were scanned and images were analysed by AGCC (GeneChip Command Console Software). CEL files generated from AGCC were imported into the Expression Console 1.3 software and subsequently underwent RMA normalization to generate the quality control (QC) metrics, which were used to determine data quality.

Generally, the probe level data was used as the quality assessment metrics. The data consisted of perfect match (PM) mean and background (bgrd) mean. PM mean is the mean of the raw intensity for all the PM probes, while bgrd mean is the mean of the raw intensity for the probes used to calculate background prior to any intensity transformations. These could be used to assess whether the chip produced proper signal intensity. All the 6 arrays produced lower bgrd_mean, compared to PM_mean, pointing to good separation between background and true signal (Figure 3.39A).

Apart from that, the Pos vs Neg area under the curve (AUC), which was used to compare signal values of positive controls to the negative controls, were used as another QC metric. A group of recognized exon based probe sets from recognized housekeeping genes, was used as the positive control. The negative control consisted of known intron based probe sets from known housekeeping genes, which usually have very low signal values. The ROC curve was plotted by evaluating the separation of the positive and negative controls, with the postulation that the negative and positive controls represents false and true positive, respectively. Perfect separation generates an

AUC of 1 while an AUC of 0.5 denotes no separation. The 6 samples used in the study generated acceptable values of above 0.77 (Figure 3.39B).

Proper hybridization was usually assessed by the signal intensity from bacterial spike control. Pre-labeled bacterial spike controls prepared in staggered concentration, were hybridized to probe sets. All the samples showed correct concentration of bacterial spike controls, indicating good hybridization (Figure 3.39C).

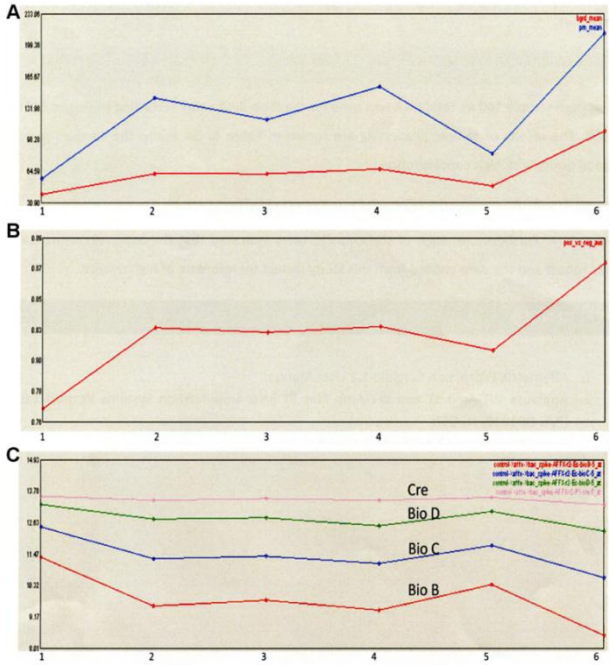

Figure 3.39. Array QC metrics. (A) PM_mean and Bgrd_mean. The 6 samples produced a lower bgrd_mean than PM_mean indicating good quality data. (B) Pos vs Neg AUC. All 6 samples have Pos vs Neg AUC values above 0.77. (C) Bacterial spike control for all 6 samples showed similar intensity for the 4 spike controls in staggered concentration, which indicated good hybridization. 1: 231.siC1QBP A, 2: 231.siC1QBP B, 3: 231.siC1QBP C, 4: 231.NT A, 5: 231.NT B, 6: 231.NT C.

The QC test for total RNA processing and array chip indicated that the assay performance was robust and the data produced should be of high quality.

3.13.3 Data analysis of Human GeneChip ST2.0 microarray

Using FS450_0002 fluidics, the hybridized sense target cDNA was stained and subsequently, scanned by Affymetrix 3000 7G scanner to produce the raw data of all probesets in the form of CEL files. The hierarchical clustering showed that the replicates of 231.siC1QBP had different expressions from the replicates of 231.NT (Figure 3.40A). The two groups showed that differential gene expressions existed after C1QBP was silenced.

A volcano plot was constructed from the data to visualize the changes of gene expression after knockdown of C1QBP (Figure 3.40B). Although a majority of the genes were not affected, a number of genes were differentially expressed by more than 1.5 folds with high statistical significance. A total of 77 genes were significantly up-regulated and 109 genes were down-regulated after knockdown of C1QBP. The list of these genes is shown in Supplementary Table 1.

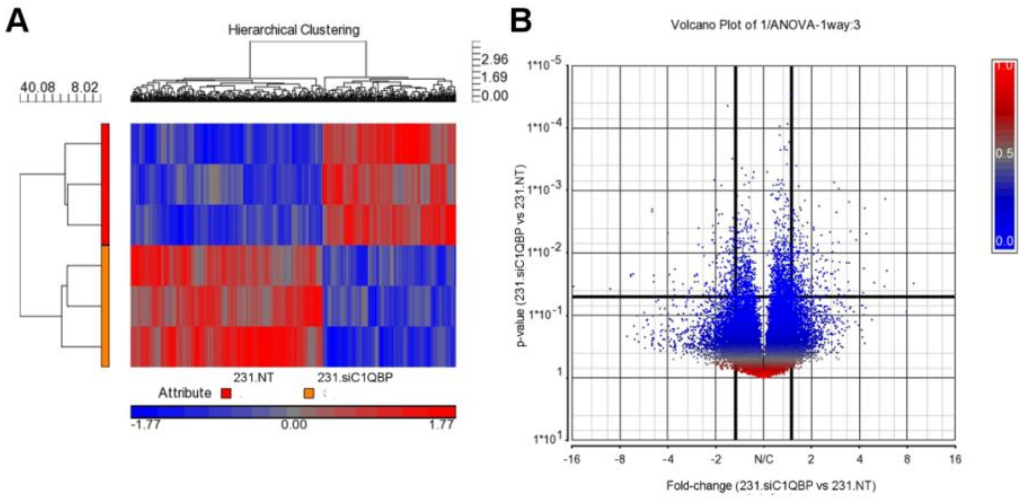

Figure 3.40. (A) Hierarchical clustering and (B) volcano plot of the Human GeneChip ST 2.0 microarray data. In the volcano plot, spots on the outside of the thick vertical lines and above the thick horizontal line have an absolute fold change of 1.5 with $P<0.05$.

3.13.4 Validation of differential gene expressions based on microarray data analysis

Five up-regulated and 10 down-regulated genes were examined using real-time PCR for validation purposes. The majority of the genes showed consistent patterns when compared to the microarray data (Figure 3.41).

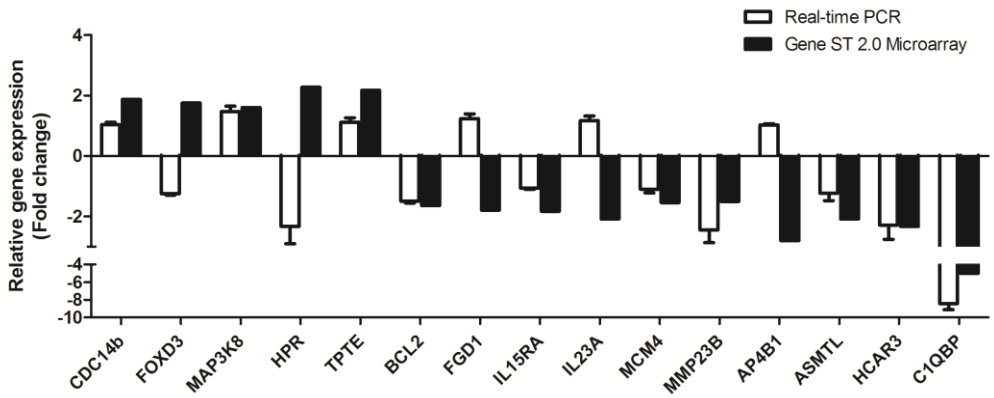

Figure 3.41. Validation of up-regulated and down-regulated genes obtained from the Gene ST 2.0 microarray data. The relative gene expression was obtained from real-time PCR and values are presented as mean of triplicates ± SEM. This was compared to the fold change value obtained from the gene microarray. Experiments were done in triplicates and repeated three times.

3.13.5 Functional classification of microarray data

To have a general understanding of the data, the differentially expressed genes were clustered based on enrichment of gene ontologies for biological functions, using the Partek Genomics Suite 6.6 software (Figure 3.42). Notably, the differentially expressed genes were primarily enriched for growth functions which were consistent with the clinical and *in vitro* data.

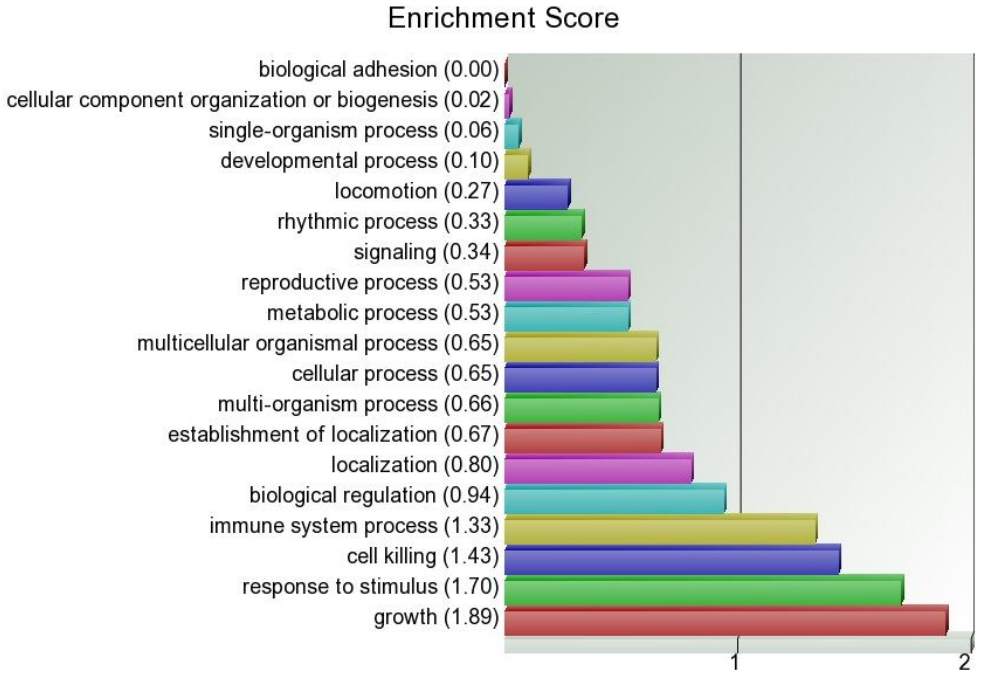

Figure 3.42. Enrichment scores for biological functions of genes affected by knockdown of C1QBP in MDA-MB-231 breast cancer cells.

In addition, the DAVID (Database for Annotation, Visualization and Integrated Discovery) software was also used to categorise the differentially expressed genes based on gene ontology for biological processes, as shown in Table 3.11. These genes were categorized into various functions, such as, transcription, immune response, cell motion, phosphorylation, cell cycle and others.

Table 3.11. Functional categorization of genes that were affected after knockdown of C1QBP in MDA-MB-231 breast cancer cells

Function	Gene ID	Gene name	Gene Entrez ID
Transcription elongation factor	TCEANC	Transcription elongation factor A (SII) N-terminal and central d	170082
	TCEB3C	Transcription elongation factor B polypeptide 3C (elongin A3)	728929
	TCEA2	Transcription elongation factor A (SII), 2	6919
Metal-ion binding	FGD1	FYVE, RhoGEF and PH domain containing 1	2245
	ZBTB9	Zinc finger and BTB domain containing 9	221504
	QTRT1	Queuine tRNA-ribosyltransferase 1	81890
	ZFP112	Zinc finger protein 112 homolog	7771
	TRIM65	Tripartite motif containing 65	201292
	OSR1	Odd-skipped related 1	130497
	RASGRP1	RAS guanyl releasing protein 1 (calcium and DAG-regulated)	10125
	ZNF735	Zinc finger protein 735	168417
	TCEA2	Transcription elongation factor A (SII), 2	6919
	DNAJA4	DnaJ (Hsp40) homolog, subfamily A, member 4	55466
	ZNF575	Zinc finger protein 575	284346
	CRIP1	Cysteine-rich protein 1 (intestinal)	1396
	BRF1	RNA polymerase III transcription initiation factor 90	2972
	MTA2	Metastasis associated 1 family, member 2	9219
	SIRT4	Sirtuin 4	23409
	KLF15	Kruppel-like factor 15	28999
	ZNF37A	Zinc finger protein 37A	7587
	ZSWIM5	Zinc finger, SWIM-type containing 5	57643
	TRIM56	Tripartite motif containing 56	81844
	RNF44	Ring finger protein 44	22838
	EBF4	Early B-cell factor 4	57593

Function	Gene ID	Gene name	Gene Entrez ID
	ZFYVE27	Zinc finger, FYVE domain containing 27	118813
	MMP23B	Matrix metallopeptidase 23B	8510
	TOP3A	Topoisomerase (DNA) III alpha	7156
	ZNHIT1	Zinc finger, HIT-type containing 1	10467
	UPF1	UPF1 regulator of nonsense transcripts homolog	5976
	MAP3K8	Mitogen-activated protein kinase kinase kinase 8	1326
	POLL	Polymerase (DNA directed), lambda	27343
	KCND1	Potassium voltage-gated channel, Shal-related subfamily, member 1	3750
	NME3	NME/NM23 nucleoside diphosphate kinase 3	4832
	KCNK10	Potassium channel, subfamily K, member 10	54207
	SMOC2	SPARC related modular calcium binding 2	64094
	ITIH1	Inter-alpha-trypsin inhibitor heavy chain 1	3697
	TREX2	Three prime repair exonuclease 2	11219
	SNTN	Sentan, cilia apical structure protein	132203
Neurogenesis	PSPN	Persephin	5623
	OSR1	Odd-skipped related 1	130497
	BCL2	B-cell CLL/lymphoma 2	596
	GREM1	Gremlin 1, DAN family BMP antagonist	26585
	LCE2A	Late cornified envelope 2A	353139
Regulation of transcription	POLL	Polymerase (DNA directed), lambda	27343
	SOX10	SRY (sex determining region Y)-box 10	6663
	ZBTB9	Zinc finger and BTB domain containing 9	221504
	MTA2	Metastasis associated 1 family, member 2	9219

Function	Gene ID	Gene name	Gene Entrez ID
	KLF15	Kruppel-like factor 15	28999
	ZFP112	Zinc finger protein 112 homolog	7771
	MCM4	Minichromosome maintenance complex component 4	4173
	ZNF37A	Zinc finger protein 37A	7587
	HIST2H4B	Histone cluster 2, H4b	8370
	HIF1A	Hypoxia inducible factor 1, alpha subunit (basic helix-loop	3091
	EBF4	Early B-cell factor 4	57593
	GTF2IRD1	GTF2I repeat domain containing 1	9569
	HES2	Hairy and enhancer of split 2	54626
	TOP3A	Topoisomerase (DNA) III alpha	7156
	HIST1H3B	Histone cluster 1, H3b	126961
	ZNF735	Zinc finger protein 735	168417
	TCEA2	Transcription elongation factor A (SII), 2	6919
	ZNF575	Zinc finger protein 575	284346
	NAT14	N-acetyltransferase 14 (GCN5-related, putative)	57106
	FOXD3	Forkhead box D3	27022
	TCEANC	Transcription elongation factor A (SII) N-terminal and central d	170082
	POLR2J	Polymerase (RNA) II (DNA directed) polypeptide J, 13.3kDa	5439
	BRF1	RNA polymerase III transcription initiation factor 90	2972
	UPF1	UPF1 regulator of nonsense transcripts homolog	5976
	TCEB3C	Transcription elongation factor B polypeptide 3C (elongin A3)	728929
	BCL2	B-cell CLL/lymphoma 2	596
	PSMD9	Proteasome (prosome, macropain) 26S subunit, non-ATPase, 9	5715
	VOPP1	Vesicular, overexpressed in cancer, prosurvival protein 1	81552
	CDC14B	Cell division cycle 14B	8555
	QTRT1	Queuine tRNA-ribosyltransferase 1	81890

Function	Gene ID	Gene name	Gene Entrez ID
	WDR55	WD repeat domain 55	54853
	OSR1	Odd-skipped related 1	130497
	IL15RA	Interleukin 15 receptor, alpha	3601
	TREX2	Three prime repair exonuclease 2	11219
	NLE1	Notchless homolog 1 (Drosophila)	54475
Immune response	MICA	MHC class I polypeptide-related sequence A	4276
	IL23A	Interleukin 23, alpha subunit p19	51561
	ITIH1	Inter-alpha-trypsin inhibitor heavy chain 1	3697
	BCL2	B-cell CLL/lymphoma 2	596
	KIR3DL1	Killer cell immunoglobulin-like receptor, three domains, long c	3811
	POLL	Polymerase (DNA directed), lambda	27343
	IGLV1-44	Immunoglobulin lambda variable 1-44	3538
	C1QBP	Complement component 1, q subcomponent binding protein	708
	HLA-L	Major histocompatibility complex, class I, L (pseudogene)	3139
	CLEC4C	C-type lectin domain family 4, member C	170482
	TPSAB1	Tryptase alpha/beta 1	7177
	GAL	Galanin/GMAP prepropeptide	51083
	HIF1A	Hypoxia inducible factor 1, alpha subunit (basic helix-loop	3091
	HPR	Haptoglobin-related protein	3250
Hormone activity	RLN1	Relaxin 1	6013
	GAL	Galanin/GMAP prepropeptide	51083
	POMC	Proopiomelanocortin	5443
	MMP23B	Matrix metallopeptidase 23B	8510
Phosphorylation activity	CDC14B	Cell division cycle 14B	8555
	BCL2	B-cell CLL/lymphoma 2	596
	CCDC155	Coiled-coil domain containing 155	147872
	TPTE	Transmembrane phosphatase with tensin homology	7179

Function	Gene ID	Gene name	Gene Entrez ID
	MAP3K8	Mitogen-activated protein kinase kinase kinase 8	1326
	PI4KAP2	Phosphatidylinositol 4-kinase, catalytic, alpha pseudogene 2	375133
	ADRBK2	Adrenergic, beta, receptor kinase 2	157
	TSSK3	Testis-specific serine kinase 3	81629
Regulation of cell motion	HIF1A	Hypoxia inducible factor 1, alpha subunit (basic helix-loop	3091
	BCL2	B-cell CLL/lymphoma 2	596
	GREM1	Gremlin 1, DAN family BMP antagonist	26585
Enzymatic activity	TPSAB1	Tryptase alpha/beta 1	7177
	TPSD1	Tryptase delta 1	23430
	HPR	Haptoglobin-related protein	3250
	MMP23B	Matrix metallopeptidase 23B	8510
	USP50	Ubiquitin specific peptidase 50	373509
	ASB18	Ankyrin repeat and SOCS box containing 18	401036
	PSMD9	Proteasome (prosome, macropain) 26S subunit, non-ATPase, 9	5715
	CDC14B	Cell division cycle 14B	8555
	TREX2	Three prime repair exonuclease 2	11219
	PNPLA6	Patatin-like phospholipase domain containing 6	10908
	TPTE	Transmembrane phosphatase with tensin homology	7179
Homeostasis	HIF1A	Hypoxia inducible factor 1, alpha subunit (basic helix-loop	3091
	BCL2	B-cell CLL/lymphoma 2	596
	NARFL	Nuclear prelamin A recognition factor-like	64428
	SLC2A4	Solute carrier family 2 (facilitated glucose transporter), member	6517
	HPR	Haptoglobin-related protein	3250
	TFF1	Trefoil factor 1	7031
Stress response	POLL	Polymerase (DNA directed), lambda	27343

Function	Gene ID	Gene name	Gene Entrez ID
	MICA	MHC class I polypeptide-related sequence A	4276
	HIF1A	Hypoxia inducible factor 1, alpha subunit (basic helix-loop	3091
	UPF1	UPF1 regulator of nonsense transcripts homolog	5976
	BCL2	B-cell CLL/lymphoma 2	596
	TREX2	Three prime repair exonuclease 2	11219
	TOP3A	Topoisomerase (DNA) III alpha	7156
	MCM4	Minichromosome maintenance complex component 4	4173
Response to hormone stimulus	BCL2	B-cell CLL/lymphoma 2	596
	TFF1	Trefoil factor 1	7031
	GAL	Galanin/GMAP prepropeptide	51083
Sensory perception	OR2T4	Olfactory receptor, family 2, subfamily T, member 4	127074
	OR14I1	Olfactory receptor, family 14, subfamily I, member 1	401994
	ADRBK2	Adrenergic, beta, receptor kinase 2	157
	OR51F2	Olfactory receptor, family 51, subfamily F, member 2	119694
	OR5A1	Olfactory receptor, family 5, subfamily A, member 1	219982
	TAS2R19	Taste receptor, type 2, member 19	259294
	TAS2R31	Taste receptor, type 2, member 31	259290
	P2RY8	Purinergic receptor P2Y, G-protein coupled, 8	286530
	GPR20	G protein-coupled receptor 20	2843
	POMC	Proopiomelanocortin	5443
	LRP10	Low density lipoprotein receptor-related protein 10	26020
	CLEC9A	C-type lectin domain family 9, member A	283420
	IL15RA	Interleukin 15 receptor, alpha	3601
	KIR3DL1	Killer cell immunoglobulin-like receptor, three domains, long c	3811
	GAL	Galanin/GMAP prepropeptide	51083

Function	Gene ID	Gene name	Gene Entrez ID
Chromatin organization	MTA2	Metastasis associated 1 family, member 2	9219
	HIST1H3B	Histone cluster 1, H3b	126961
	HIST2H4B	Histone cluster 2, H4b	8370
Voltage-gated ion channel activity	KCND1	Potassium voltage-gated channel, Shal-related subfamily, member 1	3750
	CLCNKA	Chloride channel, voltage-sensitive Ka	1187
	KCNK10	Potassium channel, subfamily K, member 10	54207
	TPTE	Transmembrane phosphatase with tensin homology	7179
	SLC16A2	Solute carrier family 16, member 2 (thyroid hormone transporter	6567
	SLC2A4	Solute carrier family 2 (facilitated glucose transporter), member	6517
	TOMM6	Translocase of outer mitochondrial membrane 6 homolog (yeast)	100188893
	NECAP2	NECAP endocytosis associated 2	55707
	AP4B1	Adaptor-related protein complex 4, beta 1 subunit	10717
Cell death	FGD1	FYVE, RhoGEF and PH domain containing 1	2245
	MICA	MHC class I polypeptide-related sequence A	4276
	NME3	NME/NM23 nucleoside diphosphate kinase 3	4832
	ZFYVE27	Zinc finger, FYVE domain containing 27	118813
	BCL2	B-cell CLL/lymphoma 2	596
	GREM1	Gremlin 1, DAN family BMP antagonist	26585
	PNPLA6	Patatin-like phospholipase domain containing 6	10908
	GAL	Galanin/GMAP prepropeptide	51083
	RASGRP1	RAS guanyl releasing protein 1 (calcium and DAG-regulated)	10125

Function	Gene ID	Gene name	Gene Entrez ID
	MAP3K8	Mitogen-activated protein kinase kinase kinase 8	1326
Cytoskeleton	GABARAPL1	GABA(A) receptor-associated protein like 1	23766
	TREX2	Three prime repair exonuclease 2	11219
	TUBA4B	Tubulin, alpha 4b (pseudogene)	80086
	FAM110A	Family with sequence similarity 110, member A	83541
Kinase activity and nucleotide binding	MAP3K8	Mitogen-activated protein kinase kinase kinase 8	1326
	ADRBK2	Adrenergic, beta, receptor kinase 2	157
	TSSK3	Testis-specific serine kinase 3	81629
	CBWD1	COBW domain containing 1	55871
	UPF1	UPF1 regulator of nonsense transcripts homolog	5976
	MCM4	Minichromosome maintenance complex component 4	4173
	BCL2	B-cell CLL/lymphoma 2	596
	PI4KAP2	Phosphatidylinositol 4-kinase, catalytic, alpha pseudogene 2	375133
	GCDH	Glutaryl-CoA dehydrogenase	2639
	NME3	NME/NM23 nucleoside diphosphate kinase 3	4832
	TOP3A	Topoisomerase (DNA) III alpha	7156
	PCCB	Propionyl CoA carboxylase, beta polypeptide	5096
	SIRT4	Sirtuin 4	23409
	RAB44	RAB44, member RAS oncogene family	401258
	TUBA4B	Tubulin, alpha 4b (pseudogene)	80086
	PABPC1L	Poly(A) binding protein, cytoplasmic 1-like	80336
Cell cycle	UPF1	UPF1 regulator of nonsense transcripts homolog	5976
	BCL2	B-cell CLL/lymphoma 2	596
	MAP3K8	Mitogen-activated protein kinase kinase kinase 8	1326
	TREX2	Three prime repair exonuclease 2	11219
	TOP3A	Topoisomerase (DNA) III alpha	7156

Function	Gene ID	Gene name	Gene Entrez ID
	PSMD9	Proteasome (prosome, macropain) 26S subunit, non-ATPase, 9	5715
Catabolic processes	MMP23B	Matrix metallopeptidase 23B	8510
	TPSAB1	Tryptase alpha/beta 1	7177
	TPSD1	Tryptase delta 1	23430
	USP50	Ubiquitin specific peptidase 50	373509
	HPR	Haptoglobin-related protein	3250
	ASB18	Ankyrin repeat and SOCS box containing 18	401036
	PSMD9	Proteasome (prosome, macropain) 26S subunit, non-ATPase, 9	5715
	UPF1	UPF1 regulator of nonsense transcripts homolog	5976
Protein transport	TOMM6	Translocase of outer mitochondrial membrane 6 homolog (yeast)	100188893
	NECAP2	NECAP endocytosis associated 2	55707
	AP4B1	Adaptor-related protein complex 4, beta 1 subunit	10717
	RAB44	RAB44, member RAS oncogene family	401258

Besides that, pathway analysis using Partek Genomics Suite 6.6 software identified a few genes involved in the MAPK and JAK-STAT pathway (Table 3.12). The full list of the pathway analysis is available in Supplementary Table 2.

Table 3.12. Pathway analysis done on gene microarray using Partek Genomics Suite 6.6

Pathway Name	Enrichment Score	Genes
Jak-STAT signaling pathway	1.37955	IL15RA, IL23A
MAPK signaling pathway	0.743159	MAP3K8, RASGRP1

3.14 PathScan® Intracellular Signaling Array

Aside from the gene expression profile, the PathScan® Intracellular Signaling Array was used to elucidate the possible signalling pathways that were utilized by C1QBP. The array enabled the simultaneous investigation of 18 established and important signalling molecules, which are shown in Figure 3.43.

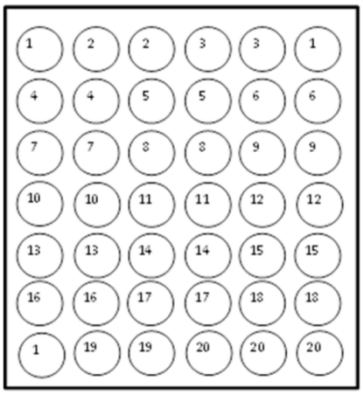

1	Positive control
2	Erk1/2 (Thr202/Tyr204)
3	Stat1 (tyr701)
4	Stat3 (Tyr705)
5	Akt (Thr308)
6	Akt (Ser473)
7	AMPKa(thr172)
8	S6 Ribosomal Protein (Ser 235/236)
9	mTOR (Ser2448)
10	Hsp27 (ser78)
11	Bad (Ser112)
12	p70 S6 Kinase (Thr389)
13	PRAS40 (Thr246)
14	p53 (ser15)
15	p38 (Thr180/Tyr182)
16	SAPK/JNK (Thr183/Tyr185)
17	PARP (Asp214)
18	Caspase-3 (Asp175)
19	GSK-3b (Ser9)
20	Negative control

Figure 3.43. Layout of the PathScan® Intracellular Signaling Array. Each array contained 42 spots. Each antibody was tested in duplicates. Three spots of positive and negative control each, were included in the array.

Protein lysate from C1QBP-overexpressing cells and control cells were prepared in triplicates and incubated with the array. The chemiluminescent signals produced from the arrays incubated with lysate from C1QBP-overexpressing cells, showed alterations for several signalling molecules, compared to the lysate from control cells (Figure 3.44A). Detailed measurements using densitometry analysis, showed that expression of phosphorylated ERK1/2 (Thr202/Tyr204) (P=0.0121) and GSK-3β (Ser9)

(*P*=0.0236) was significantly increased in C1QBP-overexpressing cells. Additionally, phosphorylation of STAT3 (Tyr705) (*P*=0.0576), AKT (Ser473) (*P*=0.0635) and S6 ribosomal protein (Ser235/236) (*P*=0.0596) was augmented with borderline significance (Figure 3.44B).

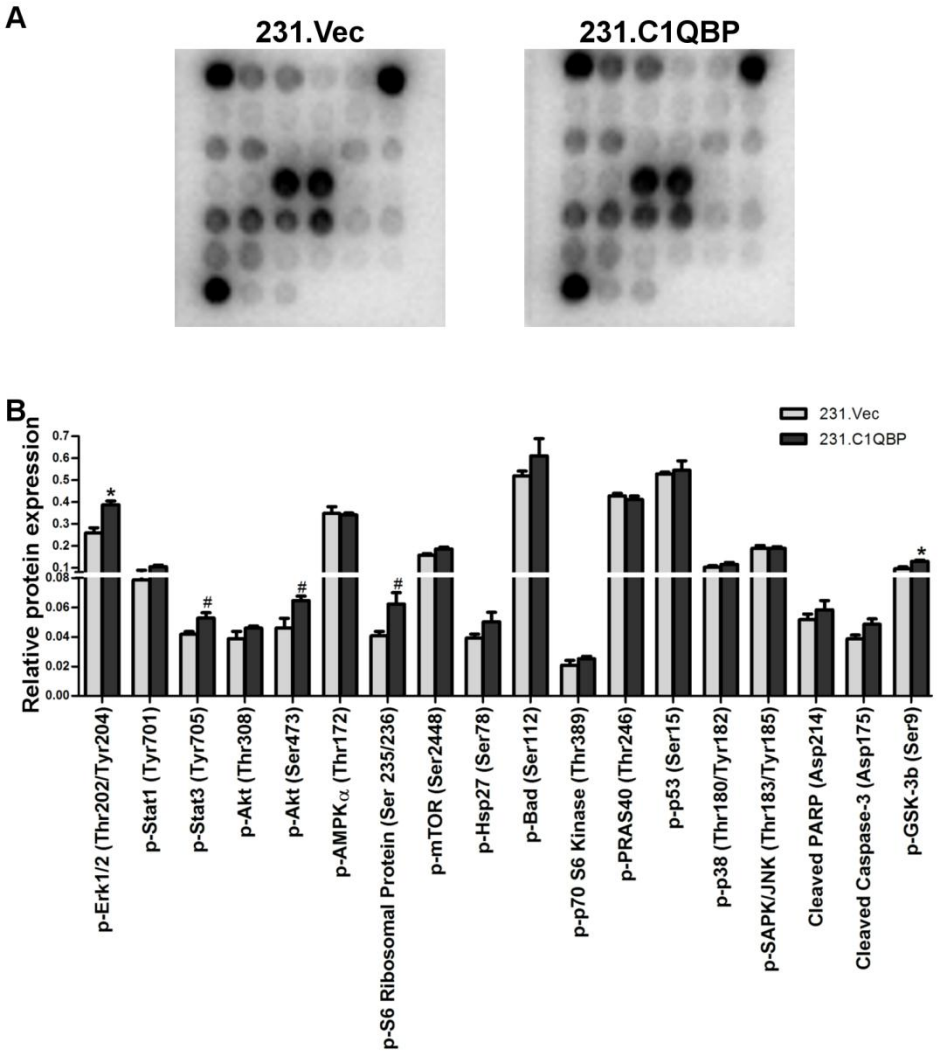

Figure 3.44. Assessment of changes in activity of signalling molecules in C1QBP-overexpressing cells via the PathScan® Intracellular Signaling Array Kit. (A) Representative images of array for 231.Vec and 231.C1QBP cells after processing. (B) Protein expression of various signalling molecules in MDA-MB-231 cells overexpressing C1QBP or empty vector. Relative protein expression was measured by obtaining the ratio of $O.D._{\text{target proteins}}$ to $O.D._{\text{positive control}}$. Values are presented as mean of triplicates ± SEM. Statistical significance was achieved at $^{*}P<0.05$. $^{\#}$ represented borderline significance, where *P*-values of p-STAT3(Tyr705), p-Akt(Ser473) and p-S6 Ribosomal Protein(Ser235/236) are 0.0576, 0.0635 and 0.0596, respectively.

3.15 Association of C1QBP with the ERK1/2 pathway

From the analysis of the PathScan® Intracellular Signaling Array, a marked increase was observed for p-ERK1/2 after overexpression of C1QBP. Together with pathway analysis from the gene microarray, differential expression of *RASGRP1* and *MAP3K8* after knockdown of C1QBP in MDA-MB-231 cells, indicated that C1QBP could potentially be involved in the MAPK/ERK pathway. Therefore, the expression of activated proteins along the MAPK/ERK pathway was evaluated. In C1QBP-overexpressing cells, the expression of p-ERK1/2 was significantly increased, validating the results obtained from the Pathscan array (P=0.0240, Figure 3.45). In addition, there was also a significant up-regulation of activated MEK1/2 in C1QBP-overexpressing cells (P=0.0441, Figure 3.45). The expression of p-MSK1 and p-c-RAF was not altered (Figure 3.45).

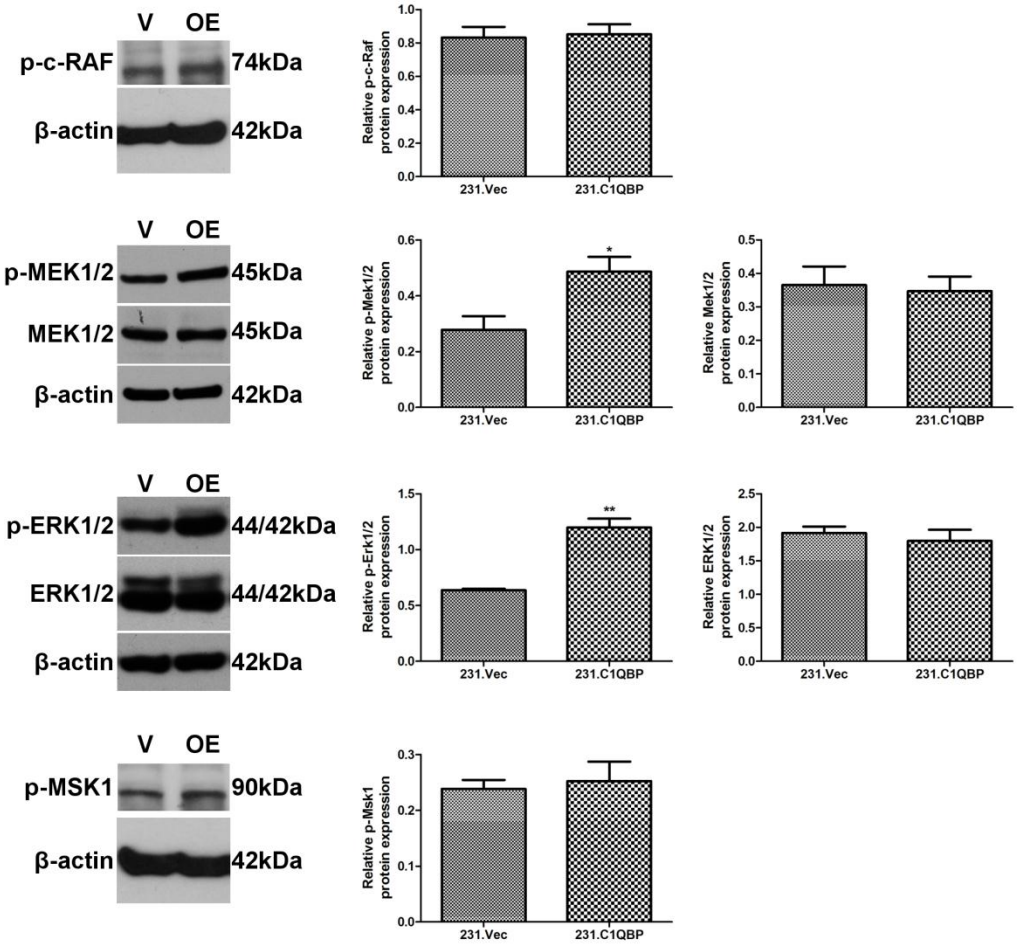

Figure 3.45. Protein expressions of p-ERK1/2 and p-ERK1/2-related proteins in MDA-MB-231 cells stably overexpressing C1QBP. The left panel shows the western blot representation of the respective proteins. V stands for 231.Vec and OE stands for 231.C1QBP. The right panel shows the densitometry analyses of the bands obtained. A statistically significant increase was observed for p-ERK1/2 and p-MEK1/2 expressions. The bar charts were presented as mean of O.D. ratio ± SEM. **P*<0.05, ***P*<0.01. Experiments were done in triplicates and repeated twice.

3.16 Association of C1QBP with the STAT3 pathway

Further analysis of the gene expression profile after knockdown of C1QBP, combined with data from Pathscan array revealed that C1QBP could also be associated to the STAT3 pathway. The gene microarray pathway analysis data detected a differential expression of *IL23A* and *IL15RA* expression – proteins involved in STAT3 pathway – after knockdown of C1QBP. Additionally, the Pathscan array showed that the overexpression of C1QBP caused an increase in p-STAT3 (Tyr705) expression. Hence, the expression of downstream targets of p-STAT3 was evaluated. Overexpression of C1QBP caused a significant increase of p-STAT3 (Tyr705) shown by western blot (P=0.0411, Figure 3.46), verifying the results obtained from the Pathscan array. The protein expression of BCL2 and MCL1 were also increased, following overexpression of C1QBP (P=0.0436 and P=0.0550, respectively, Figure 3.46). Further investigation also showed down-regulation of p53 in C1QBP-overexpressing cells (P=0.0158, Figure 3.46).

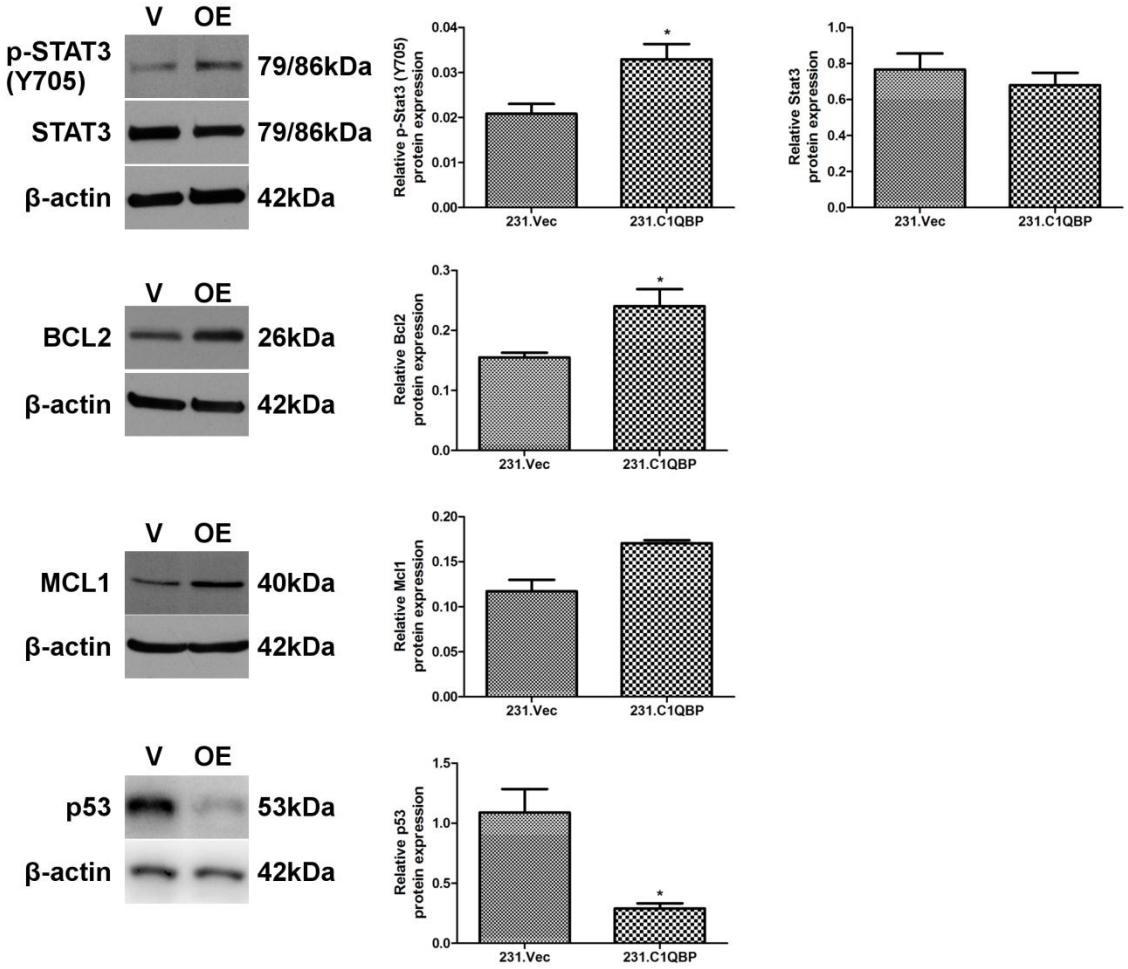

Figure 3.46. Expressions of p-STAT3(Y705) and its downstream targets after overexpression of C1QBP. The western blot representations were shown on the left side of the diagram together with its respective quantification on the right side. The overexpression of C1QBP in MDA-MB-231 led to an increase in p-STAT3(Y705), followed by up-regulation of BCL2 and MCL1, as well as down-regulation of p53. Values are presented as mean of O.D. ratio ± SEM. **P*<0.05. Experiments were done in triplicates and repeated at least twice.

3.16.1 Down-regulation of STAT3 in C1QBP-overexpressing cells

As p-STAT3 (Tyr705) has been implicated in carcinogenesis, and the data supported an association between C1QBP and p-STAT3 (Tyr705), the effects of STAT3 attenuation in C1QBP-overexpressing cells were explored. Knockdown of STAT3 using siRNA targeting STAT3 reduced the expression of p-STAT3 in C1QBP-overexpressing cells by approximately 82% (Figure 3.47B).

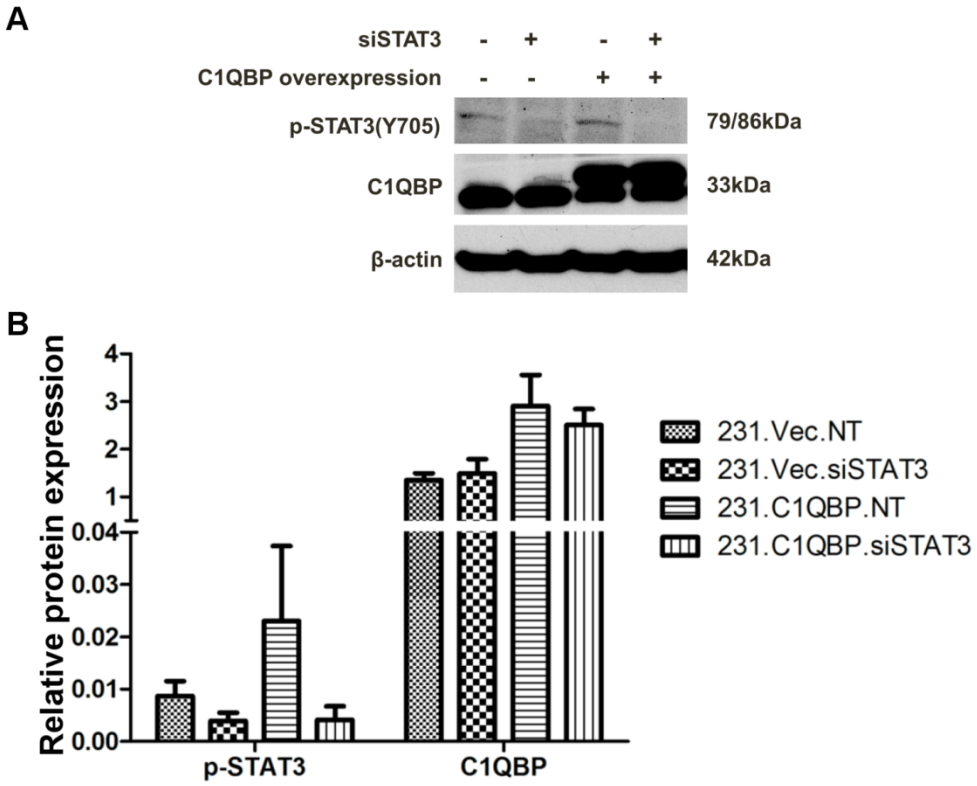

Figure 3.47. (A) Western blot representation of p-STAT3 (Y705) knockdown after siSTAT3 transfection in 231.Vec and 231.C1QBP cells. (B) Expression of p-STAT3(Y705) in C1QBP-overexpressing cells was decreased by 82% while in 231.Vec cells, p-STAT3(Y705) was decreased by 55%. Experiments were done in triplicates and repeated twice.

3.16.1.1 Effect of STAT3 attenuation in C1QBP-overexpressing cells on cell proliferation

The down-regulation of STAT3 in C1QBP-overexpressing cells was accompanied by diminished cell growth, measured by alamarBlue assay over 144 h (Figure 3.48). As perceived from Figure 3.48, the overexpression of C1QBP increased cell growth, compared to vector-expressing cells (*P*=0.0040). The knockdown of STAT3 in 231.Vec cells caused a significant decrease in cell growth (*P*=0.0257). In C1QBP-overexpressing cells, the attenuation of STAT3 significantly decreased cell growth to similar levels as 231.Vec cells with STAT3 knockdown (*P*=0.0006).

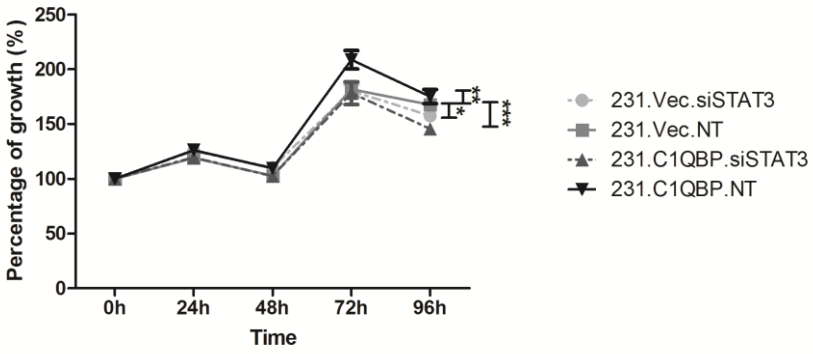

Figure 3.48. Cell growth curve of C1QBP-overexpressing cells after knockdown of STAT3. The overexpression of C1QBP increased the cell growth rate of MDA-MB-231 cells. Knockdown of STAT3 caused a drastic decrease of cell growth in 231.C1QBP and 231.Vec cells. There was no statistical difference between cell growth rate of 231.C1QBP.siSTAT3 and 231.Vec.siSTAT3 cells. ***, *P*<0.001, **, *P*<0.01, *, *P*<0.05. Experiments were done in quadruplicates and repeated twice.

3.16.1.2 Silencing of STAT3 in C1QBP-overexpressing cells altered cell migration and cell invasion

Cell migration was significantly increased after C1QBP overexpression (P<0.05). In addition, the knockdown of STAT3 in 231.Vec cells decreased cell migration (P<0.001). After knockdown of STAT3 in C1QBP-overexpressing cells, the ability of cells to migrate was significantly lowered (P<0.001) to approximately the same level as 231.Vec.siSTAT3 cells (Figure 3.49).

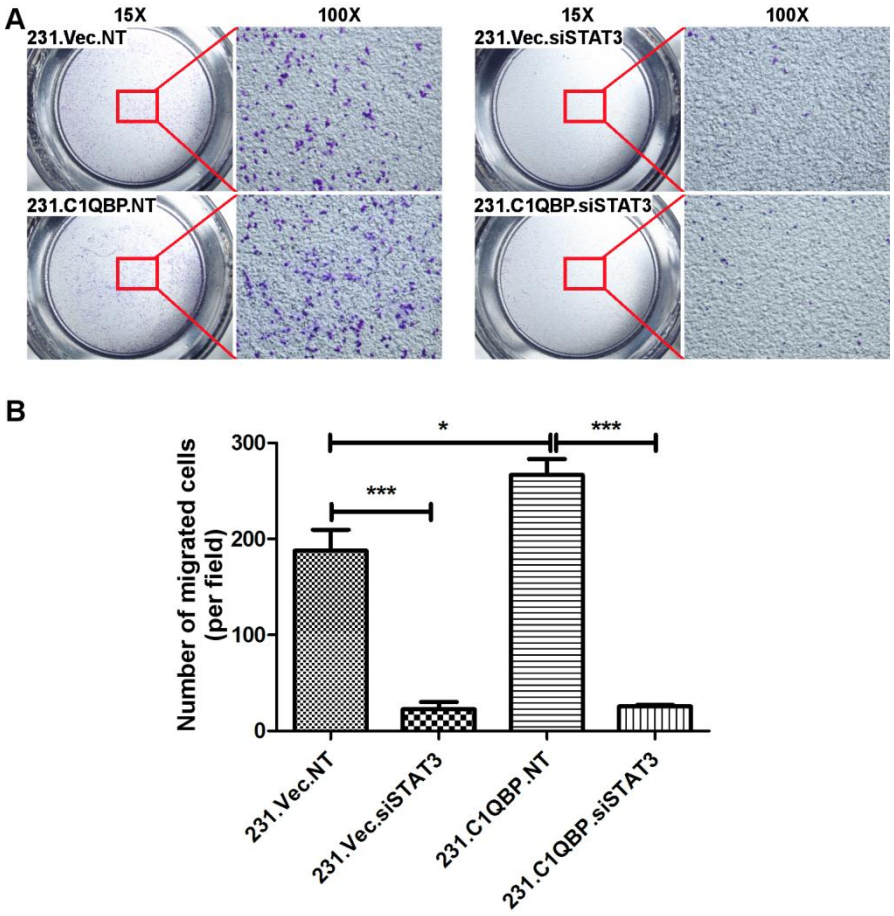

Figure 3.49. Cell migration was reduced after knockdown of STAT3 in both 231.Vec and 231.C1QBP cells. The overexpression of C1QBP increased cell migration, and the subsequent reduction of STAT3 was accompanied by a dramatic decrease in the ability of cells to migrate. Cell count are presented as mean of cells/field ± SEM. *P<0.05, ***P<0.001. Experiments were done in triplicates.

A similar phenomenon was observed for cell invasion after knockdown of STAT3 in C1QBP-overexpressing cells. Overexpression of C1QBP caused an increase of cell invasion (P<0.05). However, although a decrease of cell invasion was observed when STAT3 was knockdown in 231.Vec cells, the difference was not statistically significant. Subsequently, knockdown of STAT3 in C1QBP-overexpressing cells diminished the cell invasiveness of the cells (P<0.01, Figure 3.50).

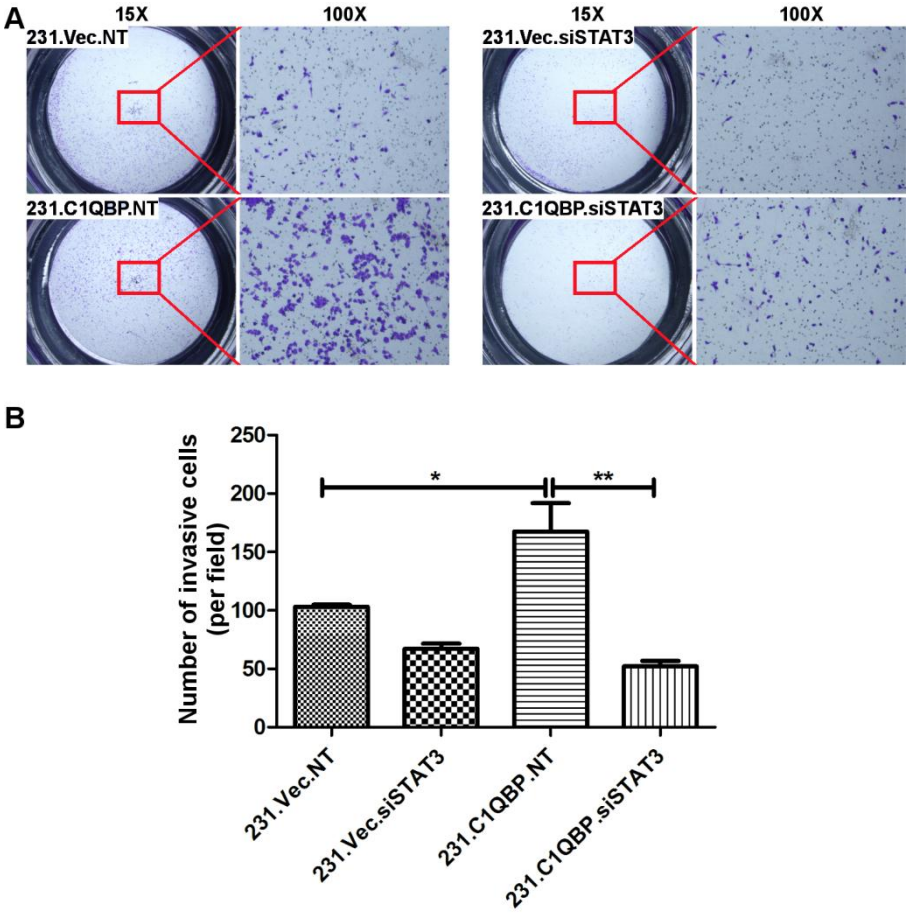

Figure 3.50. Cell invasion was decreased after knockdown of STAT3. C1QBP-overexpressing cells were more invasive compared to empty vector-expressing cells. However, the knockdown of STAT3 decreased both the invasive capabilities of 231.Vec and 231.C1QBP cells. Cell count of invasive cells are presented as mean of cells/field ± SEM. *P<0.05, **P<0.01. Experiments were done in triplicates.

3.17 SILAC-immunoprecipitation Quantitative Proteomics of C1QBP interacting partners

Next, SILAC-immunoprecipitation quantitative proteomics was carried out to determine the C1QBP interactome. Table 3.13 listed the interacting partners of C1QBP. Additional information such as Protein IDs and Peptide counts can be found in Supplementary Table 3.

Table 3.13. Interacting partners of C1QBP with a ratio H/L of above 2

Protein names	**Gene names**	**Sequence coverage [%]**	**Ratio H/L**
Complement component 1 Q subcomponent-binding protein, mitochondrial	C1QBP	51.4	67.376
Bifunctional lysine-specific demethylase and histidyl-hydroxylase NO66	NO66	44	59.393
Centromere protein V	CENPV	37.1	51.369
Ribosomal RNA processing protein 1 homolog A	RRP1	14.8	45.853
N-acylneuraminate cytidylyltransferase	CMAS	42.6	45.504
THO complex subunit 4	ALYREF	34.2	40.451
ATP-dependent RNA helicase DDX54	DDX54	31.3	38.316
Melanoma-associated antigen D2	MAGED2	31.8	33.31
Coiled-coil-helix-coiled-coil-helix domain-containing protein 2, mitochondrial;Putative coiled-coil-helix-coiled-coil-helix domain-containing protein CHCHD2P9, mitochondrial	CHCHD2 ; CHCHD2 P9	31.1	24.503
Nuclease-sensitive element-binding protein 1	YBX1	51.2	20.563
Protein LSM14 homolog B	LSM14B	34.3	20.43
E3 ubiquitin-protein ligase ZFP91	ZFP91; ZFP91-CNTF	17	20.072
40S ribosomal protein S7	RPS7	40.7	19.184

Protein names	Gene names	Sequence coverage [%]	Ratio H/L
40S ribosomal protein S17-like;40S ribosomal protein S17	RPS17L; RPS17	56.3	18.032
60S ribosomal protein L28	RPL28	59.4	15.03
Fragile X mental retardation syndrome-related protein 2	FXR2	23.8	13.896
Fragile X mental retardation syndrome-related protein 1	FXR1	31.6	13.774
Mannosyl-oligosaccharide glucosidase	MOGS	11.2	11.476
Protein PRRC2A	PRRC2A	8.2	10.753
60S ribosomal protein L27a	RPL27A	38	10.532
40S ribosomal protein S26;Putative 40S ribosomal protein S26-like 1	RPS26; RPS26P11	31.3	10.49
Plasminogen activator inhibitor 1 RNA-binding protein	SERBP1	29.5	10.434
60S ribosomal protein L11	RPL11	22.6	9.725
Protein PRRC2C	PRRC2C	5.5	8.9975
60S ribosomal protein L32	RPL32	30.1	7.6816
60S ribosomal protein L23a	RPL23A	14.7	6.4511
40S ribosomal protein S6	RPS6	25.7	5.649
Pre-rRNA-processing protein TSR1 homolog	TSR1	10.8	5.5874
40S ribosomal protein S14	RPS14	37.7	4.9595
40S ribosomal protein S18	RPS18	62.5	4.7925
ATP-dependent RNA helicase DDX3X;ATP-dependent RNA helicase DDX3Y	DDX3X; DDX3Y	33.6	4.3595
Lamin-B receptor	LBR	12.8	4.2938
40S ribosomal protein S2	RPS2	32.1	3.7432
rRNA 2-O-methyltransferase fibrillarin	FBL	34.9	3.4512
60S ribosomal protein L23	RPL23	44.3	3.0869
Heterogeneous nuclear ribonucleoprotein U	HNRNPU	8.4	2.3757

STRING analysis showed the interaction of the listed proteins (Figure 3.51).

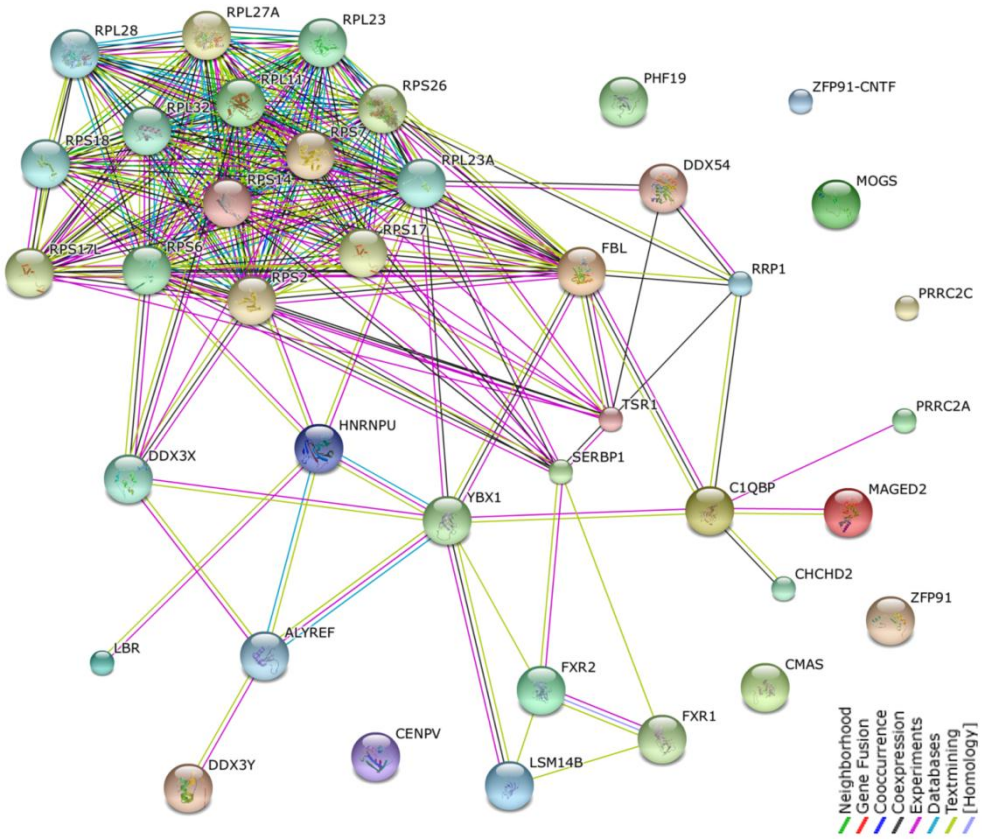

Figure 3.51. STRING analysis displayed the association of C1QBP and its interacting partners.

DAVID analysis indicated that the C1QBP interactome was generally involved in ribonucleoprotein complex, RNA processing, DNA binding, ATP binding, DEAD box binding, cell death and transcription regulation (Table 3.14). Common functions identified between DAVID analyses done on gene microarray with depletion of C1QBP, and C1QBP interactome, include transcription regulation and cell death.

Table 3.14. DAVID analysis of C1QBP interactome

Functions	Genes	Protein name	Gene ID
Ribonucleoprotein	RPS26P11	Putative 40S ribosomal protein S26-like 1	441502
	RPL27A	60S ribosomal protein L27a	6157
	RPL23A	60S ribosomal protein L23a	6147
	RPS2	40S ribosomal protein S2	6187
	RPS6	40S ribosomal protein S6	6194
	RPL28	60S ribosomal protein L28	6158
	FBL	rRNA 2-O-methyltransferase fibrillarin	2091
	HNRNPU	Heterogeneous nuclear ribonucleoprotein U	3192
	RPS7	40S ribosomal protein S7	6201
	LSM14B	Protein LSM14 homolog B	149986
	RPS26	40S ribosomal protein S26	6231
	RPS18	40S ribosomal protein S18	6222
	RPL23	60S ribosomal protein L23	9349
	RPL32	60S ribosomal protein L32	6161
	RPS17	40S ribosomal protein S17-like;40S ribosomal protein S17	6218
	RPS14	40S ribosomal protein S14	6208
	RPL11	60S ribosomal protein L11	6135
	RRP1	Ribosomal RNA processing protein 1 homolog A	8568
	FXR2	Fragile X mental retardation syndrome-related protein 2	9513
	YBX1	Nuclease-sensitive element-binding protein 1	4904
	FXR1	Fragile X mental retardation syndrome-related protein 1	8087
	TSR1	Pre-rRNA-processing protein TSR1 homolog	55720
	CENPV	Centromere protein V	201161
	DDX54	ATP-dependent RNA helicase DDX54	79039

Functions	Genes	Protein name	Gene ID
	ZFP91-CNTF	E3 ubiquitin-protein ligase ZFP91	386607
	ZFP91	E3 ubiquitin-protein ligase ZFP91	80829
RNA processing	RRP1	Ribosomal RNA processing protein 1 homolog A	8568
	TSR1	Pre-rRNA-processing protein TSR1 homolog	55720
	RPS17	40S ribosomal protein S17-like;40S ribosomal protein S17	6218
	RPS14	40S ribosomal protein S14	6208
	RPL11	60S ribosomal protein L11	6135
	RPS6	40S ribosomal protein S6	6194
	FBL	rRNA 2-O-methyltransferase fibrillarin	2091
	RPS7	40S ribosomal protein S7	6201
	DDX54	ATP-dependent RNA helicase DDX54	79039
	HNRNPU	Heterogeneous nuclear ribonucleoprotein U	3192
	YBX1	Nuclease-sensitive element-binding protein 1	4904
	RPL23	60S ribosomal protein L23	9349
	FXR1	Fragile X mental retardation syndrome-related protein 1	8087
	DDX3X	ATP-dependent RNA helicase DDX3X	1654
	C1QBP	Complement component 1 Q subcomponent-binding protein, mitochondrial	708
mRNA stability	SERBP1	Plasminogen activator inhibitor 1 RNA-binding protein	26135
	HNRNPU	Heterogeneous nuclear ribonucleoprotein U	3192
	YBX1	Nuclease-sensitive element-binding protein 1	4904
	RPS26	40S ribosomal protein S26	6231
	RPS14	40S ribosomal protein S14	6208

Functions	Genes	Protein name	Gene ID
DEAD box, DNA and ATP binding	DDX3X	ATP-dependent RNA helicase DDX3X	1654
	DDX3Y	ATP-dependent RNA helicase DDX3Y	8653
	DDX54	ATP-dependent RNA helicase DDX54	79039
	ZFP91-CNTF	E3 ubiquitin-protein ligase ZFP91	386607
	RRP1	Ribosomal RNA processing protein 1 homolog A	8568
	TSR1	Pre-rRNA-processing protein TSR1 homolog	55720
	CMAS	N-acylneuraminate cytidylyltransferase	55907
	FBL	rRNA 2-O-methyltransferase fibrillarin	2091
	YBX1	Nuclease-sensitive element-binding protein 1	4904
	HNRNPU	Heterogeneous nuclear ribonucleoprotein U	3192
	ZFP91	E3 ubiquitin-protein ligase ZFP91	80829
	SERBP1	Plasminogen activator inhibitor 1 RNA-binding protein	26135
	CENPV	Centromere protein V	201161
	LBR	Lamin-B receptor	3930
	RPS18	40S ribosomal protein S18	6222
	FXR2	Fragile X mental retardation syndrome-related protein 2	9513
	FXR1	Fragile X mental retardation syndrome-related protein 1	8087
	MOGS	Mannosyl-oligosaccharide glucosidase	7841
	RPL23A	60S ribosomal protein L23a	6147
Macromolecular complex subunit organization	TSR1	Pre-rRNA-processing protein TSR1 homolog	55720
	RPS14	40S ribosomal protein S14	6208
	CENPV	Centromere protein V	201161

Functions	Genes	Protein name	Gene ID
	ZFP91-CNTF	E3 ubiquitin-protein ligase ZFP91	386607
	ZFP91	E3 ubiquitin-protein ligase ZFP91	80829
Programmed cell death	ZFP91-CNTF	E3 ubiquitin-protein ligase ZFP91	386607
	ZFP91	E3 ubiquitin-protein ligase ZFP91	80829
	RPL11	60S ribosomal protein L11	6135
	RPS6	40S ribosomal protein S6	6194
Transcription regulation	ZFP91-CNTF	E3 ubiquitin-protein ligase ZFP91	386607
	ZFP91	E3 ubiquitin-protein ligase ZFP91	80829
	DDX54	ATP-dependent RNA helicase DDX54	79039
	YBX1	Nuclease-sensitive element-binding protein 1	4904
	RPS14	40S ribosomal protein S14	6208

3.18 Interaction of C1QBP to YB-1

Since STRING analysis showed a strong connection between C1QBP and YB-1, and YB-1 has been shown to interact with C1QBP (Matsumoto et al., 2005), YB-1 was selected for further investigations. The effects of the interaction of C1QBP and YB-1, on cell proliferation, migration and invasion were carried out.

3.18.1 Physical interaction of C1QBP and YB-1

Co-immunoprecipitation was done to determine the physical interaction of C1QBP and YB-1 in MDA-MB-231 cells (Figure 3.52). Using antibody against YB-1, it was discovered that C1QBP was also pulled down with the YB-1 protein. In addition, anti-myc was also able to pull down the

myc-tagged C1QBP together with the YB-1 protein. This indicated a physical interaction existed between C1QBP and YB-1.

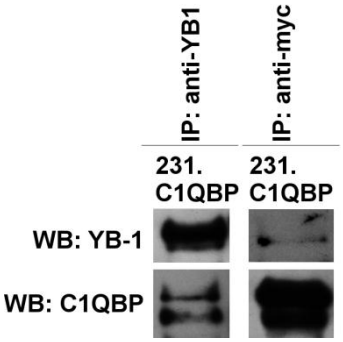

Figure 3.52. Co-immunoprecipitation blot of interaction between C1QBP and YB-1 in MDA-MB-231 cell line overexpressing C1QBP. The C1QBP protein was pulled down by anti-YB-1 and YB-1 was detected when anti-myc was used for immunoprecipitation. WB: Antibodies used for western blot; IP: Antibodies used for immunoprecipitation. Experiments were repeated at two independent times.

In addition, immunofluorescence staining of C1QBP and YB-1 were carried out to determine whether co-localization existed between these two proteins. Since C1QBP and YB-1 antibodies were both derived from rabbit, mouse anti-myc was used to represent C1QBP staining in MDA-MB-231 cells overexpressing myc-tagged C1QBP. Firstly, myc staining was performed to determine whether it could represent C1QBP staining. As seen in Figure 3.53, myc staining perfectly co-localized with C1QBP staining. Thus, anti-myc can be used to represent C1QBP staining to determine its co-localization with YB-1.

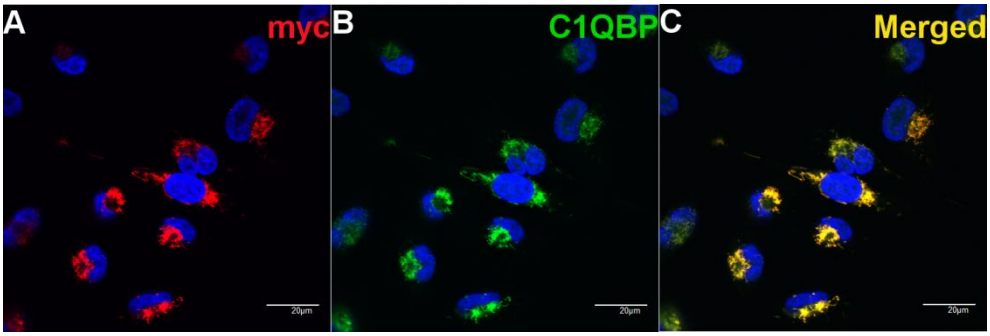

Figure 3.53. Co-localization of myc tag and C1QBP. (A) Myc and (B) C1QBP staining was co-localized perfectly as indicated by the yellow staining, showing that myc staining can be used to represent C1QBP staining in C1QBP-overexpressing cells. Scale bar: 20 µm.

Then, the co-localization of C1QBP represented by myc staining, and YB-1 was determined in MDA-MB-231 cells overexpressing C1QBP. Judging from the images, co-localization between C1QBP and YB-1 was observed in the mitochondria (Figure 3.54).

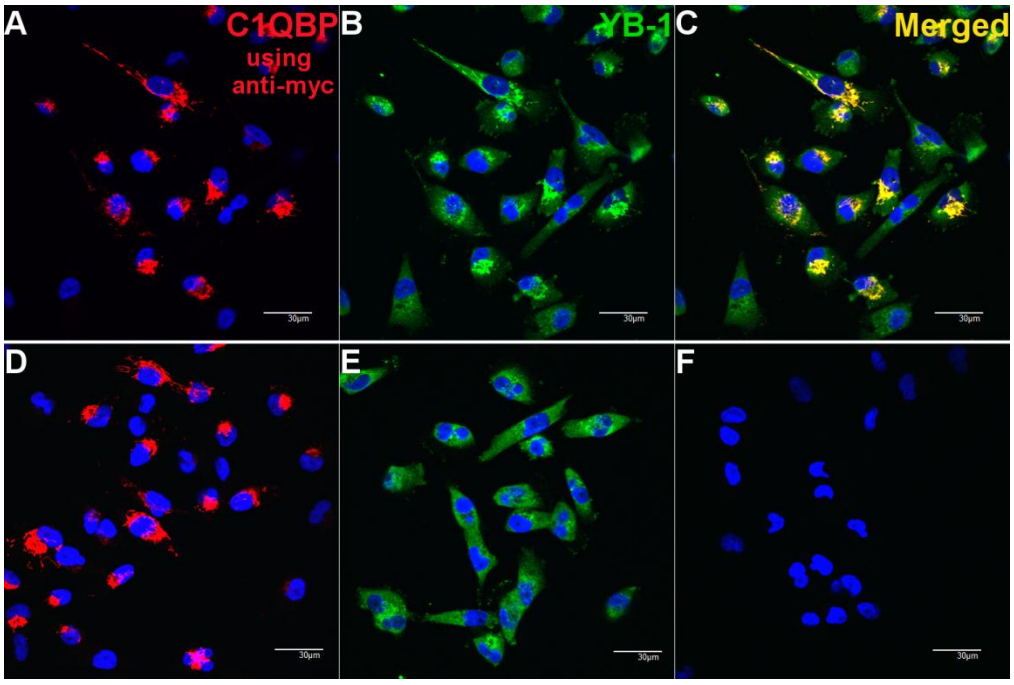

Figure 3.54. Co-localization of YB-1 and C1QBP in C1QBP-overexpressing cells. (A) Mouse anti-myc was used to represent C1QBP and (B) rabbit anti-YB-1 was used to stain YB-1. (C) Merged image showed co-localization of these two proteins in yellow. (D) Single stain control for C1QBP, where YB-1 antibody was omitted. (E) Single stain control for YB-1, where C1QBP antibody was omitted. (F) Negative control where both antibodies were omitted. Scale bar: 30 µm.

3.18.2 Correlation of expression between C1QBP and YB-1

Correlation of expression between C1QBP and YB-1 was first identified in breast cancer tissue samples. Gene expressions of C1QBP and YB-1 were obtained from TissueScan array (Panel 1). A statistically significant correlation was observed and Pearson's R was recorded as 0.5688 (P<0.0001, Figure 3.55).

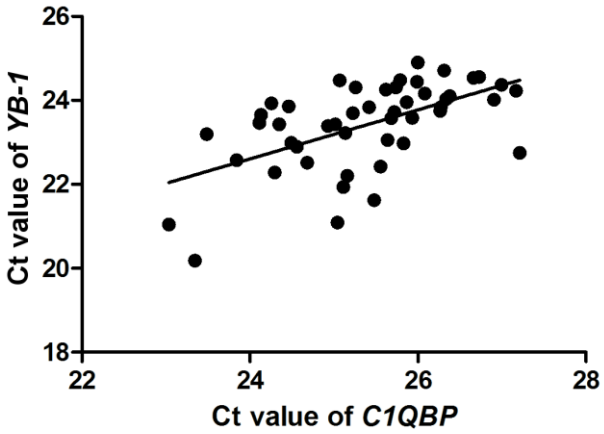

Figure 3.55. Correlation of mRNA levels of *C1QBP* and *YB-1* in breast cancer tissue samples. 48 breast cancer tissue samples obtained from TissueScan array were used. Pearson's correlation = 0.5688 with P<0.0001.

Similarly, the expression of YB-1 based on WAI score was correlated to C1QBP in breast cancer tissue samples. The Pearson's R value obtained is 0.1982 and *P*-value= 0.0626 (Figure 3.56).

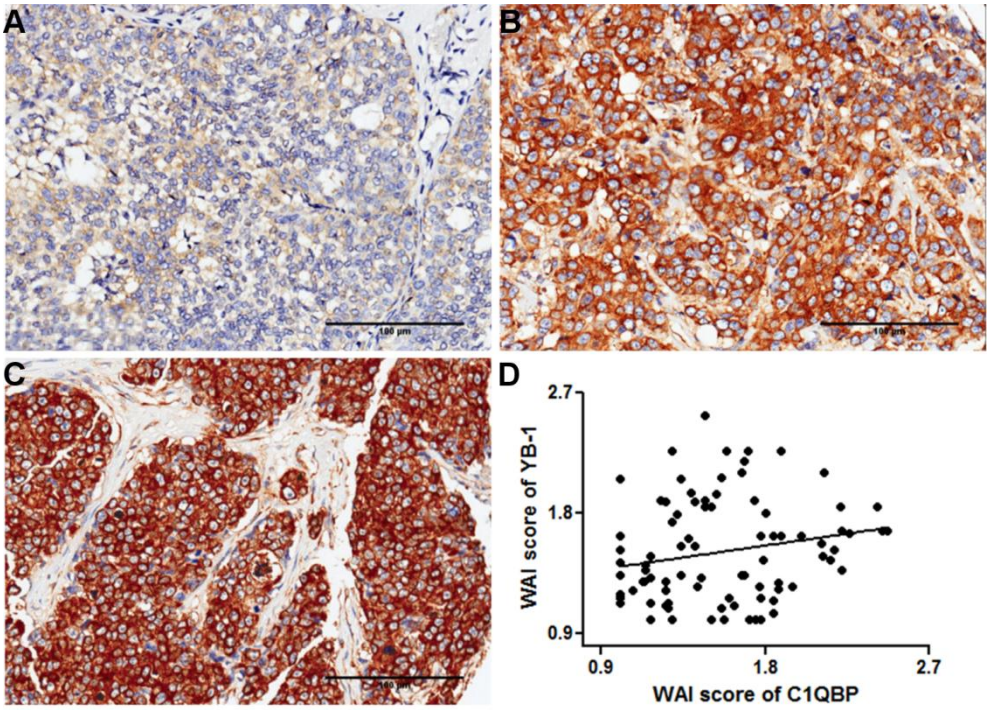

Figure 3.56. Representative image of YB-1 staining in breast cancer TMAs. Scoring was done according to the scoring method of C1QBP in the TMAs where (A) 1+ denotes weak staining, (B) 2+ denotes moderate staining and (C) 3+ denotes strong staining. Scale bar: 100 µm. (D) Correlation of C1QBP and YB-1 expression in breast cancer TMAs with Pearson's R= 0.1982 (*P*-value= 0.0626).

Subsequently, the gene and protein expressions of C1QBP and YB-1 in various breast cancer cell lines were obtained to determine its correlation. Similar to the gene expression of C1QBP, the lowest gene level of YB-1 was present in ZR-75-1 cells. T47D contained the highest gene expression of YB-1 while MDA-MB-231 and MCF7 contained moderate levels of the YB-1 gene (Figure 3.57A). Pearson's correlation test was conducted to determine the correlation between the expressions of these two genes in the breast cancer cell lines. Correlation between the gene expression of C1QBP and YB-1 was observed with Pearson's R=0.6245 (*P*=0.0299, Figure 3.57B).

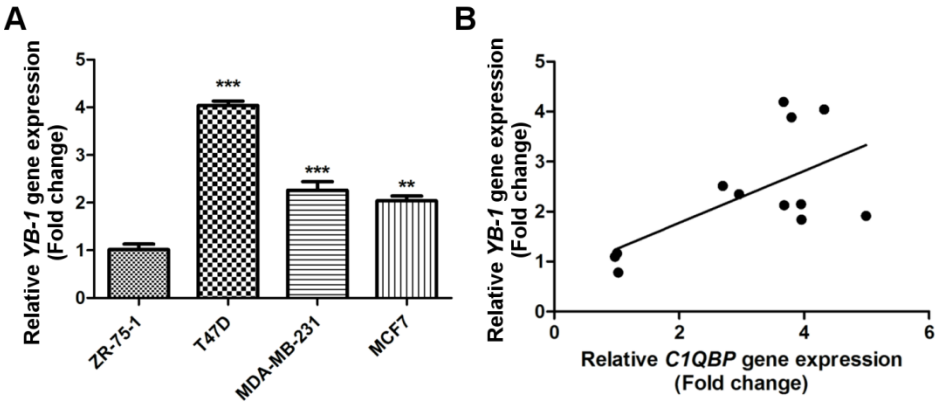

Figure 3.57. Gene expression of *YB-1* and correlation to *C1QBP* expression in breast cancer cell lines. (A) Relative gene expression of *YB-1* in breast cancer cell lines. ΔCt values of each cell lines were obtained by normalization to the corresponding Ct values of GAPDH. Subsequently, the relative expressions of *YB-1* gene expression in the breast cancer cell lines were determined by comparison to ZR-75-1. Bar chart represents mean ± SEM. ***P*<0.01 and ****P*<0.001. (B) Correlation between the gene expression of *YB-1* and *C1QBP* in breast cancer cell lines with Pearson's correlation R= 0.6245 and **P* value= 0.0299. Experiments were done in triplicates and repeated twice.

The protein expressions of C1QBP and YB-1 were also evaluated to determine its correlation. In accordance to its gene level, the YB-1 protein was least expressed in ZR-75-1 cells while highly expressed in T47D cells (Figure 3.58A). With a Pearson's correlation of 0.2643, the correlation between

C1QBP and YB-1 protein expression in breast cancer cell lines was not significant (Figure 3.58B)

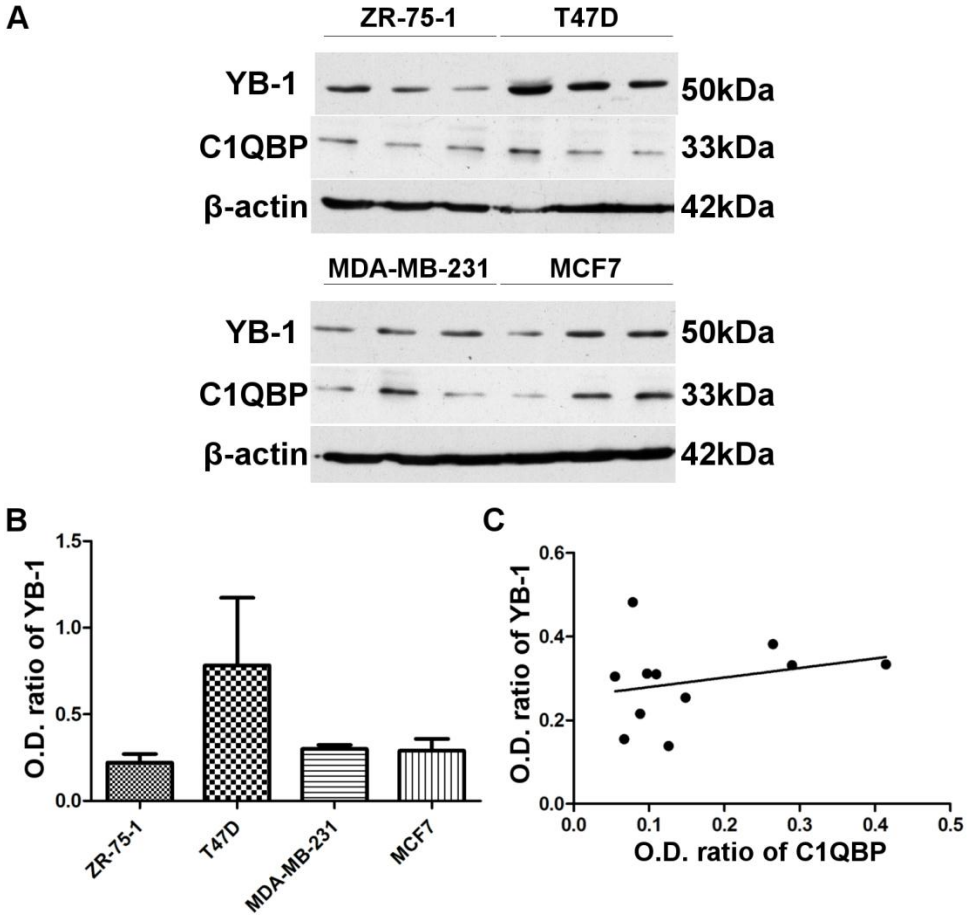

Figure 3.58. Protein expression of YB-1 in breast cancer cell lines and its correlation with the protein expression of C1QBP. (A) Western blot representations for protein expression of C1QBP in ZR-75-1, T47D, MDA-MB-231 and MCF7. (B) Expression of YB-1 in breast cancer cell lines. Each bar represents mean of O.D. ratio ± SEM. (C) Correlation of C1QBP and YB-1 protein expression with Pearson's R=0.2643. Experiments were done in triplicates and repeated twice.

3.18.3 Double knockdown of C1QBP and YB-1 in MDA-MB-231 cells

Reduced expression of YB-1 has been shown to diminish cell proliferation, migration and invasion (Yu, 2010). Hence, double knockdown of C1QBP and YB-1 was done in MDA-MB-231 cells, to determine whether the knockdown of these two proteins concurrently could produce a synergistic effect on cell proliferation, migration or invasion. The efficiency of the double knockdown on the YB-1 and C1QBP genes are shown in Figure 3.59A and on the proteins in Figure 3.59B.

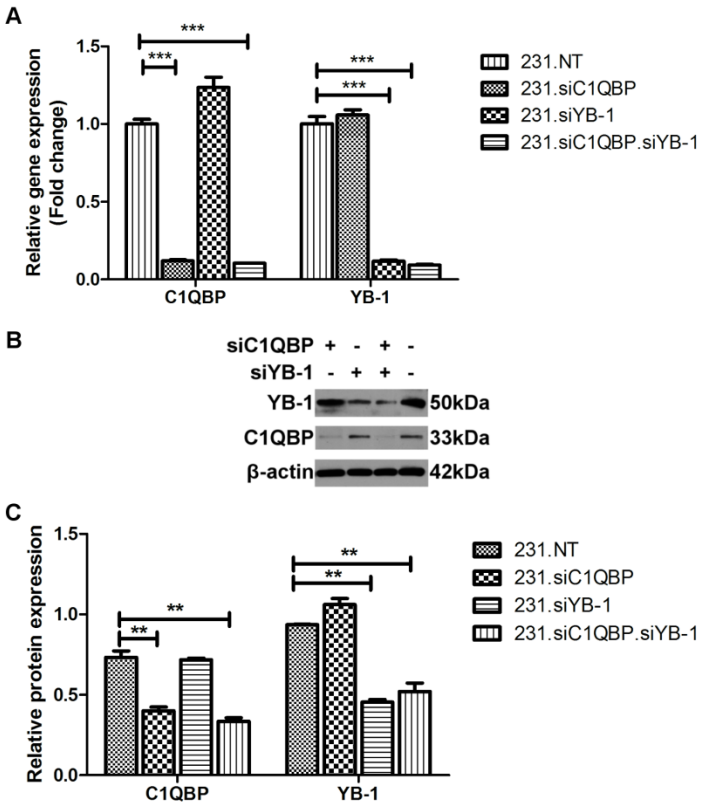

Figure 3.59. Double knockdown of C1QBP and YB-1 in MDA-MB-231 cells. (A) More than 80% of the C1QBP and YB-1 genes were knockdown after transfection with both siC1QBP and siYB-1 in MDA-MB-231 cells at the gene level, with ****P*<0.001. (B) Western blot representations after double knockdown of C1QBP and YB-1 in MDA-MB-231 cells. (C) At the protein level, C1QBP and YB-1 expressions were decreased with statistical significance. ***P*<0.01. Values are presented as mean ± SEM. Experiments were done in triplicates and repeated twice.

3.18.3.1 Effect of C1QBP and YB-1 knockdown on cell proliferation in MDA-MB-231 cells

Attenuation of C1QBP and YB-1, respectively decreased cell proliferation over 120h. The knockdown of both C1QBP and YB-1 in the cells also caused a significant decrease in cell proliferation; however, a synergistic effect was not observed (Figure 3.60).

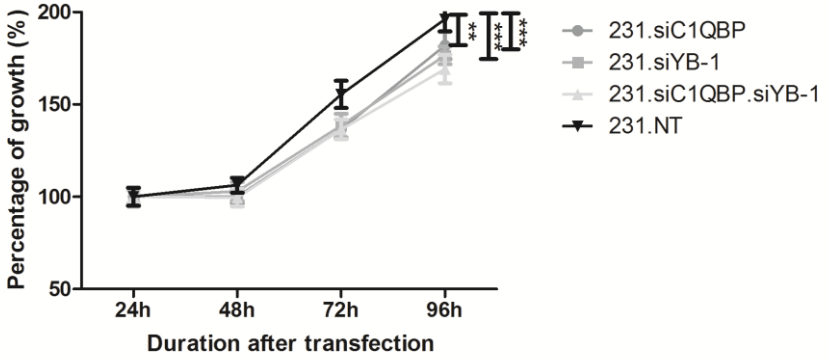

Figure 3.60. Cell growth curve was plotted using alamarBlue assay over 120h. The knockdown of C1QBP and YB-1 separately was able to significantly reduce the cell proliferation rate. Double knockdown of C1QBP and YB-1 did not synergistically reduce cell proliferation rate. Proliferation rate after attenuation of C1QBP and YB-1 was similar to knockdown of YB-1 alone. $^{**}P<0.01$, $^{***}P<0.001$. Values are presented as mean ± SEM. Experiments were done in triplicates and repeated twice.

3.18.3.2 Effect of double knockdown of C1QBP and YB-1 on cell migration and invasion in MDA-MB-231 cell

MDA-MB-231 cells treated with siC1QBP and siYB-1 respectively, showed a significant decrease in cell migration (P<0.05). The migratory ability of MDA-MB-231 cells was also significantly diminished after double knockdown of C1QBP and YB-1, although synergistic decrease was not observed (Figure 3.61).

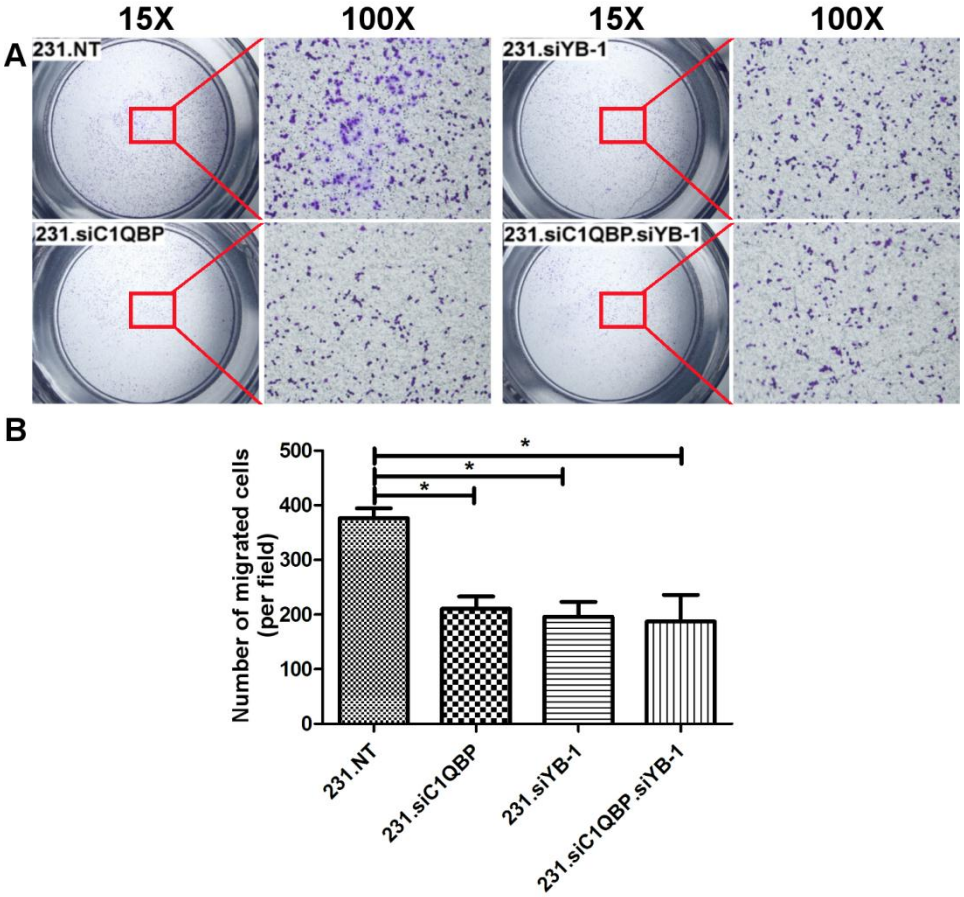

Figure 3.61. Simultaneous knockdown of C1QBP and YB-1 in MDA-MB-231 cells decreased cell migration but the effect was not synergistic. Knockdown of C1QBP and YB-1 respectively, decreased cell migration to the same level as cells with double knockdown of C1QBP and YB-1. *P<0.05. Values are presented as mean ± SEM. Experiments were done in triplicates and repeated twice.

Likewise, the simultaneous reduction of C1QBP and YB-1 in MDA-MB-231 cells did not show a synergistic decrease of cell invasion, although reduction of YB-1 alone showed diminished cell invasion.

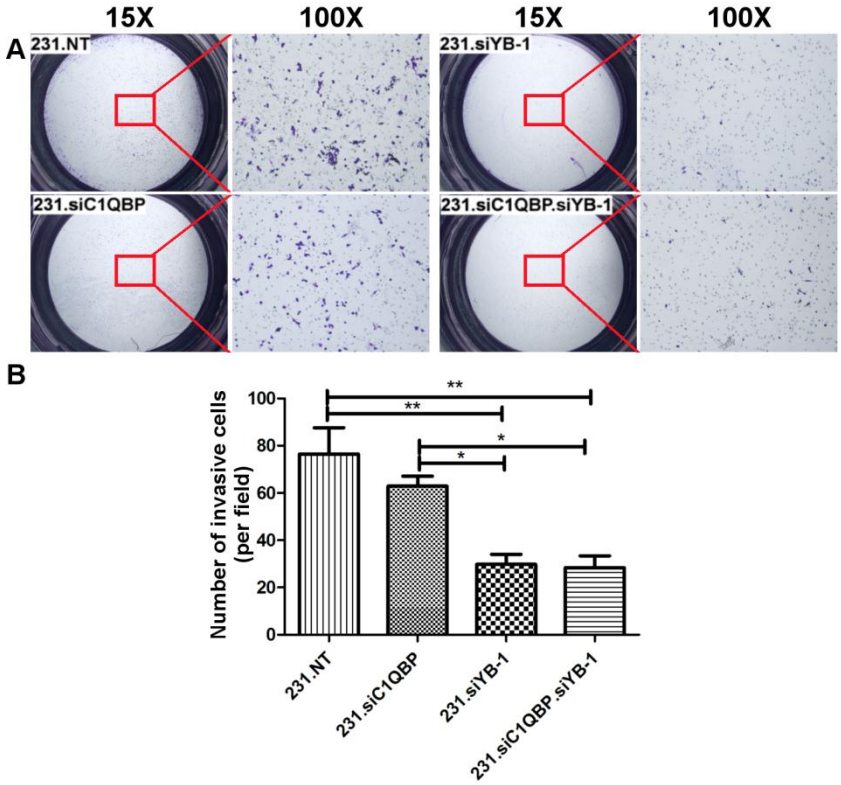

Figure 3.62. The cell invasiveness of MDA-MB-231 cells with double knockdown of C1QBP and YB-1 was similar to cell invasiveness of MDA-MB-231 cells with knockdown of YB-1 itself. No statistical significance was observed for the decrease in cell invasiveness after knockdown of C1QBP. *P<0.05, **P<0.01. Values are presented as mean ± SEM. Experiments were done in triplicates and repeated twice.

3.18.4 Functional significance of C1QBP in YB-1 overexpressing cells

Overexpression of YB-1 has been reported to increase cancer progression. Among others, the overexpression of YB-1 has been reported to increase cell migration and invasion in breast cancer (Yu, 2010). It is therefore interesting to determine whether reduction of C1QBP expression in the context of YB-1 overexpression would produce an effect to cancer progression.

3.18.4.1 Silencing efficiency of siC1QBP in YB-1 overexpressing cells

Firstly, previously established MDA-MB-231 cells stably overexpressing YB-1 were verified to contain higher levels of YB-1 expression (Yu, 2010). The YB-1 gene expression of the cells was up-regulated by 3.7 times in the YB-1-overexpressing cells compared to the control cells (*P*=0.003, Figure 3.63A). Analysis of the YB-1 protein levels by western blot also showed higher expression of YB-1 in MDA-MB-231 cells overexpressing YB-1, compared to MDA-MB-231 cells containing the empty vector (Figure 3.63B). Quantitatively, the protein expression was elevated by 53.5% in the YB-1-overexpressing cells (*P*=0.0402, Figure 3.63C).

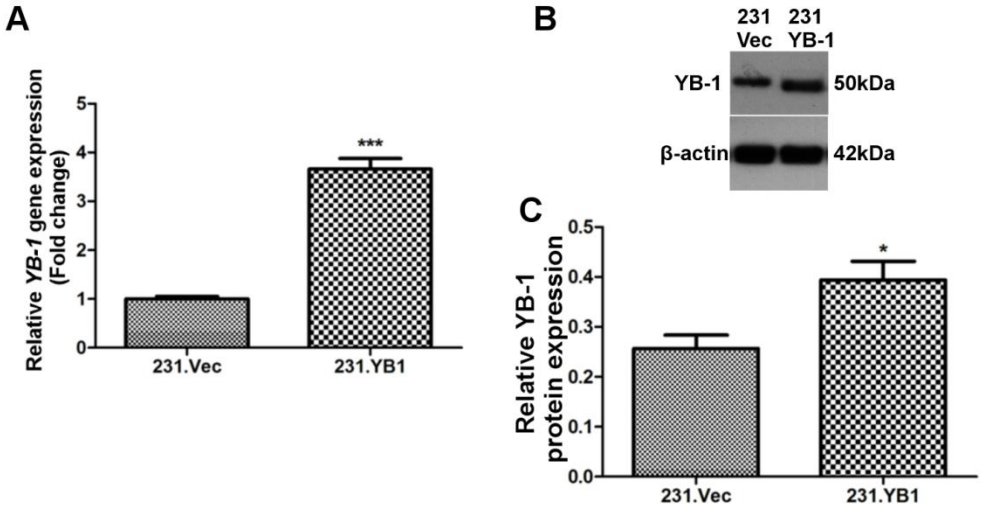

Figure 3.63. (A) The *YB-1* gene expression was overexpressed by approximately 3.7 times in MDA-MB-231 breast cancer cells. Relative *YB-1* gene expression are presented as mean ± SEM and ****P*<0.001. (B) Increased YB-1 protein expression in 231.YB1 cells as seen in western blot. (C) The protein expression of YB-1 was approximately 53.5% higher in YB-1 overexpressing cells compared to control cells. Values are presented as mean of O.D. ratio ± SEM. **P*<0.05. Experiments were done in triplicates.

Following that, knockdown of C1QBP was done in both 231.Vec and 231.YB-1 cell lines by siC1QBP transfection. The level of C1QBP was significantly reduced by 92%, 48 hours after transfection (P<0.0001).

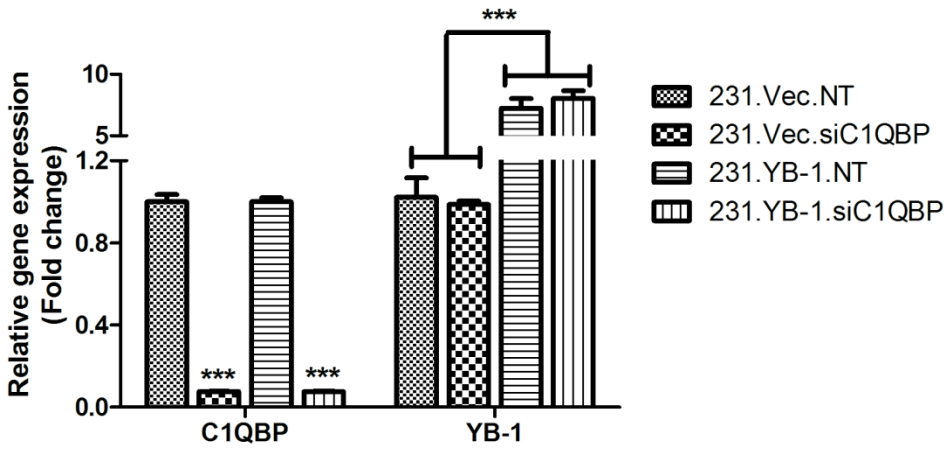

Figure 3.64. Gene expression of C1QBP and YB-1 in MDA-MB-231 cells overexpressing YB-1, 48 h after transfection with siC1QBP. Gene levels of C1QBP were decreased by 92%. ***P<0.0001. Values are presented as mean ± SEM. Experiments were done in triplicates and repeated twice.

3.18.4.2 Down-regulation of C1QBP in MDA-MB-231 cells with YB-1 overexpression altered cell growth

Cell proliferation was measured by MTS assay at 48 h and 72 h after transfection. Cell proliferation was significantly diminished at 48 h and 72 h after transfection (*P*=0.0220, Figure 3.65A; *P*=0.0069, Figure 3.65B). Further clarification was made by examining the cell growth curve of YB-1 overexpressing cells after knockdown of C1QBP. AlamarBlue assay was used to measure and plot the cell growth curve. A decrease trend was observed for cells with knockdown of C1QBP, although the difference was not statistically significant (Figure 3.65C).

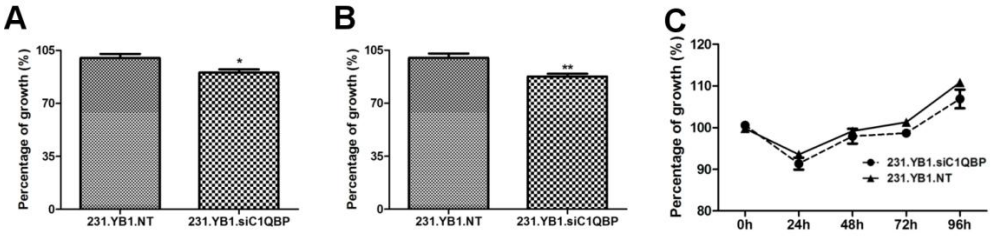

Figure 3.65. Down-regulation of C1QBP decreased proliferation and cell growth of YB-1 overexpressing cells. Measurement of cell viability was done by MTS assay at (A) 48 h and (B) 72 h, post-transfection. Values are presented as mean of absorbance at 490 nm ± SEM. **P*<0.05 and ***P*<0.01. (C) Cell growth curves of 231.YB1.NT and 231.YB1.siC1QBP cells were plotted over 96 h by repeated measurements of alamarBlue absorbance every 24 h. The difference between the two curves were not statistically significant. Values are presented as mean ± SEM. Experiments were done in quadruplicates and repeated twice.

3.18.4.3 Cell migration and invasion was altered after knockdown of C1QBP in YB-1 overexpressing cells

Overexpression of YB-1 has been associated with increased cell migration and cell invasion abilities (Yu, 2010). Using the transwell migration system, knockdown of C1QBP decreased cell migration of YB-1-overexpressing cells (Figure 3.66). However, upon further inspection, it was discovered that the level of cell migration did not return to the original level i.e. to the migration level of 231.Vec.NT cells.

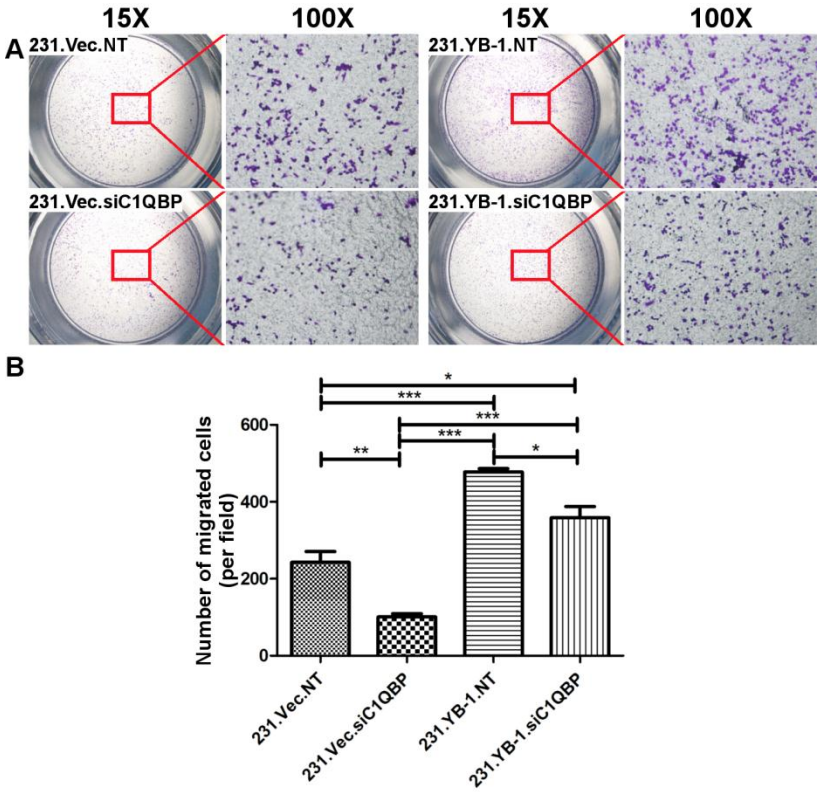

Figure 3.66. Cell migration was mitigated after knockdown of C1QBP in YB-1 overexpressing cells. (A) Cells which have migrated through the membrane were stained with fixed and stained with crystal violet. (B) The attenuation of C1QBP in MDA-MB-231 cells overexpressing YB-1 significantly reduced the ability of cells to migrate through the transwell membrane; however the reduction was not sufficient to return cell migration level to the level of 231.Vec.NT cells. Bar chart represents mean of number of migrated cells ± SEM. ***P<0.0001, **P<0.01, *P<0.01. Experiments were done in triplicates and repeated twice.

Similarly, cell invasion was decreased after knockdown of C1QBP in YB-1 overexpressing cells (Figure 3.67A). However, the knockdown of C1QBP by itself was not sufficient to reduce the number of invasive cells to that of 231.Vec.NT cells (Figure 3.67B; $P<0.05$). Therefore, it can be postulated that the interaction of C1QBP and YB-1 affected cell migration and invasion but other factors or proteins were also involved in these processes.

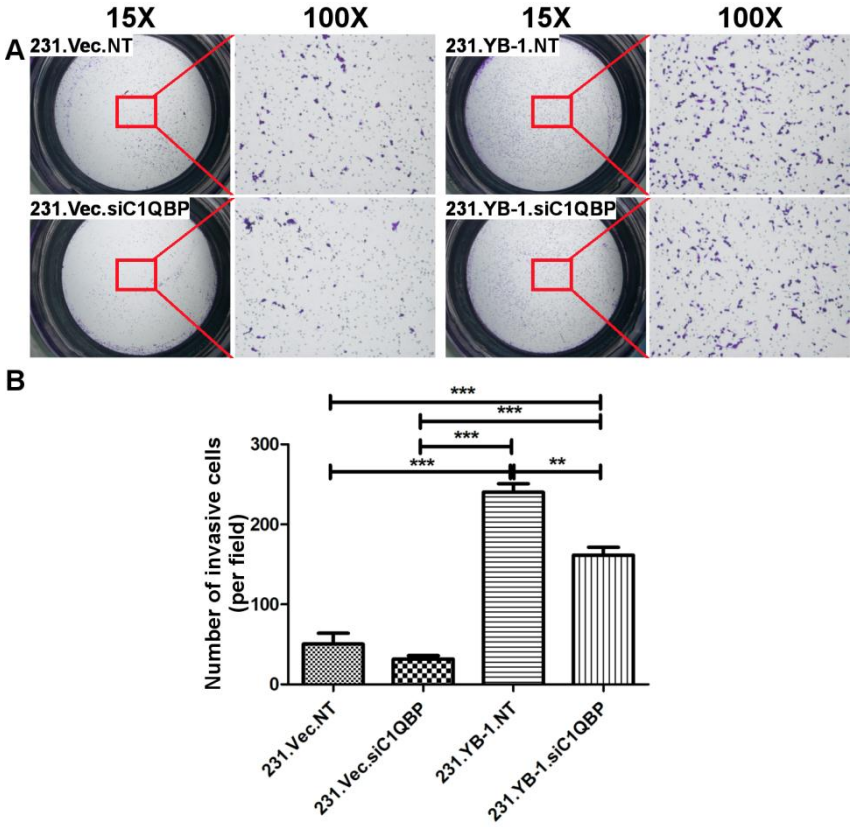

Figure 3.67. The invasiveness of MDA-MB-231 overexpressing YB-1 was diminished after knockdown of C1QBP. (A) Representative images of cells with invasive capability in the control and C1QBP-knockdown group. Cells were fixed with methanol and stained with crystal violet dye. (B) The number of invasive cells in YB-1-overexpressing cells treated with siC1QBP decreased but treatment of cells with siC1QBP was not enough to return cell invasiveness to its original state. Bar chart represents mean number of invasive cells/field ± SEM with $^{**}P<0.01$. Experiments were done in triplicates and repeated twice.

CHAPTER 4
DISCUSSION

4 DISCUSSION

4.1 Association of C1QBP with cell proliferation

One of the fundamental traits of cancer cells is the ability to sustain chronic proliferation (Hanahan and Weinberg, 2011). In normal tissues and organs, cell growth and number are tightly regulated by a balance of cell loss and organized cell proliferation (Rue and Martinez Arias, 2015). However, cancer develops due to an accumulation of genetic and epigenetic alterations to oncogenes and tumor suppressor genes, which among other characteristics, provides a growth advantage to cancer cells (Corn and El-Deiry, 2002).

In breast cancer tissue samples examined in the present study, the mRNA expression of C1QBP was observed to be upregulated in advanced stages of breast cancer (Stages IIb and higher) and in tumor size of more than 5 cm (T3). The results were further corroborated by immunohistochemical analyses of C1QBP in breast cancer TMAs, whereby overexpression of C1QBP was significantly associated with tumor size. Furthermore, multivariate analysis showed that the expression of C1QBP can independently predict tumor size in PR-positive breast cancer tissue samples. In addition, the expression of C1QBP was significantly correlated to PCNA, a proliferative marker which has been associated with mitotic index and tumor size in breast cancer (Agarwal et al., 1997). Prior reports have revealed that higher expression of C1QBP was observed in malignant tissues, compared to their normal counterpart (Chen et al., 2009b; Dembitzer et al., 2012). Comparatively, analysis of the expression of C1QBP in breast cancer TMAs done by Zhang et al. (2013) showed a significant association to the TNM

staging of breast cancer, although a correlation between tumor size and C1QBP was not detected. Cell proliferation, being a hallmark of cancer has been extensively attributed to tumor growth and progression (Hanahan and Weinberg, 2011). Additionally, standard breast cancer treatments, such as chemotherapy and radiotherapy, are largely based on the proliferative activity of breast cancer. In particular, treatment for luminal receptor-positive subtype of breast cancer is generally based on the evaluation of proliferation (Nilsson et al., 2013).

Hence, further studies on proliferation were conducted on breast cancer cell lines. The attenuation of C1QBP in PR-positive T47D breast cancer cell line and triple negative MDA-MB-231 breast cancer cell line reduced cell proliferation and cell growth rate. Consistent with the findings, previous reports have shown that knockdown of C1QBP in breast cancer and prostate cancer cell lines decreased cell proliferation (Amamoto et al., 2011; McGee et al., 2011). Complementarily, overexpression of C1QBP in MDA-MB-231 breast cancer cells increased cell proliferation and cell growth rate. Similar findings were reported after overexpression of C1QBP in a liver carcinoma cell line (Kaul et al., 2012). A deeper analysis into the cell cycle profile of MDA-MB-231 cells overexpressing C1QBP, indicated an increase in cell survival and G1 to S phase progression. In agreement with the data obtained, knockdown of C1QBP in PC3 prostate cancer cells resulted in cell cycle arrest at the G1 to S phase (Amamoto et al., 2011). Moreover, the alteration of cell cycle progression observed in MDA-MB-231 cells after manipulation of C1QBP, was accompanied by changes in the expression of Cyclin D1 and its

relevant cyclin-dependent kinases (CDKs). From the data obtained, up-regulation of C1QBP increased Cyclin D1 and CDK6.

Cancer cells with uncontrolled cell cycle progression, as an effect of dysregulated growth signals, consequently affect other biological properties such as cell survival (Hanahan and Weinberg, 2011). Regulation of cell cycle is highly dependent on cyclin-dependent protein kinases (CDKs), which require binding to cyclins (Sherr, 1996; Casimiro et al., 2014). The G1 phase is a critical point in the cell cycle process, where the decision to proceed with cell division, or withdraw from the cycle and enter resting phase was made (Sherr, 1994). In cancer cells, the G1 phase transition to S phase continues unrestricted, and as cell cycle exit expedites cell maturation and differentiation, these processes are subsequently subverted as well (Sherr, 1996). Upon entering the G1 phase, CDK4 and CDK6 form complexes with D-type cyclins (Cyclins D1, D2, D3). The G1-S phase transition is restricted by the inhibitory effect of retinoblastoma susceptibility protein (Rb) (Giacinti and Giordano, 2006). This restriction is overcome by hyperphosphorylation of the Rb protein by sequential phosphorylation of CDK4/6-Cyclin D and CDK2-Cyclin E, which consequently, releases E2F transcription factors, causing activation of genes necessary for S-phase DNA replication (Casimiro et al., 2014). The CDK/cyclin complexes are negatively regulated by the INK4 family and the Cip/Kip family, together forming the CDK inhibitors (CKIs). The INK4 family consisting of p15, p16, p18 and p19, specifically inhibits CDK4 and CDK6. Conversely, the Cip/Kip family (p21, p27 and p57) appears to broadly affect cyclin D-, E-, A- and B-dependent kinase complexes (Albrecht et al., 1998; Sherr and Roberts, 1999; Corn and El-Deiry, 2002).

The Cyclin D-CDK complex sequesters Cip/Kip family members, which relieve Cyclin E-CDK2 from the inhibitory effect, facilitating the activation of Cyclin E-CDK2 in the later stages of the G1 phase (Sherr and Roberts, 1999).

Cyclin D1, a part of the D-type cyclin family is a well-established regulator of the G1 to S phase progression of the cell cycle (Heichman and Roberts, 1994; Sherr, 1996; Pestell, 2013; Casimiro et al., 2014). The overexpression of Cyclin D1 has been widely reported in haematological malignancies of the lymphoid lineage and cancer of the breast, lung, prostate, bladder and endometrium (Pestell, 2013; Casimiro et al., 2014). Augmentation of CDK4/6-Cyclin D1 complex levels titrates Cip/Kip family mainly $p21^{Cip1}$ and $p27^{Kip1}$ away from the CDK2-Cyclin E complex, resulting in the increase hyperphosphorylation of Rb, hence enhancing entry into S-phase and subsequently, encouraging cell cycle progression (Casimiro et al., 2014). Previous *in vitro* studies in liver and prostate cancer cell lines showed a positive relationship between C1QBP and Cyclin D1 (Amamoto et al., 2011; Kaul et al., 2012). Additionally, the expression of $p21^{Cip1}$ was found to be inversely correlated with Cyclin D1 expression after knockdown or overexpression of C1QBP in prostate and liver cancer cell lines, respectively (Amamoto et al., 2011; Kaul et al., 2012).

Taken together, it can be postulated that C1QBP enhanced G1 to S phase progression in MDA-MB-231 breast cancer cell line, by regulating the expression of Cyclin D1 and CDK6, which could subsequently increase hyperphosphorylation of Rb, thereby promoting breast cancer proliferation. The process is illustrated in Figure 4.1.

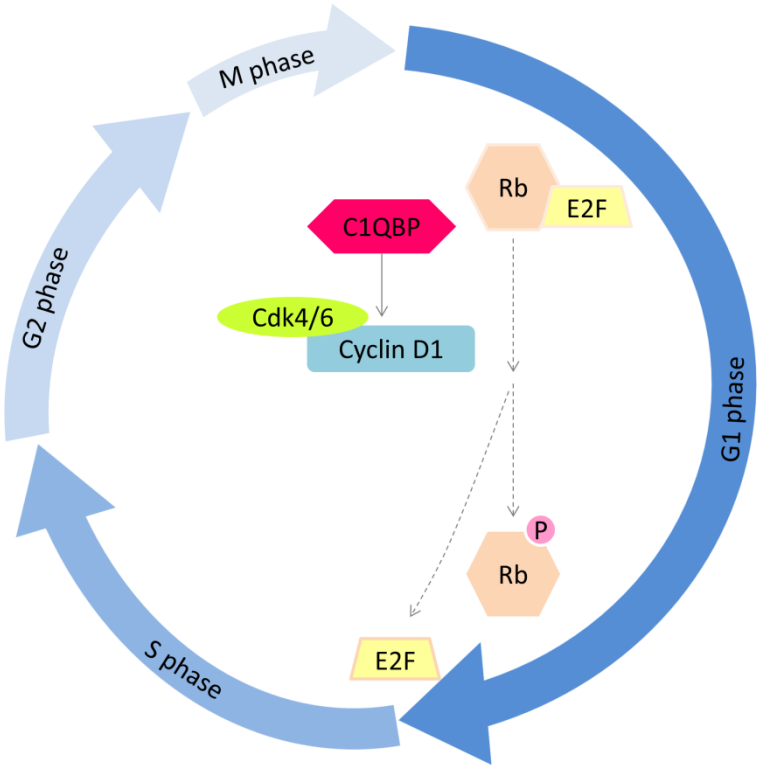

Figure 4.1. The expression of C1QBP affected the G1 to S phase progression in the cell cycle by altering Cyclin D1 and CDK4/6 expression. Augmentation of Cyclin D1 and CDK6 expression by C1QBP leads to hyperphosphorylation of Rb protein, which releases E2F transcription factors, necessary for cell cycle progression.

4.2 Association of C1QBP with metastasis

The immunohistochemical analysis of breast cancer TMAs in the current study, indicated that C1QBP overexpression was associated with lymph node spread. This was also corroborated by analysis of C1QBP gene expression in breast cancer tissues, where the mRNA expression of C1QBP was higher in breast cancer cases with positive lymph node spread, and advanced stages of breast cancer. In agreement to this, it has been shown that overexpression of C1QBP mRNA was associated with lymph node metastasis in breast cancer tissue samples (Chen et al., 2009b). Zhang et al. (2013) also shown that overexpression of C1QBP in breast cancer tissue samples was associated with

distant metastasis to the lung and liver, although an association with lymph node spread was not observed (Zhang et al., 2013).

In the present study, C1QBP has been demonstrated to promote cell migration and cell invasion in MDA-MB-231 cells. Changes in cytoskeletal structure was observed in C1QBP-overexpressing cells, as evident by prominent F-actin stress fibres formation in these cells compared to control cells. The re-organization of actin molecules at the leading edge of cells and the formation of actin stress fibres are necessary for cell migration (Vallenius, 2013). In addition, the expression of vinculin – a focal adhesion molecule – appeared to be less intense compared to control cells indicating a reduction of cell adhesion. It has been shown that loss of vinculin promotes migration and invasion. Also, it is indicative of poor prognosis in colorectal cancer (Li et al., 2014). A recent study has shown that C1QBP interacts with PKCζ upon stimulation with epidermal growth factor, causing modulation of cell polarity and chemotaxis (Zhang et al., 2013). In addition, ligand-induced lamellipodia formation requires the expression of C1QBP, and it is present in lamellipodial protrusions together with lamellipodial components, such as, CD44, F-actin, p-FAK and GM1 upon growth stimulation (Kim et al., 2011). Another way by which C1QBP mediates migration is by interacting with $\alpha_v\beta_3$ integrin, which induces the NFκβ signalling pathway, leading to an increase of MT1-MMP expression and subsequently, activates MMP2 (Prakash et al., 2011). *In vivo* studies using mice reinforced the role of C1QBP in metastasis, whereby C1QBP-attenuated cells showed a decrease in metastatic potential, when introduced into the animal models (Kim et al., 2011; Zhang et al., 2013).

4.3 Mechanistic pathways for C1QBP

As mentioned earlier, genetic and epigenetic changes that lead to uncontrolled cell growth and migration are the impelling causes of cancer progression. Often, these alterations can be mapped to various cell signalling transduction pathways, such as, pathways that control cell growth and proliferation, cell motility and cell death. Consequently, dysregulation of these signalling transduction pathways will affect wider signalling networks, that promotes cancer progression, by altering tumor microenvironment, angiogenesis and inflammation (Sever and Brugge, 2015).

As such, it is imperative to elucidate whether C1QBP was involved in any cancer signalling transduction pathways. To do this, genome wide analysis of MDA-MB-231 cells after knockdown of C1QBP was carried out. In addition, MDA-MB-231 cells overexpressing C1QBP were subjected to a panel of antibodies targeting the main regulators of various signalling pathways, including the MAPK pathways, JAK-STAT pathway and Akt signalling pathway.

4.3.1 Involvement of C1QBP in the ERK1/2 pathway

4.3.1.1 The MAPK pathways – focusing on ERK1/2 pathway

The MAPK pathways are evolutionary conserved kinase proteins, that transduce extracellular signal to intracellular signals and facilitate cell biological processes, such as cell growth, proliferation, migration, differentiation and apoptosis (Dhillon et al., 2007; Roskoski, 2012). A few signalling families constitute the MAPK pathways, namely the ERK family,

BMK1 family, p38 kinase family and c-Jun N-terminal kinase family (Roskoski, 2012; Burotto et al., 2014). Generically, the MAPK pathways consist of at least a three-tier system of which, MAPK kinase kinase (MAP3K) phosphorylates MAPK kinase (MAP2K) which subsequently, phosphorylates MAPK. The phosphorylation of other substrate proteins by activated MAPK, such as transcription factors and other functional proteins, follows the phosphorylation of MAPK, resulting in different biological processes (Roskoski, 2012). Identified MAPKs include ERK1- ERK8, p38α/β/γ/δ and JNK1-JNK3 (Schaeffer and Weber, 1999; Chen et al., 2001; Kyriakis and Avruch, 2001; Dhillon et al., 2007; Roskoski, 2012).

Among these, the ERK pathway is the first and most widely studied, and accounts for approximately one third of all human cancers (Seger and Krebs, 1995; Dhillon et al., 2007). This cascade plays a central role in signal transduction of many extracellular agents via numerous receptors. In general, the activation of these receptors stimulates transformation of RAS to its active form, which enables the recruitment of RAF (a-RAF, b-RAF, c-RAF), the first kinase of the ERK pathway to the plasma membrane, inducing its activation (Plotnikov et al., 2011; Burotto et al., 2014; Samatar and Poulikakos, 2014). Once activated, RAF phosphorylates and activates MEK (MEK1/2), which in turn, phosphorylates ERK1/2 – the final effectors of the ERK pathway (Robinson and Cobb, 1997; Burotto et al., 2014). Activation of ERK phosphorylates multiple substrates, which execute various processes, including but not limited to; cell cycle progression, cell adhesion, cell differentiation, cell survival and cell migration (Roskoski, 2012; Samatar and Poulikakos, 2014).

4.3.1.2 Overexpression of C1QBP affects the ERK pathway

In the present study, two genes - *RASGRP1* and *MAP3K8* - involved in the MAPK pathways were identified after performing pathway analysis of gene microarray studies, following knockdown of C1QBP in the MDA-MB-231 breast cancer cell line. RASGRPs are a group of guanine nucleotide exchange factors, which regulates conversion of small GTPase Ras from its inactive GDP-bound form to its active GTP-bound form (Ksionda et al., 2013). In this study, the *RASGRP1* gene expression decreased by 1.6 folds after knockdown of C1QBP in MDA-MB-231 breast cancer cell line. RASGRP1 has been reported to activate the Ras-Raf-Mek-Erk signalling cascade in blood cells, especially T cells (Dower et al., 2000; Stone, 2011). In addition, overexpression of RASGRP1 has been shown to cause resistance to treatment of acute myeloid leukemia by MEK1 inhibitor, but most importantly, the attenuation of RASGRP1 expression in acute myeloid leukemia restored the sensitivity to MEK1 inhibitors (Lauchle et al., 2009; Ksionda et al., 2013).

Unexpectedly, the gene microarray analysis also revealed an up-regulation of *MAP3K8* gene expression, after knockdown of C1QBP in MDA-MB-231 cells. While MAP3K8 has been implicated in the activation of the ERK pathway, the functional role of MAP3K8 in cancer is still unclear, as both tumor promoter and tumor suppressor functions have been reported for this protein (Vougioukalaki et al., 2011). Contrarily, the overexpression of C1QBP in MDA-MB-231 cells caused a significant increase of phosphorylated ERK1/2 as detected by Pathscan® Intracellular Signaling Array. In addition, further validation of active regulators in the ERK1/2

signalling cascade, revealed that overexpression of C1QBP also caused an increased in p-MEK1/2. In line with this, Kaul et al. (2012) has shown that the expression of p-ERK increased after overexpression of C1QBP in liver carcinoma cell line. Together with p-Akt and β-catenin, the group reported an increase in survival of HepG2 liver carcinoma cell line after overexpression of C1QBP (Kaul et al., 2012).

The ERK1/2 pathway has long been known as a growth-promoting and proliferation pathway (Katz et al., 2007). For example, using dominant-negative inactive MEK1 mutants or anti-sense RNA targeting ERK1/2, it has been shown that by blocking activation of the ERK1/2 pathway, fibroblast cell proliferation was inhibited (Pages et al., 1993; Seger et al., 1994). Furthermore, the ERK pathway, through several machineries, could induce cell cycle progression by influencing each phase of the cell cycle process (Chambard et al., 2007; Katz et al., 2007). For instance, the ERK pathway supported DNA synthesis during S phase by phosphorylation of carbamoyl phosphate synthase II, which has a role in pyrimidine biosynthesis (Graves et al., 2000). Blocking MEK or ERK activation not only retarded G2/M transition, but also prolonged the duration of mitosis (Chambard et al., 2007). However, ERK1/2 pathway has been shown to be a master regulator particularly of the G1 to S progression in the cell cycle process (Meloche and Pouyssegur, 2007). One way in which it regulates G1 to S progression, is by targeting the D-type cyclins (Meloche and Pouyssegur, 2007). It was deduced that the activation of ERK1/2 could possibly induce the expression of Cyclin D1 (Lavoie et al., 1996). This could be possible due to the presence of AP-1 site in the promoter region of Cyclin D1, which was activated by AP-1

transcription factors such as Fos and Jun (Albanese et al., 1995). Notably, sustained activation of ERK1/2 has been shown to increase expression of certain AP-1 proteins, such as Fra-1, c-Jun and JunB, as well as Cyclin D1 accumulation (Balmanno and Cook, 1999; Cook et al., 1999). Other than the Fos and Jun family, ERK could also regulate the transcription of Cyclin D1 via myc, wherein activation of ERK, phosphorylated and stabilized myc, which in turn, induced Cyclin D1 transcription (Seth et al., 1991; Daksis et al., 1994; Chambard et al., 2007). Furthermore, ERK1/2 may also promote the degradation of $p27^{Kip}$, a CDK inhibitor, hence, removing its inhibitory effect on Cyclin E-CDK2 complex (Kawada et al., 1997). Moreover, activation of MEK1/2 has been shown to regulate the assembly of Cyclin D1 and CDK4, thus further assisting in the sequestration of $p27^{Kip}$, thereby enhancing G1 to S progression (Cheng et al., 1998; Meloche and Pouyssegur, 2007).

From the current study, C1QBP has been shown to promote cell proliferation by enhancing G1 to S progression in MDA-MB-231 cells. This was accompanied by changes in expression of Cyclin D1 as well as CDK4/6. Hence, it could be postulated that overexpression of C1QBP increased activation of ERK, which could subsequently promote proliferation in the cells, by enhancing cell cycle progression via induction of Cyclin D1.

Apart from a well-established role of the ERK pathway in cell growth, the ERK pathway has also been frequently implicated in cell migration and invasion (Katz et al., 2007). Several downstream effectors such as Rho family GTPases, integrins and associated matrix adhesion proteins, extracellular proteases, cell-cell adhesion complexes and transcription factors of proteins relating to cell migration are regulated by the ERK signalling cascade (Viala

and Pouyssegur, 2004; Sever and Brugge, 2015). The lack of ERK activation has been shown to impair growth factor-stimulated migration by insulin, epidermal growth factor, fibroblast growth factor and vascular endothelial growth factor (Katz et al., 2007). Furthermore, the ERK pathway also induces expression of proteolytic enzymes, such as matrix metalloproteinases, and epithelial to mesenchymal-related factors, such as twist, vimentin, slug and fibronectin, thus promoting extracellular matrix protein degradation, as well as cell motility, and consequently, encourages invasion and migration (Chakraborti et al., 2003; Katz et al., 2007; Chen et al., 2009a; Kim and Choi, 2015; Sever and Brugge, 2015). In addition, the ERK1/2 cascade has been shown to regulate actin polymerization, as well as focal adhesion sites, by phosphorylating proteins, such as paxillin, myosin light chain kinase, calpain and focal adhesion kinase (Huang et al., 2004a; Katz et al., 2007; Kim and Choi, 2010). Through control of the interplay between these proteins, the ERK1/2 cascade promotes lamellipodia protrusion, thereafter inducing cell migration (Katz et al., 2007).

In human lung adenocarcinoma cells, C1QBP has been reported to co-localize at the lamellipodia raft. In addition to disruption of lamellipodia formation and migration ability after knockdown of C1QBP, growth factor-induced phosphorylation of ERK and AKT was also repressed (Eliseeva et al., 2011). In the present study, knockdown of C1QBP has been shown to decrease cell migration ability in MDA-MB-231 breast cancer cells. Complementarily, overexpression of C1QBP showed an obvious increase in cell migration alongside cell invasion, which was accompanied by up-regulation of p-ERK1/2 and p-MEK1/2. Thus, it is possible that the augmentation of cell

migration and invasion ability could be due to increased activity of the ERK1/2 pathway. The summary of the signalling pathway involved in C1QBP-mediated cell proliferation and metastasis is shown in Figure 4.2.

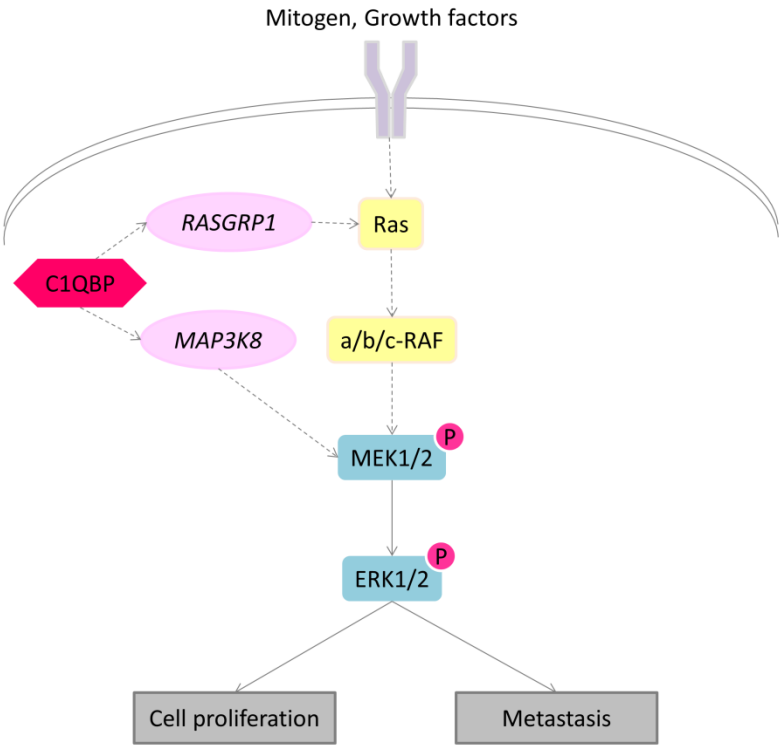

Figure 4.2. Role of ERK1/2 signalling pathway in C1QBP-mediated cell proliferation and metastasis. Alteration of *RASGRP1* and *MAP3K8* by C1QBP could affect Ras and p-MEK1/2 expression, respectively. This could activate the MAPK cascade. Overexpression of C1QBP increased the expression of p-MEK1/2 and p-ERK1/2, which are the main regulators of the MAPK cascade. The activation of this cascade could eventually cause cell proliferation and metastasis.

4.3.2 Involvement of C1QBP in the STAT3 pathway

4.3.2.1 The JAK-STAT pathway

The JAK-STAT pathway has been shown to be frequently dysregulated in diverse types of cancer (Sansone and Bromberg, 2012). The canonical JAK-STAT pathway begins with signal transduction from cytokines to its cognate receptors, inducing conformational changes, which lead to reorientation of preformed receptor dimers or dimerization of receptors (Li,

2008; Vainchenker and Constantinescu, 2013). This process activates JAK proteins, which are linked to the receptors' cytoplasmic flank, prompting receptor tyrosine phosphorylation, creating a docking site for cytoplasmic proteins, such as STAT proteins (Mohr et al., 2012). Tyrosine phosphorylation of STAT proteins by JAK will cause homodimerization of the STAT proteins (Mohr et al., 2012; Vainchenker and Constantinescu, 2013). In doing so, the STAT dimers will translocate to and retain in the nucleus, acting as transcription factors (Li, 2008; Vainchenker and Constantinescu, 2013). Additional posttranscriptional modifications to the STAT proteins, such as, serine phosphorylation, lysine acetylation and ubiquitination, regulate the transcriptional functions of STAT, contributing considerably to STAT-induced gene response (Lim and Cao, 2006; Mohr et al., 2012).

The STAT family comprised of 7 members i.e. STAT1-4, 5A, 5B and 6 (Li, 2008). Of these, STAT3 and STAT5 have been reported to play significant roles in tumor progression (Haura et al., 2005; Yu et al., 2014). While both STAT3 and STAT5 displayed prominent roles in cell proliferation and survival in cancer, STAT3 was also involved in the recruitment of immune cells to the tumor microenvironment, enhancing tumor progression, and at the same time, it has been shown to equip cells with the ability to evade the immune system (Haura et al., 2005; Kortylewski and Yu, 2008; Herrmann et al., 2010; Yu et al., 2014). In contrast to normal cells, where STAT3 activity is transient, cancer cells exhibit constitutive activation of STAT3 (Sellier et al., 2013). For example, STAT3 mutations have been shown to cause constitutive phosphorylation of STAT3 at Tyr705, in human inflammatory hepatocellular adenoma (Pilati et al., 2011). Likewise, mutations in the STAT3

protein were present in 40% of patients with large granular lymphocytic leukemia, together with up-regulation of its downstream targets, such as BCL2L1, JAK2 and IFNGR2 (Koskela et al., 2012). Apart from these, activation of STAT3 has also been shown to affect processes essential for tumorigenesis, such as, cell cycle progression, cell survival, angiogenesis, cancer inflammation, invasion and metastasis (Yu and Jove, 2004; Haura et al., 2005).

4.3.2.2 C1QBP affects STAT3 activation and its downstream targets

Pathway analysis done on data from gene microarray in the current study, has identified JAK-STAT signalling pathway, as one of the enriched pathways involved after silencing of C1QBP in MDA-MB-231 cells. Two genes – *IL15RA* and *IL23A* – were downregulated after knockdown of C1QBP in MDA-MB-231 cells. The IL15RA is a subunit of the IL15 receptor, which is part of the IL2R receptor family (Marra et al., 2014; Buchert et al., 2015). The IL15RA has been reported to bind to IL15 with the highest affinity compared to other IL15R subunits (Anderson et al., 1995). The binding of IL15 or IL2 to receptor systems in activated T cells, including the IL15 receptors, has been shown to induce activation of STAT3 and STAT5 (Lin et al., 1995; Tagaya et al., 1996). At the same time, IL15 signalling has also been shown to induce anti-apoptotic Bcl2, as well as the ERK signalling pathway (Miyazaki et al., 1995; Tagaya et al., 1996). A recent study indicated that IL15RA was overexpressed in triple negative breast cancers, especially in the immunomodulatory subtypes (Marra et al., 2014). Further, IL15RA was only discovered in basal-like breast cancer cell lines and absent in luminal-like cell

lines. Upon silencing of IL15RA in the cell lines, growth defects, as well as apoptotic cell death were observed (Marra et al., 2014).

The other downregulated gene related to the JAK-STAT signalling pathway, identified after knockdown of C1QBP in MDA-MB-231 cells is the *IL23A* gene. The *IL23A* gene encodes the p19 subunit of the IL23 ligand (Oppmann et al., 2000; Tindall and Hayes, 2010). IL23 binds to receptor complexes, which consist of the IL12 receptor β1 chain and IL23 receptor subunit. Since the IL12 receptors and IL23 receptor subunits recruit STAT4 and STAT3, respectively, signal transmission through IL23 could activate both STAT3 and STAT4 (Buchert et al., 2015). In the tumor microenvironment, STAT3 signalling appeared to transcriptionally activate *IL23A*, which promotes the tumor-enhancing IL23 program, while suppressing transcription of *IL12-p35* subunit, which favours the antitumor IL12 program (Kortylewski et al., 2009). Notably, the mRNA expression of *IL23A* has been shown to be up-regulated in various cancers, including breast, colon and ovarian cancers, compared to its normal adjacent tissues (Langowski et al., 2006). Moreover, IL23A knockout mice displayed resistance to tumor induction, tumor growth and tumor promotion (Langowski et al., 2006).

Whereas knockdown of C1QBP appeared to decrease signal transducers of the JAK-STAT signalling pathway, overexpression of C1QBP caused an increase in phosphorylation of STAT3 at Tyr705, as depicted by analysis from the Pathscan® Intracellular Signaling Array. MDA-MB-231 cells overexpressing C1QBP also displayed higher survival rates, evidenced by a decrease in sub-G1 phase. As previously cited, the Tyr705 phosphorylation of STAT3 is an important step in the canonical function of

STAT3 (Sellier et al., 2013). Activation of STAT3 has been shown to prevent apoptosis and hence enhance cell survival by regulating the anti-apoptotic Bcl2 family gene (Yu and Jove, 2004). One of the first evidence illustrating the role of STAT3 in cell survival, showed that constitutive activation of STAT3 increased expression of *Bcl-XL* and was essential in the survival of multiple myeloma cells (Catlett-Falcone et al., 1999). In addition, other members of the anti-apoptotic Bcl2 family, such as Bcl2 and Mcl1, have also been shown to be dependent on STAT3 activation (Zushi et al., 1998; Rahaman et al., 2002; Bhattacharya et al., 2005). Another target of STAT3 activation is the p53 protein. p53 is widely known as both an inhibitor of cell proliferation and a promoter of cell apoptosis. STAT3 could suppress p53 expression and more importantly, the attenuation of STAT3 signalling was able to restore the apoptosis function of p53 in cancer cells (Yu and Jove, 2004). As phosphorylation of STAT3 (Y705) was increased in conjunction with overexpression of C1QBP in MDA-MB-231 cells, the expression of Bcl2, Mcl1 and p53 – downstream targets of p-STAT3 – were explored in this study. The results obtained showed that overexpression of C1QBP in MDA-MB-231 cells, not only increased phosphorylation of STAT3 at Tyr705, but also augmented the expression of Bcl2 and Mcl1 while diminished p53. In addition, looking back at the gene microarray analysis, *Bcl2* gene expression was also decreased after knockdown of C1QBP. Thus, the increase in cell survival of MDA-MB-231 cells stably overexpressing C1QBP could be due to the increased activity of STAT3, which subsequently promoted the expression of pro-survival Bcl2 family.

In the current study, C1QBP has been shown to influence chemosensitivity of MDA-MB-231 cells to Doxorubicin hydrochloride treatment. In addition, the constitutive expression of C1QBP was higher in doxorubicin-resistant MCF7 breast cancer cells compared to parental MCF7 cells, indicating a role of C1QBP in mediating chemoresistance. Correspondingly, p-STAT3 and its downstream targets tested have also been implicated in chemoresistance. Chemoresistance arising from phosphorylation of STAT3, in particular at Tyr705 has been accounted for various types of cancers such as brain, breast, colorectal, cervical, bladder and prostate cancer (Spitzner et al., 2014). The STAT3-dependent modulation of Bcl2 expression in breast cancer cells has been shown to affect sensitivity to chemotherapeutic drugs (Real et al., 2002). In addition, chemoresistance due to STAT3-mediated Mcl1 expression has also been reported (Liu et al., 2011; Becker et al., 2014). Notably, in melanoma with B-RAF^{V600} mutation, B-RAF initiated the activation of p-STAT3 (Y705) which led to the accumulation of Mcl1, thought to be responsible for chemoresistance in this subtype of cancer (Becker et al., 2014). This also shows a possible crosstalk between the MAPK and STAT3 pathway through Tyr705 phosphorylation of STAT3 (Becker et al., 2014).

Aside from cell survival and chemoresistance, the activation of STAT3 has also been shown to regulate the expression of cell cycle-related proteins, such as c-myc and Cyclin D1 which controls G1-S progression (Kiuchi et al., 1999; Sinibaldi et al., 2000; Yu and Jove, 2004; Haura et al., 2005). Thus, in the present study, the increase of cell proliferation observed in MDA-MB-231 cells after overexpression of C1QBP could be due to an increase in activation

of p-STAT3 (Y705), which subsequently accumulates Cyclin D1, and as a consequence, expedited G1 to S progression.

Furthermore, STAT3 activity has also been reported to govern cell motility and invasion, greatly contributing to cancer metastasis (Kamran et al., 2013; Teng et al., 2014; Wendt et al., 2014). One way in which STAT3 regulates cell invasion is through the regulation of matrix metalloproteinases, (MMPs) such as MMP1, MMP2, MMP7 and MMP9 (Xie et al., 2004; Li et al., 2011; Kamran et al., 2013). After knockdown of C1QBP in MDA-MB-231 cells, gene microarray analysis revealed down-regulation of *MMP23B* gene, belonging to the MMP family. In the context of embryo implantation, a recent study showed that stimulation of IL11 in trophoblastic cells regulated STAT3 and ERK signalling pathways, which increased expression of Jun, Fos, MUC1, PDPN and MMP23B, thereby increasing cell invasiveness (Suman et al., 2012). Hence, activation of STAT3 could affect cell invasiveness through MMP23B, although further investigation needs to be done. STAT3 could also regulate cell migration by interacting with the Rho GTPases family (Debidda et al., 2005; Teng et al., 2009; Kamran et al., 2013). As an example, STAT3 binding to βPIX, an activator of RAC1, has been shown to control the organization of actin cytoskeleton and directional migration (Teng et al., 2009). In addition, epithelial to mesenchymal transition, one of the key mechanisms of cell migration, is highly intertwined with the STAT3 signalling pathway (Wendt et al., 2014). For instance, aberrant up-regulation of IL6 has been shown to increase STAT3 activity, as well as Twist. Overexpression of Twist further stimulates the production of IL6, which consequently leads to autocrine activation of STAT3, creating a positive feedback loop which also

feeds cancer EMT programs (Wendt et al., 2014). Hence, the increase phosphorylation of STAT3 (Y705) observed in the present study could possibly explain the increase in cell migration and invasion of MDA-MB-231 cells after overexpression of C1QBP. C1QBP-mediated JAK-STAT signalling and the effects on functional processes is illustrated in Figure 4.3.

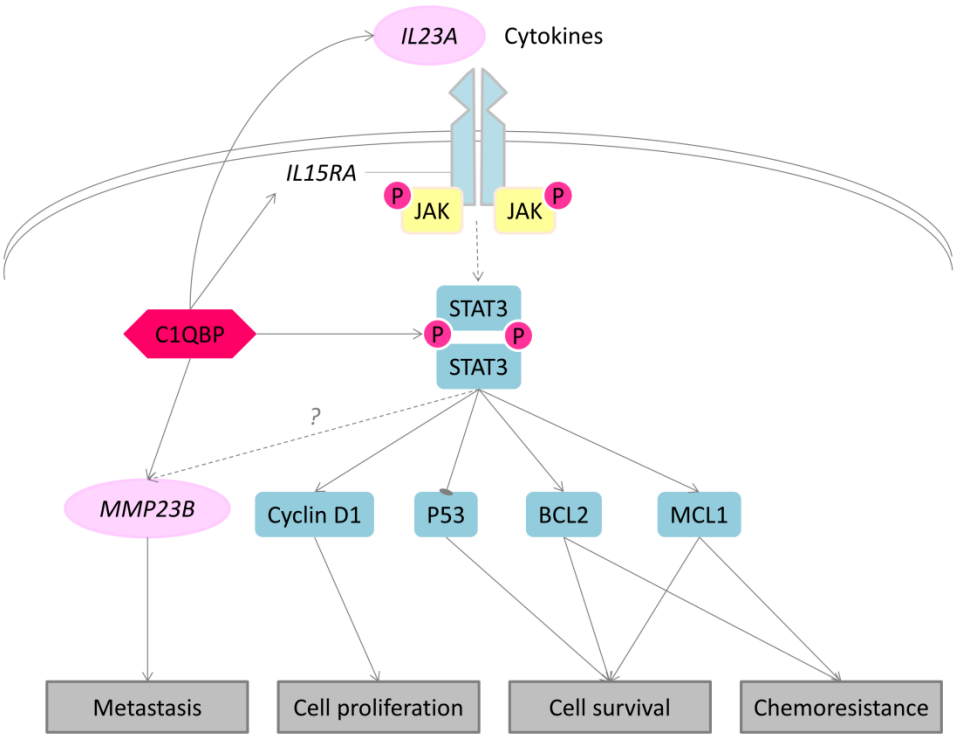

Figure 4.3. Role of C1QBP in the JAK/STAT pathway. C1QBP has been shown to alter *IL15RA*, a subunit of the IL15 interleukin receptor and *IL23A*, a subunit of the IL23 ligand. Interleukin and its receptors are important activators of the JAK-STAT pathway. Upon activation, p-JAK will activate p-STAT3. In the present study, C1QBP was shown to increase p-STAT3(Y705) expression and its downstream targets, which are involved in cell proliferation, survival and chemoresistance. In addition, C1QBP also altered the expression of MMP23B, which belongs to the MMP family. This could possibly contribute to cell invasion and subsequently, metastasis.

4.3.3 Potential involvement of C1QBP in the Akt-signalling pathway

From the Pathscan® Intracellular Signalling array analysis, the activity of three other molecules i.e. p-Akt (Ser473), p-S6 ribosomal protein (ser235/236) and p-GSK3β (Ser9) were up-regulated. These three proteins

have been implicated in the PI3K-Akt signalling pathway. The PI3K-Akt signalling pathway is a widely known regulator of cell proliferation, cell survival and resistance to anticancer therapy (Polivka and Janku, 2014; Sever and Brugge, 2015). Akt activation is triggered by stimulation of the growth factor receptor-associated PI3K, which forms 3'-polyphosphoinositides PIP3 and PIP2 at the plasma membrane (Bellacosa et al., 2005). These two molecules bind to the PH domain and recruits Akt to the membrane. The relocalization of Akt from cytoplasm to the membrane, primes it for activation by phosphorylation at Thr308 and Ser473 (Bellacosa et al., 2005; Toker and Marmiroli, 2014). Phosphorylation of Akt is a well proven factor of tumor progression, having roles in cell proliferation, growth, survival and metastasis (Cheung and Testa, 2013).

GSK3, a molecular target of activated Akt, is a serine/threonine kinase, which has been initially shown to be involved in metabolism. Further studies have shown that GSK3 is an important regulatory enzyme, having roles in various disorders, such as cancer, immune system disorders, neurological disorders and metabolic disorders (McCubrey et al., 2014). GSK3 is highly expressed in various tissues, and it has been shown to negatively regulate many proto-oncogenes and cell cycle regulators, hence being reputed as a tumor suppressor (Takahashi-Yanaga, 2013). The GSK3 protein comprises of the GSK3α and GSK3β isoforms. The functions of GSK3 are usually inhibited by phosphorylation at Ser21 in GSK3α and Ser9 in GSK3β (Takahashi-Yanaga, 2013). GSK3β has been shown to target Mcl1 and Cyclin D1 (Maurer et al., 2006; Sever and Brugge, 2015). The phosphorylation of these proteins by GSK3β marked them for degradation (Bellacosa et al., 2005). Therefore,

the phosphorylation of GSK3β by Akt will lead to stabilization of the Cyclin D1 and Mcl1 proteins (Bellacosa et al., 2005; Manning and Cantley, 2007). Consistent with the data obtained, increased in Akt activity (Ser473) was accompanied by increased phosphorylation of GSK3β (Ser9). In addition, p-GSK3β could potentially suppress the degradation of Mcl1 and Cyclin D1, leading to accumulation of these two proteins, which enhanced cell survival, proliferation and chemoresistance (Brown and Toker, 2015).

In conjunction with an increase of GSK3β phosphorylation, data from the Pathscan® array also showed that p-Akt (Ser473) up-regulation was coupled with p-S6 ribosomal protein (Ser235/236). In the Akt machinery, activation of mTOR by p-Akt will stimulate phosphorylation of p70 S6 kinase (p70S6K) and eukaryotic initiation factor 4E binding protein 1, 2, and 3 (4E-BPs). Activated p70S6K will phosphorylate S6 ribosomal protein which leads to increase translation and protein synthesis, mediating cell growth and proliferation (Dufner and Thomas, 1999). Additionally, S6 ribosomal protein has been shown to increase p-Akt (Ser473) and mTORC2 in a positive feedback loop (Yano et al., 2014). The activation of 4E-BPs phosphorylates the eIF4-binding protein, which releases the eIF4 cap binding factor and promotes cap-dependent translation of mRNA such as Cyclin D1, c-Myc and VEGF (Bellacosa et al., 2005). The potential role of C1QBP in the Akt signalling pathway is illustrated in Figure 4.4.

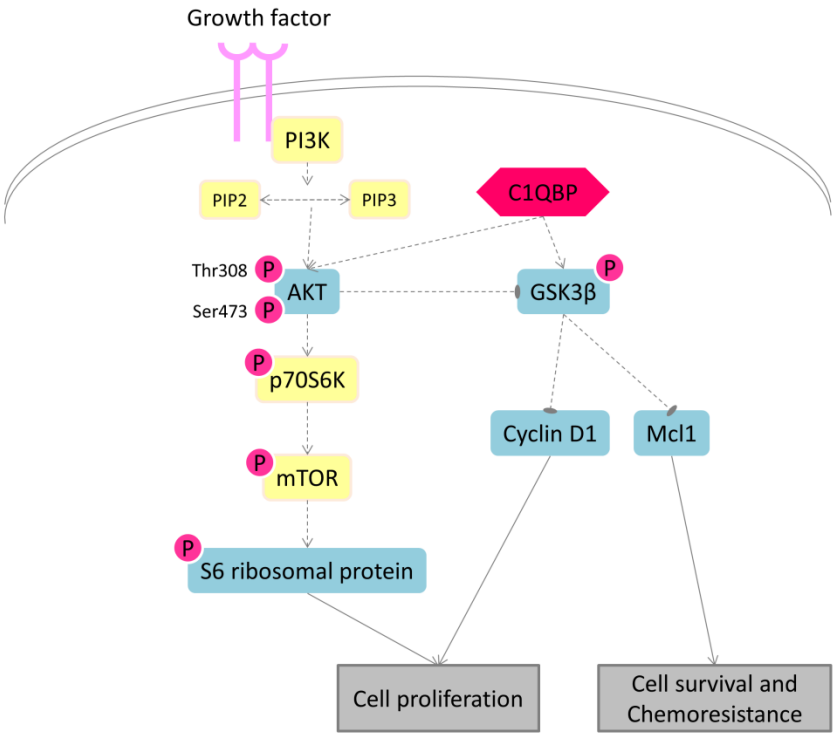

Figure 4.4. Potential role of C1QBP in the AKT signalling pathway. Overexpression of C1QBP increased p-AKT (Ser473). The phosphorylation of AKT promotes the phosphorylation of GSK3β, which relieves its inhibitory effects on Cyclin D1 and Mcl1. In addition, activation of AKT also leads to phosphorylation of S6 ribosomal protein, which enhances cell proliferation. Altogether, C1QBP could affect cell proliferation, survival and chemoresistance by regulating the AKT signalling pathway.

4.3.4 Interaction of C1QBP with YB-1

A key step in understanding a protein's function is to identify its interacting partners. To determine the C1QBP interactome, SILAC-immunoprecipitation quantitative proteomics was done. This method offers various advantages over other quantitative proteomics, such as chemical labelling of proteins or peptides. Firstly, metabolic labelling of the cells in SILAC culture takes place before any sample processing, thus minimizing variability due to subsequent biochemical or mass spectrometry procedures (Sap and Demmers, 2012). Complete incorporation of metabolic labelling encompassing proteins and peptides lead to extremely accurate and sensitive

data (Trinkle-Mulcahy, 2012). In comparison, labelling by chemical methods was done at later stages of sample treatment, which potentially introduces variability and hence, reducing its accuracy (Sap and Demmers, 2012). Additionally, apart from direct interactions, SILAC immunoprecipitation enabled the detection of low affinity or indirect interacting partners (Emmott and Goodfellow, 2014).

The data obtained showed that the C1QBP interactome was involved in RNA-binding and DNA-binding activities, such as, RNA processing, DEAD-box helicase activity and transcription factor regulation, demonstrated by DAVID analysis. In addition, transcription regulation was also identified as one of the enriched functional annotations in DAVID analysis of gene microarray performed, after knockdown of C1QBP. Thus, a specific protein, YB-1 was chosen for further studies. YB-1 is a multi-functional cold shock domain protein (Eliseeva et al., 2011). It is present in the cytoplasm, nucleus and can be secreted from cells. Likewise, YB-1 is involved in almost all DNA and mRNA-dependent processes, including DNA replication, DNA repair, transcription, pre-mRNA splicing and mRNA stabilization (Eliseeva et al., 2011). The overexpression of YB-1 in various cancers, such as breast cancer, gastric cancer, prostate tumor and rectal cancer, has been associated with poor prognosis (Janz et al., 2002; Huang et al., 2004b; Yasen et al., 2005; Habibi et al., 2008; Kosnopfel et al., 2014; Zhang et al., 2015). YB-1 has been reported to promote cell proliferation and metastatic potential in cancer cells. In addition, the nuclear translocation of YB-1 has been shown to be an early marker of multidrug resistance in tumor cells (Eliseeva et al., 2011).

Previous studies have shown that C1QBP interacts with YB-1 (Matsumoto et al., 2005; Wang et al., 2015). Matsumoto et al. (2005) showed that C1QBP relieves the mRNA translational repression of YB-1. In renal carcinoma cells, C1QBP seemed to repress functions of YB-1, by inhibiting phosphorylation and nuclear translocation of YB-1 (Wang et al., 2015). In the current study, the interaction of YB-1 and C1QBP was studied, in terms of cell proliferation, migration and invasion. In breast cancer cell lines and tissue samples, a positive correlation was observed between the gene expression of C1QBP and YB-1. C1QBP was found to co-localize with YB-1 in the mitochondria of MDA-MB-231 cells overexpressing C1QBP. Double knockdown of C1QBP and YB-1 did not show synergistic decrease for cell proliferation, migration and invasion. When C1QBP was diminished in YB-1-overexpressing cells, there was a decrease in cell proliferation, migration and invasion, but it did not return to the basal levels. Taken together, the interaction of C1QBP with YB-1 alone was not sufficient to induce cell proliferation, migration or invasion, implying that perhaps there are other factors which may also influence these functions.

4.4 Conclusion

In this study, the role of C1QBP in breast carcinogenesis has been explored, by a series of different functional analyses in breast cancer cell lines and breast cancer tissue samples. In breast cancer cell lines, C1QBP was shown to promote cell proliferation and survival, mainly by regulating the G1 to S transition in the cell cycle process through Cyclin D1 and CDK4/6. Accordingly, the expression of C1QBP was highly correlated with tumor size

at both the mRNA and protein levels in breast cancer TMAs. Furthermore, the expression of C1QBP independently predicted tumor size in PR-positive breast cancer patients, as observed by multivariate analysis.

High expression of C1QBP at the gene and protein level in breast cancer tissue samples, were associated with lymph node spread, although on further analysis, it was revealed that the expression of C1QBP was not independently associated with lymph node spread. Nonetheless, knockdown or overexpression of C1QBP in MDA-MB-231 breast cancer cell line, indicated a role of C1QBP in cell migration and invasion.

Gene microarray, Pathscan® Intracellular Array and interactome studies done after manipulating C1QBP expression have provided clues on the signalling pathways that were affected. From the gene microarray analysis, *RASGRP1* and *MAP3K8* were identified as potential regulators of the ERK1/2 pathway. In agreement with this, the antibody array used revealed a significant up-regulation of ERK1/2 activity after overexpression of C1QBP. Further investigations showed that C1QBP overexpression affected the expression of p-ERK1/2 and p-MEK1/2, both of which are important regulators of the ERK1/2 signalling pathway. Since the ERK1/2 signalling pathway has a widely established role in various cell functions, it can be postulated that C1QBP could mediate its functions in tumorigenesis through this pathway.

The analysis of gene microarray data also identified *IL15RA* and *IL23A*, both of which are involved in the JAK/STAT signalling pathway. In addition, antibody signalling array showed an increase of STAT3 (Y705) activation in C1QBP-overexpressing cells. Thereafter, the expression of downstream

targets of STAT3 was elucidated. Indeed, C1QBP was found to promote STAT3 (Y705) activity, which also enhanced the expression of Mcl1 and Bcl2 and reduced the expression of p53. This could account for the increased cell survival capability observed in C1QBP-overexpressing cells. Additionally, the survival-promoting property of the cells could contribute to increased Doxorubicin hydrochloride chemoresistance, observed in C1QBP-overexpressing cells. Apart from cell survival, phosphorylation of STAT3 (Y705) has also been shown to promote cell migration and invasion by various ways, including regulation of MMPs. In this study, gene microarray analysis also showed a decrease of *MMP23B*, after down-regulation of C1QBP. Although a direct link of p-STAT3 and MMP23B has not been reported, a previous study showed that STAT3 activation could lead to increased expression of MMP23B, and eventually promote cell invasion (Suman et al., 2012).

Additionally, Pathscan® Intracellular Signaling array has also revealed an up-regulation of p-Akt (Ser473), p-GSK3β (Ser9) and p-S6 ribosomal protein (Ser235/236), which are proteins involved in the Akt signalling pathway. This signalling pathway encompasses many cell processes, including cell growth and proliferation. The increase of p-S6 ribosomal protein has been known to increase cell proliferation. In addition, inhibition of GSK3β activity has also been shown to increase cell survival and proliferation, by preventing degradation of proteins, such as Cyclin D1 and Mcl1. However, the role of C1QBP in this pathway needs to be validated.

Together with the Akt signalling pathway, ERK1/2 signalling pathway and STAT3 signalling pathway have also been extensively associated to cell

proliferation, especially in promoting Cyclin D1 expression. Hence, it can also be proposed that these pathways influence the expression of Cyclin D1. In cooperation with CDK4/6, the accumulation of Cyclin D1 will increase cell proliferation.

Studies done using SILAC-immunoprecipitation quantitative proteomics, identified interacting partners with functions which are generally associated with DNA and RNA binding. A protein of interest, YB-1, a cold shock domain protein with prominent roles in DNA and RNA binding, was selected for further investigation on the role of its interaction with C1QBP, on functions such as, cell proliferation, migration and invasion. A correlation of C1QBP and YB-1 in breast cancer cell lines and tissue samples was observed at the gene level. In C1QBP-overexpressing cells, YB-1 and C1QBP seemed to be co-localized at the mitochondria. Although a synergistic effect was not observed upon double knockdown of C1QBP and YB-1, the knockdown of C1QBP in YB-1 overexpressing cells decreased cell proliferation, migration and invasion. However, this was not sufficient to reduce cell proliferation, migration and invasion to its original level. Hence, the role of C1QBP in these processes was only partially mediated by YB-1 and perhaps, other interacting partners were needed. Altogether, C1QBP could mediate cell proliferation, metastasis and chemoresistance, through ERK1/2, STAT3 and Akt signalling pathways. These cell processes could also be partially mediated through YB-1. The potential signalling pathways that C1QBP could be involved in is summarized in Figure 4.5.

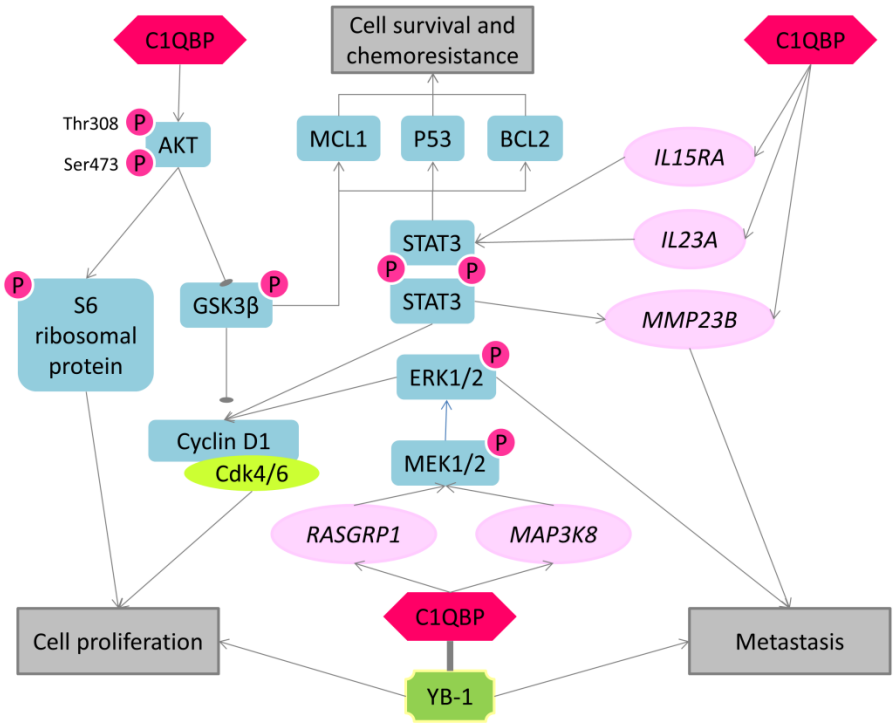

Figure 4.5. Potential signalling pathways mediated by C1QBP.

Given the multifunctional roles of C1QBP in breast cancer progression, particularly cell proliferation, migration and invasion, and its involvement in major cancer signalling pathways, such as the ERK1/2 and STAT3 pathways, C1QBP appears to be a promising molecular target for breast cancer. In fact, a monoclonal antibody, which targets C1QBP on cell surfaces has been shown to consistently block cell proliferation in lymphoma cell lines (Peerschke and Ghebrehiwet, 2014), paving the way for C1QBP as a therapeutic target in cancer.

4.5 Future studies

Since C1QBP has great potential as a molecular target in cancer, additional investigations on C1QBP could ensure its future development as a therapeutic target. Firstly, although this study has shown that C1QBP was involved in the ERK1/2 pathway and STAT3 pathway, specific targets of this

pathway was not verified. For instance, the role of MMP23B in C1QBP-mediated activation of STAT3 could be further investigated. In addition, Pathscan® Intracellular Signalling array has also shown that p-Akt (Ser473), p-GSK3β (Ser9) and p-S6 ribosomal protein (Ser235/236) were increased in C1QBP-overexpressing cells. Thus, the involvement of C1QBP in the Akt signalling pathway should be validated.

Apart from up-regulation of the anti-apoptotic Bcl2 family, the mechanism in which C1QBP induces chemoresistance should also be investigated. It would be interesting to determine the cancer stem cell-like properties of C1QBP-overexpressing cells as cancer stem cells have been shown to play key roles in recurrence following chemotherapy (Abdullah and Chow, 2013). In addition, the role of ATP-binding cassette (ABC) transporters should also be taken into account in C1QBP-mediated Doxorubicin resistance.

As reported, co-localization of YB-1 and C1QBP was detected in the mitochondria. The unique localization of YB-1 in the mitochondria warrants further investigation. YB-1 bound to nuclear-encoded mitochondrial oxidative phosphorylation mRNAs has been shown to be present at the outer membrane of mitochondria (Matsumoto et al., 2012). A more prominent mitochondrial localization of YB-1 has also been reported to significantly contribute to mitochondrial DNA mismatch-binding and mismatch-repair (de Souza-Pinto et al., 2009). Hence, it would be worthwhile to determine whether interaction of C1QBP and YB-1 could affect this activity, as disruption of mitochondrial DNA mismatch repair has been linked to DNA microsatellite instability and mitochondrial DNA instability, which has been implicated in cancer and aging (de Souza-Pinto et al., 2009).

Finally, the study of C1QBP's interactome has revealed interactions of proteins which have not been reported previously. Therefore, a deeper insight on C1QBP's functions could be attained by further exploring the interaction of C1QBP with these proteins.

REFERENCES

5 REFERENCES

Abdullah, L.N., and Chow, E.K. (2013). Mechanisms of chemoresistance in cancer stem cells. Clin Transl Med *2*, 3.

Agarwal, S., Jain, R., Rusia, U., and Gupta, R.L. (1997). Proliferating cell nuclear antigen immunostaining in breast carcinoma and its relationship to clinical and pathological variables. Indian J Pathol Microbiol *40*, 11-16.

Albanese, C., Johnson, J., Watanabe, G., Eklund, N., Vu, D., Arnold, A., and Pestell, R.G. (1995). Transforming p21ras mutants and c-Ets-2 activate the cyclin D1 promoter through distinguishable regions. J Biol Chem *270*, 23589-23597.

Albrecht, J.H., Poon, R.Y., Ahonen, C.L., Rieland, B.M., Deng, C., and Crary, G.S. (1998). Involvement of p21 and p27 in the regulation of CDK activity and cell cycle progression in the regenerating liver. Oncogene *16*, 2141-2150.

Amamoto, R., Yagi, M., Song, Y., Oda, Y., Tsuneyoshi, M., Naito, S., Yokomizo, A., Kuroiwa, K., Tokunaga, S., Kato, S., *et al.* (2011). Mitochondrial p32/C1QBP is highly expressed in prostate cancer and is associated with shorter prostate-specific antigen relapse time after radical prostatectomy. Cancer Sci *102*, 639-647.

Anderson, D.M., Kumaki, S., Ahdieh, M., Bertles, J., Tometsko, M., Loomis, A., Giri, J., Copeland, N.G., Gilbert, D.J., Jenkins, N.A., *et al.* (1995). Functional characterization of the human interleukin-15 receptor alpha chain and close linkage of IL15RA and IL2RA genes. J Biol Chem *270*, 29862-29869.

Anderson, K.N., Schwab, R.B., and Martinez, M.E. (2014). Reproductive risk factors and breast cancer subtypes: a review of the literature. Breast Cancer Res Treat *144*, 1-10.

Austreid, E., Lonning, P.E., and Eikesdal, H.P. (2014). The emergence of targeted drugs in breast cancer to prevent resistance to endocrine treatment and chemotherapy. Expert Opin Pharmacother *15*, 681-700.

Balmanno, K., and Cook, S.J. (1999). Sustained MAP kinase activation is required for the expression of cyclin D1, p21Cip1 and a subset of AP-1 proteins in CCL39 cells. Oncogene *18*, 3085-3097.

Bardia, A., and Baselga, J. (2014). Preoperative chemotherapy for operable breast cancer. In Diseases of the breast, J.R. Harris, M.E. Lipman, M. Morrow, and C.K. Osborne, eds. (Philadelphia: Wolters Kluwer/Lippincott Williams & Wilkins Health), pp. 743-753.

Becker, T.M., Boyd, S.C., Mijatov, B., Gowrishankar, K., Snoyman, S., Pupo, G.M., Scolyer, R.A., Mann, G.J., Kefford, R.F., Zhang, X.D., *et al.* (2014). Mutant B-RAF-Mcl-1 survival signaling depends on the STAT3 transcription factor. Oncogene *33*, 1158-1166.

Bellacosa, A., Kumar, C.C., Di Cristofano, A., and Testa, J.R. (2005). Activation of AKT kinases in cancer: implications for therapeutic targeting. Adv Cancer Res *94*, 29-86.

Benson, J.R. (2013). The biological basis for breast cancer screening and its relevance to treatment. In Early breast cancer from screening to multidisciplinary management, J.R. Benson, G. Gui, and T.M. Tuttle, eds. (Boca Raton: CRC Press Taylor & Francis Group), pp. 50-66.

Berg, W.A., Madsen, K.S., Schilling, K., Tartar, M., Pisano, E.D., Larsen, L.H., Narayanan, D., Ozonoff, A., Miller, J.P., and Kalinyak, J.E. (2011). Breast cancer: comparative effectiveness of positron emission mammography and MR imaging in presurgical planning for the ipsilateral breast. Radiology *258*, 59-72.

Bhattacharya, S., Ray, R.M., and Johnson, L.R. (2005). STAT3-mediated transcription of Bcl-2, Mcl-1 and c-IAP2 prevents apoptosis in polyamine-depleted cells. Biochem J *392*, 335-344.

Bleicher, R.J. (2014). Management of the palpable breast mass. In Diseases of the breast, J.R. Harris, M.E. Lipman, M. Morrow, and C.K. Osborne, eds. (Philadelphia: Wolters Kluwer/Lippincott Williams & Wilkins Health), pp. 29-37.

Bombonati, A., and Sgroi, D.C. (2011). The molecular pathology of breast cancer progression. J Pathol *223*, 307-317.

Bosetti, C., Bertuccio, P., Levi, F., Chatenoud, L., Negri, E., and La Vecchia, C. (2012). The decline in breast cancer mortality in Europe: an update (to 2009). Breast *21*, 77-82.

Brokstad, K.A., Kalland, K.H., Russell, W.C., and Matthews, D.A. (2001). Mitochondrial protein p32 can accumulate in the nucleus. Biochem Biophys Res Commun *281*, 1161-1169.

Brown, K.K., and Toker, A. (2015). The phosphoinositide 3-kinase pathway and therapy resistance in cancer. F1000Prime Rep *7*, 13.

Buchert, M., Burns, C.J., and Ernst, M. (2015). Targeting JAK kinase in solid tumors: emerging opportunities and challenges. Oncogene *In Press*.

Burotto, M., Chiou, V.L., Lee, J.M., and Kohn, E.C. (2014). The MAPK pathway across different malignancies: a new perspective. Cancer *120*, 3446-3456.

Cailleau, R., Young, R., Olive, M., and Reeves, W.J., Jr. (1974). Breast tumor cell lines from pleural effusions. J Natl Cancer Inst *53*, 661-674.

Cancer, C.G.o.H.F.i.B. (2012). Menarche, menopause, and breast cancer risk: individual participant meta-analysis, including 118 964 women with breast cancer from 117 epidemiological studies. Lancet Oncol *13*, 1141-1151.

Carey, L.A., Cheang, M.C.U., and Perou, C.M. (2014). Genomics, prognosis and therapeutic interventions. In Diseases of the breast, J.R. Harris, M.E.

Lipman, M. Morrow, and C.K. Osborne, eds. (Philadelphia: Wolters Kluwer/Lippincott Williams & Wilkins Health), pp. 452-472.

Casimiro, M.C., Velasco-Velazquez, M., Aguirre-Alvarado, C., and Pestell, R.G. (2014). Overview of cyclins D1 function in cancer and the CDK inhibitor landscape: past and present. Expert Opin Investig Drugs *23*, 295-304.

Catlett-Falcone, R., Landowski, T.H., Oshiro, M.M., Turkson, J., Levitzki, A., Savino, R., Ciliberto, G., Moscinski, L., Fernandez-Luna, J.L., Nunez, G., *et al.* (1999). Constitutive activation of Stat3 signaling confers resistance to apoptosis in human U266 myeloma cells. Immunity *10*, 105-115.

Chakraborti, S., Mandal, M., Das, S., Mandal, A., and Chakraborti, T. (2003). Regulation of matrix metalloproteinases: an overview. Mol Cell Biochem *253*, 269-285.

Chambard, J.C., Lefloch, R., Pouyssegur, J., and Lenormand, P. (2007). ERK implication in cell cycle regulation. Biochim Biophys Acta *1773*, 1299-1310.

Chattopadhyay, C., Hawke, D., Kobayashi, R., and Maity, S.N. (2004). Human p32, interacts with B subunit of the CCAAT-binding factor, CBF/NF-Y, and inhibits CBF-mediated transcription activation in vitro. Nucleic Acids Res *32*, 3632-3641.

Chen, H., Zhu, G., Li, Y., Padia, R.N., Dong, Z., Pan, Z.K., Liu, K., and Huang, S. (2009a). Extracellular signal-regulated kinase signaling pathway regulates breast cancer cell migration by maintaining slug expression. Cancer Res *69*, 9228-9235.

Chen, Y.B., Jiang, C.T., Zhang, G.Q., Wang, J.S., and Pang, D. (2009b). Increased expression of hyaluronic acid binding protein 1 is correlated with poor prognosis in patients with breast cancer. J Surg Oncol *100*, 382-386.

Chen, Z., Gibson, T.B., Robinson, F., Silvestro, L., Pearson, G., Xu, B., Wright, A., Vanderbilt, C., and Cobb, M.H. (2001). MAP kinases. Chem Rev *101*, 2449-2476.

Cheng, M., Sexl, V., Sherr, C.J., and Roussel, M.F. (1998). Assembly of cyclin D-dependent kinase and titration of p27Kip1 regulated by mitogen-activated protein kinase kinase (MEK1). Proc Natl Acad Sci U S A *95*, 1091-1096.

Cheung, M., and Testa, J.R. (2013). Diverse mechanisms of AKT pathway activation in human malignancy. Curr Cancer Drug Targets *13*, 234-244.

Chiarelli, A.M., Majpruz, V., Brown, P., Theriault, M., Shumak, R., and Mai, V. (2009). The contribution of clinical breast examination to the accuracy of breast screening. J Natl Cancer Inst *101*, 1236-1243.

Chowdhury, A.R., Ghosh, I., and Datta, K. (2008). Excessive reactive oxygen species induces apoptosis in fibroblasts: role of mitochondrially accumulated hyaluronic acid binding protein 1 (HABP1/p32/gC1qR). Exp Cell Res *314*, 651-667.

Clarke, M., Collins, R., Darby, S., Davies, C., Elphinstone, P., Evans, V., Godwin, J., Gray, R., Hicks, C., James, S., *et al.* (2005). Effects of radiotherapy and of differences in the extent of surgery for early breast cancer on local recurrence and 15-year survival: an overview of the randomised trials. Lancet *366*, 2087-2106.

Claus, E.B., Risch, N., and Thompson, W.D. (1994). Autosomal dominant inheritance of early-onset breast cancer. Implications for risk prediction. Cancer *73*, 643-651.

Colditz, G.A., Bohlke, K., and Berkey, C.S. (2014). Breast cancer risk accumulation starts early: prevention must also. Breast Cancer Res Treat *145*, 567-579.

Cook, S.J., Aziz, N., and McMahon, M. (1999). The repertoire of fos and jun proteins expressed during the G1 phase of the cell cycle is determined by the duration of mitogen-activated protein kinase activation. Mol Cell Biol *19*, 330-341.

Corn, P.G., and El-Deiry, W.S. (2002). Derangement of growth and differentiation control in oncogenesis. Bioessays *24*, 83-90.

Cox, J., and Mann, M. (2008). MaxQuant enables high peptide identification rates, individualized p.p.b.-range mass accuracies and proteome-wide protein quantification. Nat Biotechnol *26*, 1367-1372.

Daksis, J.I., Lu, R.Y., Facchini, L.M., Marhin, W.W., and Penn, L.J. (1994). Myc induces cyclin D1 expression in the absence of de novo protein synthesis and links mitogen-stimulated signal transduction to the cell cycle. Oncogene *9*, 3635-3645.

Dang, C., and Hudis, C.A. (2014). Adjuvant systemic chemotherapy in early breast cancer. In Diseases of the breast, J.R. Harris, M.E. Lipman, M. Morrow, and C.K. Osborne, eds. (Philadelphia: Wolters Kluwer/Lippincott Williams & Wilkins Health), pp. 635-648.

Dang, C.V. (2010). p32 (C1QBP) and cancer cell metabolism: is the Warburg effect a lot of hot air? Mol Cell Biol *30*, 1300-1302.

de Souza-Pinto, N.C., Mason, P.A., Hashiguchi, K., Weissman, L., Tian, J., Guay, D., Lebel, M., Stevnsner, T.V., Rasmussen, L.J., and Bohr, V.A. (2009). Novel DNA mismatch-repair activity involving YB-1 in human mitochondria. DNA Repair (Amst) *8*, 704-719.

Debidda, M., Wang, L., Zang, H., Poli, V., and Zheng, Y. (2005). A role of STAT3 in Rho GTPase-regulated cell migration and proliferation. J Biol Chem *280*, 17275-17285.

Dedio, J., Jahnen-Dechent, W., Bachmann, M., and Muller-Esterl, W. (1998). The multiligand-binding protein gC1qR, putative C1q receptor, is a mitochondrial protein. J Immunol *160*, 3534-3542.

Dembitzer, F.R., Kinoshita, Y., Burstein, D., Phelps, R.G., Beasley, M.B., Garcia, R., Harpaz, N., Jaffer, S., Thung, S.N., Unger, P.D., *et al.* (2012). gC1qR expression in normal and pathologic human tissues: differential expression in tissues of epithelial and mesenchymal origin. J Histochem Cytochem *60*, 467-474.

Dhillon, A.S., Hagan, S., Rath, O., and Kolch, W. (2007). MAP kinase signalling pathways in cancer. Oncogene *26*, 3279-3290.

Dower, N.A., Stang, S.L., Bottorff, D.A., Ebinu, J.O., Dickie, P., Ostergaard, H.L., and Stone, J.C. (2000). RasGRP is essential for mouse thymocyte differentiation and TCR signaling. Nat Immunol *1*, 317-321.

Dufner, A., and Thomas, G. (1999). Ribosomal S6 kinase signaling and the control of translation. Exp Cell Res *253*, 100-109.

Dumalaon-Canaria, J.A., Hutchinson, A.D., Prichard, I., and Wilson, C. (2014). What causes breast cancer? A systematic review of causal attributions among breast cancer survivors and how these compare to expert-endorsed risk factors. Cancer Causes Control *25*, 771-785.

Eisner, A., and Luoh, S.W. (2011). Breast cancer medications and vision: effects of treatments for early-stage disease. Curr Eye Res *36*, 867-885.

Eliseeva, I.A., Kim, E.R., Guryanov, S.G., Ovchinnikov, L.P., and Lyabin, D.N. (2011). Y-box-binding protein 1 (YB-1) and its functions. Biochemistry (Mosc) *76*, 1402-1433.

Emmott, E., and Goodfellow, I. (2014). Identification of protein interaction partners in mammalian cells using SILAC-immunoprecipitation quantitative proteomics. J Vis Exp *89*, 51656.

Engel, L.W., Young, N.A., Tralka, T.S., Lippman, M.E., O'Brien, S.J., and Joyce, M.J. (1978). Establishment and characterization of three new continuous cell lines derived from human breast carcinomas. Cancer Res *38*, 3352-3364.

Evans, D.G. (2013). Genetic predisposition and breast screening. In Early breast cancer, J.R. Benson, G. Gui, and T.M. Tuttle, eds. (Boca Raton: CRC Press Taylor and Francis Group), pp. 17-27.

Evans, D.G., Shenton, A., Woodward, E., Lalloo, F., Howell, A., and Maher, E.R. (2008). Penetrance estimates for BRCA1 and BRCA2 based on genetic testing in a Clinical Cancer Genetics service setting: risks of breast/ovarian cancer quoted should reflect the cancer burden in the family. BMC Cancer *8*, 155.

Ferlay, J., Soerjomataram I, Ervik M, Dikshit R, Eser S, Mathers C, Rebelo M, Parkin DM, Forman D, Bray, F (2013). GLOBOCAN 2012 v1.0, Cancer Incidence and Mortality Worldwide: IARC CancerBase No. 11 [Internet] (Lyon, France: International Agency for Research on Cancer).

Fogal, V., Richardson, A.D., Karmali, P.P., Scheffler, I.E., Smith, J.W., and Ruoslahti, E. (2010). Mitochondrial p32 protein is a critical regulator of tumor metabolism via maintenance of oxidative phosphorylation. Mol Cell Biol *30*, 1303-1318.

Ghebrehiwet, B., Lim, B.L., Peerschke, E.I., Willis, A.C., and Reid, K.B. (1994). Isolation, cDNA cloning, and overexpression of a 33-kD cell surface glycoprotein that binds to the globular "heads" of C1q. J Exp Med *179*, 1809-1821.

Ghebrehiwet, B., and Peerschke, E.I. (1998). Structure and function of gC1q-R: a multiligand binding cellular protein. Immunobiology *199*, 225-238.

Giacinti, C., and Giordano, A. (2006). RB and cell cycle progression. Oncogene *25*, 5220-5227.

Goldhirsch, A., Ingle, J.N., Gelber, R.D., Coates, A.S., Thurlimann, B., and Senn, H.J. (2009). Thresholds for therapies: highlights of the St Gallen International Expert Consensus on the primary therapy of early breast cancer 2009. Ann Oncol *20*, 1319-1329.

Graves, L.M., Guy, H.I., Kozlowski, P., Huang, M., Lazarowski, E., Pope, R.M., Collins, M.A., Dahlstrand, E.N., Earp, H.S., and Evans, D.R. (2000). Regulation of carbamoyl phosphate synthetase by MAP kinase. Nature *403*, 328-332.

Gunaratne, J., Goh, M.X., Swa, H.L., Lee, F.Y., Sanford, E., Wong, L.M., Hogue, K.A., Blackstock, W.P., and Okumura, K. (2011). Protein interactions of phosphatase and tensin homologue (PTEN) and its cancer-associated G20E mutant compared by using stable isotope labeling by amino acids in cell culture-based parallel affinity purification. J Biol Chem *286*, 18093-18103.

Habibi, G., Leung, S., Law, J.H., Gelmon, K., Masoudi, H., Turbin, D., Pollak, M., Nielsen, T.O., Huntsman, D., and Dunn, S.E. (2008). Redefining prognostic factors for breast cancer: YB-1 is a stronger predictor of relapse and disease-specific survival than estrogen receptor or HER-2 across all tumor subtypes. Breast Cancer Res *10*, R86.

Hanahan, D., and Weinberg, R.A. (2011). Hallmarks of cancer: the next generation. Cell *144*, 646-674.

Harris, J.R. (2014). Staging of breast cancer. In Diseases of the breast, J.R. Harris, M.E. Lipman, M. Morrow, and C.K. Osborne, eds. (Philadelphia: Wolters Kluwer/Lippincott Williams & Wilkins Health), pp. 495-503.

Harris, J.R., and Morrow, M. (2014). Breast-conserving Therapy. In Diseases of the breast, J.R. Harris, M.E. Lipman, M. Morrow, and C.K. Osborne, eds. (Philadelphia: Wolters Kluwer/Lippincott Williams & Wilkins Health), pp. 514-535.

Haura, E.B., Turkson, J., and Jove, R. (2005). Mechanisms of Disease: insights into the emerging role of signal transducers and activators of transcription in cancer. Nat Clin Prac Oncol *2*, 315-324.

Heichman, K.A., and Roberts, J.M. (1994). Rules to replicate by. Cell *79*, 557-562.

Herrmann, A., Kortylewski, M., Kujawski, M., Zhang, C., Reckamp, K., Armstrong, B., Wang, L., Kowolik, C., Deng, J., Figlin, R., *et al.* (2010). Targeting Stat3 in the myeloid compartment drastically improves the in vivo antitumor functions of adoptively transferred T cells. Cancer Res *70*, 7455-7464.

Huang, C., Jacobson, K., and Schaller, M.D. (2004a). MAP kinases and cell migration. J Cell Sci *117*, 4619-4628.

Huang, X., Ushijima, K., Komai, K., Takemoto, Y., Motoshima, S., Kamura, T., and Kohno, K. (2004b). Co-expression of Y box-binding protein-1 and P-glycoprotein as a prognostic marker for survival in epithelial ovarian cancer. Gynecol Oncol *93*, 287-291.

Itahana, K., and Zhang, Y. (2008). Mitochondrial p32 is a critical mediator of ARF-induced apoptosis. Cancer Cell *13*, 542-553.

Janz, M., Harbeck, N., Dettmar, P., Berger, U., Schmidt, A., Jurchott, K., Schmitt, M., and Royer, H.D. (2002). Y-box factor YB-1 predicts drug resistance and patient outcome in breast cancer independent of clinically relevant tumor biologic factors HER2, uPA and PAI-1. Int J Cancer *97*, 278-282.

Jiang, J., Zhang, Y., Krainer, A.R., and Xu, R.M. (1999). Crystal structure of human p32, a doughnut-shaped acidic mitochondrial matrix protein. Proc Natl Acad Sci U S A *96*, 3572-3577.

Jochelson, M.S. (2014). New breast imaging techniques. In Diseases of the breast, J.R. Harris, M.E. Lipman, M. Morrow, and C.K. Osborne, eds. (Philadelphia: Wolters Kluwer/Lippincott Williams & Wilkins Health), pp. 149-160.

Kamproh, S., and Fungpong, S. (2008). Effects of breast self-examination (BSE) program for detection early stage of breast cancer. J Med Assoc Thai *91 Suppl 3*, S147-151.

Kamran, M.Z., Patil, P., and Gude, R.P. (2013). Role of STAT3 in cancer metastasis and translational advances. Biomed Res Int *2013*, 421821.

Kao, J., Salari, K., Bocanegra, M., Choi, Y.L., Girard, L., Gandhi, J., Kwei, K.A., Hernandez-Boussard, T., Wang, P., Gazdar, A.F., *et al.* (2009). Molecular profiling of breast cancer cell lines defines relevant tumor models and provides a resource for cancer gene discovery. PLoS One *4*, e6146.

Katz, M., Amit, I., and Yarden, Y. (2007). Regulation of MAPKs by growth factors and receptor tyrosine kinases. Biochim Biophys Acta *1773*, 1161-1176.

Kaul, R., Saha, P., Saradhi, M., Prasad, R.L., Chatterjee, S., Ghosh, I., Tyagi, R.K., and Datta, K. (2012). Overexpression of hyaluronan-binding protein 1 (HABP1/p32/gC1qR) in HepG2 cells leads to increased hyaluronan synthesis

and cell proliferation by up-regulation of cyclin D1 in AKT-dependent pathway. J Biol Chem *287*, 19750-19764.

Kawada, M., Yamagoe, S., Murakami, Y., Suzuki, K., Mizuno, S., and Uehara, Y. (1997). Induction of p27Kip1 degradation and anchorage independence by Ras through the MAP kinase signaling pathway. Oncogene *15*, 629-637.

Keydar, I., Chen, L., Karby, S., Weiss, F.R., Delarea, J., Radu, M., Chaitcik, S., and Brenner, H.J. (1979). Establishment and characterization of a cell line of human breast carcinoma origin. Eur J Cancer *15*, 659-670.

Khan, A., and Haffty, B.G. (2014). Postmastectomy radiation therapy. In Diseases of the breast, J.R. Harris, M.E. Lipman, M. Morrow, and C.K. Osborne, eds. (Philadelphia: Wolters Kluwer/Lippincott Williams & Wilkins Health), pp. 604-617.

Kim, E.K., and Choi, E.J. (2010). Pathological roles of MAPK signaling pathways in human diseases. Biochim Biophys Acta *1802*, 396-405.

Kim, E.K., and Choi, E.J. (2015). Compromised MAPK signaling in human diseases: an update. Arch Toxicol *89*, 867-882.

Kim, K.B., Yi, J.S., Nguyen, N., Lee, J.H., Kwon, Y.C., Ahn, B.Y., Cho, H., Kim, Y.K., Yoo, H.J., Lee, J.S., *et al.* (2011). Cell-surface receptor for complement component C1q (gC1qR) is a key regulator for lamellipodia formation and cancer metastasis. J Biol Chem *286*, 23093-23101.

Kiuchi, N., Nakajima, K., Ichiba, M., Fukada, T., Narimatsu, M., Mizuno, K., Hibi, M., and Hirano, T. (1999). STAT3 is required for the gp130-mediated full activation of the c-myc gene. J Exp Med *189*, 63-73.

Kortylewski, M., Xin, H., Kujawski, M., Lee, H., Liu, Y., Harris, T., Drake, C., Pardoll, D., and Yu, H. (2009). Regulation of the IL-23 and IL-12 balance by Stat3 signaling in the tumor microenvironment. Cancer Cell *15*, 114-123.

Kortylewski, M., and Yu, H. (2008). Role of Stat3 in suppressing anti-tumor immunity. Curr Opin Immunol *20*, 228-233.

Koskela, H.L., Eldfors, S., Ellonen, P., van Adrichem, A.J., Kuusanmaki, H., Andersson, E.I., Lagstrom, S., Clemente, M.J., Olson, T., Jalkanen, S.E., *et al.* (2012). Somatic STAT3 mutations in large granular lymphocytic leukemia. N Engl J Med *366*, 1905-1913.

Kosnopfel, C., Sinnberg, T., and Schittek, B. (2014). Y-box binding protein 1-a prognostic marker and target in tumour therapy. Eur J Cell Biol *93*, 61-70.

Ksionda, O., Limnander, A., and Roose, J.P. (2013). RasGRP Ras guanine nucleotide exchange factors in cancer. Front Biol (Beijing) *8*, 508-532.

Kyriakis, J.M., and Avruch, J. (2001). Mammalian mitogen-activated protein kinase signal transduction pathways activated by stress and inflammation. Physiol Rev *81*, 807-869.

Langowski, J.L., Zhang, X., Wu, L., Mattson, J.D., Chen, T., Smith, K., Basham, B., McClanahan, T., Kastelein, R.A., and Oft, M. (2006). IL-23 promotes tumour incidence and growth. Nature *442*, 461-465.

Lauchle, J.O., Kim, D., Le, D.T., Akagi, K., Crone, M., Krisman, K., Warner, K., Bonifas, J.M., Li, Q., Coakley, K.M., *et al.* (2009). Response and resistance to MEK inhibition in leukaemias initiated by hyperactive Ras. Nature *461*, 411-414.

Lavoie, J.N., L'Allemain, G., Brunet, A., Muller, R., and Pouyssegur, J. (1996). Cyclin D1 expression is regulated positively by the p42/p44MAPK and negatively by the p38/HOGMAPK pathway. J Biol Chem *271*, 20608-20616.

Lee, C.I., and Elmore, J.G. (2014). Breast cancer screening. In Diseases of the breast, J.R. Harris, M.E. Lipman, M. Morrow, and C.K. Osborne, eds. (Philadelphia: Wolters Kluwer/Lippincott Williams & Wilkins Health), pp. 90-105.

Lewin, J.M. (2011). Radiologic techniques for early detection and diagnosis. In Early diagnosis and treatment of cancer series: breast cancer, L.J.A. Finlayson, ed. (Saint Louis: W.B. Saunders), pp. 125-139.

Li, H., Huang, C., Huang, K., Wu, W., Jiang, T., Cao, J., Feng, Z., and Qiu, Z. (2011). STAT3 knockdown reduces pancreatic cancer cell invasiveness and matrix metalloproteinase-7 expression in nude mice. PLoS One *6*, e25941.

Li, T., Guo, H., Song, Y., Zhao, X., Shi, Y., Lu, Y., Hu, S., Nie, Y., Fan, D., and Wu, K. (2014). Loss of vinculin and membrane-bound beta-catenin promotes metastasis and predicts poor prognosis in colorectal cancer. Mol Cancer *13*, 263.

Li, W.X. (2008). Canonical and non-canonical JAK-STAT signaling. Trends Cell Biol *18*, 545-551.

Lim, C.P., and Cao, X. (2006). Structure, function, and regulation of STAT proteins. Mol Biosyst *2*, 536-550.

Lin, J.X., Migone, T.S., Tseng, M., Friedmann, M., Weatherbee, J.A., Zhou, L., Yamauchi, A., Bloom, E.T., Mietz, J., John, S., *et al.* (1995). The role of shared receptor motifs and common stat proteins in the generation of cytokine pleiotropy and redundancy by IL-2, IL-4, IL-7, IL-13, and IL-15. Immunity *2*, 331-339.

Liu, H., Tekle, C., Chen, Y.W., Kristian, A., Zhao, Y., Zhou, M., Liu, Z., Ding, Y., Wang, B., Maelandsmo, G.M., *et al.* (2011). B7-H3 silencing increases paclitaxel sensitivity by abrogating Jak2/Stat3 phosphorylation. Mol Cancer Ther *10*, 960-971.

Lumachi, F., Luisetto, G., Basso, S.M., Basso, U., Brunello, A., and Camozzi, V. (2011). Endocrine therapy of breast cancer. Curr Med Chem *18*, 513-522.

Lutas, A., Wahlmark, C.J., Acharjee, S., and Kawasaki, F. (2012). Genetic analysis in Drosophila reveals a role for the mitochondrial protein p32 in synaptic transmission. G3 (Bethesda) *2*, 59-69.

Manning, B.D., and Cantley, L.C. (2007). AKT/PKB signaling: navigating downstream. Cell *129*, 1261-1274.

Marieb, E.N., Wilhelm, P.B., and Mallatt, J.B. (2014). Human anatomy, 7th edn (Edinburg Gate, Harlow, Essex: Pearson Education Limited).

Marra, P., Mathew, S., Grigoriadis, A., Wu, Y., Kyle-Cezar, F., Watkins, J., Rashid, M., De Rinaldis, E., Hessey, S., Gazinska, P., *et al.* (2014). IL15RA drives antagonistic mechanisms of cancer development and immune control in lymphocyte-enriched triple-negative breast cancers. Cancer Res *74*, 4908-4921.

Maruti, S.S., Willett, W.C., Feskanich, D., Rosner, B., and Colditz, G.A. (2008). A prospective study of age-specific physical activity and premenopausal breast cancer. J Natl Cancer Inst *100*, 728-737.

Mathew, J., and Cheung, K. (2013). Clinical assessment of symptomatic patients. In Early breast cancer from screening to multidisciplinary management, J.R. Benson, G. Gui, and T.M. Tuttle, eds. (Boca Raton: CRC Press Taylor & Francis Group), pp. 119-128.

Matos, P., Horn, J.A., Beards, F., Lui, S., Desforges, M., and Harris, L.K. (2014). A role for the mitochondrial-associated protein p32 in regulation of trophoblast proliferation. Mol Hum Reprod *20*, 745-755.

Matsumoto, K., Tanaka, K.J., and Tsujimoto, M. (2005). An acidic protein, YBAP1, mediates the release of YB-1 from mRNA and relieves the translational repression activity of YB-1. Mol Cell Biol *25*, 1779-1792.

Matsumoto, S., Uchiumi, T., Saito, T., Yagi, M., Takazaki, S., Kanki, T., and Kang, D. (2012). Localization of mRNAs encoding human mitochondrial oxidative phosphorylation proteins. Mitochondrion *12*, 391-398.

Maughan, K.L., Lutterbie, M.A., and Ham, P.S. (2010). Treatment of breast cancer. Am Fam Physician *81*, 1339-1346.

Maurer, U., Charvet, C., Wagman, A.S., Dejardin, E., and Green, D.R. (2006). Glycogen synthase kinase-3 regulates mitochondrial outer membrane permeabilization and apoptosis by destabilization of MCL-1. Mol Cell *21*, 749-760.

McCubrey, J.A., Steelman, L.S., Bertrand, F.E., Davis, N.M., Sokolosky, M., Abrams, S.L., Montalto, G., D'Assoro, A.B., Libra, M., Nicoletti, F., *et al.* (2014). GSK-3 as potential target for therapeutic intervention in cancer. Oncotarget *5*, 2881-2911.

McGee, A.M., and Baines, C.P. (2011). Complement 1q-binding protein inhibits the mitochondrial permeability transition pore and protects against oxidative stress-induced death. Biochem J *433*, 119-125.

McGee, A.M., Douglas, D.L., Liang, Y., Hyder, S.M., and Baines, C.P. (2011). The mitochondrial protein C1qbp promotes cell proliferation, migration and resistance to cell death. Cell Cycle *10*, 4119-4127.

Meenakshi, J., Anupama, Goswami, S.K., and Datta, K. (2003). Constitutive expression of hyaluronan binding protein 1 (HABP1/p32/gC1qR) in normal fibroblast cells perturbs its growth characteristics and induces apoptosis. Biochem Biophys Res Commun *300*, 686-693.

Meloche, S., and Pouyssegur, J. (2007). The ERK1/2 mitogen-activated protein kinase pathway as a master regulator of the G1- to S-phase transition. Oncogene *26*, 3227-3239.

Miyazaki, T., Liu, Z.J., Kawahara, A., Minami, Y., Yamada, K., Tsujimoto, Y., Barsoumian, E.L., Perlmutter, R.M., and Taniguchi, T. (1995). Three distinct IL-2 signaling pathways mediated by bcl-2, c-myc, and lck cooperate in hematopoietic cell proliferation. Cell *81*, 223-231.

Mohr, A., Chatain, N., Domoszlai, T., Rinis, N., Sommerauer, M., Vogt, M., and Muller-Newen, G. (2012). Dynamics and non-canonical aspects of JAK/STAT signalling. Eur J Cell Biol *91*, 524-532.

Morrow, M. (2014). Physical examination of the breast. In Diseases of the breast, J.R. Harris, M.E. Lipman, M. Morrow, and C.K. Osborne, eds. (Philadelphia: Wolters Kluwer/Lippincott Williams & Wilkins Health), pp. 25-28.

Morrow, M., and Golshan, M. (2014). Mastectomy. In Diseases of the breast, J.R. Harris, M.E. Lipman, M. Morrow, and C.K. Osborne, eds. (Philadelphia: Wolters Kluwer/Lippincott Williams & Wilkins Health), pp. 504-510.

Munagala, R., Aqil, F., and Gupta, R.C. (2011). Promising molecular targeted therapies in breast cancer. Indian J Pharmacol *43*, 236-245.

Muta, T., Kang, D., Kitajima, S., Fujiwara, T., and Hamasaki, N. (1997). p32 protein, a splicing factor 2-associated protein, is localized in mitochondrial matrix and is functionally important in maintaining oxidative phosphorylation. J Biol Chem *272*, 24363-24370.

NBOCC (2009). Breast cancer risk factors: A review of the evidence, N.B.O.C. Centre, ed. (Surry Hills, NSW).

Nilsson, C., Koliadi, A., Johansson, I., Ahlin, C., Thorstenson, S., Bergkvist, L., Hedenfalk, I., and Fjallskog, M.L. (2013). High proliferation is associated with inferior outcome in male breast cancer patients. Mod Pathol *26*, 87-94.

NRDO (2015). Singapore Cancer Registry Interim Annual Report. Trends in cancer incidence in Singapore 2010-2014 (Singapore: Ministry of Health).

Odle, T.G. (2014). Adverse effects of breast cancer treatment. Radiol Technol *85*, 297M-319M; quiz 320M-323M.

Oppmann, B., Lesley, R., Blom, B., Timans, J.C., Xu, Y., Hunte, B., Vega, F., Yu, N., Wang, J., Singh, K., *et al.* (2000). Novel p19 protein engages IL-

12p40 to form a cytokine, IL-23, with biological activities similar as well as distinct from IL-12. Immunity *13*, 715-725.

Pages, G., Lenormand, P., L'Allemain, G., Chambard, J.C., Meloche, S., and Pouyssegur, J. (1993). Mitogen-activated protein kinases p42mapk and p44mapk are required for fibroblast proliferation. Proc Natl Acad Sci U S A *90*, 8319-8323.

Peerschke, E.I., and Ghebrehiwet, B. (2007). The contribution of gC1qR/p33 in infection and inflammation. Immunobiology *212*, 333-342.

Peerschke, E.I., and Ghebrehiwet, B. (2014). cC1qR/CR and gC1qR/p33: observations in cancer. Mol Immunol *61*, 100-109.

Peerschke, E.I., Minta, J.O., Zhou, S.Z., Bini, A., Gotlieb, A., Colman, R.W., and Ghebrehiwet, B. (2004). Expression of gC1q-R/p33 and its major ligands in human atherosclerotic lesions. Mol Immunol *41*, 759-766.

Pestell, R.G. (2013). New roles of cyclin D1. Am J Pathol *183*, 3-9.

Petersen-Mahrt, S.K., Estmer, C., Ohrmalm, C., Matthews, D.A., Russell, W.C., and Akusjarvi, G. (1999). The splicing factor-associated protein, p32, regulates RNA splicing by inhibiting ASF/SF2 RNA binding and phosphorylation. EMBO J *18*, 1014-1024.

Pilati, C., Amessou, M., Bihl, M.P., Balabaud, C., Nhieu, J.T., Paradis, V., Nault, J.C., Izard, T., Bioulac-Sage, P., Couchy, G., *et al.* (2011). Somatic mutations activating STAT3 in human inflammatory hepatocellular adenomas. J Exp Med *208*, 1359-1366.

Plotnikov, A., Zehorai, E., Procaccia, S., and Seger, R. (2011). The MAPK cascades: signaling components, nuclear roles and mechanisms of nuclear translocation. Biochim Biophys Acta *1813*, 1619-1633.

Pointon, L.J., and Down, S.K. (2013). An introduction to screening for breast cancer. In Early breast cancer, J.R. Benson, G. Gui, and T.M. Tuttle, eds. (Boca Raton: CRC Press Taylor and Francis Group), pp. 1-12.

Polivka, J., Jr., and Janku, F. (2014). Molecular targets for cancer therapy in the PI3K/AKT/mTOR pathway. Pharmacol Ther *142*, 164-175.

Pozarowski, P., and Darzynkiewicz, Z. (2004). Analysis of cell cycle by flow cytometry. Methods Mol Biol *281*, 301-311.

Prakash, M., Kale, S., Ghosh, I., Kundu, G.C., and Datta, K. (2011). Hyaluronan-binding protein 1 (HABP1/p32/gC1qR) induces melanoma cell migration and tumor growth by NF-kappa B dependent MMP-2 activation through integrin alpha(v)beta(3) interaction. Cell Signal *23*, 1563-1577.

Prier, E. (2011). Surgical biopsy. In Early diagnosis and treatment of cancer series: breast cancer, L.J.C.A. Finlayson, ed. (Saint Louis: W.B. Saunders), pp. 175-183.

Rahaman, S.O., Harbor, P.C., Chernova, O., Barnett, G.H., Vogelbaum, M.A., and Haque, S.J. (2002). Inhibition of constitutively active Stat3 suppresses proliferation and induces apoptosis in glioblastoma multiforme cells. Oncogene *21*, 8404-8413.

Real, P.J., Sierra, A., De Juan, A., Segovia, J.C., Lopez-Vega, J.M., and Fernandez-Luna, J.L. (2002). Resistance to chemotherapy via Stat3-dependent overexpression of Bcl-2 in metastatic breast cancer cells. Oncogene *21*, 7611-7618.

Rimawi, M.F., and Osborne, C.K. (2014). Adjuvant systemic therapy: endocrine therapy. In Diseases of the breast, J.R. Harris, M.E. Lipman, M. Morrow, and C.K. Osborne, eds. (Philadelphia: Wolters Kluwer/Lippincott Williams & Wilkins Health), pp. 618-634.

Robinson, M.J., and Cobb, M.H. (1997). Mitogen-activated protein kinase pathways. Curr Opin Cell Biol *9*, 180-186.

Roskoski, R., Jr. (2012). ERK1/2 MAP kinases: structure, function, and regulation. Pharmacol Res *66*, 105-143.

Rossi, R.E., Pericleous, M., Mandair, D., Whyand, T., and Caplin, M.E. (2014). The role of dietary factors in prevention and progression of breast cancer. Anticancer Res *34*, 6861-6875.

Rozanov, D.V., Ghebrehiwet, B., Ratnikov, B., Monosov, E.Z., Deryugina, E.I., and Strongin, A.Y. (2002). The cytoplasmic tail peptide sequence of membrane type-1 matrix metalloproteinase (MT1-MMP) directly binds to gC1qR, a compartment-specific chaperone-like regulatory protein. FEBS Lett *527*, 51-57.

Rubinstein, D.B., Stortchevoi, A., Boosalis, M., Ashfaq, R., Ghebrehiwet, B., Peerschke, E.I., Calvo, F., and Guillaume, T. (2004). Receptor for the globular heads of C1q (gC1q-R, p33, hyaluronan-binding protein) is preferentially expressed by adenocarcinoma cells. Int J Cancer *110*, 741-750.

Rue, P., and Martinez Arias, A. (2015). Cell dynamics and gene expression control in tissue homeostasis and development. Mol Syst Biol *11*, 792.

Samatar, A.A., and Poulikakos, P.I. (2014). Targeting RAS-ERK signalling in cancer: promises and challenges. Nat Rev Drug Discov *13*, 928-942.

Sansone, P., and Bromberg, J. (2012). Targeting the interleukin-6/Jak/Stat pathway in human malignancies. J Clin Oncol *30*, 1005-1014.

Sap, K.A., and Demmers, J.A.A. (2012). Labeling methods in mass spectrometry based quantitative proteomics. In Integrative Proteomics, H.-C.E. Leung, ed. (Rijeka: InTech), pp. 111-132.

Schaeffer, H.J., and Weber, M.J. (1999). Mitogen-activated protein kinases: specific messages from ubiquitous messengers. Mol Cell Biol *19*, 2435-2444.

Schaerer, M.T., Kannenberg, K., Hunziker, P., Baumann, S.W., and Sigel, E. (2001). Interaction between GABA(A) receptor beta subunits and the multifunctional protein gC1q-R. J Biol Chem *276*, 26597-26604.

Schnitt, S.J. (2010). Classification and prognosis of invasive breast cancer: from morphology to molecular taxonomy. Mod Pathol *23*, S60-S64.

Sedgwick, E.L. (2014). Imaging analysis: ultrasonography. In Diseases of the breast, J.R. Harris, M.E. Lipman, M. Morrow, and C.K. Osborne, eds. (Philadelphia: Wolters Kluwer/Lippincott Williams & Wilkins Health), pp. 123-132.

Seger, R., and Krebs, E.G. (1995). The MAPK signaling cascade. FASEB J *9*, 726-735.

Seger, R., Seger, D., Reszka, A.A., Munar, E.S., Eldar-Finkelman, H., Dobrowolska, G., Jensen, A.M., Campbell, J.S., Fischer, E.H., and Krebs, E.G. (1994). Overexpression of mitogen-activated protein kinase kinase (MAPKK) and its mutants in NIH 3T3 cells. Evidence that MAPKK involvement in cellular proliferation is regulated by phosphorylation of serine residues in its kinase subdomains VII and VIII. J Biol Chem *269*, 25699-25709.

Sellier, H., Rebillard, A., Guette, C., Barre, B., and Coqueret, O. (2013). How should we define STAT3 as an oncogene and as a potential target for therapy? JAKSTAT *2*, e24716.

Seth, A., Alvarez, E., Gupta, S., and Davis, R.J. (1991). A phosphorylation site located in the NH2-terminal domain of c-Myc increases transactivation of gene expression. J Biol Chem *266*, 23521-23524.

Sever, R., and Brugge, J.S. (2015). Signal transduction in cancer. Cold Spring Harb Perspect Med *5*, pii: a006098.

Sherr, C.J. (1994). G1 phase progression: cycling on cue. Cell *79*, 551-555.

Sherr, C.J. (1996). Cancer cell cycles. Science *274*, 1672-1677.

Sherr, C.J., and Roberts, J.M. (1999). CDK inhibitors: positive and negative regulators of G1-phase progression. Genes Dev *13*, 1501-1512.

Shevchenko, A., Tomas, H., Havlis, J., Olsen, J.V., and Mann, M. (2006). In-gel digestion for mass spectrometric characterization of proteins and proteomes. Nat Protoc *1*, 2856-2860.

Simos, G., and Georgatos, S.D. (1994). The lamin B receptor-associated protein p34 shares sequence homology and antigenic determinants with the splicing factor 2-associated protein p32. FEBS Lett *346*, 225-228.

Simpson, P.T., Reis-Filho, J.S., Gale, T., and Lakhani, S.R. (2005). Molecular evolution of breast cancer. J Pathol *205*, 248-254.

Sinibaldi, D., Wharton, W., Turkson, J., Bowman, T., Pledger, W.J., and Jove, R. (2000). Induction of p21WAF1/CIP1 and cyclin D1 expression by the Src

oncoprotein in mouse fibroblasts: role of activated STAT3 signaling. Oncogene *19*, 5419-5427.

Sinn, H.P., and Kreipe, H. (2013). A Brief Overview of the WHO Classification of Breast Tumors, 4th Edition, Focusing on Issues and Updates from the 3rd Edition. Breast Care (Basel) *8*, 149-154.

Soltys, B.J., Kang, D., and Gupta, R.S. (2000). Localization of P32 protein (gC1q-R) in mitochondria and at specific extramitochondrial locations in normal tissues. Histochem Cell Biol *114*, 245-255.

Sonnenblick, A., Fumagalli, D., Sotiriou, C., and Piccart, M. (2014). Is the differentiation into molecular subtypes of breast cancer important for staging, local and systemic therapy, and follow up? Cancer Treat Rev *40*, 1089-1095.

Soule, H.D., Vazguez, J., Long, A., Albert, S., and Brennan, M. (1973). A human cell line from a pleural effusion derived from a breast carcinoma. J Natl Cancer Inst *51*, 1409-1416.

Spitzner, M., Ebner, R., Wolff, H.A., Ghadimi, B.M., Wienands, J., and Grade, M. (2014). STAT3: a novel molecular mediator of resistance to chemoradiotherapy. Cancers (Basel) *6*, 1986-2011.

Stone, J.C. (2011). Regulation and function of the RasGRP family of Ras activators in blood cells. Genes Cancer *2*, 320-334.

Storz, P., Hausser, A., Link, G., Dedio, J., Ghebrehiwet, B., Pfizenmaier, K., and Johannes, F.J. (2000). Protein kinase C [micro] is regulated by the multifunctional chaperon protein p32. J Biol Chem *275*, 24601-24607.

Suman, P., Godbole, G., Thakur, R., Morales-Prieto, D.M., Modi, D.N., Markert, U.R., and Gupta, S.K. (2012). AP-1 transcription factors, mucin-type molecules and MMPs regulate the IL-11 mediated invasiveness of JEG-3 and HTR-8/SVneo trophoblastic cells. PLoS One *7*, e29745.

Sung, J.S., and Comstock, C.E. (2014). Image-guided biopsy of nonpalpable breast lesions. In Diseases of the breast, J.R. Harris, M.E. Lipman, M. Morrow, and C.K. Osborne, eds. (Philadelphia: Wolters Kluwer/Lippincott Williams & Wilkins Health), pp. 161-172.

Tagaya, Y., Bamford, R.N., DeFilippis, A.P., and Waldmann, T.A. (1996). IL-15: a pleiotropic cytokine with diverse receptor/signaling pathways whose expression is controlled at multiple levels. Immunity *4*, 329-336.

Tai, S.K., Tan, O.J., Chow, V.T., Jin, R., Jones, J.L., Tan, P.H., Jayasurya, A., and Bay, B.H. (2003). Differential expression of metallothionein 1 and 2 isoforms in breast cancer lines with different invasive potential: identification of a novel nonsilent metallothionein-1H mutant variant. Am J Pathol *163*, 2009-2019.

Takahashi-Yanaga, F. (2013). Activator or inhibitor? GSK-3 as a new drug target. Biochem Pharmacol *86*, 191-199.

Teng, T.S., Lin, B., Manser, E., Ng, D.C., and Cao, X. (2009). Stat3 promotes directional cell migration by regulating Rac1 activity via its activator betaPIX. J Cell Sci *122*, 4150-4159.

Teng, Y., Ross, J.L., and Cowell, J.K. (2014). The involvement of JAK-STAT3 in cell motility, invasion, and metastasis. JAKSTAT *3*, e28086.

Tindall, E.A., and Hayes, V.M. (2010). Comprehensive sequence analysis of the human IL23A gene defines new variation content and high rate of evolutionary conservation. DNA Res *17*, 117-122.

Toker, A., and Marmiroli, S. (2014). Signaling specificity in the Akt pathway in biology and disease. Adv Biol Regul *55*, 28-38.

Torre, L.A., Bray, F., Siegel, R.L., Ferlay, J., Lortet-Tieulent, J., and Jemal, A. (2015). Global cancer statistics, 2012. CA Cancer J Clin *65*, 87-108.

Trinkle-Mulcahy, L. (2012). Resolving protein interactions and complexes by affinity purification followed by label-based quantitative mass spectrometry. Proteomics *12*, 1623-1638.

Tye, A.J., Ghebrehiwet, B., Guo, N., Sastry, K.N., Chow, B.K., Peerschke, E.I., and Lim, B.L. (2001). The human gC1qR/p32 gene, C1qBP. Genomic organization and promoter analysis. J Biol Chem *276*, 17069-17075.

Vainchenker, W., and Constantinescu, S.N. (2013). JAK/STAT signaling in hematological malignancies. Oncogene *32*, 2601-2613.

Vallenius, T. (2013). Actin stress fibre subtypes in mesenchymal-migrating cells. Open Biol *3*, 130001.

Viala, E., and Pouyssegur, J. (2004). Regulation of tumor cell motility by ERK mitogen-activated protein kinases. Ann N Y Acad Sci *1030*, 208-218.

Viale, G. (2012). The current state of breast cancer classification. Ann Oncol *23 Suppl 10*, x207-210.

Vougioukalaki, M., Kanellis, D.C., Gkouskou, K., and Eliopoulos, A.G. (2011). Tpl2 kinase signal transduction in inflammation and cancer. Cancer Lett *304*, 80-89.

Wang, Y., Yue, D., Xiao, M., Qi, C., Chen, Y., Sun, D., Zhang, N., and Chen, R. (2015). C1QBP negatively regulates the activation of oncoprotein YBX1 in the renal cell carcinoma as revealed by interactomics analysis. J Proteome Res *14*, 804-813.

Weinstein, S.P., and Roth, S.O. (2014). Imaging analysis: magnetic resonance imaging. In Diseases of the breast, J.R. Harris, M.E. Lipman, M. Morrow, and C.K. Osborne, eds. (Philadelphia: Wolters Kluwer/Lippincott Williams & Wilkins Health), pp. 133-148.

Wendt, M.K., Balanis, N., Carlin, C.R., and Schiemann, W.P. (2014). STAT3 and epithelial-mesenchymal transitions in carcinomas. JAKSTAT *3*, e28975.

Xie, T.X., Wei, D., Liu, M., Gao, A.C., Ali-Osman, F., Sawaya, R., and Huang, S. (2004). Stat3 activation regulates the expression of matrix metalloproteinase-2 and tumor invasion and metastasis. Oncogene *23*, 3550-3560.

Yagi, M., Uchiumi, T., Takazaki, S., Okuno, B., Nomura, M., Yoshida, S., Kanki, T., and Kang, D. (2012). p32/gC1qR is indispensable for fetal development and mitochondrial translation: importance of its RNA-binding ability. Nucleic Acids Res *40*, 9717-9737.

Yalcin, B. (2013). Staging, risk assessment and screening of breast cancer. Exp Oncol *35*, 238-245.

Yano, T., Ferlito, M., Aponte, A., Kuno, A., Miura, T., Murphy, E., and Steenbergen, C. (2014). Pivotal role of mTORC2 and involvement of ribosomal protein S6 in cardioprotective signaling. Circ Res *114*, 1268-1280.

Yao, Z.Q., Eisen-Vandervelde, A., Ray, S., and Hahn, Y.S. (2003). HCV core/gC1qR interaction arrests T cell cycle progression through stabilization of the cell cycle inhibitor p27Kip1. Virology *314*, 271-282.

Yasen, M., Kajino, K., Kano, S., Tobita, H., Yamamoto, J., Uchiumi, T., Kon, S., Maeda, M., Obulhasim, G., Arii, S., *et al.* (2005). The up-regulation of Y-box binding proteins (DNA binding protein A and Y-box binding protein-1) as prognostic markers of hepatocellular carcinoma. Clin Cancer Res *11*, 7354-7361.

Yoshikawa, H., Komatsu, W., Hayano, T., Miura, Y., Homma, K., Izumikawa, K., Ishikawa, H., Miyazawa, N., Tachikawa, H., Yamauchi, Y., *et al.* (2011). Splicing factor 2-associated protein p32 participates in ribosome biogenesis by regulating the binding of Nop52 and fibrillarin to preribosome particles. Mol Cell Proteomics *10*, M110 006148.

Youlden, D.R., Cramb, S.M., Dunn, N.A., Muller, J.M., Pyke, C.M., and Baade, P.D. (2012). The descriptive epidemiology of female breast cancer: an international comparison of screening, incidence, survival and mortality. Cancer Epidemiol *36*, 237-248.

Yu, G., and Wang, J. (2013). Significance of hyaluronan binding protein (HABP1/P32/gC1qR) expression in advanced serous ovarian cancer patients. Exp Mol Pathol *94*, 210-215.

Yu, H., and Jove, R. (2004). The STATs of cancer-new molecular targets come of age. Nat Rev Cancer *4*, 97-105.

Yu, H., Lee, H., Herrmann, A., Buettner, R., and Jove, R. (2014). Revisiting STAT3 signalling in cancer: new and unexpected biological functions. Nat Rev Cancer *14*, 736-746.

Yu, H., Liu, Q., Xin, T., Xing, L., Dong, G., Jiang, Q., Lv, Y., Song, X., Teng, C., Huang, D., *et al.* (2013). Elevated expression of hyaluronic acid binding protein 1 (HABP1)/P32/C1QBP is a novel indicator for lymph node and

peritoneal metastasis of epithelial ovarian cancer patients. Tumour Biol *34*, 3981-3987.

Yu, L., Loewenstein, P.M., Zhang, Z., and Green, M. (1995). In vitro interaction of the human immunodeficiency virus type 1 Tat transactivator and the general transcription factor TFIIB with the cellular protein TAP. J Virol *69*, 3017-3023.

Yu, Y.N. (2010). Functional studies of Y-box binding protein 1 in breast cancer. Dissertation. (Singapore: Department of Anatomy, National University of Singapore).

Zhang, X., Zhang, F., Guo, L., Wang, Y., Zhang, P., Wang, R., Zhang, N., and Chen, R. (2013). Interactome analysis reveals that C1QBP (complement component 1, q subcomponent binding protein) is associated with cancer cell chemotaxis and metastasis. Mol Cell Proteomics *12*, 3199-3209.

Zhang, Y., Zhao, P.W., Feng, G., Xie, G., Wang, A.Q., Yang, Y.H., Wang, D., and Du, X.B. (2015). The expression level and prognostic value of Y-box binding protein-1 in rectal cancer. PLoS One *10*, e0119385.

Zhao, J., Liu, T., Yu, G., and Wang, J. (2015). Overexpression of HABP1 correlated with clinicopathological characteristics and unfavorable prognosis in endometrial cancer. Tumour Biol *36*, 1299-1306.

Ziauddin, M.F., Hua, D., and Tang, S.C. (2014). Emerging strategies to overcome resistance to endocrine therapy for breast cancer. Cancer Metastasis Rev *33*, 791-807.

Zushi, S., Shinomura, Y., Kiyohara, T., Miyazaki, Y., Kondo, S., Sugimachi, M., Higashimoto, Y., Kanayama, S., and Matsuzawa, Y. (1998). STAT3 mediates the survival signal in oncogenic ras-transfected intestinal epithelial cells. Int J Cancer *78*, 326-330.

SUPPLEMENTARY DATA

Supplementary Table 1

Transcript ID	Gene Symbol	Gene name	RefSeq	p-value (Attribute)	p-value (siybap1 vs. nt)	Ratio (siybap1 vs. nt)	Fold-Change (siybap1 vs. nt)	F(Attribute)	SS(Attribute)	SS(Error)	F(Error)
16761518	TAS2R31	Taste receptor, type 2, member 31	NM_176885	0.0130177	0.0130177	2.43929	2.43929	18.1771	2.48248	0.546288	1
16820947	HPR	Haptoglobin-related protein	NM_020995	0.0352038	0.0352038	2.26608	2.26608	9.79348	2.08931	0.853347	1
16924149	TPTE	Transmembrane phosphatase with tensin homology	ENST00000415664	0.0136987	0.0136987	2.16776	2.16776	17.6378	1.86888	0.423834	1
16801028	RNA5SP395	RNA, 5S ribosomal pseudogene 395	ENST00000516567	0.0499184	0.0499184	2.14439	2.14439	7.71751	1.81688	0.941693	1
16992195	MIR378E	MicroRNA 378e	NR_039609	0.0479144	0.0479144	2.13078	2.13078	7.94241	1.78666	0.899809	1
17051439	RNU7-73P	RNA, U7 small nuclear 73 pseudogene	ENST00000458743	0.0105224	0.0105224	2.06486	2.06486	20.5829	1.64131	0.318966	1
17008025	RAB44	RAB44, member RAS oncogene family	NM_001257357	0.00393404	0.00393404	2.05404	2.05404	35.742	1.61761	0.181032	1
16721212	OR51F2	Olfactory receptor, family 51, subfamily F, member 2	ENST00000322110	0.0268037	0.0268037	1.95385	1.95385	11.6899	1.40067	0.479277	1
16898567	GKN2	Gastrokine 2	NM_182536	0.0357134	0.0357134	1.93535	1.93535	9.70058	1.36115	0.561265	1
17091932	CBWD1	COBW domain containing 1	NM_018491	0.00996034	0.00996034	1.89753	1.89753	21.2463	1.28101	0.241173	1
16979330	FLJ14186	Uncharacterized LOC401149	NR_037596	0.00903048	0.00903048	1.89212	1.89212	22.4772	1.26961	0.225938	1
16810972	SNORD18B	Small nucleolar RNA, C/D box 18B	NR_002442	0.0054852	0.0054852	1.88865	1.88865	29.7664	1.2623	0.169627	1
17118419	CDC14B	Cell division cycle 14B	ENST00000481149	0.00759399	0.00759399	1.86621	1.86621	24.8066	1.2153	0.195963	1
17046586	SNORA22	Small nucleolar RNA, H/ACA box 22	NR_002961	0.0327419	0.0327419	1.86355	1.86355	10.2726	1.20974	0.471057	1
16774764	RNY3P2	RNA, Ro-associated Y3 pseudogene 2	ENST00000362918	0.00917447	0.00917447	1.8395	1.8395	22.2744	1.15979	0.208274	1
16888454	FSIP2	Fibrous sheath interacting protein 2	NM_173651	0.0274427	0.0274427	1.8231	1.8231	11.5154	1.12595	0.39111	1
17093018	EQTN	Equatorin, sperm acrosome associated	NM_020641	0.00143389	0.00143389	1.81232	1.81232	61.367	1.10383	0.071949	1
16761514	TAS2R19	Taste receptor, type 2, member 19	ENST00000390673	0.0413512	0.0413512	1.80937	1.80937	8.79088	1.0978	0.499517	1

16760825	CLEC4C	C-type lectin domain family 4, member C	BC114338	0.0122955	0.0122955	1.7908	1.7908	18.7974	1.05992	0.225547	1
17111801	IGBP1-AS1	IGBP1 antisense RNA 1	ENST00000366397	0.0423266	0.0423266	1.76075	1.76075	8.65231	0.99924	0.461953	1
16665507	FOXD3	Forkhead box D3	NM_012183	0.00367629	0.00367629	1.75292	1.75292	37.087	0.98356	0.106081	1
17115154	TREX2	Three prime repair exonuclease 2	NM_080701	0.0422422	0.0422422	1.73375	1.73375	8.66412	0.945401	0.436467	1
16942369	SNTN	Sentan, cilia apical structure protein	ENST00000343837	0.0333035	0.0333035	1.72339	1.72339	10.1586	0.92493	0.364197	1
17117114	BCORP1	BCL6 corepressor pseudogene 1	NR_033732	0.0163674	0.0163674	1.72119	1.72119	15.86	0.920585	0.232177	1
16788669	SNORD114-17	Small nucleolar RNA, C/D box 114-17	NR_003210	0.0290858	0.0290858	1.71756	1.71756	11.0938	0.91344	0.329352	1
16830343	SLC2A4	Solute carrier family 2 (facilitated glucose transporter), member	NM_001042	0.00487364	0.00487364	1.71049	1.71049	31.7786	0.899565	0.113229	1
17112362	MIR4328	MicroRNA 4328	NR_036258	0.0301389	0.0301389	1.70784	1.70784	10.8419	0.89438	0.329971	1
16865060	MIR517A	MicroRNA 517a	NR_030201	0.00189589	0.00189589	1.702	1.702	52.9378	0.882966	0.066717	1
16755223	KRT19P2	Keratin 19 pseudogene 2	NR_036685	0.0430275	0.0430275	1.66399	1.66399	8.5557	0.80955	0.378485	1
17108740	P2RY8	Purinergic receptor P2Y, G-protein coupled, 8	ENST00000460672	0.0237277	0.0237277	1.66232	1.66232	12.6261	0.806379	0.255464	1
17046422	ZNF735	Zinc finger protein 735	NM_001159524	0.010731	0.010731	1.65518	1.65518	20.3501	0.792771	0.155827	1
16803618	MIR184	MicroRNA 184	NR_029705	0.0196718	0.0196718	1.65475	1.65475	14.183	0.791958	0.223354	1
16878888	MIR558	MicroRNA 558	NR_030285	0.025101	0.025101	1.65445	1.65445	12.1868	0.791372	0.259747	1
16814628	TPSD1	Tryptase delta 1	NM_012217	0.0319127	0.0319127	1.65202	1.65202	10.4463	0.786757	0.301258	1
16941704	ITIH1	Inter-alpha-trypsin inhibitor heavy chain 1	NM_001166434	0.0102624	0.0102624	1.65014	1.65014	20.883	0.7832	0.150017	1
16812373	LOC100133746	Uncharacterized LOC100133746	ENST00000548231	0.0197171	0.0197171	1.64507	1.64507	14.163	0.773611	0.218488	1
16934881	SOX10	SRY (sex determining region Y)-box 10	NM_006941	0.039498	0.039498	1.64284	1.64284	9.06821	0.769392	0.33938	1
17005790	HIST2H4B	Histone cluster 2, H4b	ENST00000354348	0.0095927	0.0095927	1.64185	1.64185	21.7115	0.76753	0.141405	1
16731054	MIR34B	MicroRNA 34b	NR_029839	0.0384154	0.0384154	1.63941	1.63941	9.23947	0.762938	0.330295	1
16831527	CCDC144A	Coiled-coil domain containing 144A	ENST00000443444	0.0402288	0.0402288	1.63901	1.63901	8.95654	0.762174	0.340388	1
16895337	POMC	Proopiomelanocortin	NM_001035256	0.0323654	0.0323654	1.63019	1.63019	10.3506	0.745614	0.288143	1

16659794	CLCNKA	Chloride channel, voltage-sensitive Ka	NM_004070	0.031585	0.031585	1.62784	1.62784	10.5169	0.741219	0.281916	1
16705992	MIR4676	MicroRNA 4676	NR_039823	0.034681	0.034681	1.61913	1.61913	9.89091	0.725003	0.2932	1
17107371	SRD5A1P1	Steroid-5-alpha-reductase, alpha polypeptide 1 pseudogene 1	NR_028597	0.0458398	0.0458398	1.6169	1.6169	8.19069	0.720845	0.352031	1
16703659	MAP3K8	Mitogen-activated protein kinase kinase kinase 8	AB209539	0.00793012	0.00793012	1.59747	1.59747	24.2051	0.68504	0.113206	1
16747917	FAM66C	Family with sequence similarity 66, member C	NR_026788	0.0333728	0.0333728	1.59684	1.59684	10.1447	0.683887	0.269653	1
17095020	NMRK1	Nicotinamide riboside kinase 1	NR_023352	0.0252456	0.0252456	1.58741	1.58741	12.1426	0.666679	0.219616	1
16785083	HIF1A	Hypoxia inducible factor 1, alpha subunit (basic helix-loop	ENST00000554177	0.0329583	0.0329583	1.58611	1.58611	10.2283	0.664318	0.259796	1
16927749	IGLV1-44	Immunoglobulin lambda variable 1-44	ENST00000390297	0.023334	0.023334	1.58288	1.58288	12.7592	0.658459	0.206427	1
16909760	ASB18	Ankyrin repeat and SOCS box containing 18	NM_212556	0.0360273	0.0360273	1.579	1.579	9.64435	0.651438	0.270184	1
16852921	LOC284294	Uncharacterized LOC284294	NR_033881	0.00617287	0.00617287	1.57756	1.57756	27.8715	0.648843	0.093119	1
16748275	CLEC9A	C-type lectin domain family 9, member A	NM_207345	0.0166945	0.0166945	1.57568	1.57568	15.672	0.645455	0.164741	1
16862815	ZNF575	Zinc finger protein 575	NM_174945	0.0448975	0.0448975	1.57563	1.57563	8.30913	0.645356	0.310673	1
16969155	MIR3684	MicroRNA 3684	NR_037455	0.0330968	0.0330968	1.56999	1.56999	10.2002	0.635232	0.249106	1
16873160	ZFP112	Zinc finger protein 112 homolog	NM_001083335	0.03461	0.03461	1.56926	1.56926	9.90432	0.633923	0.256018	1
16678946	LOC100506810	Uncharacterized LOC100506810	NR_038856	0.00234529	0.00234529	1.5632	1.5632	47.2635	0.623077	0.052732	1
17014798	SMOC2	SPARC related modular calcium binding 2	NM_022138	0.0471266	0.0471266	1.56271	1.56271	8.03474	0.622195	0.309753	1
16811577	LOC283731	Uncharacterized LOC283731	NR_027073	0.0212716	0.0212716	1.56145	1.56145	13.5157	0.619947	0.183474	1
16803469	DNAJA4	DnaJ (Hsp40) homolog, subfamily A, member 4	NM_018602	0.0271638	0.0271638	1.56123	1.56123	11.5908	0.619556	0.213809	1
16701634	OR14I1	Olfactory receptor, family 14, subfamily I, member 1	ENST00000342623	0.010847	0.010847	1.56073	1.56073	20.2235	0.618673	0.122367	1

16954705	LINC00696	Long intergenic non-protein coding RNA 696	NR_027331	0.0190837	0.0190837	1.55961	1.55961	14.4492	0.616686	0.170718	1
16958638	KLF15	Kruppel-like factor 15	NM_014079	0.00203996	0.00203996	1.55624	1.55624	50.9155	0.610687	0.047977	1
16697272	LOC100288079	Microtubule-associated protein 1 light chain 3 beta pseudo	NR_038424	0.039607	0.039607	1.55339	1.55339	9.05136	0.605634	0.267644	1
16673341	RNA5SP65	RNA, 5S ribosomal pseudogene 65	ENST00000363166	0.042946	0.042946	1.54523	1.54523	8.56681	0.591249	0.276065	1
16778677	LINC00330	Long intergenic non-protein coding RNA 330	AK056732	0.0313837	0.0313837	1.54379	1.54379	10.5608	0.588709	0.22298	1
16809123	USP50	Ubiquitin specific peptidase 50	NM_203494	0.0100706	0.0100706	1.54204	1.54204	21.1119	0.585633	0.110958	1
16679799	OR2T4	Olfactory receptor, family 2, subfamily T, member 4	NM_001004696	0.0318457	0.0318457	1.54202	1.54202	10.4606	0.585598	0.223924	1
16799776	OIP5-AS1	OIP5 antisense RNA 1	ENST00000558945	0.0347324	0.0347324	1.53624	1.53624	9.88123	0.575486	0.232961	1
16927742	IGLV7-46	Immunoglobulin lambda variable 7-46 (gene/pseudogene)	ENST00000390295	0.0340871	0.0340871	1.53516	1.53516	10.0043	0.573606	0.229344	1
16788731	MIR1193	MicroRNA 1193	NR_036132	0.0164339	0.0164339	1.52923	1.52923	15.8214	0.563296	0.142414	1
16804062	TM6SF1	Transmembrane 6 superfamily member 1	NM_023003	0.00223439	0.00223439	1.52746	1.52746	48.503	0.560234	0.046202	1
16704027	ZNF37A	Zinc finger protein 37A	NM_001007094	0.0152454	0.0152454	1.52651	1.52651	16.5503	0.558585	0.135003	1
16849597	C1QTNF1-AS1	C1QTNF1 antisense RNA 1	NR_040018	0.0433442	0.0433442	1.52573	1.52573	8.51281	0.557226	0.26183	1
16667481	DPYD-AS1	DPYD antisense RNA 1	NR_046590	0.0116713	0.0116713	1.52374	1.52374	19.3792	0.553798	0.114307	1
16725084	OR5A1	Olfactory receptor, family 5, subfamily A, member 1	ENST00000302030	0.00858497	0.00858497	1.52101	1.52101	23.1366	0.549097	0.094931	1
16926043	TFF1	Trefoil factor 1	ENST00000291527	0.0368823	0.0368823	1.51829	1.51829	9.49486	0.544416	0.229352	1
16865498	KIR3DL1	Killer cell immunoglobulin-like receptor, three domains, long c	NM_013289	0.040739	0.040739	1.51015	1.51015	8.88038	0.530494	0.238951	1
16858756	GCDH	Glutaryl-CoA dehydrogenase	NM_000159	0.0393276	0.0393276	0.666147	-1.50117	9.09469	0.51525	0.226616	1
16826619	LOC100132339	Uncharacterized LOC100132339	ENST00000559802	0.0432994	0.0432994	0.665876	-1.50178	8.51885	0.516279	0.242417	1
16657895	MMP23B	Matrix metallopeptidase 23B	NM_006983	0.00553606	0.00553606	0.665351	-1.50297	29.6143	0.518284	0.070005	1
16812517	LOC80154	Golgin A2 pseudogene	NR_026811	0.0249706	0.0249706	0.664977	-1.50381	12.2269	0.519717	0.170024	1

17069141	LOC286177	Uncharacterized LOC286177	NR_038874	0.0109349	0.0109349	0.662864	-1.5086	20.1289	0.527856	0.104895	1
16848692	HID1	HID1 domain containing	NM_030630	0.0300424	0.0300424	0.661961	-1.51066	10.8644	0.531363	0.195634	1
17042805	GET4	Golgi to ER traffic protein 4 homolog (S. cerevisiae)	NM_015949	0.0420725	0.0420725	0.659264	-1.51684	8.68794	0.541931	0.24951	1
16686376	ZSWIM5	Zinc finger, SWIM-type containing 5	NM_020883	0.00694559	0.00694559	0.657235	-1.52153	26.0879	0.54998	0.084327	1
17008529	TOMM6	Translocase of outer mitochondrial membrane 6 homolog (yeast)	AJ420506	0.0161474	0.0161474	0.656565	-1.52308	15.9897	0.552657	0.138253	1
16942389	THOC7-AS1	THOC7 antisense RNA 1	ENST00000468961	0.0496952	0.0496952	0.65602	-1.52434	7.74189	0.554838	0.286668	1
16659881	NECAP2	NECAP endocytosis associated 2	NM_018090	0.0152683	0.0152683	0.6554	-1.52579	16.5354	0.557332	0.134821	1
16703758	RNU7-22P	RNA, U7 small nuclear 22 pseudogene	ENST00000516673	0.0441043	0.0441043	0.655306	-1.526	8.4118	0.55771	0.265204	1
17068782	MCM4	Minichromosome maintenance complex component 4	NM_005914	0.0380317	0.0380317	0.650849	-1.53646	9.30193	0.575867	0.247633	1
16920876	LOC100128310	Uncharacterized LOC100128310	AK097866	0.0298676	0.0298676	0.650784	-1.53661	10.9055	0.576132	0.211318	1
16916158	MIR941-1	MicroRNA 941-1	NR_030637	0.0324546	0.0324546	0.649299	-1.54012	10.332	0.582276	0.225427	1
16910854	EBF4	Early B-cell factor 4	NM_001110514	0.0363486	0.0363486	0.648818	-1.54126	9.58756	0.584278	0.243765	1
16780268	LOC100652869	Uncharacterized LOC100652869	XR_171060	0.00617201	0.00617201	0.648237	-1.54265	27.8737	0.586701	0.084194	1
17063975	CTAGE6	CTAGE family, member 6	NM_178561	0.0381603	0.0381603	0.64822	-1.54269	9.2809	0.586772	0.252895	1
16708061	ZFYVE27	Zinc finger, FYVE domain containing 27	NM_144588	0.0459347	0.0459347	0.647782	-1.54373	8.17896	0.588601	0.287861	1
16914117	PABPC1L	Poly(A) binding protein, cytoplasmic 1-like	NM_001124756	0.0426532	0.0426532	0.646879	-1.54588	8.60699	0.592391	0.275307	1
17057897	VOPP1	Vesicular, overexpressed in cancer, prosurvival protein 1	NM_030796	0.0118575	0.0118575	0.64688	-1.54588	19.2008	0.592387	0.123409	1
16671049	LCE2A	Late cornified envelope 2A	NM_178428	0.0158713	0.0158713	0.646083	-1.54779	16.1562	0.595745	0.147496	1
16681127	HES2	Hairy and enhancer of split 2	NM_019089	0.0345635	0.0345635	0.646077	-1.5478	9.91312	0.595768	0.240396	1
16728141	GAL	Galanin/GMAP prepropeptide	ENST00000265643	0.0449885	0.0449885	0.64506	-1.55024	8.29753	0.600076	0.289279	1

16928428	ADRBK2	Adrenergic, beta, receptor kinase 2	NM_005160	0.0292868	0.0292868	0.644519	-1.55154	11.0446	0.602373	0.21816	1
16664438	LINC00853	Long intergenic non-protein coding RNA 853	NR_047498	0.00392191	0.00392191	0.644396	-1.55184	35.8023	0.602895	0.067358	1
17092187	RLN1	Relaxin 1	NM_006911	0.00601878	0.00601878	0.641863	-1.55797	28.2677	0.613754	0.086849	1
16798951	GREM1	Gremlin 1, DAN family BMP antagonist	ENST00000300177	0.0467654	0.0467654	0.641705	-1.55835	8.07785	0.614435	0.304256	1
17118281	LOC100506458	Putative uncharacterized protein LOC65996-like	AK097034	0.039974	0.039974	0.640889	-1.56033	8.99512	0.617963	0.274799	1
16822548	NARFL	Nuclear prelamin A recognition factor-like	NM_022493	0.0279976	0.0279976	0.640866	-1.56039	11.3689	0.618064	0.217458	1
17016363	HIST1H3B	Histone cluster 1, H3b	NM_003537	0.0075093	0.0075093	0.63827	-1.56673	24.9645	0.62939	0.100846	1
16932782	PI4KAP2	Phosphatidylinositol 4-kinase, catalytic, alpha pseudogene 2	NR_003700	0.0100812	0.0100812	0.637439	-1.56878	21.099	0.633052	0.120015	1
17049667	TRIM56	Tripartite motif containing 56	ENST00000306085	0.0303044	0.0303044	0.636306	-1.57157	10.8035	0.638063	0.236242	1
17004339	PSMG4	Proteasome (prosome, macropain) assembly chaperone 4	AK096543	0.0496349	0.0496349	0.635179	-1.57436	7.7485	0.643074	0.331973	1
16858263	QTRT1	Queuine tRNA-ribosyltransferase 1	NM_031209	0.0424447	0.0424447	0.634868	-1.57513	8.63587	0.644462	0.298505	1
16739317	MTA2	Metastasis associated 1 family, member 2	NM_004739	0.0435419	0.0435419	0.634777	-1.57536	8.48628	0.644872	0.30396	1
17101605	TCEANC	Transcription elongation factor A (SII) N-terminal and central d	NM_152634	0.0225791	0.0225791	0.633589	-1.57831	13.024	0.650197	0.199692	1
17081850	GPR20	G protein-coupled receptor 20	NM_005293	0.0215886	0.0215886	0.633532	-1.57845	13.3924	0.650454	0.194276	1
17117486	LOC387720	Uncharacterized LOC387720	AK127642	0.0166138	0.0166138	0.632389	-1.58131	15.7179	0.655612	0.166844	1
16910645	FAM110A	Family with sequence similarity 110, member A	ENST00000381941	0.0166047	0.0166047	0.631965	-1.58237	15.7231	0.657532	0.167278	1
17104947	SLC16A2	Solute carrier family 16, member 2 (thyroid hormone transporter	NM_006517	0.0311806	0.0311806	0.631733	-1.58295	10.6055	0.658586	0.248395	1

17073290	GPIHBP1	Glycosylphosphatidylinositol anchored high density lipoprotein	NM_178172	0.00588708	0.00588708	0.630145	-1.58694	28.6186	0.66582	0.093061	1
16864084	CCDC155	Coiled-coil domain containing 155	NM_144688	0.0240895	0.0240895	0.62944	-1.58871	12.5067	0.669053	0.213982	1
16822801	NME3	NME/NM23 nucleoside diphosphate kinase 3	ENST00000219302	0.0194712	0.0194712	0.627934	-1.59252	14.2725	0.675997	0.189455	1
16857242	LOC100131094	Uncharacterized LOC100131094	NM_001242901	0.0406088	0.0406088	0.626812	-1.59537	8.89968	0.6812	0.306168	1
16757873	SIRT4	Sirtuin 4	NM_012240	0.0206501	0.0206501	0.625628	-1.59839	13.7657	0.686728	0.199547	1
16753962	MIR3913-1	MicroRNA 3913-1	NR_037475	0.0485542	0.0485542	0.623832	-1.603	7.86908	0.695175	0.353371	1
17013520	SASH1	SAM and SH3 domain containing 1	NM_015278	0.049728	0.049728	0.621149	-1.60992	7.7383	0.707932	0.365937	1
16806538	GOLGA8R	Golgin A8 family, member R	ENST00000544495	0.032288	0.032288	0.621122	-1.60999	10.3668	0.708062	0.273203	1
16729290	TSKU	Tsukushi, small leucine rich proteoglycan	NM_001258210	0.00953557	0.00953557	0.618969	-1.61559	21.7862	0.718422	0.131904	1
16990146	WDR55	WD repeat domain 55	ENST00000358337	0.0256844	0.0256844	0.61618	-1.6229	12.011	0.732015	0.243782	1
16715223	C10orf105	Chromosome 10 open reading frame 105	NM_001164375	0.0457697	0.0457697	0.615783	-1.62395	8.19937	0.733965	0.358059	1
17110700	KCND1	Potassium voltage-gated channel, Shal-related subfamily, member 1	NM_004979	0.00600062	0.00600062	0.613899	-1.62893	28.3154	0.74327	0.104999	1
16857630	PNPLA6	Patatin-like phospholipase domain containing 6	NM_001166111	0.00386235	0.00386235	0.613384	-1.6303	36.1026	0.74583	0.082635	1
16774623	LRCH1	Leucine-rich repeats and calponin homology (CH) domain cont	ENST00000311191	0.00434677	0.00434677	0.613272	-1.6306	33.8429	0.746387	0.088218	1
16795755	TTC7B	Tetratricopeptide repeat domain 7B	NM_001010854	0.0133899	0.0133899	0.61314	-1.63095	17.8772	0.747042	0.16715	1
17033279	MICA	MHC class I polypeptide-related sequence A	NR_036523	0.0103894	0.0103894	0.610552	-1.63786	20.735	0.76002	0.146616	1
16855673	BCL2	B-cell CLL/lymphoma 2	ENST00000398117	0.0204666	0.0204666	0.60862	-1.64306	13.8417	0.769815	0.222462	1
17060983	POLR2J	Polymerase (RNA) II (DNA directed) polypeptide J, 13.3kDa	NM_006234	0.0433766	0.0433766	0.603216	-1.65778	8.50846	0.797715	0.375022	1

16741549	ALG1L9P	Asparagine-linked glycosylation 1-like 9, pseudogene	NR_073388	0.0140843	0.0140843	0.60178	-1.66174	17.35	0.805255	0.18565	1
16807195	RASGRP1	RAS guanyl releasing protein 1 (calcium and DAG-regulated)	NM_005739	0.0479793	0.0479793	0.598616	-1.67052	7.9349	0.822058	0.414401	1
16662108	TSSK3	Testis-specific serine kinase 3	NM_052841	0.021244	0.021244	0.59463	-1.68172	13.5266	0.843605	0.249466	1
17003077	RNF44	Ring finger protein 44	NM_014901	4.37E-05	4.37E-05	0.592431	-1.68796	367.338	0.855672	0.009318	1
17049702	ZNHIT1	Zinc finger, HIT-type containing 1	NM_006349	0.0394297	0.0394297	0.592168	-1.68871	9.0788	0.857124	0.377638	1
16797285	BRF1	RNA polymerase III transcription initiation factor 90	ENST00000546474	0.0421155	0.0421155	0.590962	-1.69216	8.6819	0.86381	0.397982	1
16867657	PSPN	Persephin	NM_004158	0.0382368	0.0382368	0.589907	-1.69518	9.26843	0.869686	0.375333	1
17041421	ZBTB9	Zinc finger and BTB domain containing 9	ENST00000395064	0.0438848	0.0438848	0.587237	-1.70289	8.44069	0.884702	0.419256	1
17032957	HLA-L	Major histocompatibility complex, class I, L (pseudogene)	ENST00000491405	0.0169509	0.0169509	0.585126	-1.70903	15.5285	0.896712	0.230984	1
16842070	TOP3A	Topoisomerase (DNA) III alpha	NM_004618	0.0292841	0.0292841	0.584694	-1.7103	11.0453	0.899185	0.325635	1
16795567	KCNK10	Potassium channel, subfamily K, member 10	NM_021161	0.00668772	0.00668772	0.581317	-1.72023	26.6486	0.918699	0.137898	1
16946016	PCCB	Propionyl CoA carboxylase, beta polypeptide	NM_000532	0.0413342	0.0413342	0.580743	-1.72193	8.79333	0.922048	0.419431	1
16817212	RNA5SP405	RNA, 5S ribosomal pseudogene 405	ENST00000363059	0.0341409	0.0341409	0.578528	-1.72853	9.99393	0.935064	0.374253	1
16848961	TRIM65	Tripartite motif containing 65	NM_173547	0.0321262	0.0321262	0.578186	-1.72955	10.4009	0.937083	0.360384	1
16748304	GABARAPL1	GABA(A) receptor-associated protein like 1	ENST00000266458	0.0218829	0.0218829	0.576816	-1.73365	13.2803	0.945216	0.284697	1
16995888	LOC648987	Uncharacterized LOC648987	ENST00000503152	0.03522	0.03522	0.576709	-1.73398	9.7905	0.945855	0.386438	1
16859874	UPF1	UPF1 regulator of nonsense transcripts homolog	NM_002911	0.0407804	0.0407804	0.572561	-1.74654	8.87427	0.970827	0.437592	1

17057813	COBL	Cordon-bleu WH2 repeat protein	NM_015198	0.0257134	0.0257134	0.571697	-1.74918	12.0024	0.976094	0.325301	1
16916221	TCEA2	Transcription elongation factor A (SII), 2	BC098585	0.00983256	0.00983256	0.569842	-1.75487	21.4051	0.987474	0.184531	1
16814619	TPSAB1	Tryptase alpha/beta 1	NM_003294	0.0458649	0.0458649	0.567337	-1.76262	8.18758	1.003	0.490012	1
16902679	LOC389033	Placenta-specific 9 pseudogene	NR_026740	0.0474685	0.0474685	0.566148	-1.76632	7.99438	1.01044	0.505577	1
16894824	OSR1	Odd-skipped related 1	NM_145260	0.00987536	0.00987536	0.558694	-1.78989	21.3516	1.05807	0.19822	1
17111464	FGD1	FYVE, RhoGEF and PH domain containing 1	NM_004463	0.0119947	0.0119947	0.558614	-1.79014	19.0721	1.05859	0.222019	1
16865693	NAT14	N-acetyltransferase 14 (GCN5-related, putative)	NM_020378	0.0282187	0.0282187	0.557613	-1.79336	11.3117	1.06512	0.376645	1
16843376	NLE1	Notchless homolog 1 (Drosophila)	NM_001014445	0.0354797	0.0354797	0.552428	-1.81019	9.74294	1.09947	0.45139	1
16723100	MIR610	MicroRNA 610	NR_030341	0.00238537	0.00238537	0.552107	-1.81124	46.8369	1.10162	0.094082	1
16722295	RNA5SP332	RNA, 5S ribosomal pseudogene 332	ENST00000391063	0.0278526	0.0278526	0.546166	-1.83095	11.4068	1.14212	0.400505	1
16711484	IL15RA	Interleukin 15 receptor, alpha	NM_001243539	0.0291015	0.0291015	0.545693	-1.83253	11.0899	1.14539	0.413128	1
16808340	CATSPER2P1	Cation channel, sperm associated 2 pseudogene 1	NR_002318	0.040096	0.040096	0.544994	-1.83488	8.9766	1.15024	0.512551	1
17000121	LOC340073	Uncharacterized LOC340073	NR_037895	0.00807635	0.00807635	0.544351	-1.83705	23.9553	1.15472	0.192813	1
16758186	PSMD9	Proteasome (prosome, macropain) 26S subunit, non-ATPase, 9	NM_002813	0.0448884	0.0448884	0.534256	-1.87176	8.31029	1.2269	0.590545	1
16717706	POLL	Polymerase (DNA directed), lambda	NM_001174084	0.0241437	0.0241437	0.533809	-1.87333	12.4891	1.23018	0.394001	1
16855049	TCEB3C	Transcription elongation factor B polypeptide 3C (elongin A3)	NM_145653	0.020991	0.020991	0.53241	-1.87825	13.6272	1.24048	0.364119	1
17047138	GTF2IRD1	GTF2I repeat domain containing 1	NM_016328	0.0474343	0.0474343	0.531654	-1.88092	7.99839	1.24609	0.623169	1
16891225	TUBA4B	Tubulin, alpha 4b (pseudogene)	NR_003063	0.0327691	0.0327691	0.524633	-1.90609	10.267	1.29908	0.50612	1

16673883	C1orf105	Chromosome 1 open reading frame 105	ENST00000367727	0.00242651	0.00242651	0.522491	-1.91391	46.4101	1.31561	0.11339	1
16952244	ACAA1	Acetyl-CoA acyltransferase 1	NM_001607	0.0418213	0.0418213	0.514133	-1.94502	8.72349	1.38179	0.633593	1
16812083	LOC91450	Uncharacterized LOC91450	NR_026998	0.00067377	0.00067377	0.490577	-2.03842	91.0427	1.58348	0.069571	1
17056506	RP9P	Retinitis pigmentosa 9 pseudogene	NR_003500	0.00704435	0.00704435	0.489133	-2.04443	25.8814	1.59661	0.246759	1
17046559	INTS4L2	Integrator complex subunit 4-like 2	NR_027392	0.0391764	0.0391764	0.483515	-2.06819	9.11834	1.64861	0.723206	1
17035366	LOC100996357	Uncharacterized LOC100996357	ENST00000436256	0.0047095	0.0047095	0.482577	-2.07221	32.3844	1.65744	0.20472	1
17052679	IL23A	Interleukin 23, alpha subunit p19	AY532914	0.0291177	0.0291177	0.481004	-2.07899	11.0859	1.67232	0.603403	1
17108719	ASMTL	Acetylserotonin O-methyltransferase-like	ENST00000463763	0.00620783	0.00620783	0.480388	-2.08165	27.7837	1.67818	0.241606	1
16782207	LRP10	Low density lipoprotein receptor-related protein 10	ENST00000359591	0.0141519	0.0141519	0.477584	-2.09387	17.3007	1.70509	0.394225	1
16862484	CCDC97	Coiled-coil domain containing 97	NM_052848	0.0355213	0.0355213	0.457644	-2.18511	9.73536	1.90757	0.78377	1
16789743	CRIP1	Cysteine-rich protein 1 (intestinal)	NM_001311	0.0413088	0.0413088	0.436936	-2.28866	8.79701	2.14027	0.973179	1
16771801	HCAR3	Hydroxycarboxylic acid receptor 3	NM_006018	0.0339516	0.0339516	0.429125	-2.33032	10.0306	2.23454	0.891089	1
17051157	RNU7-27P	RNA, U7 small nuclear 27 pseudogene	ENST00000459281	0.00793745	0.00793745	0.413836	-2.41642	24.1925	2.43029	0.401826	1
16691129	AP4B1	Adaptor-related protein complex 4, beta 1 subunit	NM_001253852	0.0497166	0.0497166	0.356928	-2.80168	7.73954	3.3136	1.71256	1
16840284	C1QBP	Complement component 1, q subcomponent binding protein	NM_001212	0.00200878	0.00200878	0.199122	-5.02205	51.3347	8.13131	0.633592	1

Supplementary Table 2

Pathway Name	Enrichment Score	Genes
Fatty acid degradation	3.51594	ACAA1, GCDH
Valine, leucine and isoleucine degradation	3.51594	ACAA1, PCCB
Taste transduction	3.209	TAS2R19, TAS2R31
Adipocytokine signaling pathway	2.67827	POMC, SLC2A4
Non-homologous end-joining	2.56127	POLL
Olfactory transduction	2.31763	ADRBK2, OR2T4, OR5A1, OR14I1, OR51F2
mRNA surveillance pathway	2.22979	PABPC1L, UPF1
Biosynthesis of unsaturated fatty acids	2.10542	ACAA1
T cell receptor signaling pathway	2.01024	MAP3K8, RASGRP1
Pyrimidine metabolism	1.99475	NME3, POLR2J
Glyoxylate and dicarboxylate metabolism	1.98074	PCCB
HIF-1 signaling pathway	1.97945	BCL2, HIF1A
alpha-Linolenic acid metabolism	1.94286	ACAA1
Nicotinate and nicotinamide metabolism	1.83835	NMRK1
Homologous recombination	1.83835	TOP3A
Cell cycle	1.73155	CDC14B, MCM4
Propanoate metabolism	1.71654	PCCB
RNA polymerase	1.71654	POLR2J
Regulation of autophagy	1.66176	GABARAPL1
African trypanosomiasis	1.66176	HPR
Base excision repair	1.66176	POLL
Natural killer cell mediated cytotoxicity	1.64724	KIR3DL1, MICA
FoxO signaling pathway	1.62423	GABARAPL1, SLC2A4
DNA replication	1.61043	MCM4
Systemic lupus erythematosus	1.59054	HIST1H3B, HIST2H4B
Tryptophan metabolism	1.5167	GCDH
Graft-versus-host disease	1.45308	KIR3DL1
Basal transcription factors	1.4134	GTF2IRD1
Jak-STAT signaling pathway	1.37955	IL15RA, IL23A
Fatty acid metabolism	1.35751	ACAA1
Type II diabetes mellitus	1.35751	SLC2A4
Lysine degradation	1.33977	GCDH
Intestinal immune network for IgA production	1.33977	IL15RA
RNA transport	1.30902	PABPC1L, UPF1
Amyotrophic lateral sclerosis (ALS)	1.30551	BCL2
Fanconi anemia pathway	1.27279	TOP3A
Purine metabolism	1.26732	NME3, POLR2J
Tuberculosis	1.19646	BCL2, IL23A
Alcoholism	1.19646	HIST1H3B, HIST2H4B
mTOR signaling pathway	1.16873	HIF1A

Herpes simplex infection	1.14479	C1QBP, GTF2IRD1
Colorectal cancer	1.14163	BCL2
Renal cell carcinoma	1.09045	HIF1A
PPAR signaling pathway	1.06625	ACAA1
Inflammatory bowel disease (IBD)	1.06625	IL23A
Epstein-Barr virus infection	1.0367	BCL2, POLR2J
RNA degradation	1.00939	PABPC1L
Gastric acid secretion	0.987977	KCNK10
Pertussis	0.977536	IL23A
Antigen processing and presentation	0.977536	KIR3DL1
Peroxisome	0.927797	ACAA1
Apoptosis	0.881805	BCL2
Small cell lung cancer	0.881805	BCL2
GABAergic synapse	0.855826	GABARAPL1
Prostate cancer	0.847418	BCL2
Glycerophospholipid metabolism	0.839131	PNPLA6
Morphine addiction	0.83096	ADRBK2
NF-kappa B signaling pathway	0.83096	Bcl2
Rheumatoid arthritis	0.83096	IL23A
Carbon metabolism	0.776864	PCCB
Melanogenesis	0.762334	POMC
MAPK signaling pathway	0.743159	MAP3K8, RASGRP1
Toll-like receptor signaling pathway	0.720971	MAP3K8
Cytokine-cytokine receptor interaction	0.709588	IL15RA, IL23A
TNF signaling pathway	0.701456	MAP3K8
Cholinergic synapse	0.688846	BCL2
Glutamatergic synapse	0.670505	ADRBK2
Neurotrophin signaling pathway	0.641379	BCL2
Toxoplasmosis	0.641379	BCL2
Lysosome	0.630202	AP4B1
MicroRNAs in cancer	0.615074	BCL2, MIR34B
Insulin signaling pathway	0.535764	SLC2A4
Hepatitis B	0.509766	BCL2
Adrenergic signaling in cardiomyocytes	0.501455	BCL2
Pathways in cancer	0.499403	BCL2, HIF1A
Protein processing in endoplasmic reticulum	0.433732	BCL2
Transcriptional misregulation in cancer	0.394724	HIST1H3B
Huntington's disease	0.388639	POLR2J
Chemokine signaling pathway	0.368195	ADRBK2
Endocytosis	0.328479	ADRBK2
Focal adhesion	0.323569	BCL2
Viral carcinogenesis	0.321145	HIST2H4B
Regulation of actin cytoskeleton	0.30475	FGD1
Proteoglycans in cancer	0.282953	HIF1A

Ras signaling pathway	0.276762	RASGRP1
HTLV-I infection	0.213123	IL15RA
Neuroactive ligand-receptor interaction	0.191498	P2RY8
Metabolic pathways	0.135322	ACAA1, GCDH, NME3, PCCB, POLR2J
PI3K-Akt signaling pathway	0.118991	Bcl2

Supplementary Table 3

Protein IDs	Peptide counts (all)	Protein names	Gene names	Sequence coverage [%]	Mol. weight [kDa]	Sequence length	Ratio H/L G524L5
Q07021	8	Complement component 1 Q subcomponent-binding protein, mitochondrial	C1QBP	51.4	31.362	282	67.376
Q9H6W3;Q9H6W3-2	19;11	Bifunctional lysine-specific demethylase and histidyl-hydroxylase NO66	NO66	44	71.085	641	59.393
Q7Z7K6;Q7Z7K6-3;Q7Z7K6-2	7;6;5	Centromere protein V	CENPV	37.1	29.946	275	51.369
P56182;D6RE82	6;2	Ribosomal RNA processing protein 1 homolog A	RRP1	14.8	52.839	461	45.853
Q8NFW8;Q8NFW8-2;F5H296;F5GYM0	15;8;3;3	N-acylneuraminate cytidylyltransferase	CMAS	42.6	48.379	434	45.504
Q86V81;E9PB61	7;6	THO complex subunit 4	ALYREF	34.2	26.888	257	40.451
Q8TDD1;Q8TDD1-2;F8VRX4;H0YHH7	25;24;6;5	ATP-dependent RNA helicase DDX54	DDX54	31.3	98.594	881	38.316
Q9UNF1;Q9UNF1-2;Q5H909;Q5H907;Q12816-5;A0A087X070;G5E9N2;Q12816-2;Q9Y5V3;Q9Y5V3-2;Q12816-3;Q12816-4;Q12816	16;15;15;13;1;1;1;1;1;1;1;1	Melanoma-associated antigen D2	MAGED2	31.8	64.953	606	33.31
Q9Y6H1;Q5T1J5	3;2	Coiled-coil-helix-coiled-coil-helix domain-containing protein 2, mitochondrial;Putative coiled-coil-helix-coiled-coil-helix domain-containing protein CHCHD2P9, mitochondrial	CHCHD2;CHCHD2P9	31.1	15.512	151	24.503
P67809;A0A087X1S2;H0Y449;C9J5V9;Q9Y2T7	13;10;9;6;4	Nuclease-sensitive element-binding protein 1	YBX1	51.2	35.924	324	20.563
Q9BX40;Q5TBQ0;Q9BX40-2;Q5TBQ1;Q5TBP9;Q9BX40-3	9;7;7;5;4;3	Protein LSM14 homolog B	LSM14B	34.3	42.07	385	20.43

Q96JP5;Q96JP5-2;H3BTR0	8;7;5	E3 ubiquitin-protein ligase ZFP91	ZFP91;ZFP91-CNTF	17	63.444	570	20.072
P62081;B5MCP9	8;6	40S ribosomal protein S7	RPS7	40.7	22.127	194	19.184
P0CW22;P08708;H0YN88;A0A075B716;H0YN73;H3BNC9	8;8;7;7;5;2	40S ribosomal protein S17-like;40S ribosomal protein S17	RPS17L;RPS17	56.3	15.55	135	18.032
P46779-4;P46779-5;H0YLP6;H0YMF4;P46779;P46779-2;P46779-3;H0YKD8	5;5;5;5;5;5;5	60S ribosomal protein L28	RPL28	59.4	7.888	69	15.03
P51116;I3L1Z2	12;2	Fragile X mental retardation syndrome-related protein 2	FXR2	23.8	74.222	673	13.896
P51114;B4DXZ6;P51114-2;E9PFF5;P51114-3;E7EU85;C9JZE0;C9JY20;C9JAJ4;C9IZ22;H7C4S4;C9JYQ6;C9J5B4;R9WNI0;A8MQB8;Q06787-8;Q06787-6;G3V0J0;Q06787-2;Q06787-4;Q06787-5;Q06787-9;Q06787-7;Q06787-3;Q06787	17;16;15;14;14;12;4;4;3;2;2;1;1;1;1;1;1;1;1;1;1;1;1;1	Fragile X mental retardation syndrome-related protein 1	FXR1	31.6	69.72	621	13.774
Q13724-2;Q13724;C9J8D4;C9JDQ1	6;6;3;1	Mannosyl-oligosaccharide glucosidase	MOGS	11.2	80.702	731	11.476
P48634-2;P48634-3;P48634;P48634-4	13;13;13;11	Protein PRRC2A	PRRC2A	8.2	227.84	2144	10.753
E9PLL6;P46776;E9PJD9;E9PLX7	4;4;3;1	60S ribosomal protein L27a	RPL27A	38	12.201	108	10.532
P62854;Q5JNZ5	3;2	40S ribosomal protein S26;Putative 40S ribosomal protein S26-like 1	RPS26;RPS26P11	31.3	13.015	115	10.49
Q8NC51-4;Q8NC51-3;Q8NC51-2;Q8NC51	9;9;9;9	Plasminogen activator inhibitor 1 RNA-binding protein	SERBP1	29.5	42.426	387	10.434
P62913-2;P62913;Q5VVC8;Q5VVC9	4;4;3;2	60S ribosomal protein L11	RPL11	22.6	20.124	177	9.725
Q9Y520-6;Q9Y520-4;E7EPN9;Q9Y520-5;Q9Y520;Q9Y520-7;Q9Y520-2;Q9Y520-3;H7C5N8;A0A0A0MS30;Q5JSZ5-5;Q5JSZ5	14;14;14;14;14;14;13;13;4;2;1;1	Protein PRRC2C	PRRC2C	5.5	301.57	2752	8.9975
D3YTB1;P62910;F8W727	4;4;4	60S ribosomal protein L32	RPL32	30.1	15.616	133	7.6816

P62750;H7BY10;K7EJV9;K7ERT8;A8MUS3;K7EMA7	3;3;3;3;3;1	60S ribosomal protein L23a	RPL23A	14.7	17.695	156	6.4511
P62753;A2A3R7;A2A3R5	5;3;3	40S ribosomal protein S6	RPS6	25.7	28.68	249	5.649
Q2NL82;I3L1Q5	8;3	Pre-rRNA-processing protein TSR1 homolog	TSR1	10.8	91.809	804	5.5874
P62263;H0YB22;E5RH77	6;5;5	40S ribosomal protein S14	RPS14	37.7	16.273	151	4.9595
P62269;J3JS69	14;3	40S ribosomal protein S18	RPS18	62.5	17.718	152	4.7925
O00571-2;O00571;O15523-2;O15523;O15523-3;A0A087WVZ1;C9J8G5;C9J081;B4DLA0	18;18;13;13;5;3;3;3;1	ATP-dependent RNA helicase DDX3X;ATP-dependent RNA helicase DDX3Y	DDX3X;DDX3Y	33.6	71.354	646	4.3595
Q14739;C9JXK0;C9JES9	7;3;2	Lamin-B receptor	LBR	12.8	70.702	615	4.2938
P15880;H0YEN5;E9PQD7;E9PMM9;I3L404;E9PPT0;E9PM36;H3BNG3;H0YE27	8;7;7;4;3;3;3;1;1	40S ribosomal protein S2	RPS2	32.1	31.324	293	3.7432
P22087;M0QXL5;M0R2Q4;M0R0P1;M0R299;M0R2U2;M0R1H0;M0R2B0;A6NHQ2;R4GMW7;M0QXC9	11;10;10;9;9;7;7;7;2;2;1	rRNA 2-O-methyltransferase fibrillarin	FBL	34.9	33.784	321	3.4512
P62829;C9JD32;J3KT29;B9ZVP7;J3KTJ3;J3QQT9	5;4;4;3;2;1	60S ribosomal protein L23	RPL23	44.3	14.865	140	3.0869
Q00839-2;Q00839;Q5RI18	7;7;3	Heterogeneous nuclear ribonucleoprotein U	HNRNPU	8.4	88.979	806	2.3757